THE DEVELOPMENT OF IN-PROCESS MONITORING AND CONTROL TECHNIQUES FOR AEROSPACE APPLICATIONS OF FRICTION STIR WELDING

By

Brian Travis Gibson

Dissertation

Submitted to the Faculty of the

Graduate School of Vanderbilt University

in partial fulfillment of the requirements

for the degree of

DOCTOR OF PHILOSOPHY

in

Mechanical Engineering

May, 2015

Nashville, Tennessee

Approved:

Professor George E. Cook

Professor Alvin M. Strauss

Professor Jason G. Valentine

Professor D. Greg Walker

Professor D. Mitch Wilkes

For George Hayward and Ruthana Parkins Gibson

&

Camden Edward and Betty Lou Grant

ACKNOWLEDGEMENTS

I would like to thank Dr. Alvin Strauss and Dr. George Cook for providing me with an excellent opportunity. Your support and guidance over the years has been invaluable. I would like to thank Dr. Mitch Wilkes for contributing to this research in the area of signal processing and serving on my committee. Thank you also to Dr. Greg Walker and Dr. Jason Valentine for serving on my committee.

I gratefully acknowledge the funding and support provided by the Tennessee Space Grant Consortium and Vanderbilt University, without which, this research would not have been possible. I also acknowledge the assistance of Gilbert Sylva of Eclipse Aerospace, whose technical guidance regarding applications of FSW in aerospace manufacturing both inspired and enabled the pursuit of many of the research objectives presented here.

Thank you to my colleagues in the Vanderbilt University Welding Automation Laboratory, particularly Chase Cox, for assisting with this research and contributing to the graduate school experience. Thank you to Dr. David DeLapp for providing insightful guidance regarding experimental methodology and to the personnel of the Vanderbilt University Physics Machine Shop, particularly Robert Patchin, for providing timely assistance and the highest quality of work.

Finally, I would like to thank my parents, Robert and Deborah Gibson, my sister, Robin Fraker, and Chelsea Snarrenberg. You have provided me with endless love, support, and encouragement, and without you, this work would not have been possible.

TABLE OF CONTENTS

LIST OF TABLES

LIST OF FIGURES

CHAPTER I

INTRODUCTION

Overview

Research presented in this dissertation addresses issues regarding the utilization of Friction Stir Welding (FSW) as a primary joining technology for the manufacture of lightweight structures in the transportation industry. FSW is indeed finding applications in numerous industries, and certainly the lessons learned herein will potentially be applicable to challenges in automotive manufacturing; however, applications in aerospace, and in particular, solutions to the challenges presented by the use of FSW as a rivet replacement technology, are targeted with this research.

Aerospace manufacturers are currently pursuing increased utilization of novel manufacturing technologies and non-traditional materials to achieve lower manufacturing costs, weight reduction, and greater efficiency, while at the same time experiencing rapid growth in product demand. This situation has presented numerous technical challenges. FSW is a joining technology that has proven to offer many advantages to manufacturers when compared to traditional riveting operations. And, while FSW is beginning to be utilized for production aircraft assemblies, it remains in its relative infancy as a rivet replacement technology. Significant progress has been required regarding the incorporation of aerospace sealants into joining operations, development of efficient quality evaluation methods, development of novel robotic FSW control techniques, and process optimization for joining new alloys with FSW. Accordingly, research presented in this dissertation focuses on developing technologies that address these deficiencies.

Contributions

Significant contributions of this dissertation take the form of advancements in the challenging aspects of joining with FSW for aerospace applications: the incorporation of corrosion prevention measures into welded components, robotic path planning procedures, and tool wear. The utilization of process variants and the joining of an advanced alloy with non-traditional tool geometry and parameters are investigated as well. The expectation is that contributions will enhance the knowledge base, create areas of strength for manufacturers using FSW, and enable new users of FSW to emerge.

The content of Chapters III and IV addresses the use of aerospace sealants with FSW and orchestrates interactions between sealants and welding robots that have not been accomplished previously. Chapter III details the development of an in-process evaluation technique for detecting the quality of faying surface sealant application in dissimilar lap joints of 7075 and 2024 alloys. In it, the welding process itself becomes a diagnostic tool, as information is extracted from the spectral content of weld forces and correlated with sealant condition. Chapter IV builds upon observations of Chapter III and presents an innovative method for automatically tracking blind sealant paths that have been applied between sheets of lap joints of the same alloys. Chapter V examines novel FSW variant technologies, weaving and pulsing, and characterizes their impact on weld strength in the joining of 2198 aluminum-lithium alloy, a candidate material receiving significant attention from aerospace manufacturers. Chapter VI compares base material properties and the joint strengths achievable with FSW for the incumbent and candidate alloys, and finally, Chapter VII outlines the design and characterization of an adaptive torque controller that enables in-process estimation of tool wear.

CHAPTER II

LITERATURE REVIEW

Select passages of this chapter are published in:

Gibson, B.T., Lammlein, D.H., Prater, T.J., Longhurst, W.R., Cox, C.D., Ballun, M.C., Dharmaraj, K.J., Cook, G.E., Strauss, A.M., "Friction Stir Welding: Process, Automation, and Control," *SME Journal of Manufacturing Processes*, Vol 16, No 1, 2014, pp. 56-73. DOI: 10.1016/j.jmapro.2013.04.002

Friction stir welding (FSW) is a solid-state joining technique, the use of which has expanded rapidly since its development at TWI of Cambridge, UK in December 1991. It has found applications in a wide variety of industries as well, including aerospace, automotive, railway, and maritime [1, 2]. The FSW process exhibits a number of attractive advantages when compared to other welding processes, perhaps the most significant of which is the ability to weld alloys that are difficult or impossible to weld using fusion welding techniques. The FSW process takes place in the solid-phase, below the melting point of the material, and as a result does not experience problems related to resolidification, such as the formation of second phases or inclusions, porosity, embrittlement, and cracking. In addition, the lower temperature of the process enables joining with lower distortion and lower residual stresses. FSW is also an energy efficient process that uses a practically non-consumable tool, requires no filler material, and in most cases, does not require the use of a shielding gas. Furthermore, the process lacks the fumes, arc flash, and spatter associated with most fusion welding techniques. For these many reasons, FSW has become an attractive alternative for many manufacturers.

Process

Although there are several process variants, some of which will be discussed here, conventional FSW was the earliest demonstrated technique, and it remains the most basic and widely applied technique in research and industry. A rotating tool consisting of a probe and shoulder plunges into the workpiece, generating heat through both friction and plastic deformation, and traverses the joint line. Figure 1 displays a conventional FSW square butt joint.

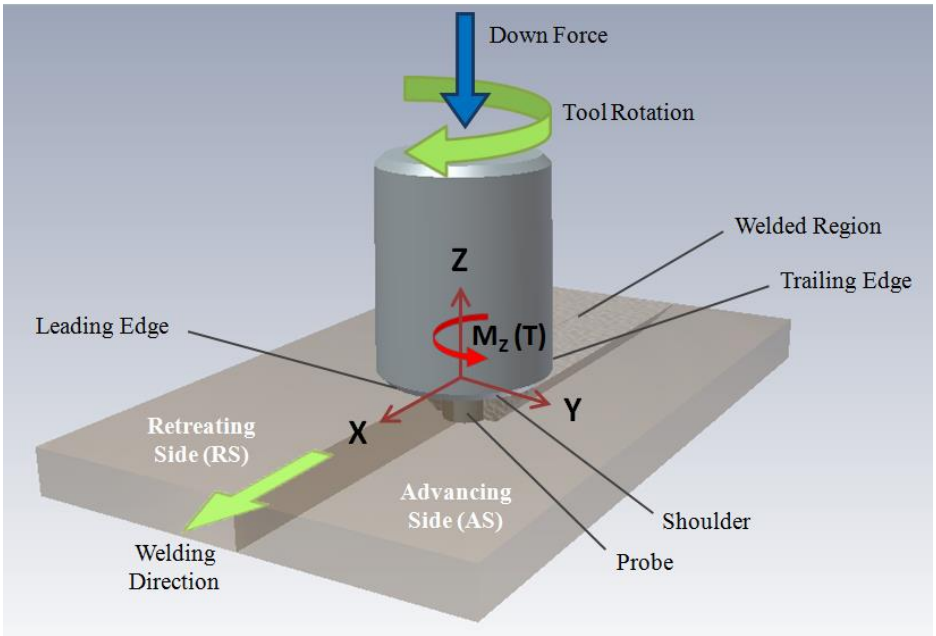

Figure 1: FSW Process

The basic terminology for describing the FSW process was outlined in an article by Threadgill [3]. Variables include the tool rotation rate, welding speed, plunge depth, tilt angle, sideways tilt angle, shoulder geometry, shoulder features (such as scrolls), probe geometry, and probe features (such as threads, flutes, flats, etc). Absent from this list are forces, which should first be well understood as dependent, reactionary variables

before they are used as inputs for control. Tool geometry, process forces, and control methodology are discussed extensively in their respective sections of this literature review.

FSW is applicable to a number of joint configurations, the most common of which are the square butt joint and the lap joint. These are pictured in Figure 2 along with a T-joint.

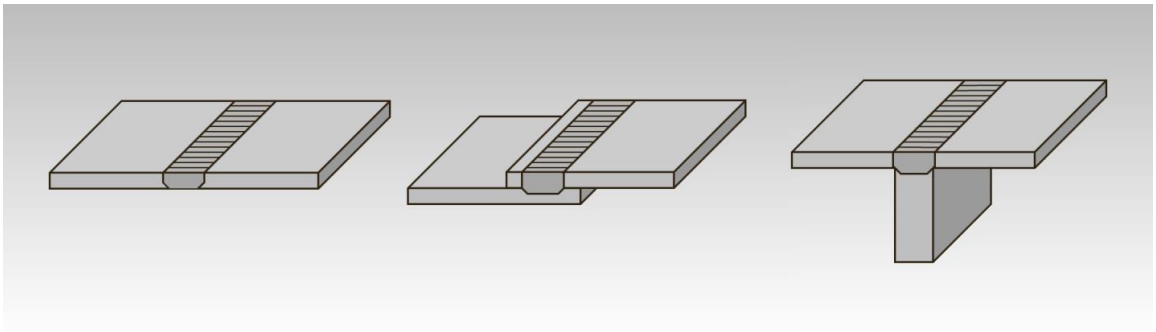

Figure 2: Common Joint Types: Square Butt, Lap, and T-Joint

Other common joint types not pictured include pipe welds, hemispherical welds, multiple lap welds, double T-joint welds, corner welds, and fillet welds. As the lap joint configuration is the primary focus of much of the work presented in this dissertation, lap joint characteristics are examined closely in their own respective section of this review. Another advantage of FSW is that typically little joint preparation is required. Butt joints can be made in the closed-square style, even when the workpiece is relatively thick (greater than 0.25 in), and FSW is usually tolerant of light oxide layers. No matter what the joint type, what is always necessary in FSW however is adequate fixturing along with a rigid backing anvil, in the case of conventional friction stir welding. A consequence is that there is usually a large capital investment on the front end of the manufacturing

process to obtain the required machinery and tooling, and setup time relative to joining time increases when production begins.

Material Flow

There are multiple facets of the material flow process within FSW that must be well understood. Multiple flow regimes will be discussed here, but the most basic phenomenon is the advancing-retreating nature of the process, which is due to differential tangential velocities on the sides of the tool resulting from simultaneous rotation and translation. The advancing side (AS) and retreating side (RS) are labeled in Figure 1. The advancing-retreating phenomenon of FSW is a dominant characteristic of the process and greatly influences how heated, plasticized material is extruded around the tool probe before it is forged together behind the probe under significant shoulder pressure. This cyclical material transfer mechanism is a topic of much research and debate, and it is often examined from both an experimental and modeling perspective.

Some of the earliest studies focused on determining material flow mechanisms within the FSW process were conducted from primarily an experimental perspective; however, the ability for researchers to study material flow in FSW and communicate effectively with one another about their findings was dependent upon standard classifications of the weld zone microstructural characteristics, so again Threadgill outlined the terminology for these classifications by describing three primary regions and one special region in the cross sections of friction stir welded joints [3]. As in fusion welding, FSW joints have a region that is affected by heat only, known as the heat affected zone (HAZ). The region outside of this, which is unaffected by heat or

deformation is the parent material. The region that is affected by both heat and plastic deformation is known as the thermo-mechanically affected zone (TMAZ), which at a minimum is defined by a trapezoid bounded by the diameter of the shoulder and the diameter of the probe at the weld root. In welds of certain materials, the TMAZ region may not be completely recrystallized. In this case, a special region within the TMAZ called the 'nugget', in which all material is recrystallized, is designated. These regions are depicted in Figure 3 for a friction stir weld cross-section of ambiguous joint type.

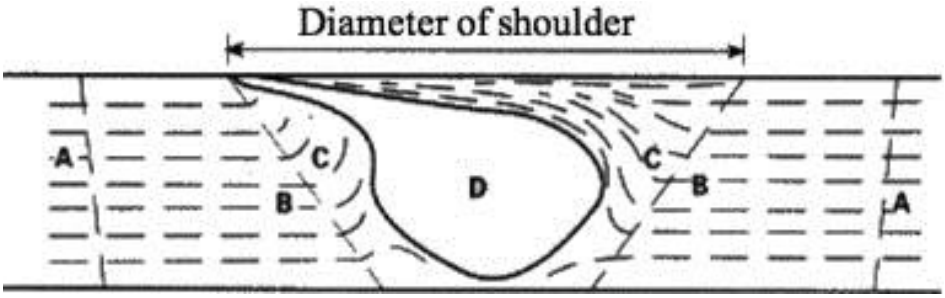

Figure 3: Depiction of Weld Cross-Section Indicating Four Characteristic Regions: (A) Parent Material, (B) HAZ, (C) TMAZ, (D) Nugget; Image adapted from [4]

Another term for the 'nugget' that is encountered in the literature is the 'dynamically recrystallized zone', sometimes abbreviated DRX or DXZ. The use of ambiguous terms such as 'stirred zone' should be avoided. These weld regions were defined so to be applicable to friction stir welds in most materials and are present no matter what the joint configuration [3].

Early experimental studies into mechanisms of material flow in FSW involved several different methodologies. Colligan classified FSW as primarily an extrusion process, conducting tracer experiments with steel shot in 6061-T6 and 7075-T6 alloy butt joints and determining that some material moves via chaotic mixing and some material is

simply extruded around the retreating side of the probe. The transfer mechanism depended on where the material originated in the joint [5]. Two techniques for evaluating material flow were utilized in this study. First, 0.38 mm diameter steel shot was imbedded into 14 different 0.75 mm x 0.3 mm grooves of various vertical and lateral positions relative to the path of the FSW tool, which had proprietary geometry, but at a minimum featured a threaded probe and concave shoulder. This was performed for both 6061-T6 and 7075-T6 plate in 6.4 mm thickness. Radiographs were used to view the position of the steel shot before welding, during interaction with the tool, and after the tool had passed. An example of one of these radiographs for a 6061-T6 specimen is displayed in Figure 4.

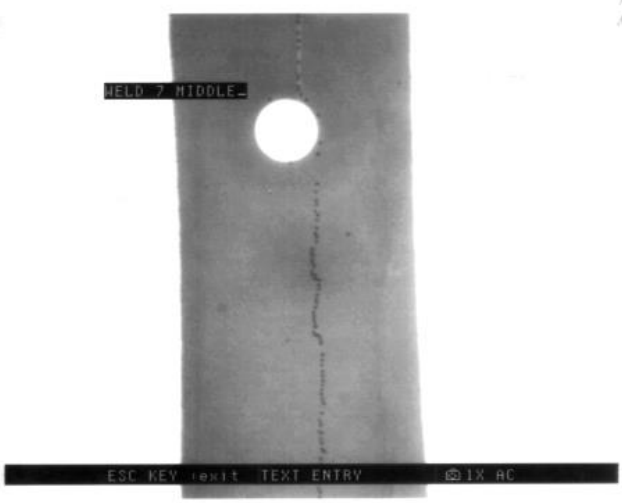

Figure 4: Radiograph of 6061-T6 Butt Weld Revealing Dispersal of Steel Shot Tracer Around Tool Probe (Visible Hole) [5]

Secondly, a ‘stop-action’ technique was used, wherein the tool traverse and rotation speed were stopped suddenly and tool retraction began simultaneously with a rotation rate that caused the threaded tool probe to simply unscrew from the workpiece. Cross-

sectioning of the retraction point, or keyhole, allowed for the study of material flow in the region adjacent to and within the tool threads. Figure 5 displays a cross-section of the keyhole retraction region for a 6061-T6 specimen.

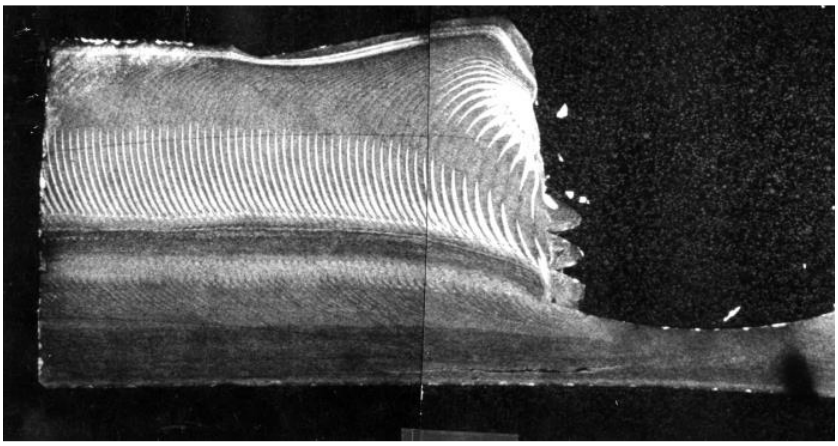

Figure 5: Cross-Section of Keyhole Retraction Region in 6061-T6 Generated with 'Stop-Action' Technique [5]

Results from both experimental methods indicate that the primary method of material transfer in FSW is simple extrusion, which occurs on the retreating side of the probe. Radiographs did indicate however that some material is stirred. This material originates near the upper portion of the tool probe and is forced downward by the threads on probe and is deposited as the tool passes. Conversely, material that is extruded rises as it passes around the tool probe. Inertial effects due to differential masses of the aluminum workpiece material and the steel tracer were deemed insignificant due to the relatively high viscosity of the plasticized aluminum, which would resist relative motion. These preliminary results formed a conceptual model for material flow in friction stir welds of aluminum alloys which could then be built upon to formulate ideal models of the process for predicting variables such as temperature profiles and forces [5].

Reynolds also classified FSW as an extrusion process, utilizing a 5454-H32 tracer to study material flow in butt welds of 2195-T8, and noting that the tool shoulder, the weld backing plate, and cold base metal outside the weld zone form a moving 'extrusion chamber' [6]. To study material flow, welds were made with tools exhibiting two different probe diameters, 10 mm and 12 mm, and workpieces of 2195-T8 that were modified to accommodate inserts of 5454-H32 at the faying surfaces of the butt joints on both advancing and retreating sides at three different heights. Post weld visualization was accomplished via metallographic etching with Keller's reagent, which readily distinguished the two alloys due to the fact that 2195 has a relatively high copper content and 5454 contains no copper. First, standard transverse cross-sections were examined to ensure that the welds that had been created were of good quality and exhibited typical characteristics of friction stir welded butt joints. Figure 6 displays these cross-sections for both tools in the study.

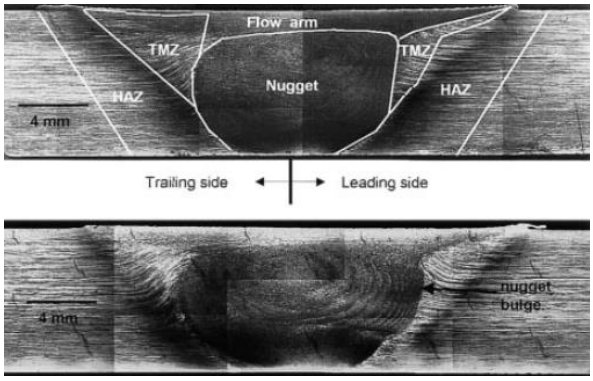

Figure 6: Initial Transverse Cross-Sections of Tracer Study Welds; Top: 10 mm Diameter Probe, Bottom: 12 mm Diameter Probe [6]

Once it was determined the cross-sections were of acceptable quality, and the extent of the dynamically recrystallized zones had been determined at various depths as well,

welds were then sectioned in the XY plane by repeatedly milling off slices of 0.25 mm thickness from the top surface, etching with Keller's reagent, and then digitally imaging the surface. The digital images of the slices at varying depths were then compiled to build a three-dimensional (3D) picture of the material flow. This is displayed in Figure 7. Reynolds used the terms 'leading side' and 'trailing side' to refer to the advancing side and retreating side of the welds, respectively.

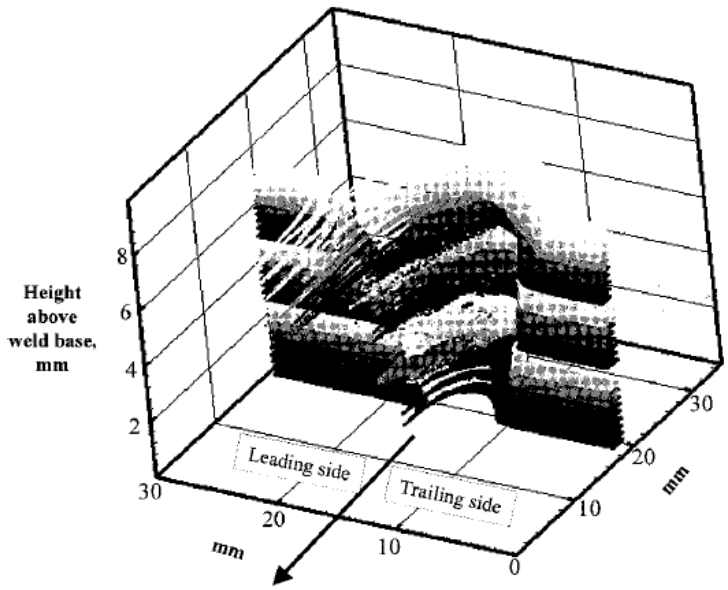

Figure 7: 3D Composite Image Compiled from 60 Successive Slices of Tracer Study Weld with 10 mm Probe Diameter [6]

Examining the flow visualizations obtained in the experiments, Reynolds asserted that FSW is an extrusion process, with the tool (including both the probe and shoulder) and the cold material on all sides of the tool, working in conjunction with the weld backing plate, forming a moving extrusion die. Reynolds stated that hot material with lower flow stress is extruded on both sides of the probe, which differs somewhat from Colligan's

assertion that extrusion primarily occurs on the retreating side [5]. Reynolds also noted however, like Colligan, that some material, which originates near the top of the weld, is stirred or circulated around the tool axis, moving primarily from the retreating to advancing side, with some deviation from this convention occurring as the point from which the material originates lowers to the middle or bottom of the weld. Finally, Reynolds described the forging aspect of FSW, which occurs as the back of the shoulder, or heel, consolidates the extruded material as it passes over [6].

Arbegast developed a metal-working model for material flow in FSW that includes the aspects of extrusion and forging observed experimentally by Colligan and Reynolds. The model describes five metal-working zones, which are pre-heating, initial deformation, extrusion, forging, and post-weld cooldown [7]. These are illustrated schematically in Figure 8.

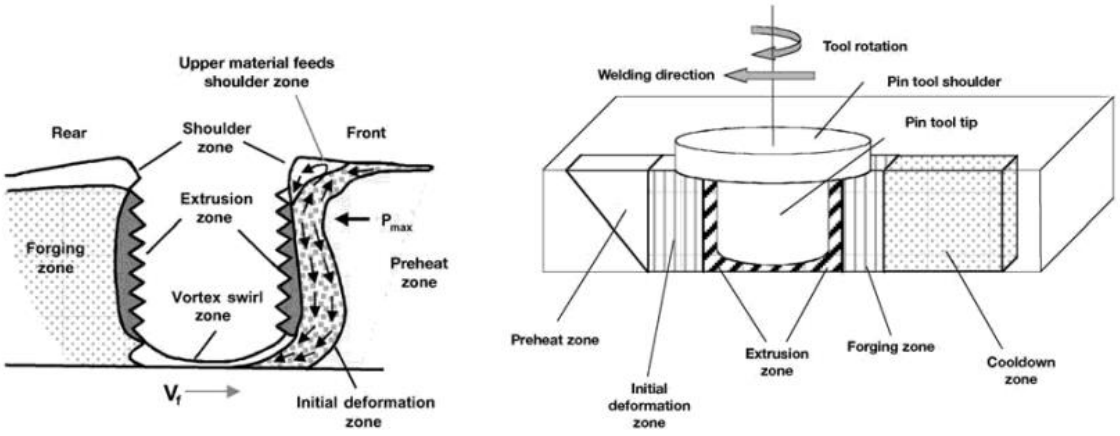

Figure 8: Arbegast's Metalworking Model for FSW [7]; Image adapted from [8]

The pre-heat zone is caused by the advancing of the FSW tool through the material, particularly the tool shoulder as it reaches the unwelded workpiece in advance of the

probe. As the workpiece is heated and softened, the initial deformation zone forms ahead of the probe. Arbegast claims that in this zone, material is first forced upward and then downward into the extrusion zone. This claim would seem dependent on having concave shoulder geometry, which appears evident in Figure 8. Once in the extrusion zone, material is transferred around the probe as it moves forward through the workpiece, and then material at the rear of the probe is forged or consolidated by pressure from the back, or heel, of the tool shoulder. The welded workpiece then cools as the tool continues to advance along the joint line [7]. This early model was serviceable in terms of gaining a basic understanding of the FSW process. It also helped explain the formation of some common defects, such as wormholes and lack of penetration [8]. Arbegast then however expanded on the model to help explain the formation of many weld defects, including wormholes, lack of penetration, lack of fusion, surface lack of fill, scalloping, surface galling, root flow defects, and nugget collapse. This was accomplished using a flow-partitioned deformation zone model along with equations for describing the motion of a multi-body dynamic system. The concept of this model has been presented, and experimental validation is underway [9].

While early experimental work from Colligan and Reynolds, along with Arbegast's metalworking model, lent great understanding to material flow mechanisms of FSW, they did not address to a great extent the cyclical nature of the process, or the periodic transfer of material around the tool probe, which is evident upon observation of welded workpiece surfaces or weld-cross sections in the form of banded structures. Krishnan classified FSW as an extrusion process as well, but went on to say that for each rotation of the tool, a cylindrical section of material is extruded around the probe and a

banded structure within the weld results. Krishnan asserted that these bands, or 'onion rings', which can appear as concentric rings or semicircles depending on which cut plane they are viewed from, result from oxidation on the surface of each semi-cylinder [10]. To examine this process from an experimental perspective, 6061 and 7075 alloys were welded with unreported tool geometry and sectioned in all three planes. Figure 9 displays a conceptual visualization of the rings or semicircles which result from planar cross-sectioning and an actual cross-section on the YZ plane showing concentric rings denoted as 'onion rings'.

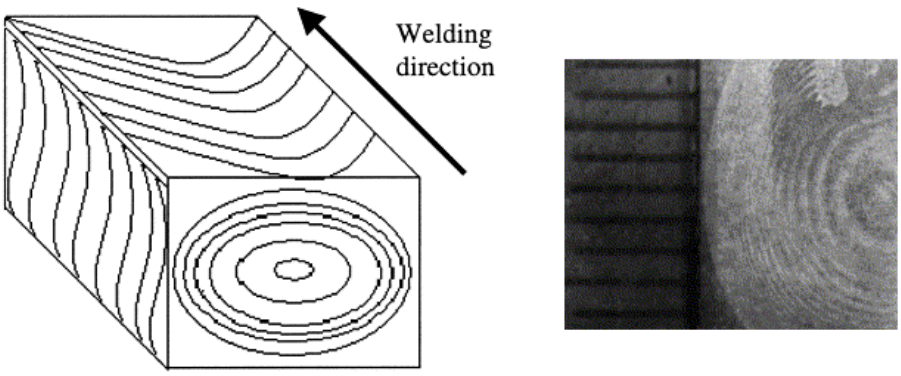

Figure 9: Visualization of Rings and Semicircles Revealed by Cross-Sectioning (left) and YZ Plane Cross-Section Showing 'Onion Rings' (right) [10]

Krishnan asserted that during the welding process, a repeated cyclical process occurs wherein the tool pauses for a short period of time while the workpiece immediately in front of the probe is heated and then forward motion of the tool shears and extrudes a sheet of plasticized metal. This process occurs once per tool rotation creating a continuous set of semicircular rings, and the resulting spacing in between the rings is equal to the distance traversed by the tool in one rotation, as illustrated in Figure 10.

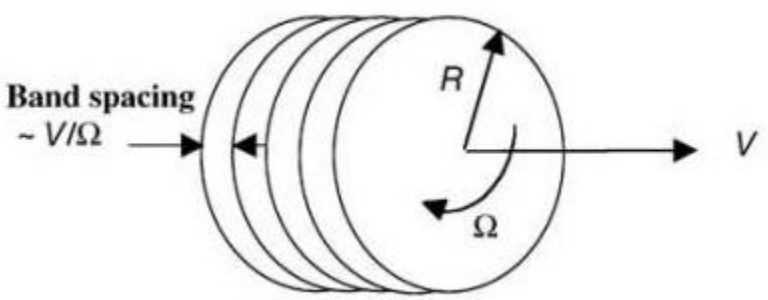

Figure 10: Spacing of Banded Structures; Image adapted from [8]

Again, Krishnan attributed the visibility of the banded structure to oxidation on the surface of each semi-cylinder [10]. While there has been some other discussion of oxidation in the literature, it is somewhat a simplistic and perhaps naïve explanation that does not take into account other important aspects of the process. For instance, Yang et al. observed banded microstructure in welds of AA2024-T351 and AA2524-T351, and concluded that it resulted from periodic variations in the size of equiaxed grains, the micro-hardness, and the concentration of base metal impurity particles. This study highlighted, through meticulous measurements of the properties of the banded structures, that while FSW has very consistent macro-scale properties, there is indeed a regular varying component at a smaller scale that is important for understanding both the underlying physics of the process and the properties of resulting welded joints [11].

Schneider et al. also studied 'onion ring' formation and banding and asserted, like Krishnan, that each 'onion ring' is formed by material transfer during a singular rotation of the tool. However, Schneider et al. also observed a secondary phenomenon at a lower frequency that was evident in the dispersal pattern of a molten lead tracer wire in a butt weld of 2195-T81 Al-Li-Cu alloy [12]. This phenomenon was referred to as interfacial

'slipping and sticking' and was theorized to result from variation in the radial distribution of the rotational field, or an oscillation in the material contact condition at the edge of the tool shoulder, as illustrated in Figure 11, although additional interactions dealing with a more comprehensive material flow model will be discussed here as well. This alternating boundary condition may however have the effect of destabilizing weld zone temperature, causing 'slip-stick' oscillations.

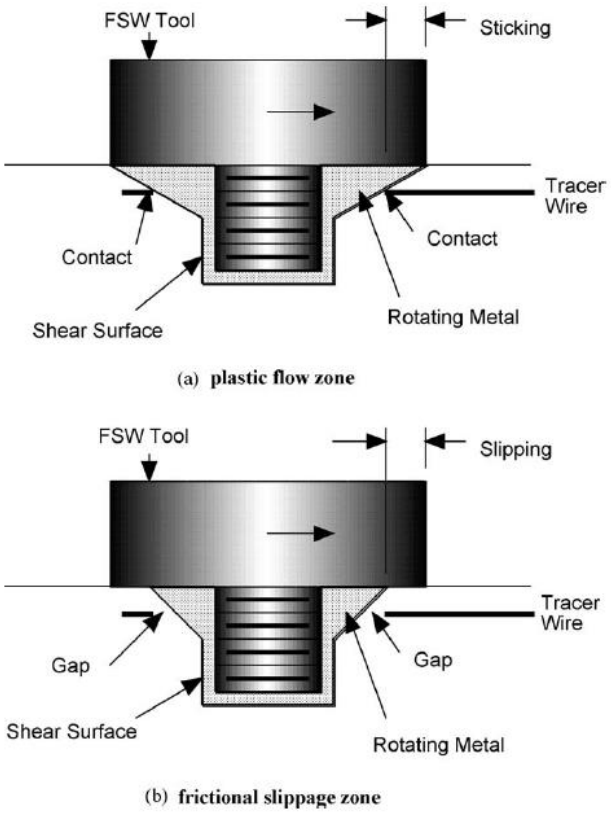

Figure 11: Visualization of Fluctuations in Contact Condition at Edge of Shoulder Leading to 'Slipping and Sticking' Conditions [12]

The phenomenon in question was observed at a frequency one order of magnitude lower than the tool rotational speed. Welding for this experiment was performed at 200 rpm

and 15 cm/min (5.9 inch/min) with a tool featuring a flat, smooth shoulder and threaded probe. Banded structures were observed via cross-section at a frequency of 200 bands/min, while fluctuations in the dispersal pattern of the molten lead tracer were observed in radiographs at approximately 20 traces/min, suggesting a 'double periodicity'. Figure 12 displays a depiction of the weld and an inverted radiograph of the lead wire dispersal pattern from 29 cm to 37 cm, while also highlighting the inconsistency of the phenomenon throughout other portions of the weld.

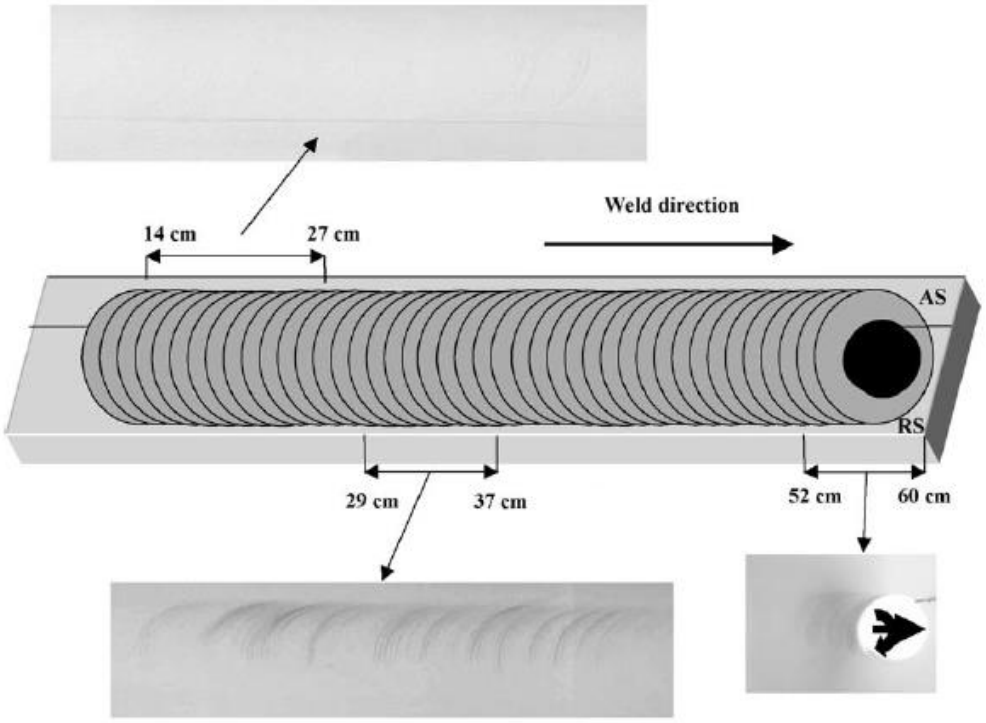

Figure 12: Lead Wire Tracer Weld Depiction with Inverted Radiographs; Image adapted from [12]

Schneider et al. questioned the effect that the slower oscillation in material contact condition would have on the structural integrity of welds, and suggested that it would perhaps be more critical than the presence of the more widely recognized, and accepted,

banded structure or 'onion rings' in the weld nugget. Schneider et al. also suggested that the incorporation of high speed torque measurements would be a way to examine and potentially verify the existence of a 'slip-stick' oscillation [12].

There are indeed studies that have incorporated relatively high speed torque measurements and observed steady oscillations in the process torque. Longhurst conducted a set of experiments to examine in-process void detection capabilities, in which spindle motor current was monitored as an indirect measurement of process torque [13]. Butt joints of 6061 in 0.25 inch thickness were prepared with holes of varying sizes (3/16 inch, 1/8 inch, 1/16 inch) drilled into the faying surface of one of the workpieces. Welds were performed with a tapered, scrolled shoulder tool with a threaded probe at 1400 rpm and 10 IPM. Figure 13 displays a portion of the spindle motor current data for the weld with 1/8 inch drilled holes.

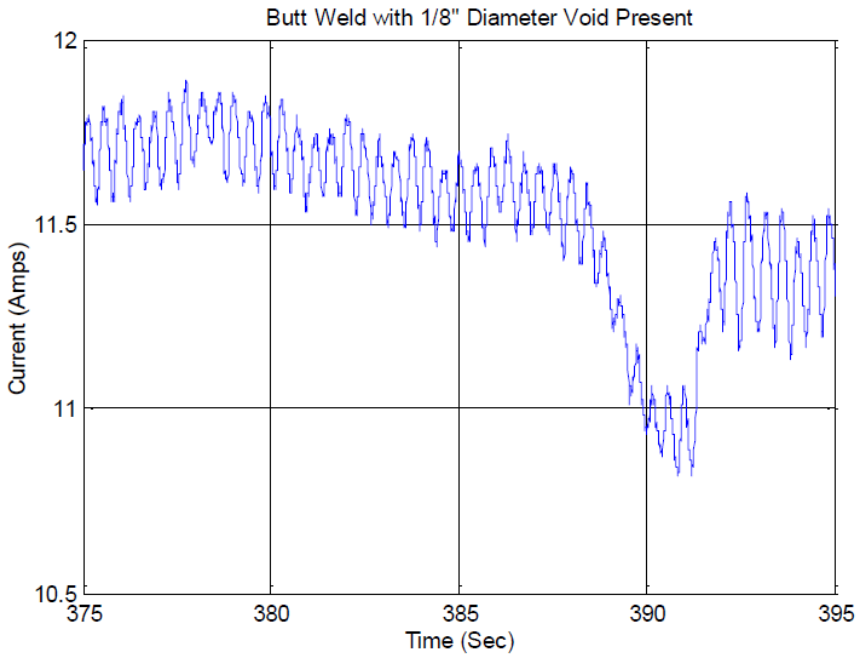

Figure 13: Spindle Current Data from Void Detection Study Showing Steady Oscillation; Decrease in Magnitude Occurred at Void Location [13]

A steady oscillation in the spindle motor current of about 1-2% of the mean is evident in Figure 13. In what may be a significant parallel to Schneider's observations, the oscillation occurs at approximately 140 oscillations/min (2.33 Hz), which is exactly one order of magnitude lower, or $1/10^{th}$ the tool rotation speed. Although it can't be confirmed due to the lack of a metric to measure flow variations, such as the dispersal pattern of a tracer, this oscillation may have been caused by a varying contact condition at the shoulder, or 'slip-stick' mechanism. Another observation from Figure 13 is the magnitude decrease in spindle current when the tool encountered the void. Perhaps more significantly however, there was also a change in oscillation frequency at the void location, which cannot be easily discerned visually, but was apparent after analyzing the frequency components of the signal using Fourier analysis [13]. These results will be discussed more in the appropriate section of this literature review.

Qian et al. also studied the apparent 'slip-stick' mechanism and 'onion ring' formation and asserted that the two processes are intimately linked, ultimately the exact same phenomenon, both occurring at the same frequency as the spindle rotation [14]. This is very different from the Schneider view of 'slip-stick' as a slower, secondary phenomenon, and ultimately may simply be a confusion of terminology. Qian et al. studied torque oscillations that occurred at the same frequency as the tool rotation speed and that resulted from cyclical material transfer in butt welds of 1100-H14 according to an analytical model developed by the authors. The observed torque oscillations were relatively high (10-20% of the mean) for a range of spindle speeds, and the model asserts that higher torques correspond to a slipping, or frictional heating condition, and lower torques correspond to a sticking condition, when a section of material is transferred or

extruded by the tool probe [14]. This is likely contrary to how most researchers think about the 'slip-stick' mechanism, but given that the authors have assigned this terminology to the cyclical material transfer of every rotation of the tool, instead of a slower, secondary oscillation, their assertions may be correct and the model may lend significant insight into material flow in FSW. It is unclear, however, how the authors calculated P, the normal pressure responsible for slipping friction, for the side of the probe and why the observed torque oscillations are so large, which has not been documented elsewhere in the literature.

While this review is not intended to be comprehensive, there are many more experimental and modeling studies into material flow in FSW that are noteworthy and should be recognized. London et al. studied the flow of material within 7050 butt joints, utilizing Al-SiC and Al-W composite markers in conjunction with metallographic and X-ray methodologies [15]. Zhao et al. visualized material flow in welds of 2014 using a LF5 Al alloy marker and three different tool geometries. Digital images of weld cross sections were compiled to build 3D composite images of flow patterns, which were confirmed to be asymmetrical, around the tool probes [16]. From a modeling perspective, the utilization of techniques such as computational fluid dynamics (CFD) or finite element analysis (FEA) is quite popular in studying material flow in FSW. Lammlein et al. used Ansys Fluent to model a number of scenarios, including the application of shoulder-less, conical tools and the welding of small diameter pipe and hemispherical geometries [17, 18, 19]. Schmidt and Hattel used a FEA technique to examine the conditions under which material is transferred properly and the space behind the tool probe is filled, resulting in quality, void-free welds [20]. And, although it will

not be discussed here at length, heat generation and weld zone temperature profiles are also the focus of many efforts in modeling, with both analytic modeling techniques and with CFD or FEA [21, 22, 23].

Perhaps one of the most noteworthy and comprehensive models of material flow in FSW, thus commanding the ultimate position in the material flow section of this literature review, is the Nunes Kinematic Model. In this model, material flow is described using kinematics and is decoupled into three incompressible flow fields that interact to form two dominant currents [8, 12, 24, 25]. A rigid body rotation flow field is induced simply by the rotation of the tool probe. Threads on the tool probe induce a ring vortex flow field, which surrounds the probe. Material trapped in the ring vortex flow field may travel around the probe multiple times, experiencing significant thermo-mechanical processing. Material not trapped in the ring vortex flow field simply moves straight by the probe in the uniform translation flow field. These three flow fields are depicted in Figure 14. A combined rendering of these flow fields is shown in Figure 15, in which the rigid body rotation flow field is referred to as the 'rotating plug' component.

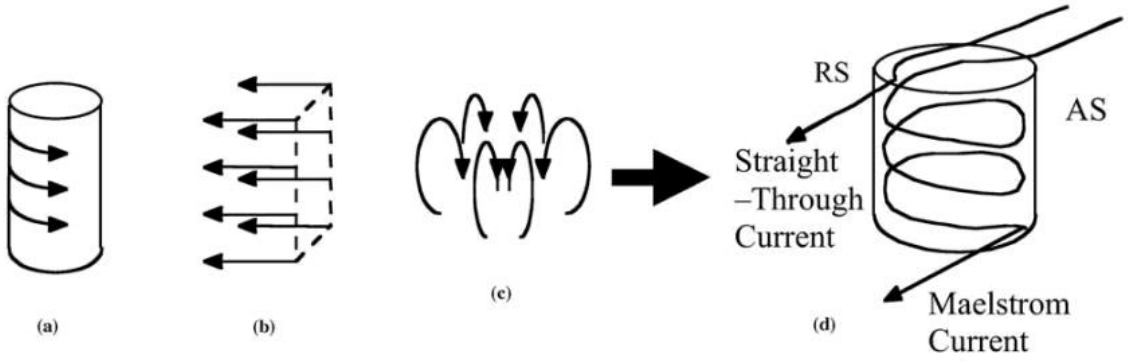

Figure 14: Flow Fields of the Nunes Kinematic Model: (a) Rigid Body Rotation, (b) Uniform Translation, (c) Ring Vortex; (d) Resulting Dominant Currents [24, 25]; Image adapted from [8]

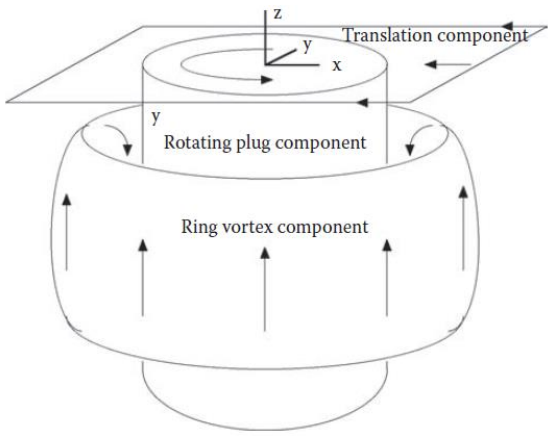

Figure 15: Superimposed View of the Three Flow Fields of the Nunes Kinematic Model [25]

The rigid body rotation flow field and the ring vortex flow field combine to form what is known as the ‘maelstrom’ current, or powerful whirlpool-like current. This current is translated down the length of the workpiece by the tool, while the other, or ‘straight-through’ current passes by the tool probe, residing primarily on the retreating side of the weld. Material in the ‘maelstrom’ current is primarily picked up on the advancing side of the weld and resides longer in the rotational flow fields around the tool, getting trapped by a continuous influx of material at the top of the probe and gradually moving downwards along the length of the probe, given the conventional downward thread direction. The circulation of the ring vortex then moves material outward and upward once it nears the bottom of the probe. Reversal of the probe thread direction would reverse the direction of the ‘maelstrom’ current and the direction of material circulation. Because of the differing nature of the two dominant currents and the difference in time that workpiece material spends trapped in each one, a variation in the amount of thermo-mechanical processing that sections of workpiece material experience, depending on where they originate in the joint, arises. From a metalworking perspective, this means

that there are variations in the hot working history of the welded joint. This phenomenon has been used to describe the nature of certain features in weld cross-sections, such as banding or 'onion rings,' as well as larger scale surface textures, as depicted in Figure 16.

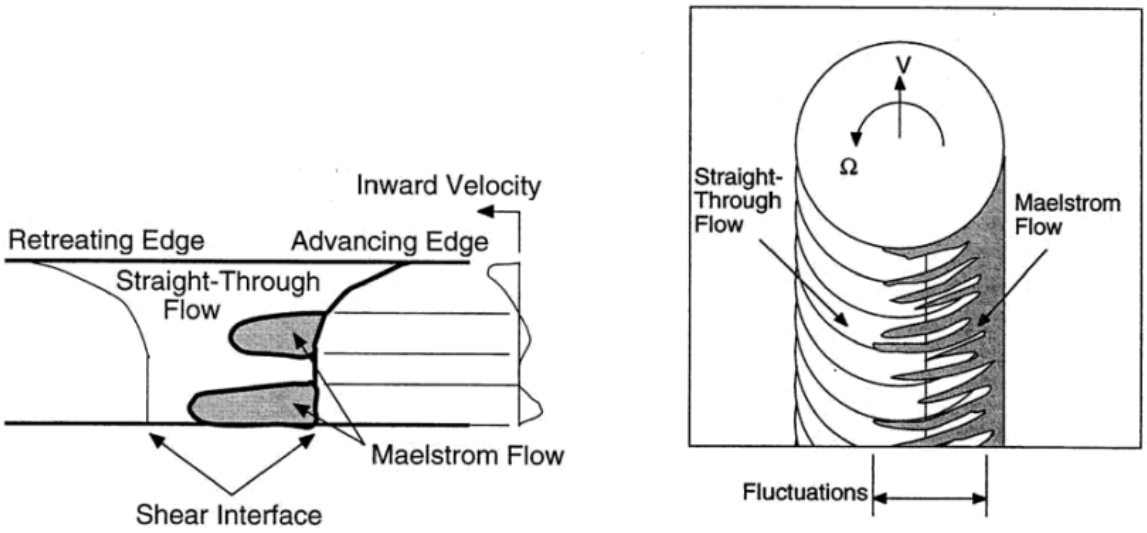

Figure 16: Interaction of Dominant Currents of the Nunes Kinematic Model [8]

Material flow from the 'maelstrom' current dominates the advancing side and the lower region of the TMAZ, assuming the conventional direction of probe threads is utilized. Material flow from the 'straight-through' current dominates on the retreating side and upper region of the TMAZ. Interactions between these currents, denoted as 'interleaving', and the inherent properties due to differences in hot working time, can cause visual surface cues, captured in the plan view of Figure 16, and has been credited with influencing material properties of the TMAZ and nugget, as in the side view in Figure 16 [8, 24, 25]. The Nunes Kinematic Model was also invoked to describe potential flow variations in the lead tracer wire work conducted by Schneider [12]. As a whole, the model provides working explanations for multiple phenomena observed in the

FSW process and takes into account tool features, such as threads, that are commonplace, yet perhaps poorly understood, and are sure to have a significant impact on the dynamics of material flow. The model also lends itself well to the study of process forces and gives insight into how they are generated and how they can be predicted.

Forces

The forces experienced by the welding tool can be significant, and as previously discussed, should first be viewed as dependent, reactionary variables before they are used as inputs for control. That is to say that forces are generated by the welding process, rather than input into the welding process, although one could argue that these scenarios are merely reactions of each other. What is critical to the welding process however is a contact condition between the workpiece and the tool, which was first achieved, and can still be achieved, without force control by simply setting a fixed tool position. As the tool then rotates and traverses during welding, the dynamic material flows react against the tool creating the axial force (F_z), the traverse force (F_x), and the side force (F_y) as well as the tool torque (M_z or T). The directions of these forces are labeled in Figure 1. Much research has indeed focused on FSW process forces, and it has been shown that force signals are excellent feedbacks for machine control and in-process quality evaluation, which will be discussed in the robotic welding section of this literature review, and they can even lend insight into resulting weld properties. Forces have been examined from both a modeling and experimental perspective, and both will be discussed here.

First, from a modeling perspective, the flows within the Nunes Kinematic Model have lent a great deal of understanding to FSW process forces, particularly with regards

to torque. The rigid body rotation flow field, which has been referred to as the 'rotating plug' component and is in intimate contact with the tool probe, has been examined to determine how torque is imparted on the tool by the workpiece material. This examination gave rise to the Nunes Rotating Plug Model, in which a rotation field is visualized adjacent to *all* tool surfaces in contact with the workpiece, which includes the shoulder, the sides of the probe, and the bottom of the probe. In other words, a thin layer, or 'plug', of material is theorized to stick to the tool surface, and at some distance away from the tool surface, a shearing interface is present [26]. Figure 17 displays a diagram of a hypothetical rotating plug of material which would be attached to the tool.

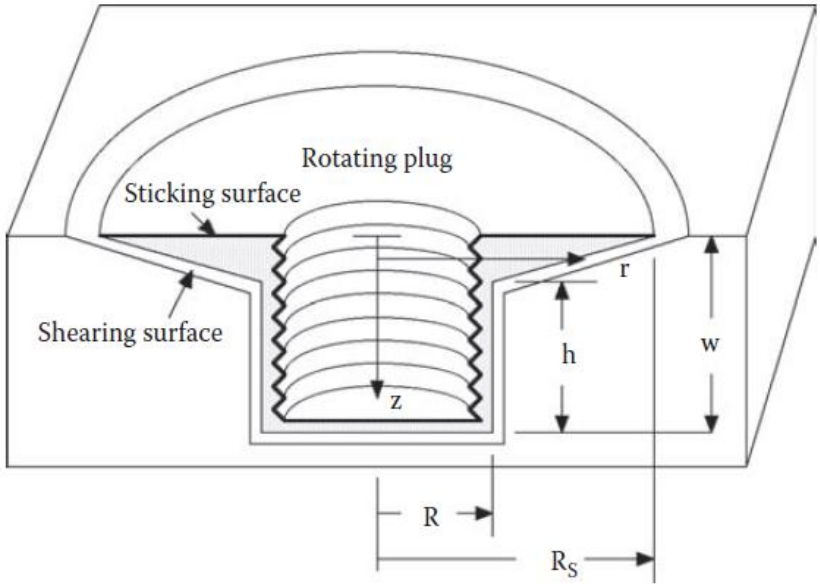

Figure 17: Rotating Plug Model Concept [25]

The shearing interface separates the rotating plug from the rest of the workpiece. The Rotating Plug Model also takes into account the ring vortex flow field that is induced by threads on the tool probe, although this flow is sometimes ignored for the purposes of

simplification when the model is used to generate equations of tool forces. These two flows, the rotating plug component and the ring vortex component, are said to transfer material via a wiping action [27]. This material flow mechanism and the existence of the rotating plug itself have indeed been examined experimentally. Figure 18 displays an XY planar cross-section of the tool probe retraction point in an FSW butt joint of 0.317 inch thick 2219-T87.

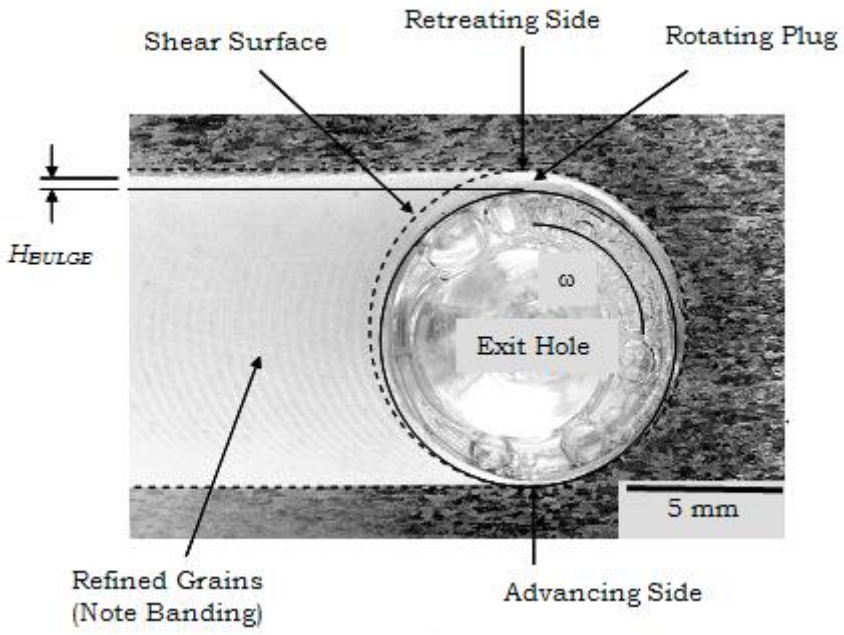

Figure 18: Experimental Confirmation of Rotating Plug [25, 28]

The parameters for the weld were 220 rpm and 3.5 IPM, and the void left behind by the tool probe was filled with mounting medium. Of note in Figure 18 is the drastic difference between the fine-grained thermo-mechanically processed material and the coarse-grained parent material, but the primary interest is that the circular shaped shear interface, or 'rotating plug,' enclosing the FSW tool is visible, with the greatest thickness

on the retreating side and the minimum thickness on the advancing side [25]. With this experimental validation of the 'rotating plug' concept, analytical models for predicting process forces could be used with confidence, given the acceptance of a number of simplifications and assumptions. For predicting process torque with the Nunes Rotating Plug Model, it is assumed that a thin layer of material sticks to all working surfaces of the tool, beyond which there is a shear interface, and that the layer of material is sufficiently thin that the dimensions of the 'rotating plug' can be taken as the same dimensions of the tool itself. Thus, a simpler geometry than what is depicted in Figure 17 for the shape of the rotating plug is assumed. Also, any effect of tool probe threads and torque arising from the ring vortex flow field is ignored as well for simplification purposes. Given that the tool is rotating against a boundary shear stress τ, the torque can be calculated as follows:

$$T_{Total} = T_{Probe\ Bottom} + T_{Probe\ Sides} + T_{Shoulder} \tag{1}$$

$$T_{Total} = \int_0^r 2\pi r^2 \tau dr + 2\pi r^2 t\tau + \int_r^R 2\pi r^2 \tau dr \tag{2}$$

$$T_{Total} = \frac{2\pi R^3}{3}\left(1 + 3\frac{r^2 t}{R^3}\right)\tau \tag{3}$$

where r = probe radius, R = shoulder radius, and t = depth of probe contact. Again, simple geometry is assumed; that is, a cylindrical probe and flat shoulder. In cases where a tapered or spherical shoulder geometry is used, which will be discussed in a latter section of this review as the Nunes Rotating Plug Model has indeed helped guide tool design, R = radius of shoulder contact with the workpiece. A final natural extension of

this analytical expression is the calculation of weld power, which can be computed by multiplying the spindle speed and the torque, given that the power or heat input component resulting from tool translation is sufficiently small [26].

The Nunes Rotating Plug Model has been used in several instances to predict process torque or to generate torque signals for FSW simulations, and in addition to torque, Nunes examined the axial, traverse, and side forces in FSW as well, developing relatively simple analytic expressions which may be helpful in understanding the process of material flow and force generation [26]. The physical principle behind the model of axial force is that the tool shoulder must maintain pressure to contain workpiece material from being expelled from the joint, which Nunes likens to the pressure necessary for an indenter to indent the workpiece surface under the softened conditions of an elevated temperature. Nunes says that the stress required to indent the surface is approximately three times the normal flow stress or six times the shear flow stress; therefore, the axial force must be approximately the product of 6τ and the apparent downward-facing tool cross-sectional area, as follows:

$$F_Z = 6\pi R^2 \tau \tag{4}$$

The apparent downward-facing tool cross-sectional area includes the area of the shoulder and the area of the bottom of the probe. These two areas can be calculated together by simply using the shoulder radius, R. Using this model as a guide, Nunes discussed anticipated trends in axial force relative to other process parameters, such as welding speed, and observed trends from experimental work will indeed be discussed here. Going

even further with the indenter concept, Nunes developed an analytical expression for traverse force as well, saying that the probe pushes into the workpiece like a hardness indenter, all while repeatedly transferring material from front to back. This expression will not be discussed at length here, nor will be the expression for the side force, which Nunes claims is driven largely by thermal differences in the welding environment as the tool moves from warmer material into colder material, creating a net reaction force towards the advancing side of the probe as material is sheared and transferred [26].

From an experimental perspective, much work has been done to examine FSW process forces and determine trends which could perhaps be exploited for feedback control purposes. Melendez et al. examined the forces exerted on the FSW tool in bead-on-plate welds of 0.25 inch thick 6061-T6 and 2195-T6 aluminum alloys [29]. A custom force measurement setup was used that will be referenced in a following section of this review. Variations in the axial, traverse, and side forces due to changes in plunge depth, welding speed, rotational speed, and tool geometry were examined and reported. Appropriate windows of force were determined for typical welding parameters for the alloys being welded, and it was also observed that the side force changes direction when the direction of tool rotation is changed. A model of side force based on thermal conditions and resulting yield strength differences between the front and the back of the tool probe was presented, paralleling ideas from the Nunes Rotating Plug Model previously discussed. The effects of weld parameters on dynamic recrystallization were discussed, and it was determined that additional work was required to quantify mechanical properties of the welded joints [29]. Cook et al. also examined FSW process forces, with a primary focus on the axial force, as they relate to welding parameters in

0.25 inch thick 6061-T651 bead-on-plate style welds [30]. Welding speed and rotation rate were varied to determine the effects on axial force, with a goal of establishing trends that could be exploited for load control purposes. This would expand the applicability of FSW to more compliant standard industrial robots. Further advantages of control will be discussed in a latter section. Figure 19 displays axial force data, as measured with a Kistler Model 9124B rotating cutting force dynamometer, and its dependence on welding parameters.

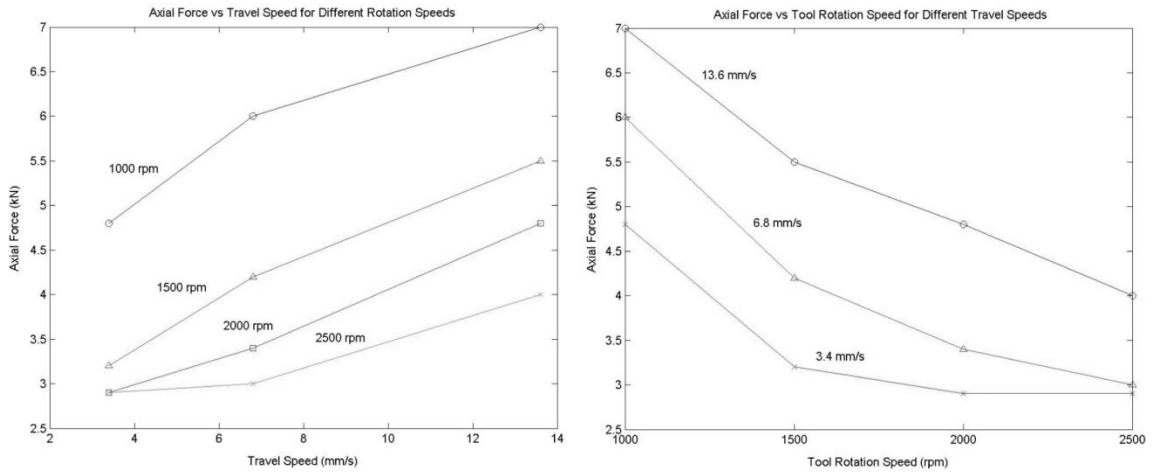

Figure 19: Axial Force Trends with Varying Welding Parameters in 0.25 inch Thick 6061-T651; Image adapted from [30]

Trends in the force data were indeed observed that could be used for control purposes or simply for force reduction purposes. It was shown that axial force increases with higher welding speeds and lower rotation rates. It was also shown that variations in axial force relative to welding parameters reached upwards of 50% of the maximum value for some parameter sets, and overall, axial force variations were observed from 1 to 15 kN [30]. Force trends such as these have been the focus of much experimental and modeling

research. Continuing from an experimental perspective, Crawford et al. attempted to examine the bounds of force trends that had been observed by Cook, with an emphasis on force reduction accomplished with relatively high 'weld pitch' parameter sets [31]. As the 'weld pitch' is defined by the rotation rate divided by the welding speed, these parameter sets exhibited high rotation rates and low welding speeds. Aluminum 6061-T6 was welded with welding speeds that ranged from 11 IPM to 63 IPM and with tool rotation rates that ranged from 1500 to 4500 rpm. It was indeed observed that force trends similar to what were documented by Cook existed between the parameter bounds for the experiment, and the limits of these trends, and thus the force reduction capacity of parameter modification, may not have been reached. Crawford then turned to modeling techniques to further examine the relationships between welding parameters and the resulting forces and torques, implementing Couette and viscoplastic mechanical models in a Fluent CFD numerical simulation. This modeling exercise served to validate experimental results, determine which mechanical model was more appropriate for simulating high pitch friction stir welding, and in addition, examine modes of defect formation, particularly weld flash, under relatively high localized temperature conditions at the tool shoulder [31]. Crawford et al. then went on to further evaluate FSW forces via modeling and simulation, with a focus on implementing the process on standard industrial robots. Force and torque capacities that would be required of such robots were determined for various parameter sets for the welding of 6061-T6 [32]. Atharifar et al. also investigated the loads carried by the FSW tool during the welding process. A 3D numerical model implemented with a CFD approach was used to analyze the viscous and inertial loads on the tool and how they varied with changing welding parameters [33].

Welding of 0.25 inch thick 6061-T6 with a concave shoulder tool featuring a threaded cylindrical probe operating at a tilt angle was considered. Temperature dependent material properties and 'slip-stick' conditions were incorporated into the model. Figure 20 displays the simulation results for a range of welding parameters.

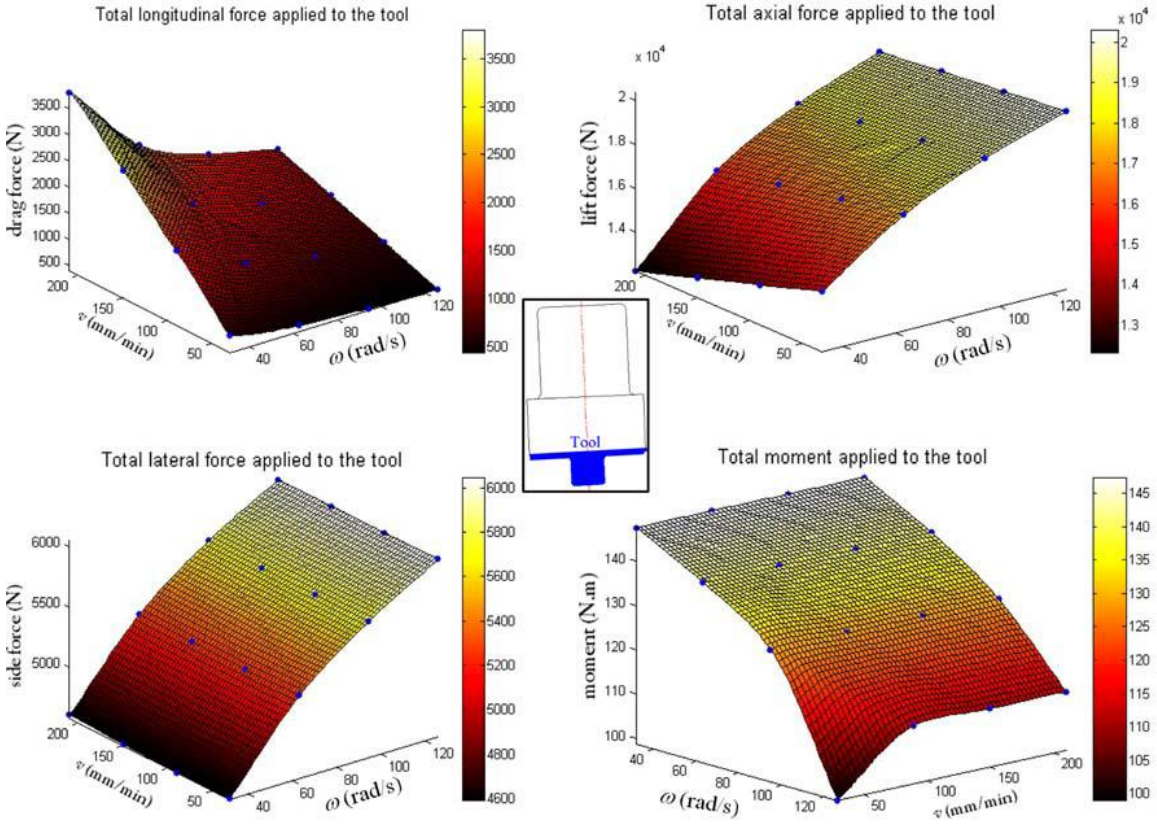

Figure 20: Loads Experienced by the FSW Tool while Welding 6061-T6 as Determined by Modeling and Simulation [33]

It is apparent that forces and torque can vary drastically depending on the selection of welding parameters of tool rotation rate and welding speed, and the results may be helpful in predicting resulting forces when parameters are selected based primarily on achieving good weld quality. It is also significant that Atharifar et al. used the 'Magnus

Effect' label when discussing the physical principal from which the side force arises. While similar concepts have been discussed elsewhere in the literature, these authors are perhaps the first to directly attribute the side force to the 'Magnus Effect,' which would be caused by the FSW tool rotating in a flow field created by tool translation through the workpiece [33]. Additional modeling efforts have been invaluable when it comes to analyzing or predicting forces as well as temperatures as process parameters are modified in a variety of materials [34]. These efforts help to lend credence to data obtained through much additional experimental work that will not be discussed here at length. Of course, in addition to basic process parameters such as welding speed and tool rotational rate, force data obtained through both modeling and experimental work is completely dependent on other variables, such as tool geometry.

Tooling and Wear

Tool design is one of the most important factors to consider when designing a FSW joining process. The tool must perform many functions, including generating heat, promoting mixing, breaking up the joint line, dispersing oxide layers, creating forging pressure, containing material within the joint thereby preventing surface weld flash, and preventing the formation (or minimizing the impact) of defects such as wormholes, sheet-thinning, or hooking defects. Additionally, tool geometry must often facilitate a stable force or torque control scheme and be compatible with a range of plunge depths.

The earliest tool designs consisted of flat, featureless shoulders and cylindrical, perhaps threaded, probes, as depicted in Figure 1. Some of the first design innovations were developed by Thomas et al. at TWI [35]. These innovations were aimed at

increasing interfacial oxide layer disruption and increasing the TMAZ width, particularly in lap welds. Designs that arose from this work were the Flared-Triflute™ tool and the Skew-Stir™ tool, which promotes mixing via an off-axis probe that increases dynamic, or swept, volume. In addition to the advantages just mentioned, these tools help to reduce differential pressure between the top and bottom sheets of lap joints, which has been found to cause top sheet thinning, a defect that leads to weaker welds that can sometimes simply peel apart during loading conditions [35]. Figure 21 displays the design concepts of the Flared-Triflute™ and Skew-Stir™ tools.

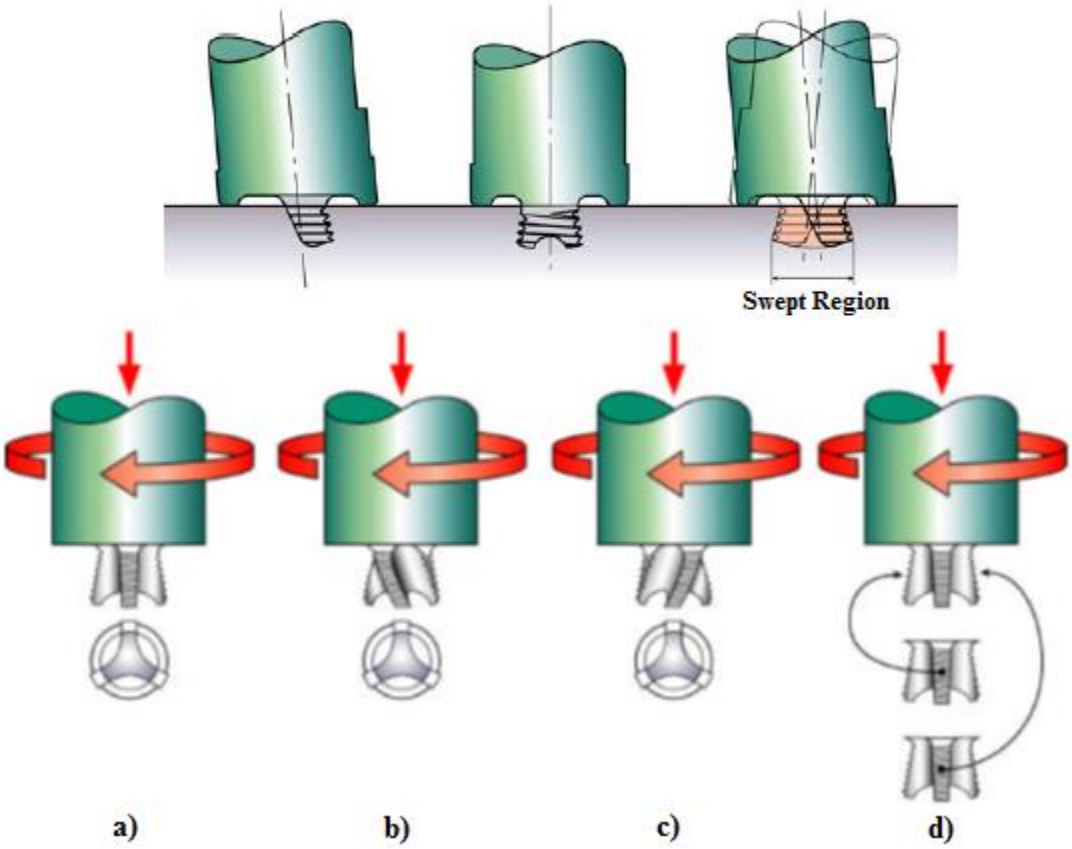

Figure 21: Skew-Stir™ Tool Design by TWI (Top); Flared-Triflute™ Tool Options: a) Neutral Flutes, b) Left-Hand Flutes, c) Right-Hand Flutes, d) Neutral, Right-Handed, or Left-Handed Threads (Bottom); Image adapted from [35, 36]

Other tool designs that originated at TWI include the Trivex™ and the MX-Trivex™ tools (shown in Figure 22), which can reduce process forces and be manufactured with relative ease [37].

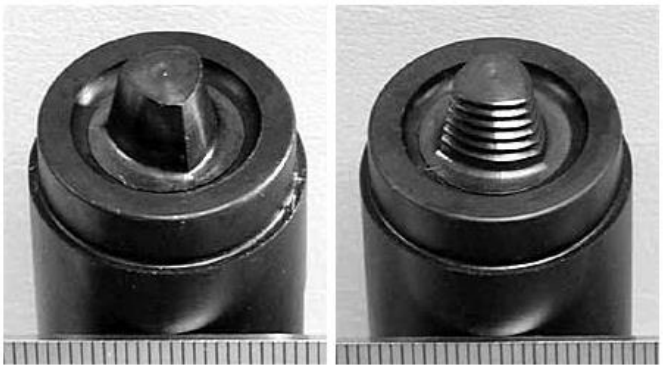

Figure 22: Trivex™ Tool (left) and MX-Trivex™ Tool [37]

Since then, numerous studies have been conducted to advance the science of tool design and deepen the understanding of tool geometries relative to resulting weld properties, primarily in aluminum alloys. As previously discussed from a materials flow perspective, Zhao et al. studied the effects of probe geometry, specifically a taper and threads, on material flow in butt welds of 2014 using an LF5 Al alloy marker insert technique. It was found that threads were critical for creating vertical material flow and reducing the likelihood of the formation of a wormhole-like defect [16]. Elangovan and Balasubramanian also studied probe geometry, testing the effects of straight cylindrical, tapered cylindrical, threaded cylindrical, square, and triangular probes on the microstructure, tensile strength, and microhardness of Al 2219 butt welds [38]. Figure 23 displays a diagram of the five different probe geometries tested. Tools exhibiting the geometry were tested at three traverse speeds. Analysis showed that the square probe

tool outperformed tools with the other geometries, from both a tensile strength perspective and a metallurgical perspective.

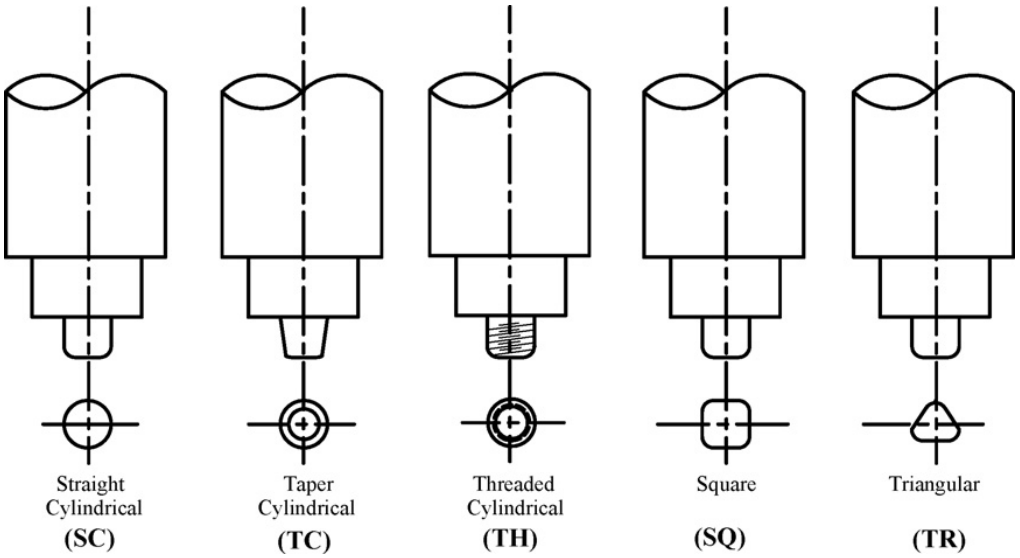

Figure 23: Five Tool Probe Geometries Evaluated by Elangovan and Balasubramanian [38]

At all three traverse speeds, the square probe tool created defect free friction stir processed regions [38]. It is likely the higher dynamic volume, which is the volume that the probe sweeps as it rotates beyond its actual static volume, of the square probe tool contributed to its better performance. This is a demonstration that tool geometries that may be thought of as unconventional when compared to simple, threaded cylindrical probes may in fact have much potential for creating quality, defect free welds. Liu and Ma investigated the effect of varying probe and shoulder diameters on the microstructure and mechanical properties of 6061-T651 butt welds in 6 mm thickness. Evaluations were performed with a focus on the effect of low hardness zones (LHZ) and how these zones formed with respect to tool geometry and welding speed [39]. Colligan et al. investigated

the welding of thick section (25.4 mm) 5083-H131 aluminum alloy with a tool featuring a threaded probe with a number of flats. It was hypothesized and indeed found to be significant that the tool travel per flat per revolution would strongly affect material flow, and by extension, process forces. Welding speed and spindle speed were also found to be significant contributors to variations in process forces [40].

Focusing primarily on shoulder geometry rather than probe geometry or interactions between the features, Scialpi et al. studied the influence of shoulder geometry on microstructure, tensile strength, and microhardness of Al 6082 butt welds. Three tools were evaluated, featuring shoulder geometries with a fillet on the outer edge, a shoulder with a fillet and a cavity, and a shoulder with a fillet and a scroll. The best results were obtained with the shoulder featuring a fillet and cavity. All tools had simple, unthreaded cylindrical probes [41]. While tools with cavities, or concave shoulder geometries, have been documented repeatedly in the literature, Sorensen and Nielsen presented a convex scrolled shoulder tool with a step spiral probe that offered wider process windows, lower process forces, and the ability to operate at a zero degree tilt angle [42]. Longhurst also found similar advantages with a hybrid flat-tapered shoulder design while examining tool design from a force control implementation perspective. Similar to using flat shoulder tools at higher tilt angles, alternative shoulder geometry was identified as a key enabler of successful force control of FSW [43, 44]. Longhurst et al. then went on to quantitatively examine shoulder profiles with a goal of determining geometry that would exhibit a nearly linear relationship between plunge depth and torque, thereby enabling the implementation a stable linear controller for a wide range of plunge depths in the torque control of FSW [45, 46]. More on this from a controls perspective will be discussed in

the appropriate section of this review, but from a tool design perspective, this was important work. Using the Nunes Rotating Plug Model to simulate process torque, Longhurst compared straight tapered and spherical shoulder geometries in terms of linearity between plunge depth and torque. First, the Nunes Rotating Plug Model equation for torque was modified to accommodate a convex shoulder rather than a flat shoulder. The general equation governing the torque developed on a convex shoulder (ignoring the probe sides and bottom) was found to be:

$$Torque\ (T) = \int_0^{PD} 2\pi r^2 \tau \sqrt{1 + \left(\frac{dr}{dz}\right)^2}\, dz \tag{5}$$

where r = radial coordinate of the shoulder (R could be substituted for continuity purposes with content already introduced), z = vertical coordinate of the shoulder, PD = plunge depth of the shoulder, and as before, τ = boundary shear stress. Next, this formula was used to determine the equation for process torque on a straight tapered shoulder with a 1 inch diameter and a 0.050 inch rise from the center to the edge of the shoulder. This equation was found to be:

$$Torque\ (T) = 2103.77\tau(PD)^3 \tag{6}$$

Finally, a tool was designed that featured a spherically tapered shoulder with radius of 3 inches over a 1 inch diameter, which yielded approximately the same plunge depth operating window of 0.050 inch that the straight tapered shoulder tool exhibited. This continuity was important in terms of maintaining equal capabilities during welding and

for comparison purposes. Again, the general equation for torque on a convex shoulder was used to determine the torque acting on this specific spherical geometry. The equation was found to be:

$$Torque\ (T) = 27\pi\tau\left[\sin^{-1}\left(\frac{-3+PD}{3}\right) + \left(\frac{1}{2}\sin 2\left(\sin^{-1}\left(\frac{-3+PD}{3}\right)\right)\right) + \frac{\pi}{2}\right] \qquad (7)$$

The two shoulder geometries were then compared in a simple numerical simulation by plotting torque for a range of shoulder plunge depths using Equations (6) and (7). The results of this simulation are displayed in Figure 24 with process torque represented by a scalar to be multiplied by the boundary shear stress.

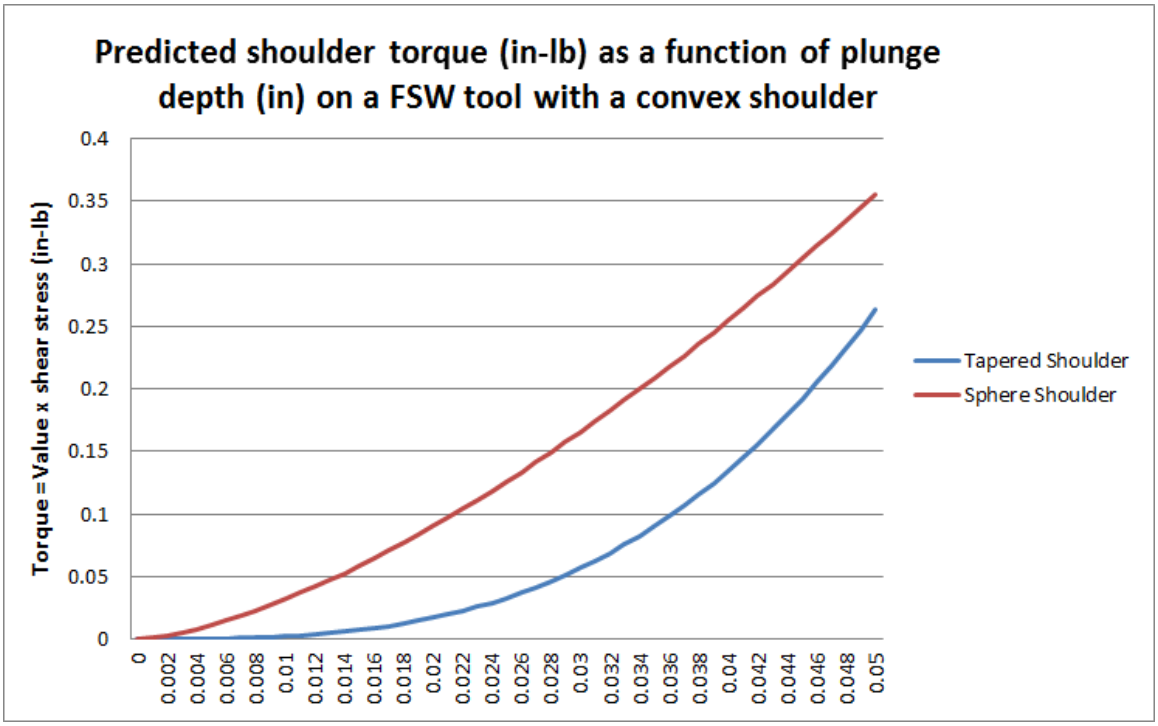

Figure 24: Torque vs. Plunge Depth Relationships for Straight Tapered and Spherical Shoulder Geometries [45, 46]

It can be clearly seen in Figure 24 that the spherical shoulder geometry creates a more linear relationship between plunge depth and torque when compared to the straight tapered shoulder geometry. This is very important for facilitating a stable torque control scheme when linear control is utilized because when the controller is tuned, stability will exist over a wider range of plunge depths given the greater linearity of the torque-plunge depth relationship. Longhurst et al. also conducted CFD simulations to study the material flow and temperature profile characteristics of the spherical shoulder tool, in conjunction with a 0.25 inch diameter threaded probe, and focusing on welding 6061 in 0.25 inch thickness. Figure 25 displays an example of the temperature contours visualized with these simulations.

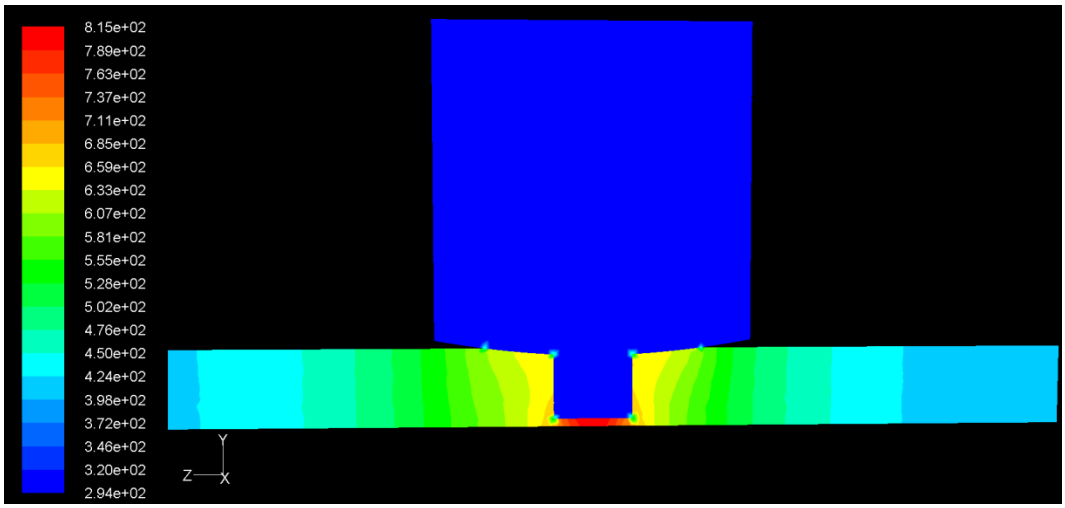

Figure 25: Temperature Contours of Spherical Shoulder Tool with Probe in Welding of 6061 in 0.25 Inch Thickness [45, 46]

The simulations suggested the spherical shoulder tool would exhibit characteristics similar to those of the straight tapered shoulder tool, which had been used previously with much success. Given these encouraging results, the spherical shoulder tool was

developed and used in a study focusing on simplifying torque control implementation by remotely monitoring spindle motor current with inexpensive off-the-shelf sensors and using it as a feedback signal [45, 46]. Figure 26 displays the spherical shoulder tool.

Figure 26: Spherical Scrolled-Shoulder Tool with Threaded Probe [45, 46]

Scrolls were incorporated in the design, as is often done to facilitate material containment and reduce flash during welding. More on the significance of this study will be covered in the controls section of this review, but the tool design exercise within it served to illustrate how analytical models of the FSW process are becoming more and more useful and are being utilized to guide tool design and facilitate stable process operation.

Additional noteworthy tool designs that will not be discussed here at length include the threaded Counterflow^{TM} tool [47], the variable penetration tool (VPT) [48], and numerous other designs, many of which are patented and were developed specifically for FSW variants, such as self-reacting welding or spot welding, or to tackle special process issues such as keyhole elimination [49, 50]. Many of these tool designed were developed with a focus on the welding of lower melting point and relatively soft materials, such as aluminum. For the friction stir welding of other materials such as steel

and titanium for example, tool design, as well as tool material, can change considerably. This is critical because in addition to the many functions the tool must perform in regards to creating quality welds, the tool must also be resistant to wear, typically to the degree of being considered a non-consumable item.

In the early stages of the FSW process development, the primary focus was on joining metals such as aluminum, magnesium, and copper. For welding these materials, tools were primarily machined from tool steels such as H13 and subsequently hardened. In research settings, these tools would typically exhibit little wear and would be considered practically non-consumable. When FSW began to find applications in the joining of higher melting point, higher hardness metals, such as steel, titanium, and nickel based superalloys, or to metal matrix composites (MMCs), significant advances in tool materials were required primarily to mitigate tool wear. Early investigations into tool wear occurring during the welding of steels were conducted by Thomas et al. [51] and Lienert et al. [52]. Several studies on tool wear have been conducted with metal matrix composites (MMCs), which have highly abrasive reinforcing particles or whiskers and tend to accelerate tool wear to the point at which the mechanisms of tool wear itself are easily studied over relatively short welded distances [53, 54]. MMCs also serve as an effective 'proving ground' for evaluating the durability of new tool materials or coatings which are intended to be wear resistant. Prater compared the durability of tools made of steel, tungsten-carbide cobalt (WC-Co), and diamond coated WC-Co in the welding of MMCs [55]. Leonhardt and Thompson documented the use of tungsten-rhenium (W-Re) and W-Re with the addition of hafnium carbide (HfC) as tool materials for welding titanium and later HSLA-65 steel [56]. Kolluri et al. also tested a W-Re tool as well as a

W-Re/cubic boron nitride (CBN) composite tool for welding P91 steel [57]. CBN, or polycrystalline cubic boron nitride (PCBN), has been utilized by many others as well, and it has exhibited fracture toughness sufficient for features to be machined on tools used in ferrous alloys [58]. Miyake et al. demonstrated the use of cobalt based alloy tools for the joining of steels [59], and Mochizuki et al. evaluated a nickel based dual two-phase intermetallic alloy tool for joining 430 stainless steel [60].

Recent advances in tool material such as these have led to the ability to successfully weld steels, titanium, and even nickel based alloys. For the welding of higher strength aluminum alloys, particularly in the 7xxx series, advances have been made in reducing wear as well, including the use of cobalt alloys like MP159 as a tool material (See *Proceedings of the 9th International Symposium on Friction Stir Welding*, TWI, Cambridge, UK, May 2012 for information on these most recent advances). A comprehensive survey of tool material selection relative to workpiece material and welding parameters encountered in the literature was compiled by Rai et al. [61], and a method of generating tool durability maps that correlate process parameters to tool life was developed by DebRoy et al. [62]. And, in cases where tool wear cannot be significantly reduced with material and parameter selection alone, processes are being developed to monitor tool wear or fracture in real time. For example, Dodds et al. successfully correlated tool fracture events with fluctuations in feedback forces [63]. Finally, Zhang et al. compiled a comprehensive review of tools for FSW from a perspective of tool type, shape, dimensions, materials, and wear characteristics [64], and any questions related to tool terminology again are addressed by Threadgill [3].

Lap Joining

As the focus of much of the research in this dissertation is on friction stir welded lap joints, this joint configuration will be discussed at length and emphasized, relative to other joint configurations, such as butt joints or T-joints. The lap joint presents a number of unique challenges, especially in regards to material flow, oxide layer disruption, and joint line remnant defects, and therefore has been the focus of much research. Furthermore, tool designs as well as weld evaluation procedures have been developed specifically for use with lap joints to address some of the unique demands of this joint configuration.

Early investigations into creating quality friction stir lap welds in aluminum were conducted by Thomas et al. [35]. Lap welds of 5083-O, in wrought sheet form, and in 6mm thickness were created using a conventional flat shouldered tool with threaded cylindrical probe that had been used successfully for creating butt welds. Welding speed was 120 mm/min and tool rotation rate was unreported. Figure 27 displays a macrograph and a bend test failure that highlight the difficulties of the lap joint configuration.

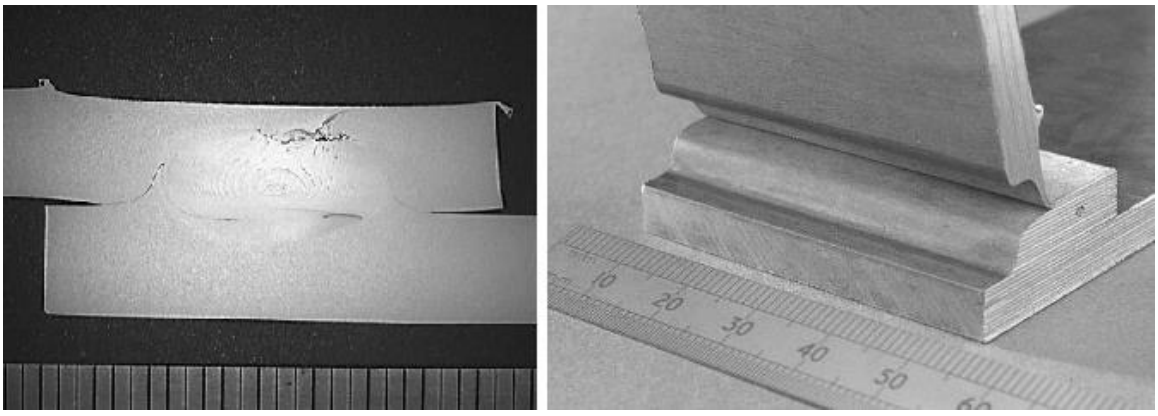

Figure 27: Macrograph Revealing Defects (left) and Bend Test Failure (right) from 5083-O Lap Weld in 6 mm Thickness; Image adapted from [35]

The FSW tool, which had been adequate for creating butt welds, did not perform well in the lap joint configuration. Thomas et al. attributed poor performance in the bend test to extreme thinning of the top sheet and thickening of the bottom sheet resulting from differential pressure. The bend test, formally called the hammer S-Bend test, is a simple method of lap weld evaluation in which the goal is to bend a clamped weld section into an S shape with repeated hammering. Colegrove et al. described it as a method of putting the sample in tension, opening any cracks that were formed in the welding process [65]. Indeed, any defects that may be present in the weld will likely lead to failure, as in Figure 27, in which the top sheet simply peeled away. Thomas et al. have also noted that bend test results typically correlate well with fatigue test results for lap welds, the difference being that crack growth and failure occur over vastly different time scales [66]. Referring again to Figure 27, it was observed by Thomas et al. that failure occurred along the original interfacial surface oxide layers, emphasizing the fact that lap welds require tooling that will fully disrupt these layers and create a wider TMAZ. Additionally, the macrograph in Figure 27 not only revealed weld porosity just below the crown, but characteristic defects that are very common in lap welds. These are the 'hooking' defect on the advancing side of the weld and the 'sheet thinning' defect, sometimes called 'top sheet thinning,' as it typically thins the top sheet and thickens the bottom sheet, or a 'cold lap' defect. The nature of the defects corresponds with the differential relative velocities on either side of the tool. The higher velocity and heat input on the advancing side can cause a sharp disruption of the joint line and oxide layers, and the lower velocity and heat input on the retreating side can result in inadequate disruption and simple migration of the joint line and oxide layers into the upper or lower sheet. Thomas et al. sometimes

generically referred to these defects as ‘notches’ and explored tool technology that would help reduce their effects on weld quality and create wider TMAZs in lap joints. The tools tested in these explorations were the Flared-Triflute™ tool and the Skew-Stir™ tool, which have already been discussed and are displayed in Figure 21. These were used to again weld 6 mm thick 5083-O at a welding speed of 240 mm/min and an unspecified tool rotation rate. Figure 28 displays resulting weld section macrographs with exploded views of the joint line remnant defects on each side.

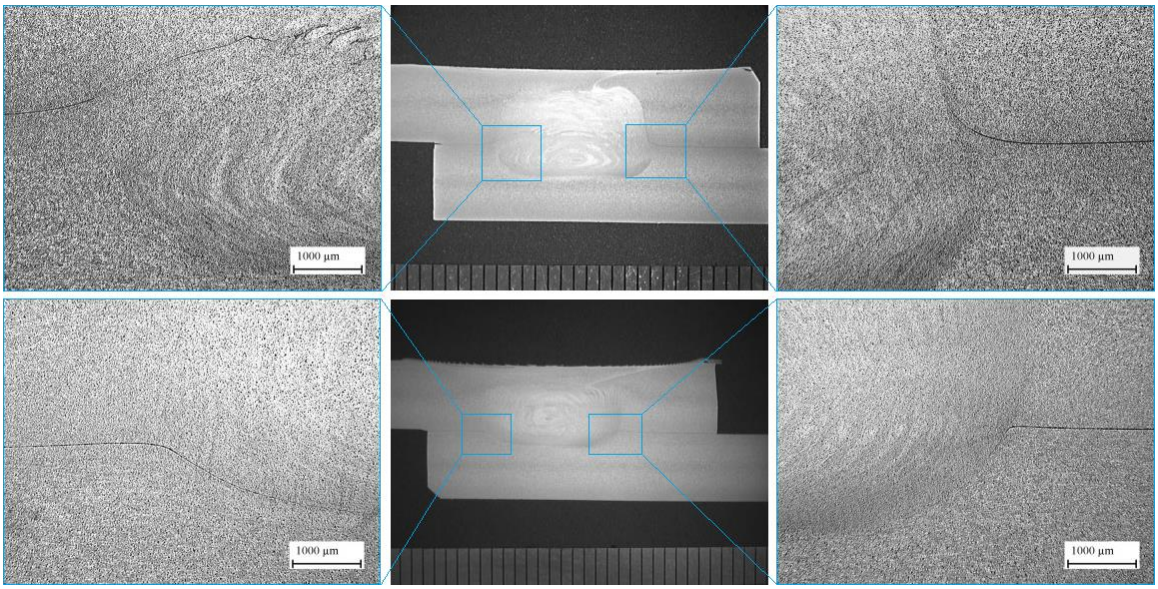

Figure 28: 5083-O Lap Welds in 6 mm Thickness made with Flared-Triflute™ Probe (Top) and Skew-Stir™ Probe (Bottom); Retreating Side on Left, Advancing Side on Right; Image adapted from [35]

The joint line remnant defects in these welds were much less pronounced however than in previous trials with the conventional threaded probe tool. Thomas et al. noted that the sheet thinning defect did not turn up or down, but remained parallel to the joint line, and the hooking defect was much less severe. Furthermore, the advanced tools created a

greater TMAZ width, which reached 190% of the plate thickness with the Flared-Triflute™ tool compared to 110% of the plate thickness with the conventional threaded probe tool. This work served to illustrate the importance of tool design in friction stir lap welds. FSW variants, specifically Re-Stir™, were also developed and evaluated for utilization in lap welding and will be discussed here in the appropriate section of this review [35].

Cederqvist and Reynolds also studied the joining of aluminum in a friction stir lap joint configuration, focusing on a dissimilar combination of Alclad 2024-T3 and 7075-T6, which are alloys commonly utilized in the aerospace industry [67]. This was a relatively early study on joining these alloys in a lap joint configuration, and was aimed at determining if FSW could be a viable rivet or resistance spot weld replacement technology. In the study, the top sheet was Alclad 2024-T3 and the bottom sheet 7075-T6 which is opposite the configuration that is encountered in more recent studies and applications. This will be discussed further in the aerospace applications section. The thickness of each sheet was 0.090 in (2.29 mm) with 0.06 mm thick cladding incorporated on both sides of the 2024-T3 sheet. Welds were made with 9 different tools, featuring different probe lengths, probe diameters, and shoulder diameters, with multiple welding speeds and tool rotation speeds, and with either a single pass or double passes, featuring varying separation distances. Welds were evaluated with tension-shear testing, optical microscopy, and hardness testing. The placement of the RS versus AS (or cold lap defect versus hooking defect, respectively) in the load path for tension-shear testing was also evaluated by creating lap weld configurations of each type. These configurations have also been called right-handed or left-handed lap welds, respectively,

in the literature, referring to the position of the top sheet as viewed from the start of the weld and assuming clockwise (CW) tool rotation. This terminology is somewhat ambiguous as tool rotation direction can often change and is not often specified in research articles. The configuration is perhaps most clearly specified by stating whether AS or RS is 'outboard,' or adjacent to the lapped edge. The configurations from the Cederqvist and Reynolds study are displayed schematically in Figure 29.

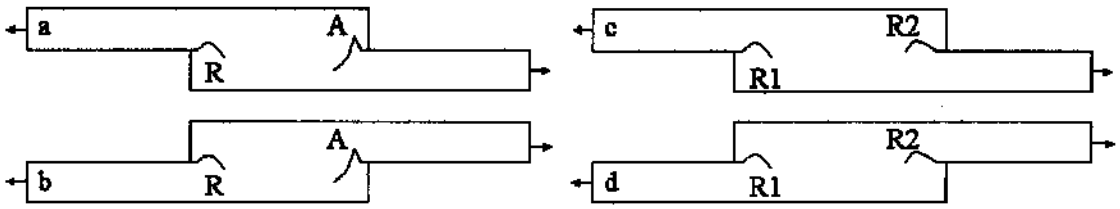

Figure 29: Lap Weld Configurations; Single Pass: a) Retreating Loaded, b) Advancing Loaded; Double Pass: c) Retreating-1 Loaded, d) Retreating-2 Loaded [67]

Much valuable information can be drawn from the results of this study regarding several different aspects of lap joining, and the authors' conclusions were:

1) Joint efficiencies for single pass welds were achieved that were at least 60% stronger than similar riveted or resistance spot welded joints, making FSW a viable alternative in applications using these joining methodologies.

2) Double pass welding modified the hardness distribution but did not reduce the overall minimum hardness.

3) Effective sheet thickness (EST) and the shape of the sheet interface are two critical factors which affect tension-shear strength, given the weld TMAZ is wide enough to prevent interfacial fracture. Sharp corners or cavities are highly undesirable.

4) A probe that is short, while still penetrating past the top sheet, creates less vertical mixing of the interface thus maximizing the EST. Less vertical mixing of the retreating side can also be achieved with a colder weld, meaning a high welding speed and low tool rotational speed combination.

5) A wide TMAZ is desirable not only in that it prevents interfacial fracture, but that it also reduces bending in a shear loading scenario, meaning larger probe diameters may be desirable.

6) Desirable weld configuration depends on the direction of 'pull up' or 'pull down' of the defects on the advancing and retreating sides. This is affected by tool geometry. For Cederqvist and Reynolds, loading the AS was most often best for single pass welds due to the downward nature of the hooking defect, and loading R2 was best for double pass welds [67].

Perhaps conclusions 4) and 6) from Cederqvist and Reynolds are most significant in terms of affecting all who investigate or develop friction stir lap joining and require the greatest amount of attention when tool geometry and process parameters change [67]. There are several hallmarks of friction stir lap joining that seem to permeate the literature now. These are flat shoulder tool geometry, high welding speed, higher than normal tilt angle, and only partial probe penetration into the bottom sheet. The high welding speed creates a colder weld, as described in 4), and means that the maximized EST on the retreating side would likely dictate an RS loading scenario is better, depending of course on tool geometry and AS characteristics as discussed in 6). The range of welding speeds tested by Cederqvist and Reynolds was 2.3 mm/s (5.4 IPM) to 5.6 mm/s (13.2 IPM) [67]. It is not uncommon to see much higher welding speeds reported in the literature. It has

been reported that for industrial aerospace applications of 2024 and 7075 alloys in a friction stir lap joint configuration the convention is to rotate the leading edge of the tool towards the upright leg of the L or Z shaped stiffener (top sheet of 7075), meaning the advancing side will be outboard or adjacent to the lapped edge, and any cold lap defect that is present on the retreating side will be placed in the load path. It has also been reported that the optimal penetration of the probe into the bottom sheet is between 22% and 35% of the top sheet thickness [68]. Tool geometry utilized in industry is often proprietary, but flat shoulder tool geometry dominates what is found in the literature. The flat shoulder tool theoretically creates a contact condition with the workpiece that is geometrically like a segment of a circle, as outlined in Figure 30.

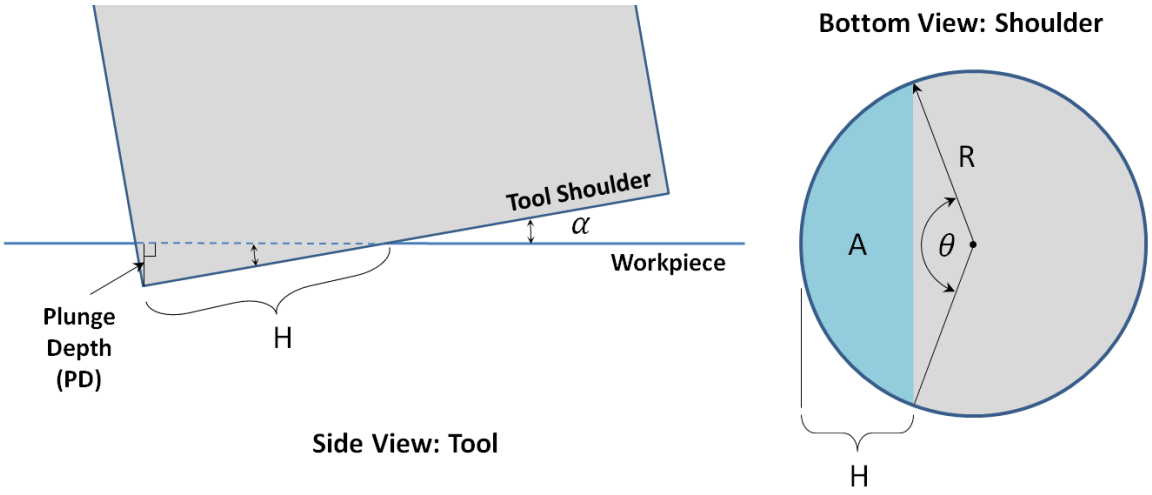

Figure 30: Flat Shoulder Tool Contact Condition

The plunge depth (PD), also called heel plunge depth, is measured vertically from the surface of the workpiece to the trailing edge of the tool shoulder. The tool tilt angle (α) determines how rapidly the tool contact condition, surface area (A), changes as the tool is

plunged into the workpiece. The area of the segment of the circle representing the contact condition can be calculated with the equation:

$$Area\ (A) = \frac{R^2}{2}(\theta - \sin\theta) \tag{8}$$

And, the sector angle (θ) corresponding to the segment can be calculated with:

$$\theta = 2\cos^{-1}\left(\frac{R-H}{R}\right) \tag{9}$$

Longhurst determined the sensitivity of various tool tilt angles with respect to changing contact condition due to changing plunge depth, first, by substituting Eq. (9) into Eq. (8) and differentiating [43]. The result is:

$$\frac{dA}{dH} = \frac{R^2}{2}\left[\frac{2}{R\left(1-\frac{(R-H)^2}{R^2}\right)^{1/2}} - \frac{2\cos\left(2\cos^{-1}\left(\frac{R-H}{R}\right)\right)}{R\left(1-\frac{(R-H)^2}{R^2}\right)^{1/2}}\right] \tag{10}$$

Then, the contact distance (H) is linearly related to a fixed plunge depth (α) by:

$$H = \frac{1}{\sin\alpha}(PD) \tag{11}$$

So, given the relationship of Eq. (11), Eq. (10) can be used to relate changes in contact surface area to plunge depth. Longhurst conducted a numerical simulation to plot dA/dH

versus plunge depth for three different tool tilt angles, and showed that sensitivity for control purposes increases as tool tilt angle decreases, noting that sensitivity cannot be defined for a tool tilt angle of 0 degrees [43]. While exercises like these, which are dependent on having a geometrical model, are incredibly valuable, the theoretical contact condition defined by a circle segment varies somewhat during welding. As the tool plunges into the workpiece at the start of a weld, material is displaced by the probe, often creating a pillow of material underneath the entire shoulder. Then, as the tool traverses along the joint line, material is pushed ahead of the shoulder, which is usually subsequently forged underneath but can sometimes be expelled as flash. This scenario has been likened to the tool 'surfing' on the plasticized workpiece material [25]. Therefore is it very important to be aware of tool contact condition and selection of plunge depth as it relates to tool tilt angle, which is usually found in the literature to be somewhat higher (2 – 3 degrees) for lap joining. Often experimental trials are required for determining the optimal parameters.

Much experimental work has indeed focused on developing processes and parameters for friction stir lap joining with a variety of materials. Dubourg et al. conducted process optimization via mechanical properties in the lap joining of 7075-T6 in 1.5 mm (0.059 inch) thickness and 2024-T3 in 2.3 mm (0.091 inch) thickness. This was done in order to simulate an aerospace application in which the 7075 (top sheet) acts as a stringer or stiffener joined to the inner surface of a 2024 (bottom sheet) aircraft skin. The configuration of AS outboard and RS in the load path was selected for single pass welds, and double pass welds and riveted specimens were created as well, for comparison. For single pass welds, low weld pitch, or colder, welds were determined to

have better properties, with the optimum welding speed and tool rotation rate determined to be 27.5 IPM and 700 rpm, respectively. More on this study will be presented in the aerospace application section of this review [69]. Jana et al. studied the effects of tool geometry on the shear strength and microstructural properties of dissimilar lap joints of Mg AZ31 and two different steels, a mild steel and a high strength low alloy (HSLA) steel [70]. Cox [71, 72] and Yang et al. [73] also studied the joining of MG AZ31 in a lap joint configuration, conducting process optimization with measurements from a number of different evaluation methodologies. Yazdanian et al. created dissimilar friction stir lap joints of Al 6065-T6 and Mg AZ31B-H24 and studied the effect of defect size, specifically size of the hooking defect, on the fracture strength while also analyzing the fracture modes [74]. And finally, Aldanondo et al. studied the effects of probe design and welding parameters on the formation of defect in dissimilar friction stir lap welds of 6082-T6 and 5754-H22 [75]. These are just a small sampling of the myriad articles that address issues related to friction stir lap joining, most of which focus only on conventional joining methodologies.

Process Variants

Since its development, the conventional FSW process has evolved and expanded into a number of process variations that include modifications to the tool-shoulder geometry as well as changes in the joining methodology from continuous welding to a discrete joining method, as in Friction Stir Spot Welding (FSSW). As most applications of FSSW are on lap joint configurations, it can be thought of as a continuous lap joining variant, and although it will not be discussed here at length, a number of variants will be

discussed here that are well established, newly developed, or have relevance relating to manufacturing issues in a variety of industries, including aerospace.

Self-Reacting FSW or SR-FSW is a variant in which the tool probe extends through the workpiece and reaches a second shoulder on the back side that replaces the anvil or backing plate. This type of tool is also sometimes referred to as a bobbin tool. The distance, or gap, between the tool shoulders can be either fixed or variable. The shoulders and probe rotate together as the tool enters the workpiece from the edge or a designated through-hole, rather than plunging, and then traverses the joint line. In the case of variable gaps tools, the shoulders are typically independently actuated, allowing for a variety of control options. The primary advantage of SR-FSW is that the large axial force associated with conventional FSW is balanced due to the symmetrical nature of the tool. This can reduce the size and complexity of the tooling (backing plate, clamps, etc.) necessary to weld larger structures. It is also advantageous that heat input and stirring from the shoulders affect the workpiece in a more balanced manner, eliminating problems associated with partial penetration, like weld root defects, and often leading to more desirable weld characteristics. Skinner and Edwards demonstrated SR-FSW weld head technology for joining 2219 and 2195 in thicknesses up to 25.4 mm [76]. Sylva et al. conducted a feasibility study in which tools and parameters were tested to advance the use of SR-FSW technology for welding thin (1.8 mm) section 6061-T6 and 6N01 aluminum alloys at relatively high (greater than 1 m/min) welding speeds [77]. Tool design is critically important to enabling a successful SR-FSW joining process. Colligan developed and tested a tapered shoulder design for SR-FSW that allows welding to be conducted at a tilt angle of zero degrees [78, 79]. Colligan et al. also conducted extensive

tool and parameter optimization for the welding of thin (as small as 3 mm) 5XXX and 6XXX series aluminum extrusions for a shipbuilding application using fixed gap bobbin tools. One of the tool designs from this study is pictured in Figure 1. Weld initiation failure was identified as a major problem in SR-FSW of thin sections than can be controlled with tool design and strict adherence to proper welding procedures [80].

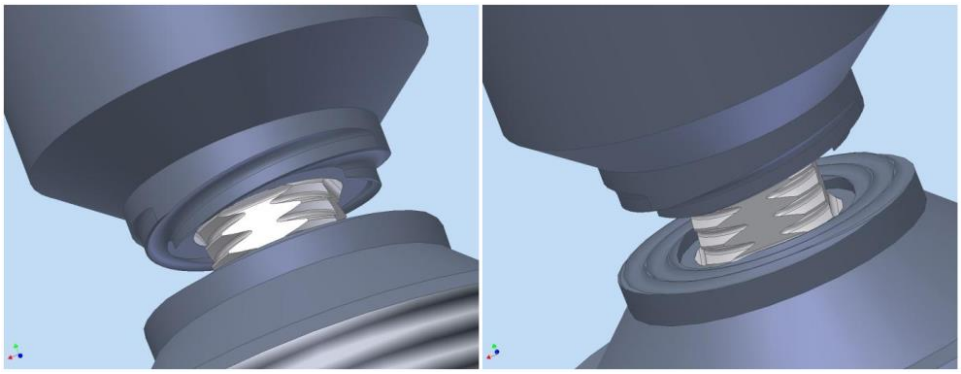

Figure 31: Fixed gap SR-FSW tool for welding thin 5xxx series aluminum, developed by Colligan et al. [80]

SR-FSW has now become a more mature process, as evidenced by its application in industry and attention in research and development efforts. NASA has used SR-FSW technology for welding the external fuel tank of the space shuttle, an application that will be discussed further here [81], has developed additional technology for advancing the SR-FSW process [82], and has extensively analyzed weld zone characteristics relative to parameter selection and tool geometry [83]. Optimization for the process has been conducted via numerical simulation [84], and similar variants, like double-sided FSW wherein top and bottom tool shoulders are not mechanically connected, are being further evaluated [85].

Assisted FSW involves using a secondary heat source that assists the primary process heating that results from friction and plastic deformation of the workpiece. Preheating the workpiece can potentially reduce tool wear, particularly in the plunge phase of welding, by softening the workpiece thereby reducing stresses in the tool. Another motivation involves lowering process forces throughout the weld to extend the applicability of FSW to machines with lower capacities. Sinclair precisely documented how preheating can significantly reduce process forces by performing a series of 6061 bead-on-plate welds with a TrivexTM tool with varying itial temperatures and process parameters. Initial temperatures ranged from room temperature to 300° C and were achieved with electrical heating elements placed below the workpiece. The average axial force decreased by a minimum of 21% for all welding speeds, and the torque was reduced significantly as well before reaching an apparent self-regulating minimum [86, 87]. Previously, Riichi et al. had shown that preheating had relatively little effect on the tensile strength of 5052-H34 welds with varying initial temperatures. Heating was performed with an electrical heating element in this study as well [88]. Other methods of assisted FSW that have been tested include the use of a TIG welding torch [89, 90], a laser welding system [91, 92], and an induction heating system [93, 94]. In another variation, electrical current was passed directly through the tool and workpiece to create secondary Ohmic heating during the weld. This was dubbed Electrically Assisted Friction Stir Welding (EAFSW) and was aimed at reducing forces to enable the utilization of smaller machines for shipyard manufacturing and in-situ maintenance and repair [95].

Pulsing, or Pulsed FSW (PFSW), is a relatively new variant of FSW that has its roots in arc welding technology and has been recently investigated on a preliminary basis. In arc welding, pulsation of the welding current between high and low values has advantages in the welding of aluminum alloys. The fluctuation in current allows for heat to be dissipated away from the weld zone more effectively, reducing the probability of the occurrence of hot cracking, which is a common problem [96]. Through the evolution of FSW technologies, researchers have looked at natural extensions of arc welding technology to determine what knowledge could be applied to FSW. Pulsing is one of these natural extensions, which if applied to FSW parameters, such as the tool rotation rate or the traverse rate, held promise for perhaps having similar impacts on heat dissipation and even enhanced material mixing. The first instance of pulsing FSW parameters was demonstrated by TWI with the Re-stir^{TM} (reversal stir welding) technique, in which the tool rotation rate is pulsed in full reversal mode. Reversal can be initiated before or after one full tool rotation. Preliminary results showed symmetries in weld zone microstructural characteristics not achievable with conventional FSW [35]. Eberl et al. explored the use of pulsing parameters in FSW to correct a problem with tool oscillation. The traverse rate was pulsed in the welding of dissimilar alloys, and not only was tool oscillation eliminated, but other advantages were observed as well. The pulsed weld exhibited higher tensile strength, a lack of volumetric flaws, and enhanced mixing between the alloys which was evident by the appearance of alternating light and dark features within the weld [97]. The largest and most comprehensive examination of pulsed FSW to date was conducted by Ballun, in which pulsing capabilities were developed for a welding robot and characterized, and a large study of pulsed tool rotation

rate butt welds of 0.25 inch thick 6061 was conducted with some preliminary, yet unreported, investigation into lap welding as well [98, 99]. Tool rotation rate was pulsed as a square wave input with an amplitude of 150 rpm about different means with different frequencies, and conventional welds were made for comparison. The output spindle speed was characterized, and it was confirmed that the workpiece material is affected by the spindle pulsation by examining process forces and by quantifying the visible evidence such as surface texture and alternating striations. Figure 32 displays the resulting surface finish.

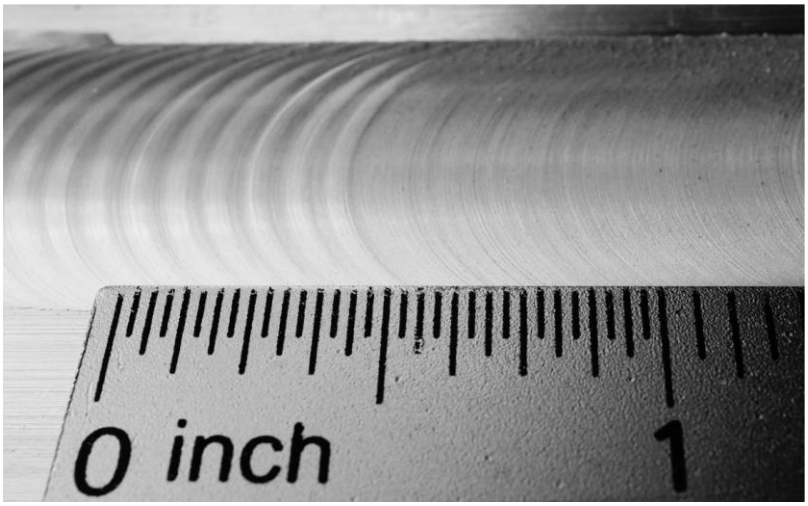

Figure 32: Comparison of Pulsed (Left) and Conventional (Right) Surface Finishes; Pulsing Frequency was 1.0 Hz [98]

Through material testing, it was determined that there was not a significant difference in tensile strength between pulsed and conventional specimens, but pulsation did in fact have a statistically significant impact on the size of the TMAZ, the greatest being for welds with the tool rotation rate pulsed at 0.25 Hz (1200 ± 150 rpm) While this understandably would have limited positive impact on butt welds, which have a finite

joint interface, a large TMAZ is critical for lap welds, showing that pulsation may have more of an impact, particularly with regards to strength, on lap welds [98, 99].

Weaving, or Weaved FSW, is another process variant that has its origins in control, specifically lateral position control. A through-the-tool tracking technique called WeaveTrack was developed for automatically tracking friction stir weld joints of different configurations [100]. The technique involves weaving the tool back and forth laterally while sensing forces to enable a controller to make decisions about adjusting and maintaining a desired lateral tool position. The controls aspects of this technique are discussed extensively in a latter section of this review. Another aspect of the technique, however, is the effect that periodic lateral tool movement has on joint characteristics. While this was evaluated on a limited basis for T-joints and lap joints in studies focused primarily on controller evaluation, a large study of the effect of weaving on lap joints was conducted by Hendricks [101]. First, Hendricks evaluated weaved welds of 0.125 inch thick 6061-T6 with a tool rotation rate of 1000 rpm and a traverse speed of 50 mm/min. Inputs of the WeaveTrack controller, weave width (2*radius) and weave rate, were varied to determine the effect on weld strength. The weave width was varied from 0.25 mm to 1.25 mm, and the weave rate, or the speed of lateral tool movement, was changed from 51 mm/min to 89 mm/min to 127 mm/min. The lap configuration was such that the AS was outboard. Figure 33 displays the strength results of weld specimens from this study. Non-weaved specimens were created for a control. Hendricks noted that on average, weaved welds exhibited a strength level 6.5% higher than that of non-weaved welds, and the increase in TMAZ width as measured in weld cross sections increased at a level equal to the weave width. Next, Hendricks welded another round of specimens with an

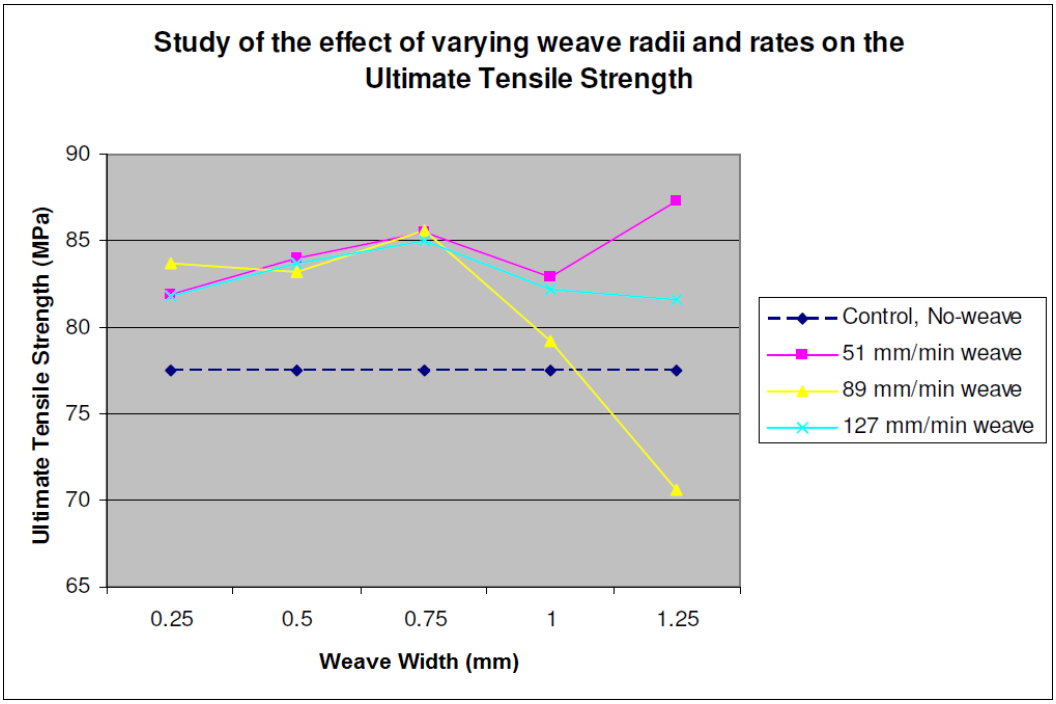

Figure 33: Strength of Weaved 0.125 inch Thick 6061-T6 Lap Welds at 1000 rpm and 50 mm/min Welding Speed [101]

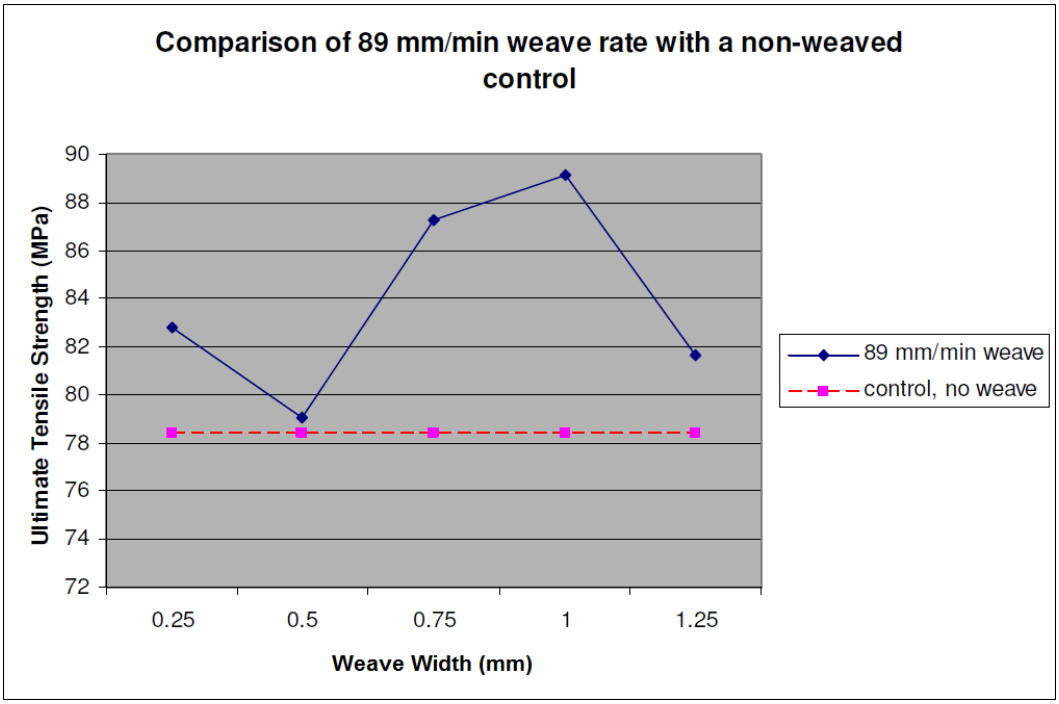

Figure 34: Strength of Weaved 0.125 inch Thick 6061-T6 Lap Welds at 1500 rpm and 50 mm/min Welding Speed [101]

increased plunge depth and an increased rotation rate, from 1000 to 1500 rpm. These measures were taken to improve material flow and eliminate some volumetric flaws that had been observed in some cross sections. Weave rate was held constant at 89 mm/min while the weave width was again varied over the same levels as before. Strength results for these weld specimens are displayed in Figure 34. Results of this second round of welds showed that weaving increased strength for all weave widths, however strength did decrease from a width of 1 mm to 1.25 mm, just as before, as seen in Figure 33, when the strength of the weaved weld fell below that of the control weld, for the 89 mm/min weave rate case. The general trend observed by Hendricks is that weaving increases strength to a point, and then further increases in weave width can lead to surface defects and drops in strength. Surface defects, like that of Figure 35, were observed for weave widths of 1 mm and 1.25 mm in the first study.

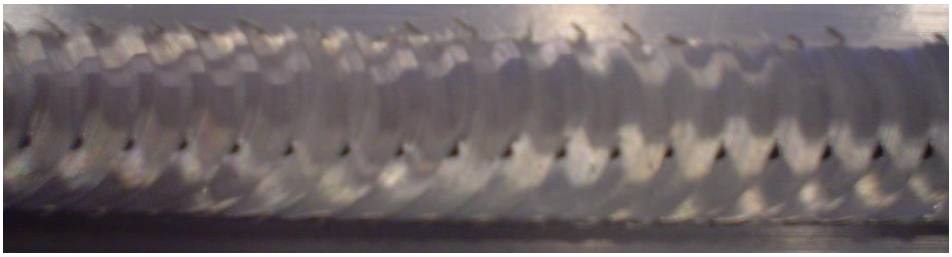

Figure 35: Repeating Surface Defect Caused by Wide Weave Radii [101]

Hendricks concluded that a balance must be struck between choosing WeaveTrack parameters for successful tracking and for desirable mechanical properties. Parameters chosen solely to achieve good tracking characteristic may not create the strongest possible welds, and conversely, parameters chosen to create the strongest, defect-free welds may not allow the tracking controller to perform at its most efficient level [101].

Robotic Welding

Friction stir welding is a unique joining process in a number of ways, and one aspect that cannot be ignored is the requirement that the process be performed by robots due to the relatively high forces involved. While hand-held FSW is a capability that is being sought by researchers, it is a long way from commercial implementation. There are multiple aspects of robotic FSW that will be discussed here, including force sensing and control, methods of automatic joint tracking, and in-process evaluation of weld quality and detection of defects.

Sensing and Control

There are a number of physical properties that can be sensed or measured during the FSW process, but the most commonly measured process output in research and in industry is force. Force sensing is an important aspect of robotic welding. Sensing forces allows for processing monitoring capability that can lend insight into resulting weld characteristics, expanded control capabilities that make FSW more adaptable to industrial robots, and even the enabling of through-the-tool joint tracking techniques. As previously discussed, the process forces of FSW are the axial force (F_z), the traversing force (F_x), the side force (F_y), and the torque (M_z or T). The directions of these forces for a conventional friction stir weld are displayed in Figure 1.

The most common method of measuring forces involves using an industrial load cell that is mounted between the FSW tool and the welding robot faceplate or head, although there are creative alternatives that have been developed. Table-type dynamometers onto which the workpiece can be mounted are also occasionally used.

Most load cells utilize strain gages or piezoelectric crystals as the sensing elements, and there are many commercially available, off-the-shelf options that are applicable to FSW. There are also systems, including the LowStir Mk.1 (Figure 36) or Mk.2, that were designed specifically to be used in FSW research or industrial applications [102, 103].

Figure 36: LowStir Mk.1 Sensing Device [104]

Often however, due to the relatively high cost of most commercially available load cells, some researchers opt to design and build custom low-cost force measurement systems [29, 105, 106, 107, 108, 109]. In addition to having open architectures, which allow for flexible measurement capabilities and easy repair, these systems are often more robust in terms of capability for withstanding potential overloading conditions and the harsh thermal environment of FSW as well. In either case, once FSW process forces can be measured, data that lends insight to weld characteristics can be collected, and data can be fed back to the robotic control system to enable closed-loop force control.

Closed-loop force control of the FSW process has been a topic of research for a number of years and can now be found widely applied in FSW joining operations in industry. There are a number of reasons force control is popular and in many cases necessary, which include the utilization of compliant standard industrial robots, the need to weld complex geometries, unknowns related to workpiece geometry or rigidity, and inconsistent workpiece thicknesses. All of these issues are related to one critical aspect of the FSW process, however, which is maintaining proper tool-workpiece engagement. Maintaining proper engagement with position control alone can fall short due to these issues, making force control necessary to create quality, consistent welds.

It has been shown that axial force can be controlled by manipulating plunge depth, traverse speed, or tool rotation rate [43, 110]. If plunge depth is chosen as the controlling variable, which is by far the most popular method, force control enables the continuous adjustment of tool-workpiece engagement in the vertical (Z-axis) direction to maintain a desired contact condition. This allows force control to compensate for the issues just previously listed. This has been especially important in the expansion of FSW in manufacturing and the utilization of standard industrial robots in welding operations.

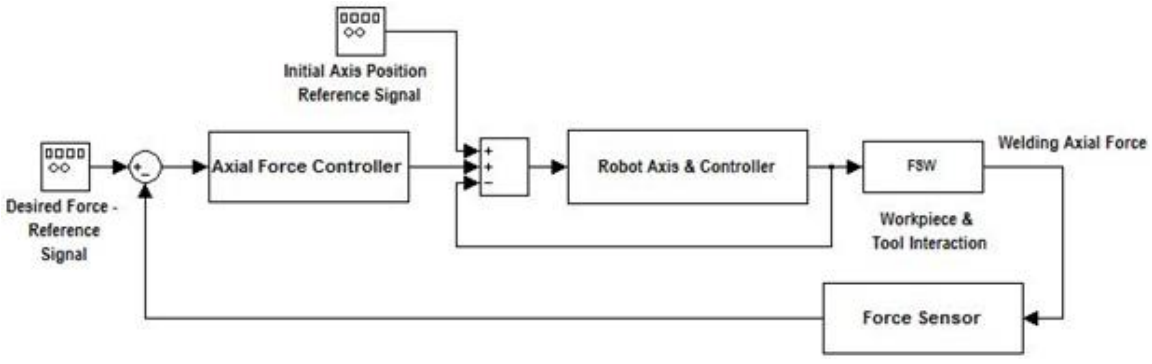

Figure 37: Common Force Control Architecture [43]

Figure 37 displays a control architecture documented by Longhurst that is commonly utilized when standard industrial robots are configured to operate with force control [43]. It is a nested loop architecture in which the position controller of the robot is enclosed by a force control loop. Force error, which would be indicative of a change in the desired tool-workpiece contact condition, is fed into the position controller, which enables continuous adjustment of tool position in the vertical direction to maintain a desired force. Smith demonstrated a relatively early example of FSW performed on a standard industrial robot using force control [111]. Since then, along with force control capabilities, robots are being purpose built to be larger and more rigid with increased load capacities to handle the higher forces of processes like FSW. Figure 38 displays an image of the ESAB Rosio FSW robot.

Figure 38: ESAB Rosio FSW Robot [112]

The ESAB Rosio FSW robot consists of an ABB IRB 7600 robot that has been modified specifically for performing FSW operations. It is capable of maintaining a down force of 13 kN (2900 lb) over a length of 2.5 m [112]. De Backer and Verheyden used an ABB IRB 7600 robot with force control capability and specialized FSW equipment provided by ESAB for developing welding procedures for three automobile components provided by Saab: floor panels, the A-structure, and wheel hoods [113]. More discussion of automotive applications of FSW will follow in the appropriate section of this review.

Apart from focusing on specific industrial applications requiring control, a significant amount of basic research has gone into characterizing force control methodologies and optimizing different technical approaches. As previously discussed, Cook et al. experimentally determined trends in axial force with varying rotational speed and welding speed that could be exploited for force control purposes (Figure 19), noting that force control is necessary in FSW to compensate for compliance in robotic arms and workpiece fixturing [30]. Cook et al. further examined controlling robotic friction stir welding with a series of bead-on-plate 6061 welding experiments focused on measuring process forces with a custom data acquisition system. Workpiece temperature, spindle power, and changes in axial force with incremental changes in axial position were examined. Again, the importance of force control capabilities in FSW were stressed, noting particularly that relatively small changes in axial position equate to large changes in axial force, which highlights the sensitivity of the controls problem [114]. Sensitivity in this context has already been discussed somewhat previously, with Longhurst examining the tool contact condition for flat shoulder geometry at different tilt angles with varying plunge depth [43]. Furthermore, focusing primarily on this tool-workpiece

contact condition, Longhurst identified key enablers of a successful force control setup. These included always keeping some portion of the tool shoulder above the surface of the workpiece, using a tool with a smooth motion profile during plunging or retracting to minimize force spikes, and increasing the tool tilt angle [44]. A smooth motion profile tool developed by Longhurst has already been discussed from a tool design perspective [45, 46], but its contribution to advances in controls has been significant as well. The spherical shoulder tool was used in a torque control study that highlighted the ability to measure process torque indirectly with relatively inexpensive, off-the-shelf spindle motor current sensors [46]. Torque control is an alternative to axial force control that has been shown to be simple and straightforward to implement, more sensitive to plunge depth, and more stable over a wide range of welding temperatures, while at the same time, lending a greater understand of the welding process [115]. Longhurst et al. welded 0.25 inch thick 6061 plates in a raster pattern, creating 10 feet of total weld length to simulate the longer welds required in many industrial applications. A torque (or current) controller was implemented and tuned using the Ziegler-Nichols method [116] so that as process torque was controlled by manipulating plunge depth, proper tool contact would be maintained as well, even as plates were put on inclines of 3 mm and 6 mm rise over 20 inches of length. Welds with torque control and welds with position control, or fixed plunge depth, were created for comparison. Figure 39 displays the controlled spindle current and the corresponding plunge depth adjustments commanded by the controller for a weld with a 6 mm rise. Figure 40 displays a comparison of surface finishes for a flat weld without control and a weld with a 6 mm rise. It was determined that spindle motor current provided a reliable indirect measurement of process torque and that torque control

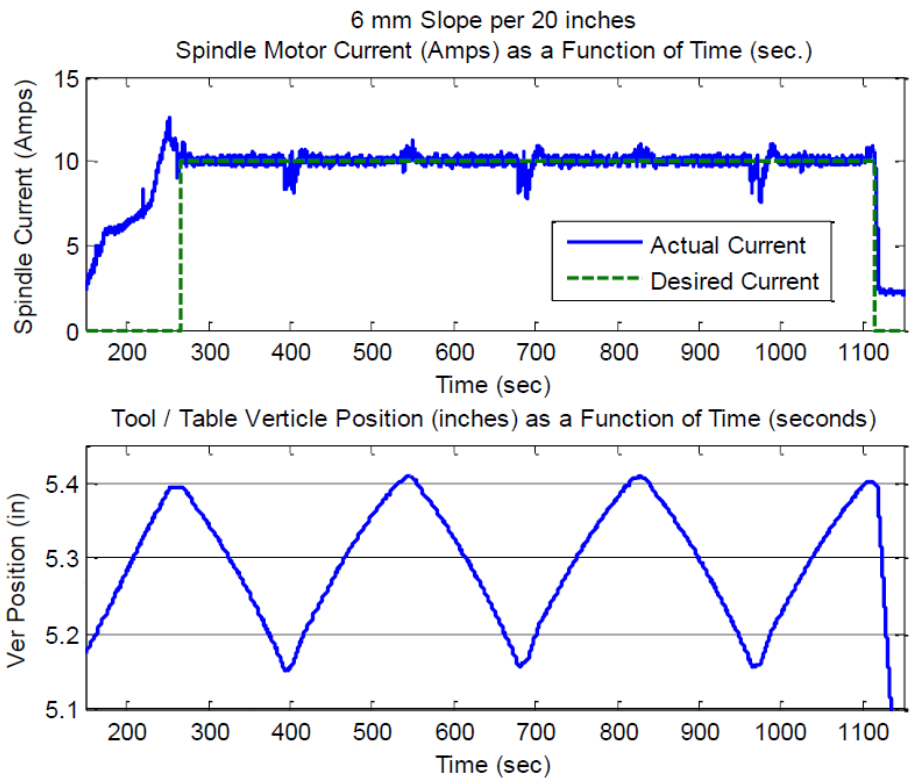

Figure 39: Controlled Spindle Current and Corresponding Vertical Position Adjustments [46]

Figure 40: Flat Weld without Torque (or Current) Control (Top); Controlled Weld with 6 mm Rise (Bottom); Image adapted from [46]

is indeed perhaps a preferred alternative to axial force control if the primary goal is to maintain proper tool-workpiece contact condition during welding [46]. Additional advances related to controls in FSW include the simulation of the interactions between control architectures, industrial robots, and manufacturing processes [117], the development of hardware that enables multi-axis force control for FSW process variants like self-reacting welding [118], and the development and characterization non-force control methodologies, such as closed-loop temperature control [119]. These advances and the ones previously discussed here at length focus primarily on maintaining proper tool position in the axial direction, but of equal importance is maintaining proper tool position in the lateral direction relative to the joint line being welded.

Joint Tracking

Proper tool-workpiece engagement or alignment is of utmost importance for creating quality friction stir welds. As discussed in the preceding section, force control or torque control via plunge depth manipulation are excellent methods for maintaining the desired plunge depth, i.e. the proper tool-workpiece alignment in the vertical direction. Of equal importance, particularly for butt joints and T-joints however, is the tool-workpiece alignment in the lateral (Y-axis) direction.

To maintain proper lateral alignment, a planned path technique with compensation or a joint tracking technique is usually necessary, with one exception being on the relatively short welds that are conducted in research laboratory settings. Planned paths can be generated from CAD models of the workpiece, even when complex 3D curved surfaces are involved [120], but when using a planned path technique on an

industrial robot, there are two important issues that can impact success: It is common for there to be slight differences between virtual and real environments in the case of offline programming, and robot deflection that gets worse with increasing welding forces can cause deviation from the planned path [121]. It is however possible to compensate for these issues by monitoring process forces and correlating them to path deviations [122, 123] or by using a vision-based tracking system.

As with most automated manufacturing processes that require tracking, the predominant method of joint tracking in FSW, particularly for butt joints, is to use a vision-based system that interfaces with the control system of the robot. This has been demonstrated at both the academic and industrial levels [121, 124]. Typically a camera, in conjunction with a computer operating line or edge detection algorithms, interfaces with the robot controller, and path corrections are made based on the relative locations of the weld joint line and the FSW tool. It is also common to incorporate laser depth sensors to give more information to the control system about the weld head or tool position relative to the workpiece, backing plate, or clamps. This adds another level of collision detection or avoidance capability.

One of the more difficult joint configurations in FSW to track properly is the blind T-joint. This joint type is characterized by an absence of visual cues on the top side of the workpiece that can be exploited for tracking purposes, and it is from the top side that the joint is welded, rather than welding the two fillet regions on either side of the vertical member as would be traditional with a fusion welding technique, although the potential for welding these regions with stationary shoulder FSW (SSFSW) technology has been developed [125]. Fleming et al. examined this joint configuration with an ‘open

air’ clamping setup with the hopes of characterizing the force properties and enabling misalignment detection and automatic joint tracking. This joint configuration and clamping setup are displayed in Figure 41.

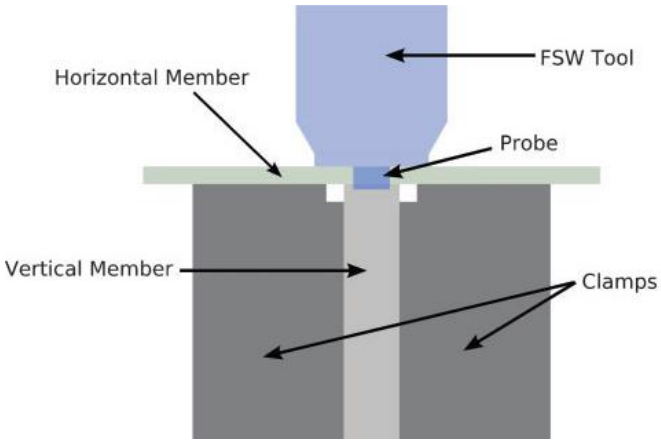

Figure 41: Blind T-Joint Configuration with 'Open Air' Clamps [123]

The ‘open air’ designation means that the clamps do not restrict the sample immediately adjacent to the joint line, making the joint configuration particularly challenging due to the potential for material expulsion from the joint in cases of severe misalignment. Fleming et al. welded 6061 T-Joints with intentional lateral tool offsets to both the advancing and retreating sides of center at increments of 0.25 mm. Axial force was monitored as a feedback signal, and welding parameters were set at 1000 rpm and 4 IPM. Figure 42 displays the variation in axial force with lateral position along with macrographs of weld cross sections at each interval. Force variation with lateral position was significant, as were weld defects with severe misalignment. Based on the encouraging results, Fleming et al. developed a lateral position estimator using a general regression neural network. The network was trained and evaluated with different

combinations of the collected force data. During testing trails, the estimator averaged an error of 0.42 mm with a standard deviation of 0.508 mm.

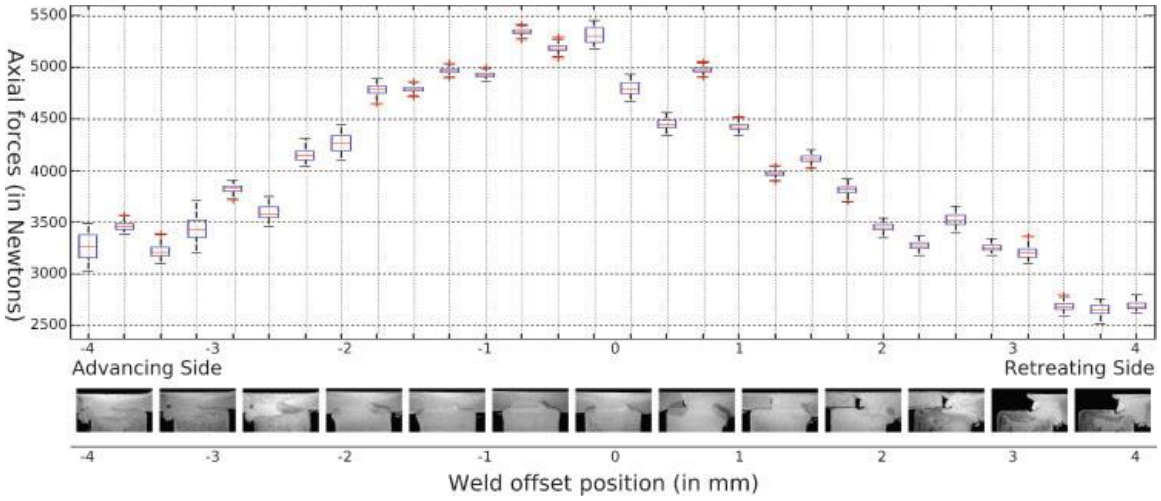

Figure 42: Axial Force Variation with Lateral Offset in T-Joints of 6061 [123]

Additional welds were then performed with intentional periodic changes in lateral position, and the estimator was used to predict the actual position. Performance was satisfactory, but Fleming et al. noted that compensation for axial force fluctuation resulting from dynamic changes in lateral position would have to be incorporated into future systems [123].

Continuing with a focus on blind T-Joints, Fleming et al. then developed a novel technique for automatically tracking the joint line, maintaining proper tool alignment relative to the vertical member [126]. As previously discussed from a strictly process-modification perspective, this lateral position control system is known as WeaveTrack [100]. WeaveTrack utilizes an extremum-seeking control methodology, wherein the tool weaves back and forth laterally while traversing the joint line, taking force measurements

at the extremes and then making lateral adjustments to the center of the weave based on force comparisons to maintain the maximum axial force, which has been shown to represent proper tool alignment with the vertical member, as seen in Figure 42. This technique creates a trapezoidal tool path, and there are a number of parameters that affect the overall performance of the system, including the tool rotation rate, the welding speed, the lateral rate of change, the weave radius, the center step change, and the pause duration at the extremes. Fleming et al., while not necessarily determining the optimal parameters, selected parameters and demonstrated the capability of the system to find and track a desired joint line after an initial offset and then track a continuously changing desired joint line. These results are shown in Figure 43.

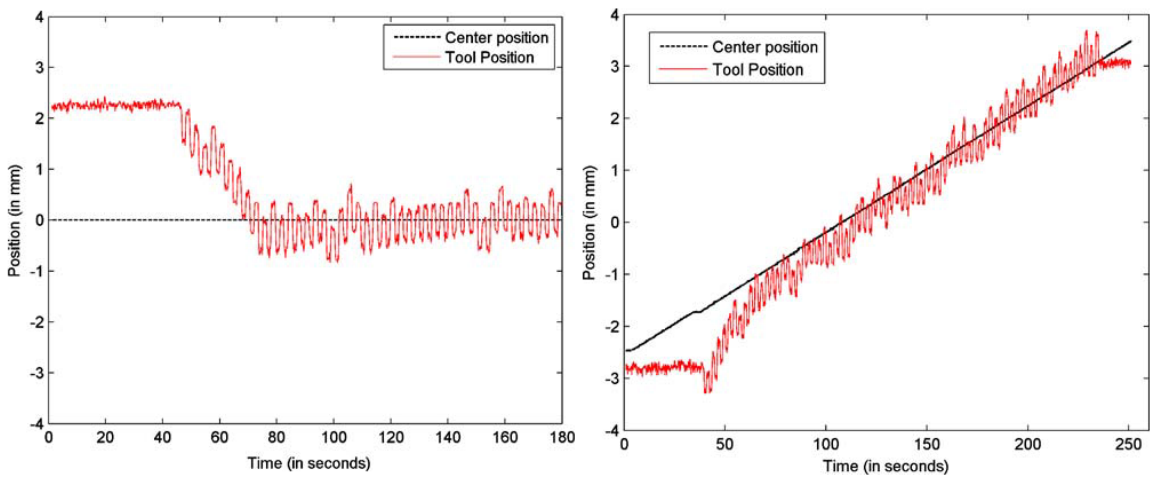

Figure 43: WeaveTrack Performance on Blind T-Joints [126]

Tracking performance was more than satisfactory, and Fleming et al. also investigated the effects of weaving on weld quality and confirmed that weaving could potentially contribute to increased weld strength, a secondary benefit of weaving that, as previously discussed, was investigated to a greater extent by Hendricks when applied to lap welds

[101]. Possible extensions and improvements to the system were discussed, which included the incorporation of axial force control between the weaving cycles and the modification of the system to allow for dynamic parameters, such as the center step change, which would vary with the magnitude of the force comparisons [126].

Fleming et al. also determined that WeaveTrack is effective at tracking lap joints when the width of the overlap region is equal to the tool shoulder diameter [127]. In this case, both axial force and torque were found to be effective feedback signals, with torque having slightly better characteristics. Again, tracking was demonstrated with initial offsets and continuously changing desired joint lines. The effect that WeaveTrack parameters have on the speed with which the system reaches the desired joint line and the presence of subsequent oscillations during tracking was discussed as well [127]. Overall, the system is an example of a through-the-tool tracking technique that can lend simplicity and lower the cost of a manufacturing process. Along these same lines, in-process evaluation of weld quality or detection of defects is an advanced capability of increasing demand and importance in FSW manufacturing processes.

In-Process Evaluation

There are a multitude of techniques that can be used for evaluating weld quality, a few of which have been discussed in preceding sections. Post-weld destructive evaluation techniques include mechanical tests such as tensile or shear testing and fatigue testing, hammer S-bend testing for lap welds, and macrograph cross-sectioning. When destructive testing is not feasible or when verification of weld quality is needed on completed structures or assemblies, there are also numerous post-weld non-destructive

evaluation (NDE) techniques available for use. These include, but are not limited to, simple visual testing, dye penetrant testing, eddy current testing, radiographic testing, ultrasonic testing, including phased-array and laser ultrasonic testing, and a number of additional advanced methodologies. While these methods are effective, they can also be both expensive and time consuming. Because of these disadvantages, there is a movement within the FSW research and development community to develop techniques for monitoring weld quality in-process (e-NDE), detecting defects as they occur, enabling the potential for corrective action to be taken, which could possibly reduce waste and the requirement for post-weld evaluation, saving time and money. Efforts such as this would mirror similar efforts in related manufacturing processes. Dave et al. developed an alternative for a qualified, small-lot inertia welding process with an in-process monitoring and control strategy [128]. A qualified manufacturing process is one in which all inputs and procedures are controlled, and the end product is found to be satisfactory or not with inspection and destructive testing along with statistical analysis. A number of factors can cause adverse effects to the system however, and these include human error, material variation, contamination, oxidation, equipment degradation, inadequate maintenance, tool wear, and marginally stable process parameters. Dave et al. used low-cost acoustic sensors, data reduction procedures, and a neural network to build a system capable of classifying bond plate contamination between copper and stainless steel welded components into three conditions: acceptable, conditional, or unacceptable. When data from the acoustic power spectrum was used as the input to the neural network, the system had an identification accuracy of 100%, virtually eliminating the need for additional post-process evaluation. Dave et al. suggested that a success of this magnitude was an

exciting development that may signal a transformation in quality control methods in manufacturing for decades to come [128]. Success stories such as this have prompted others to examine in-process quality evaluation techniques, and a few such cases in FSW will be discussed here.

Boldsaikhan et al. developed a system for detecting worm hole defects based on real-time frequency analysis of process forces [129]. It was hypothesized that the frequency components of process forces would vary as normal material flow characteristics were disrupted. Force data was analyzed from a database of previously completed 7075 butt welds in 0.25 inch thickness. Welds were created with a featureless shoulder and threaded probe at 300 rpm under axial force control. Traverse speed and forge load were varied based on experience to create good, defect free welds and bad welds with volumetric flaws. It was determined that the frequency components of in-plane (X and Y axes) forces were most indicative of weld quality. Figure 44 displays a sampling of force frequency data and corresponding weld macrographs from this study.

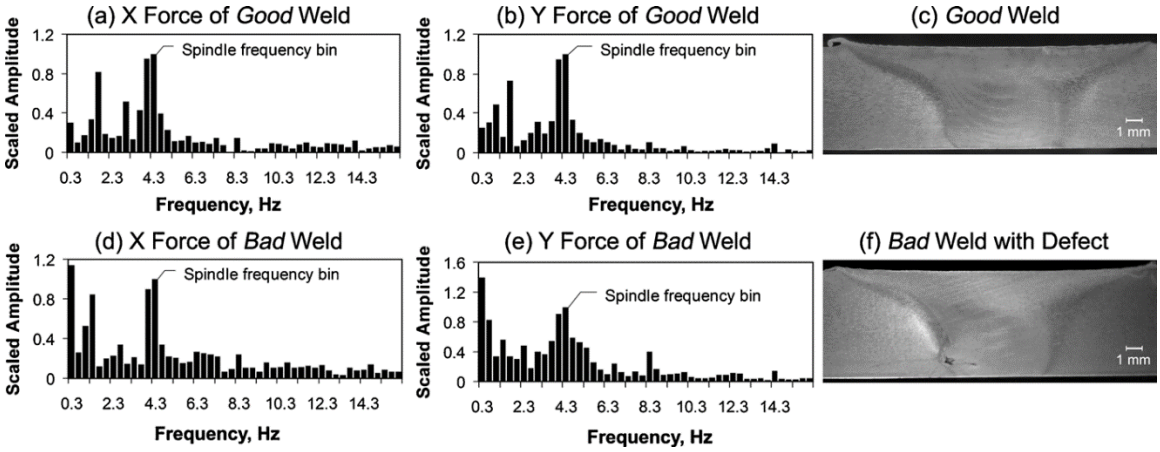

Figure 44: Variation of In-Plane Force Frequency Components with Variation in Weld Quality [129]

Boldsaikhan et al. suggested that under normal operating conditions, material is transferred at a regular rate that is equal to the spindle speed, or in other words, material is transferred during each rotation of the tool. Therefore, the dominant frequency for a good weld is the spindle frequency. When weld parameters are such that material is not transferred properly and worm hole formation is likely, magnitudes increase at frequencies lower than that of the spindle speed. These trends are evident in Figure 44. Using this information, a neural network was developed with 60 frequency bin inputs, 9 hidden units, and one output (1 = volumetric defect, 0 = no defect). Inputs in the spindle frequency range (4 to 6 Hz) and beyond 12 Hz were omitted. The neural network was trained using 180 data sets, each 3 seconds of either X or Y axis force data collected at 68.2 Hz. After training, the network properly identified 57 out of 60 testing samples. Finally, the system was tested on new welds performed under position control with other parameters varied to intentionally create defects to determine if the system could identify the locations of the defects. An example of this testing is displayed in Figure 45.

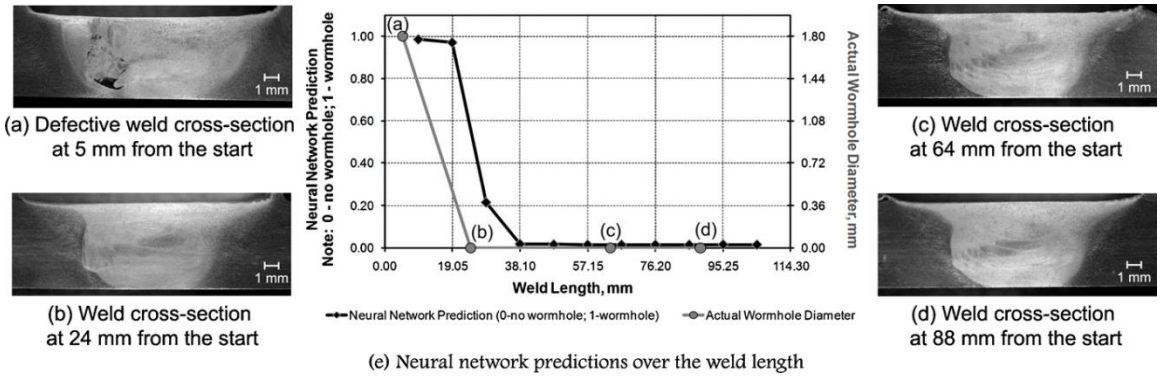

Figure 45: Comparison of Neural Network Predictions of Defect Presence over the Length of a Weld with Actual Defect Dimensions [129]

A defect at the start of the weld is identified by the neural network, and as the defect is eliminated, the network prediction of defect presence follows suit. No real-time evaluation was performed, but Boldsaikhan et al. proposed that a system of this type could be used to develop a feedback system that automatically adjusts welding parameters to eliminate worm holes as they form [129]. Updates to both this technology and concepts about force feedback analysis relative to material flow regimes in FSW have been presented [130, 131, 132].

As discussed previously from a primarily material flow perspective, Longhurst examined in-process defect detection ability with the objective of detecting pre-drilled holes at the faying surface of 0.25 inch thick 6061 butt welds by monitoring spindle motor current as an indirect measure of process torque [13]. In addition to seeing magnitude decreases in the current signal as the tool passed over the hole locations, a change in the frequency components of the current signal was observed as well. This was evident after computing the frequency spectrum using the Fast Fourier Transform (FFT) method and observing the dominant frequencies. Figure 46 displays the raw current data along with the FFT of the current data for selected regions of the weld with two 1/8 inch diameter pre-drilled holes. Frequency data is shown for each of the void regions and for a control region. At the control region, the dominant frequency in the current signal is approximately 2.3 Hz, or one order of magnitude lower than the spindle speed of 1400 rpm (23.3 Hz) as previously discussed. When the tool passed over the pre-drilled holes, creating a void, or flaw at the surface of the weld which is observable in the macrograph in Figure 46, the dominant frequency in the current signal dropped to approximately 1 Hz. Except for the fact that spindle frequency was not reported in the results by

Longhurst, and instead there was a regular oscillation at a frequency lower than that of the spindle, this decrease in dominant frequency with disruptions in regular material flow follows the previously discussed observations by Boldsaikhan et al. [129].

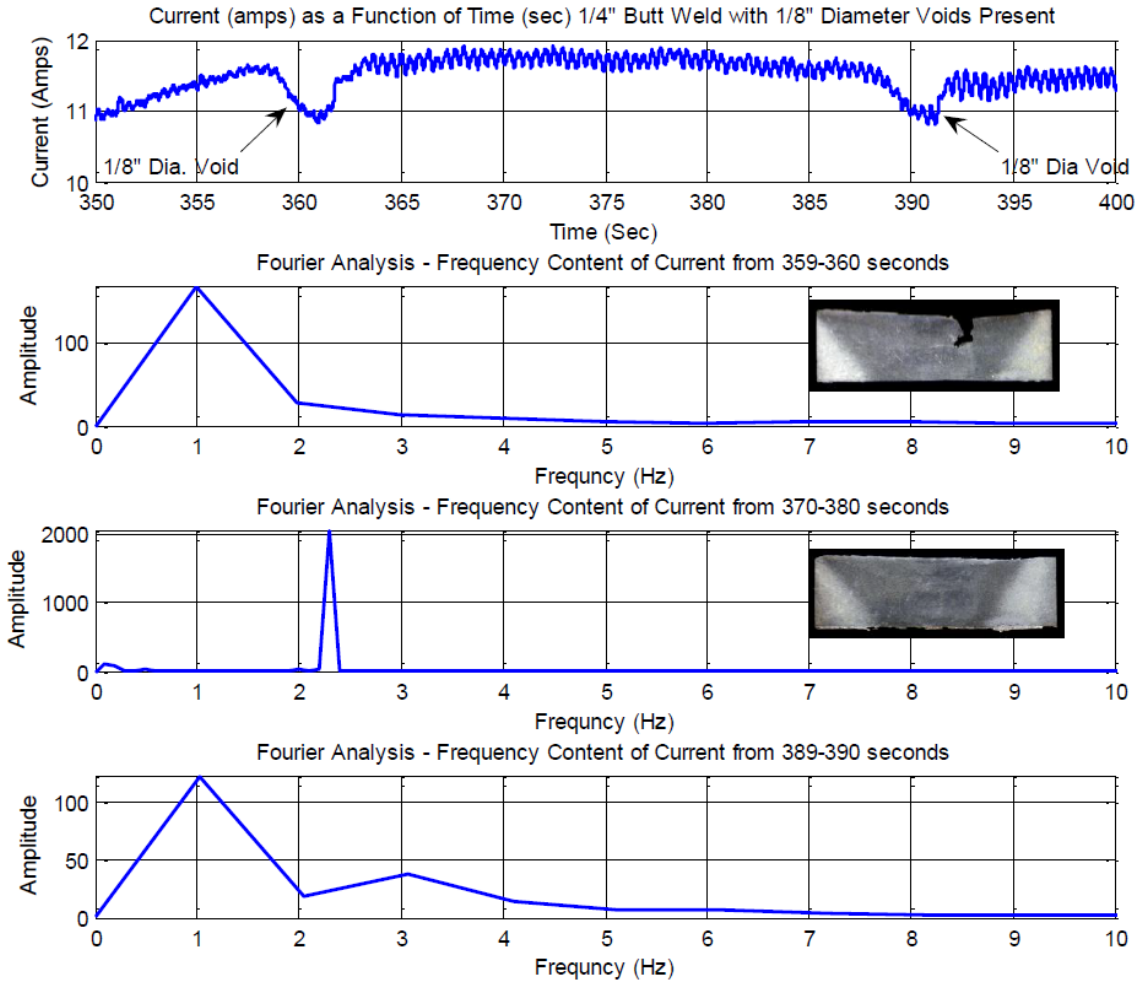

Figure 46: Variations in the Frequency Components of the Spindle Motor Current Signal with Weld Quality [13]

The same convention was observable for pre-drilled holes of other sizes as well. These results showed promise that the spindle motor current, which can be monitored remotely and relatively inexpensively may reveal much insight into weld quality as well [13].

Shifting focus somewhat, Fleming et al. developed an in-process detection of defects technique with a goal of detecting part fit-up issues in lap welds, which can lead to conditions that are detrimental to weld quality [133]. Fleming examined these conditions by welding lap joints of 1/8 inch thick 6061 with machined gaps in the bottom sheet of varying depths (0.005, 0.004, 0.003, 0.002, 0.0016, 0.0012, 0.0008, 0.0004, 0.0002 inch). Welding speed and tool rotation rate were 16 IPM and 2000 rpm, respectively, and process force signals were collected using a Kistler dynamometer sampling at 1000 Hz. Figure 47 displays the raw, or 'first-order', axial force data.

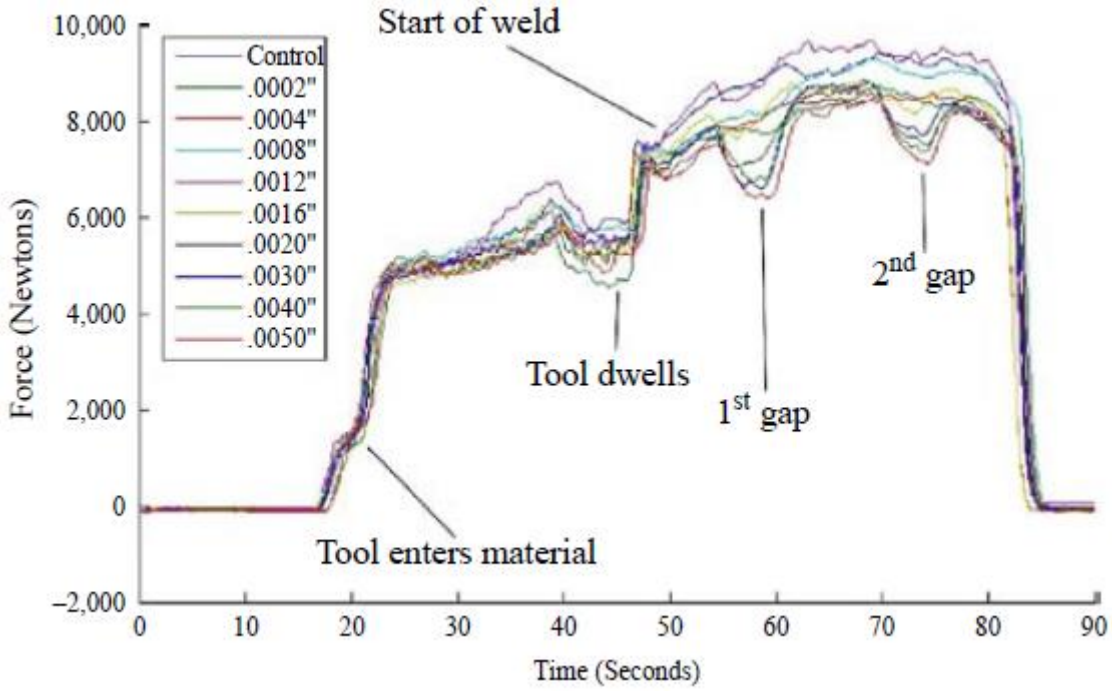

Figure 47: Raw Axial Force Data for Lap Welds with Machined Gaps in the Bottom Sheet of Various Depths [133]

In the gap sections of the welds, a decrease in axial force is evident for gap depths of 0.002 inch or greater, but not for smaller gaps. Figure 48 displays this more clearly.

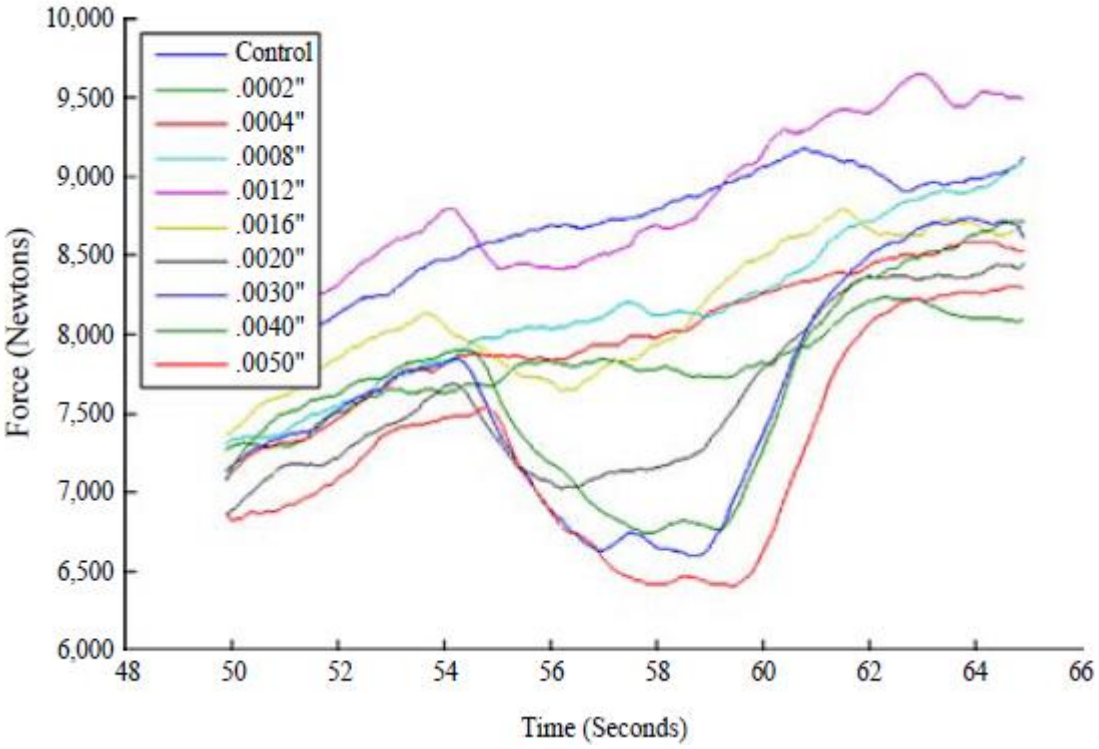

Figure 48: Enlarged View of 1st Gap Region from Figure 47 [133]

Fleming et al. noted that 'first-order' data does not always reveal evidence of fault occurrence, and further data analysis may sometimes be required. In order to extract more detailed features from the collected force data, Fleming et al. selected 2 second long windows from both the gaps regions and control regions and then computed the frequency spectra of the force windows using the FFT method. Data was grouped into 100 frequency bins for each window, meaning each point was represented in 100-dimensional space. Dimensional reduction techniques were then used to reduce redundancy in the data and create more meaningful low-dimensional data sets that could be easily qualitatively examined and compared. Principle component analysis (PCA), which is given no knowledge of the data classes, and Linear discriminant analysis (LDA), which is fed class label information, were selected for this portion of the study. Figure 49

displays a sampling of results, projected onto two dimensions, for each technique. When PCA was utilized, control and gap sections were linearly separable only when gap size was greater than 0.004 inch, for which discrimination could have been performed simply with the unprocessed raw data. PCA was unable to separate data when smaller gap sizes were grouped into the analysis, as seen in Figure 49.

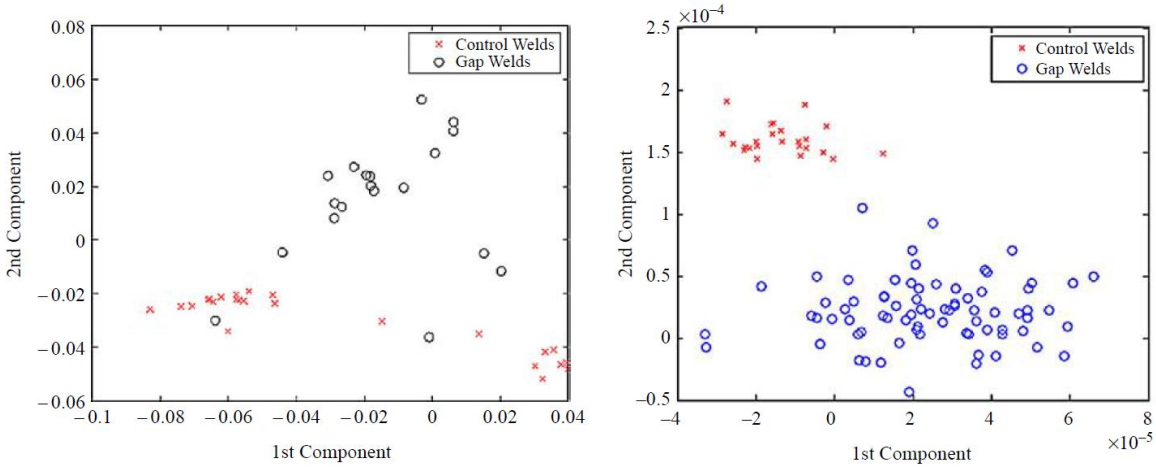

Figure 49: Results for PCA with Gaps Greater than 0.002 inch (Left); Results for LDA with Gaps Greater than 0.0002 inch (Right) [133]

When LDA, which seeks to maximize class separability, was utilized, control and gap sections became linearly separable for all gap sizes. Figure 49 displays the results for this compiled analysis with all gap sizes included. This was an excellent result that showed promise for perhaps forming the basis of a reliable and robust in-process defect detection system [133]. Systems of this nature are becoming important pieces of technology for manufacturers as more and more processes, including welding, are being performed by robots in a variety of industries and applications.

Applications

As mentioned at the top of this literature review, FSW has expanded rapidly and found use in a variety of industries, including aerospace, automotive, railway, and maritime. This section will focus primarily on the automotive and aerospace applications of FSW, along with the use of sealants in FSW, which has become an important and challenging aspect of manufacturing operations where FSW is used to create parts and assemblies expected to perform in potentially corrosive environments.

Automotive

FSW is becoming a widely implemented method of joining in the automotive industry. This is true for both conventional FSW as well as variants like FSSW. These are attractive processes for manufacturers seeking to reduce body weight by integrating lightweight aluminum alloys into their assemblies and reduce the energy consumption of their joining processes. The earliest investigation into applying FSW to automotive manufacturing began in 1998, when TWI partnered with BMW, Daimler-Chrysler, Ford, General Motors, Land Rover, Volvo, Tower Automotive, and EWI to explore FSW concepts applied to aluminum tailored blanks for door panels, drive shafts, and space frames [134]. Since then, many advances have been made, and FSW is now being used to manufacture automobiles and aftermarket components worldwide.

Mazda has used FSSW to join the aluminum rear door structure of the RX-8 since 2003. This rear door structure provides protection from side-impact and contributes to five-star rollover protection [8]. Several manufacturers have applied FSW to the joining of the center tunnel and floor structures. Ford uses continuous FSW lap joints to construct the

central tunnel for the Ford GT from aluminum stampings and extrusions. The fuel tank is housed in the central tunnel, a location that was found to be optimum based on reducing risk in collisions and maintaining a consistent weight distribution and center of gravity at different fuel levels [135]. The use of FSW also led to improved dimensional accuracy of the assembly and an increase in strength of 30% when compared to fusion welded assemblies [8]. In a similar application, for the construction of the Audi R8 high-performance sports car, FSW is used to manufacture aluminum tailored blanks of varying thickness that are press formed to create the center tunnel. In addition to achieving high dimensional accuracy, Audi found that using FSW in this manner also reduced the weight of the final component by one kilogram [136]. In addition to welding the center tunnel, Mercedes, with the help of Riftec, is joining extruded aluminum floor panels with FSW in the manufacture of the lightweight, full aluminum body of the 2012 SL model displayed in Figure 50 [137]. The application of FSW to the center tunnel led to a reduction in parts, an elimination of post-welding rework, and lower costs.

Figure 50: Mercedes SL with Friction Stir Welded Center Tunnel and Floor Panels [137]

The application of FSW to the floor panels led to an elimination of sealer, reduced weld distortion, smooth surfaces, and lower costs. Overall, the new vehicle body is 110 kg lighter and 20% stiffer than that of the predecessor [137].

A number of second-tier suppliers and aftermarket parts manufactures have implemented the use of FSW as well. Sapa joined aluminum extrusions with FSW to construct foldable rear seats for the Volvo V70 station wagon and also used FSW in the construction of a prototype engine cradle which combined several aluminum components formed using various methods. Simmons Wheels and DanStir each developed new processes for constructing lightweight wheels using FSW. Showa Denko uses FSW to manufacture suspension arms, and Tower Automotive creates suspension links from aluminum extrusions for Lincoln Town Car stretch limousines [134].

Perhaps the latest application of FSW in the automotive industry is in the manufacture of a lightweight engine cradle for the 2013 Honda Accord, depicted in Figure 51 [138].

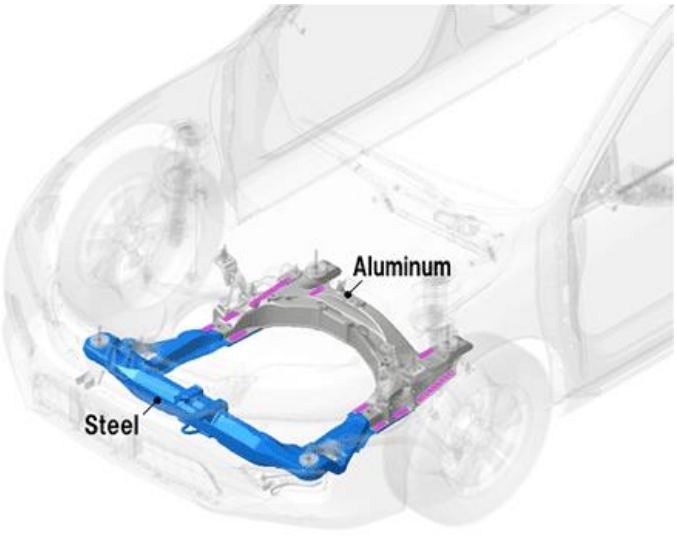

Figure 51: Honda Accord Engine Cradle [138]

The cradle is a dissimilar aluminum and steel subframe assembly joined with continuous FSW lap welds. Using an aluminum and steel hybrid structure resulted in a 25% weight reduction when compared to a full steel subframe. Additionally, by utilizing FSW, electricity consumption during the joining process dropped approximately 50%, and a redesign of the subframe and suspension mounting point was enabled, resulting in 20% greater rigidity and improved dynamic performance. Honda used standard industrial robots to implement the FSW process, and advances in non-destructive testing, including the use of an infrared camera and laser system, have also been touted by the company [138].

Aerospace

One of the first high profile implementations of FSW in industry was as an alternate joining method for space vehicle structures. NASA developed a process for welding the external fuel tank of the space shuttle with FSW, which was necessitated by a change in tank material from 2219 to an even lighter weight 2195 alloy [139]. As this process development was considered a great success, NASA has and will continue to use FSW as a joining method on future generations of spacecraft, and a number of private aerospace companies have begun using the process as well.

FSW is also rapidly gaining acceptance as a rivet replacement technology in the manufacture of aviation structures [140, 141]. In addition to weight savings, the use of FSW leads to a reduction in parts, significantly faster joining speeds, greater joint strength, and lower manufacturing costs. The most common aerospace alloys utilized are Al 2024 and 7075, which have been the focus of many studies in both dissimilar butt

joint and lap joint configurations [67, 69, 142, 143, 144, 145, 146]. A 7xxx alloy structural member, which could be a stringer, ring frame, rib, or spar, is most often welded to the inner surface of a 2xxx alloy skin panel, creating a lap joint with the weld crown on the interior of the aircraft and the smooth weld root on the exterior of the aircraft. This configuration is preferable for cosmetic and perhaps aerodynamic purposes, although the alternate configuration may actually exhibit superior mechanical characteristics [68]. The aircraft structural components just mentioned are illustrated in Figures 52 and 53.

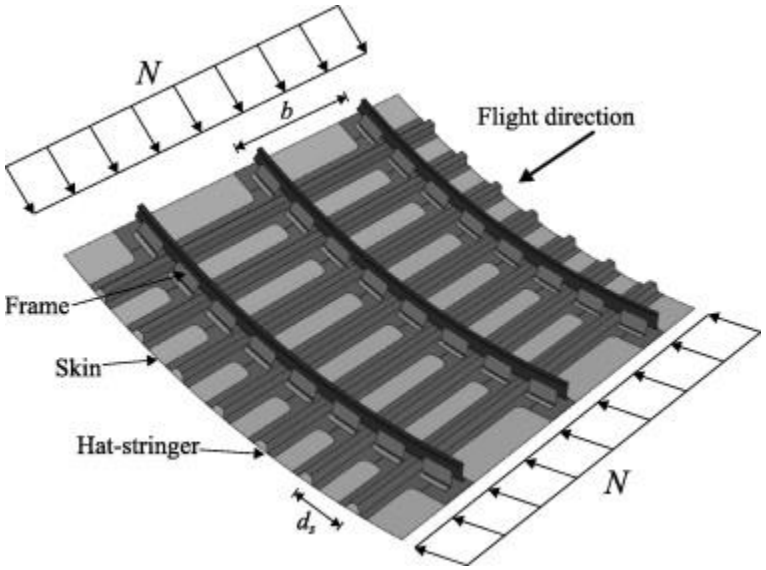

Figure 52: Aircraft Fuselage Stringer and Frame Construction [147]

The 2xxx series alloys include some of the earliest aluminum alloys produced and have been utilized extensively in the aviation industry for both skins and internal structural members. When higher strength aluminum alloys, such as the 7xxx series, were introduced, they were used to replace the internal 2xxx series structural members while

the 2xxx series skins remained. Using a higher strength alloy meant that the size of the structural members could be reduced, thereby maximizing the cabin space of the aircraft.

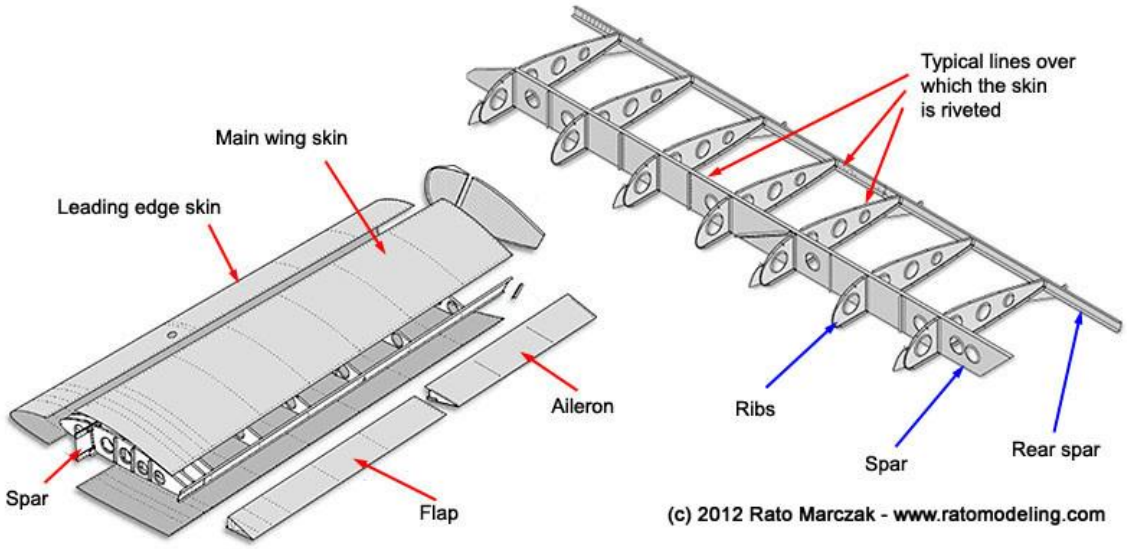

Figure 53: Classic Aircraft Wing Construction [148]

This is especially critical for smaller aircraft, such as the Eclipse 500, very light jet (VLJ). Eclipse Aerospace, formerly Eclipse Aviation, developed an FSW process to join its Eclipse 500 VLJ (pictured in Figure 54), finding that FSW enabled joining speeds 6 times faster than automated riveting (4.5 inch/min) and 60 times faster than manual riveting [124, 149]. This rapid joining speed was the primary motivation for Eclipse to first explore using FSW, as it was necessary for a business model based on high volume manufacturing, producing and selling upwards of 1500 aircraft per year [150]. The Eclipse 500 has a total of 263 friction stir welds that total 136 m in length and replace 7,378 conventional fasteners. Stringers and frames are welded to pocketed skins to construct integrally stiffened skin panels for the cabin, aft fuselage, and wings. The joints have 2.4 times the static tension (lap shear) strength of single-row riveted joints,

and the fatigue life of the FSW joints equals or exceeds the fatigue life of comparable riveted joints, easily exceeding the 8 lifetime cycle requirement [124, 149].

Figure 54: Eclipse 500 Very Light Jet; Completed RH Cabin Assembly (Left) [149], In Flight (Right) [151]

Because of successful examples of FSW used as a rivet replacement technology, as in the manufacture of the Eclipse 500 VLJ, many other commercial aerospace manufacturers have also implemented the use of FSW or are evaluating the technology for use on future aircraft. Embraer has evaluated the technology for use on its Legacy 450 and Legacy 500 models [152, 153], Bombardier has tested FSW tooling for use in the manufacture of Regional aircraft, which typically experience higher loads and longer life cycles [154], and Airbus has worked to incorporate friction stir welded skin joints on the fuselages and wings of the A340 and A350 models [155, 156].

In terms of weight reduction, FSW creates an advantage by eliminating the protruding heads of the rivets. In aviation, aluminum is the most common rivet material. Alloys include 1100, 2117, 2017, 2024, 5056, 7075. It is common for alloys other than 1100 to be anodized. Both solid shank and different types of blind rivets are utilized, depending on the joint configuration and ease of access. Two head types are most

common. These are the Universal (AN470 or MS20470) and Countersunk (AN426 or MS20426). The Universal style will have a protruding head on each side of the joint, whereas the Countersunk is flush on one side and has the shop head on the back side, which makes it appropriate for exterior skins in aerodynamically critical locations. Dubourg et al. confirmed the advantages of FSW over riveting with a comparison of a variety of aerospace appropriate lap joint configurations displayed in Figure 55.

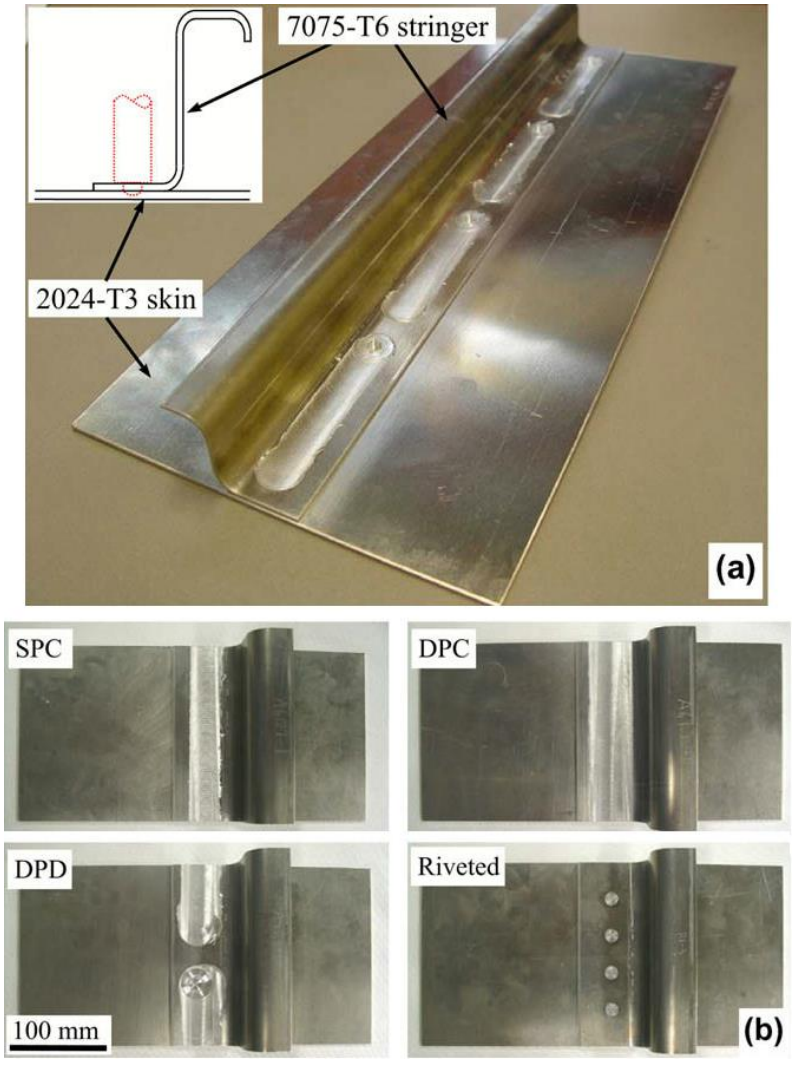

Figure 55: (a) 1.5 mm 7075-76 Stringer Welded to 2.3 mm 2024-T3 Skin; (b) Lap Joint Configurations: Single Pass Continuous (SPC), Double Pass Continuous (DPC), Double Pass Discontinuous (DPD), Riveted [69]

It was found that double pass continuous welds with overlapped advancing sides exhibited greater fatigue life than riveted sections [69], and as previously discussed, Eclipse Aerospace documented the mechanical advantages of FSW over rivets in the manufacturing of the Eclipse 500. The exact weight savings associated with FSW have not been as well documented however, although conservative estimates can be made. On the Eclipse 500 (or new model 550), if all 7,378 conventional fasteners eliminated by FSW happened to be solid shank, aluminum, universal head rivets of 1/8" diameter and 5/16" length used to join 0.063 inch thick sheet, the weight of the protruding heads, and thus the weight savings by using FSW, would be approximately 6.1 lbs. This is 0.17% of the aircraft empty weight (3,634 lb) [157] and a favorable weight savings estimate as in reality many of the eliminated fasteners would likely have been countersunk rivets. On larger aircraft, which are typically assembled using hundreds of thousands, if not millions of rivets, the weight of the protruding heads could possibly reach into the thousands of pounds, but would still likely represent a fraction of a percent of the aircraft weight. While any weight savings is perhaps significant, and this is indeed an advantage of FSW over riveting, the primary advantages of FSW over riveting are welding speed and joint strength, along with part elimination and cost reduction. There are additional studies that have examined FSW as candidate joining method in aerospace manufacturing [158], and one significant aspect of this that cannot be ignored is in-service corrosion prevention.

Corrosion Prevention

Welded components that are exposed to in-service corrosive environments, which are commonplace in automotive and aerospace applications, must have some measure of

built-in corrosion prevention. This is especially true when considering the lap joint configuration, which has faying surfaces in contact that lead directly into the weld from the side. The potential for crevice corrosion and, in some cases, galvanic corrosion must be addressed directly from the design and manufacturing phase. One method of preventing in-service corrosion is to apply sealants directly into lap joints before welding. During the welding process, the pressure of the FSW tool squeezes sealant away from the nugget, concentrating it at the faying surfaces, and the heat input from welding creates a beneficial accelerated rate of sealant curing [159]. Cured sealant then prevents ingress of corrosion for the life of the welded component. However, the incorporation of sealants into welding processes adds a level of complexity, and it can be very difficult to properly control sealant application [68]. For these reasons, this aspect of FSW in manufacturing has recently gained attention from researchers.

Li et al. examined the use of PRC 1750 sealant applied prior to welding in lap joints of 0.080 inch thick 7075-T6 [160]. Four different factors were studied from weld strength, macrograph characteristic, and corrosion prevention perspectives: conventional versus modified FSW tools, high (815 rpm, 5 IPM) versus low (815 rpm, 15 IPM) weld pitches, no sealant versus uncured or cured (clamped 48 hours prior to welding) sealant, and welding through versus welding between sealant, which was applied in beads of 1/16 inch diameter onto the bottom sheet. Figure 56 displays the two sealant configurations.

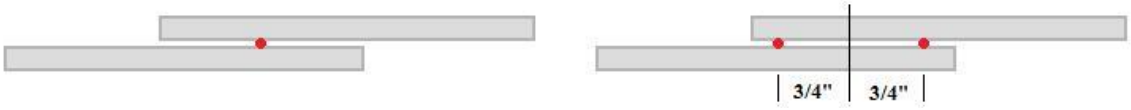

Figure 56: Two Sealant Applications Evaluated by Li et al. [160]: Welding Through Sealant (left) and Welding Between Sealant (right)

After welding, some specimens were exposed to a 500 hour salt spray. None of the specimen macrographs displayed evidence of corrosion attack at the faying surface. Corrosion was evident however at the TMAZ/HAZ on the top surface. The presence of sealant had mixed results on the size of sheet-thinning and hooking defects. The highest lap shear load of approximately 3300 psi was obtained with the modified tool at the low weld pitch with the advancing side machined outboard on the tensile specimen and with no sealant and no exposure. The presence of sealant has a significant negative impact on tensile strength for only one combination: the modified tool at the high weld pitch with the retreating side machined outboard on the tensile specimen. Interestingly, corrosion testing actually increased tensile strength in two cases: no sealant welds and sealant welds with the conventional tool. Li et al. noted that natural aging of the as-welded 7075 alloy in near W temper likely played a part, as the corrosion test specimens were pulled approximately one month after the non-exposed specimens. Corrosion testing slightly reduced the tensile strength of the sealant welds with the modified tool. Unfortunately, for all tensile strength and failure mode data presented, the authors did not distinguish between cured and uncured sealant or welding through versus welding between sealant [160].

Brown evaluated the use of PR-1432-GP sealant in Octaspot^{TM} swept friction stir spot welded specimens of 2024-T3 with various surface treatments in 1 mm (0.040 inch) thickness [161]. Surface treatments included AlClad, Alodine chemical conversion coating, and Chromic Acid Anodization (CAA). Welded specimens with no surface treatment were created for comparison as well. Specimens were tensile tested and fatigue tested, and then a second set of specimens was exposed to a 240 hour alternate immersion

cycle in a 3.5% NaCl solution after pre-fatiguing and then tensile tested and cross-sectioned for examination. Figures 57 and 58 display corroded coupons and a comparison of ultimate shear strength among pristine and corroded specimens after exposure, respectively.

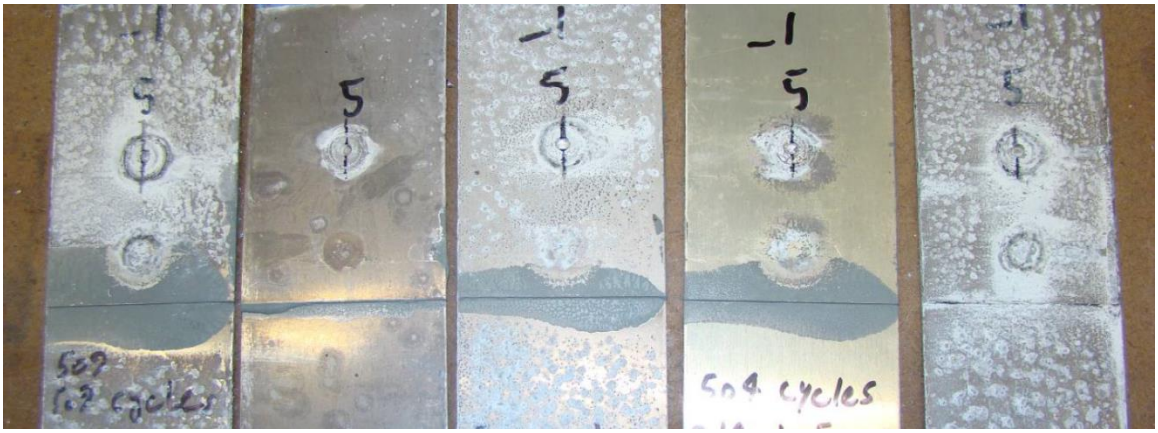

Figure 57: Corroded Swept Spot Weld Specimens (left to right): Bare with Sealant, AlClad with Sealant, CAA with Sealant, Alodine with Sealant, Bare without Sealant [161]

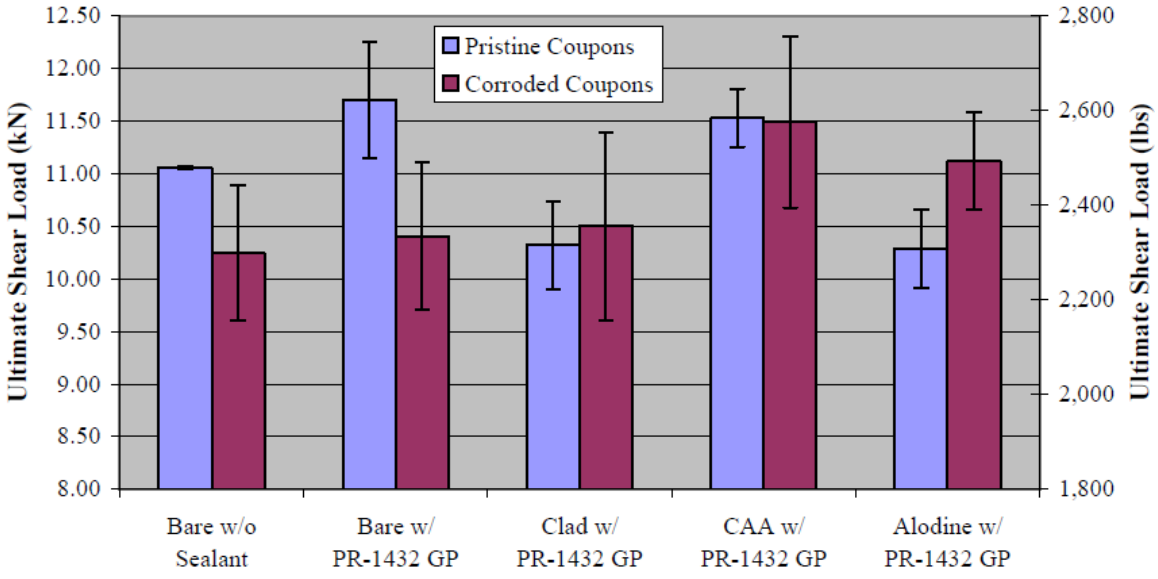

Figure 58: Swept Spot Weld Specimen Strengths Before and After Corrosion [161]

Overall, it was shown that swept friction stir spot welding can be performed successfully through sealants and surface treatments. Sealants and surface treatments indeed helped to prevent degradation from corrosive immersion; however, both corrosion exposure and the presence of sealant in joints led to greater standard deviations or less consistency in the strength of welded coupons. Sealant slightly decreased joint strength in some cases, but sealant and surface treatments had only minimal impacts to fatigue life. Brown also evaluated riveted coupons for comparison and found that on average they exhibited only 35% to 44% the strength of swept friction stir spot welded coupons in bare metal without sealant [161].

Doering investigated the friction stir welding of anodized 2024-T8 sheet in 1.18 mm (0.125 inch) thickness to anodized 357-T6 cast T-rails with the incorporation of sealants [162]. This joint configuration is depicted in Figure 59.

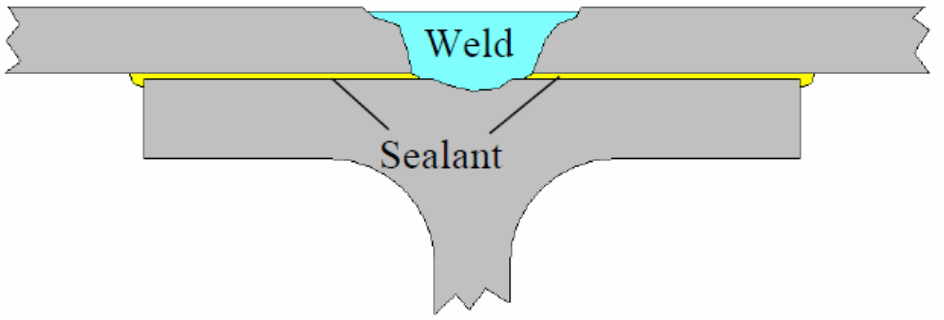

Figure 59: Lap on T-Rail Joint Configuration [162]

The purpose of incorporating sealants was to restore the fatigue life of specimens that had been exposed to a corrosive immersion. The sealants investigated were silicone rubber and nylon-11. Silicone rubber was applied in the uncured state, and nylon-11 was applied as a prefabricated sheet. Doering extensively examined the adhesive properties

of the sealants themselves to determine how they interacted with the welded joints under loading conditions. Properties of the sealants and results from weld evaluations indicated that the two sealants reach optimal utilization under different environmental conditions. The nylon-11 sealant performed best in the ambient environment and, while requiring modified welding parameters to create additional heat input, demonstrated potential for contributing to fatigue life significantly, given sufficient adhesive bond strength. The silicone rubber sealant on the other hand could be welded with the same parameters as non-sealant welds and showed promise for improving corrosion fatigue performance, given the selection of an elastomer material with sufficient elongation properties and high temperature resistance [162].

Research of this nature, with a direct focus on applications and including critical factors influencing success, such as the incorporation of corrosion prevention measures, in both the manufacturing and in-service phases, has become very important. Increased production volume in aerospace manufacturing in particular is dictating that more processes, such as sealant application, be performed by industrial robots [163]. This in turn is driving a need for automated systems that ensure conformance to standards, such as in-process sealant application quality monitoring and control capabilities. Addressing special issues in manufacturing such as these is largely the focus of the work presented in this dissertation.

CHAPTER III

IN-PROCESS DETECTION OF FAYING SURFACE SEALANT APPLICATION FLAWS

Portions of this chapter are published in:

Gibson, B.T., Wilkes, D.M., Cook, G.E., Strauss, A.M., "In-Process Detection of Faying Surface Sealant Application Flaws in Friction Stir Welding," *AIAA Journal of Aircraft*, Vol 50, No 2, 2013, pp. 567 – 575. DOI: 10.2514/1.C031939

Abstract

In this study, a process for detecting faying surface sealant application flaws in Friction Stir Welded (FSW) lap joints is developed. It utilizes a technique shown previously to enable the detection of machined gaps in the same joint type. This technique involves computing the frequency spectra of process forces and reducing the dimensions of the data using well-known methods for discrimination purposes. Aluminum alloys 2024-T3 and 7075-T6 in 0.063 inch (1.6 mm) thick sheets were welded with a variety of PR-1432-GP sealant configurations, including in both the cured and uncured state and applied in the tool path and adjacent to the tool path. It is shown that sealant flaws, such as gaps or thin spots, can indeed be discriminated from control welds with proper sealant application, and the success of this technique depends directly on the input force signal, the sealant configuration, and the dimensional reduction method. Factors affecting the real-time implementation of this technology in aerospace manufacturing are also examined.

Introduction

Friction Stir Welding (FSW) is rapidly advancing as a rivet replacement technology [140, 141]. In recent years, numerous studies have been conducted using common aerospace alloys, Al 2024 and Al 7075, in dissimilar butt joint [143, 144, 145, 146, 142] and lap joint [67, 69] configurations. In a lap joint configuration, a stringer of 7075 is often welded to the inner surface of a 2024 skin. Sealant can also be applied in the joint prior to welding, and the heat of the welding process then accelerates curing [159]. The sealant will then help to prevent the ingress of corrosion at the faying surface for the life of the joint. An example of industrial implementation of this technology is in the manufacturing of the Eclipse 500 business class jet. In this case, FSW is used to join stringers and frames to pocketed skins to construct integrally stiffened skin panels. The aircraft skins that are welded include the cabin, aft fuselage, and wing skin panels. This technology leads to a reduction in parts, decreased cycle times, lower manufacturing costs, reduced weight, and stronger joints [124, 149]. Because of these benefits, many aerospace manufacturers are working to incorporate this technology into their aircraft [152, 153, 154, 155, 156].

Increased implementation of this technology will arise from increased confidence and expertise in joining with sealants that can be gained through further research and development. Li, et al. showed that using PRC 1750 sealant in a variety of configurations, including cured and uncured, and applied in the tool path or adjacent to the tool path, would prevent crevice corrosion in FSW lap joints of 7075-T6 in 0.080 inch (2 mm) thickness. The presence of sealant also had a significant negative impact on shear strength in only one parameter combination in the study [160]. In this paper, PR-

1432-GP corrosion inhibitive sealant was used, which has been shown to prevent crevice corrosion while only slightly decreasing joint strength and having a minimal impact on fatigue life in swept Friction Stir Spot Welds (FSSW) of 2024-T3 with various surface treatments in 0.040 inch (1 mm) thicknesses [161].

An important aspect of this technology that will affect its transition from the laboratory to manufacturing applications, however, is quality control. Sealant application must be precisely controlled, and it can be challenging even when using a manual method [68]. Ensuring the quality of sealant application will become even more difficult when it must be done on a large scale in a high volume manufacturing environment, particularly if automated processes are used. The focus of this paper is the development of a process for detecting flaws in sealant applications, such as gaps or thin spots, applying a technique first used by Fleming, et al. to detect machined gaps in FSW lap joints [133]. This technique involves analyzing the frequency spectra of the process forces and reducing the dimensions of the data using well-known methods. Fleming, et al. showed it to be effective in distinguishing machined gaps as small as 0.0002 inch, and in this paper it is tested on a variety of sealant configurations with intentionally introduced flaws in the lap joints of aerospace alloys.

Technical Approach

Material and Parameter Selection

Aluminum alloys 2024-T3 and 7075-T6 in 0.063 inch (1.6 mm) thick bare sheets (AMS-QQ-A-250/4 and AMS-QQ-A-250/12 specifications, respectively) were selected

for this study. Table 1 displays the chemical composition limits for these alloys. It is believed that welding parameters (rotation rate and particularly welding speed) can affect the process of flaw detection; therefore, a parameter study of non-sealant welds was performed in order to justify the welding parameters that would be used for the sealant flaw detection portion of this study.

Table 1: 2024 and 7075 Chemical Composition Limits [164, 165]

	CHEMICAL COMPOSITION LIMITS (WT. %) *Value is maximum if range not shown. Principle alloying elements highlighted.*										
	Si	Fe	Cu	Mn	Mg	Cr	Zn	Ti	Others, each	Others, total	Al
2024	0.50	0.50	3.8 - 4.9	0.30 - 0.9	1.2 - 1.8	0.10	0.25	0.15	0.05	0.15	Balance
7075	0.40	0.50	1.2 - 2.0	0.30	2.1 - 2.9	0.18 - 0.28	5.1 - 6.1	0.20	0.05	0.15	Balance

FSW lap welds were created with a top sheet of 7075-T6, simulating a stringer, and a bottom sheet of 2024-T3, simulating an aircraft skin. Rotation rates of 600, 900, 1200, and 1500 rpm were tested along with welding speeds of 8, 14, and 20 inches per minute (IPM). Coupons 9 inches in length were welded perpendicular to the rolling direction with a 0.625 inch (15.9 mm) diameter scrolled shoulder tool with a 0.25 inch (6.35 mm) diameter threaded, fluted probe that penetrated the bottom sheet by 30% of the top sheet thickness. Figure 60 displays an image of the FSW tool. A heel plunge depth of 0.002 inch and a lead angle of 2 degrees were used. The advancing side of the weld was placed adjacent to the lapped edge which simulates rotating towards an upright leg of a stringer at the leading edge of the tool and places any cold-lap defect that may be present in the load path for shear testing. This geometry has shown to produce superior results [68, 160]. Figure 61 displays the top side of a completed weld from this parameter study.

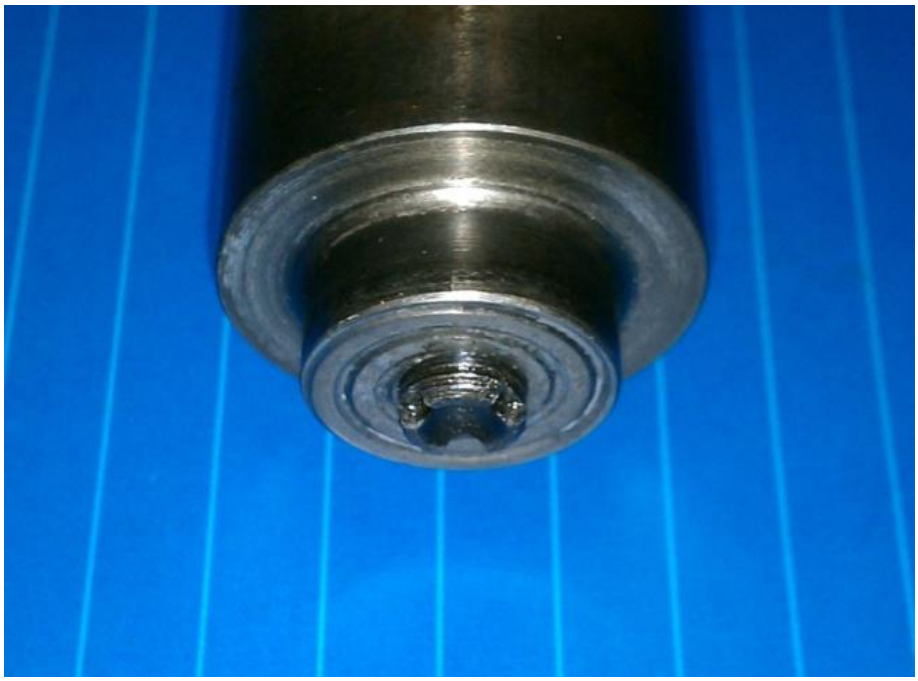

Figure 60: FSW Tool

Welds were evaluated by performing unguided tension-shear tests and hammer S-bend tests after approximately 165 hours of natural aging. Figure 62 shows a sample of tension-shear and S-bend specimens.

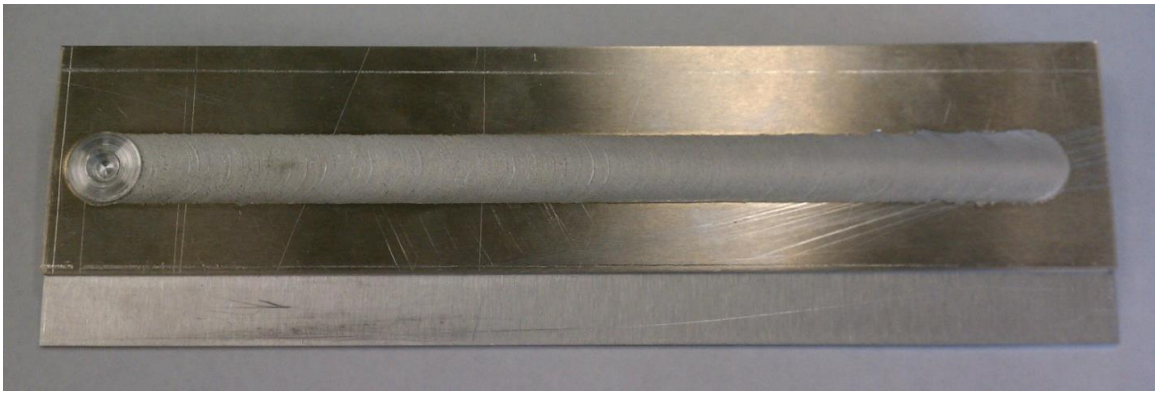

Figure 61: Parameter Study Lap Weld

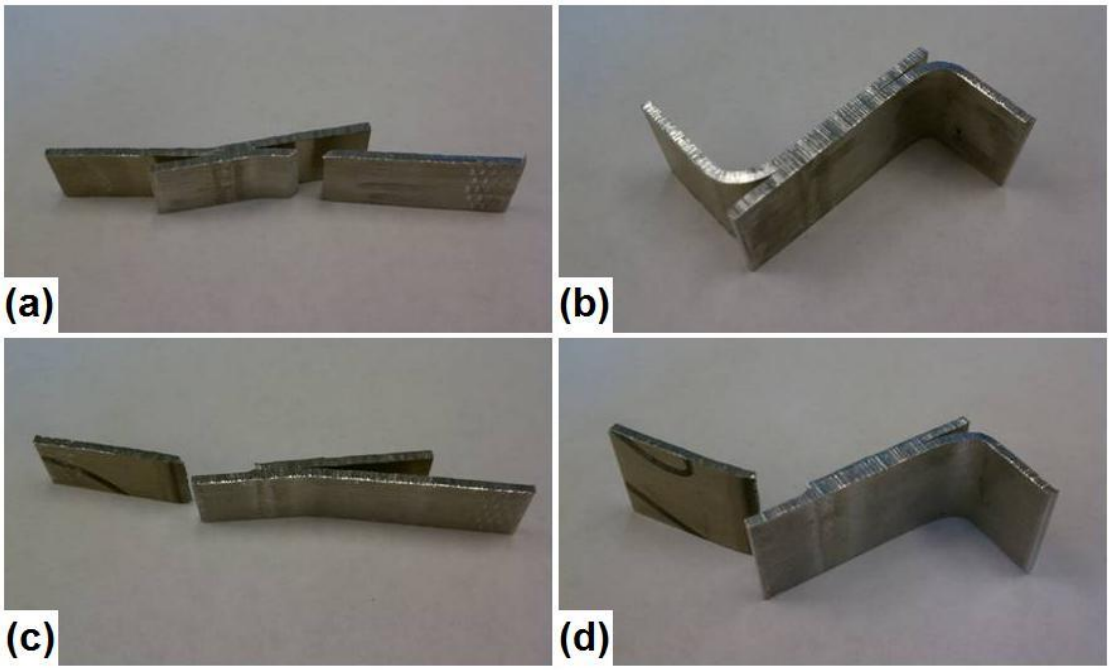

Figure 62: Tension-Shear and S-Bend Specimens: (a) Bottom sheet, parent failure; (b) Passing S-bend test; (c) Top sheet, nugget failure; (c) Failing S-bend test

During tension-shear testing, all samples exhibited pull-out fracture, failing in either the top or bottom sheet and either adjacent to the nugget or in the parent material. No samples exhibited interfacial fracture. It is for this reason that the tensile strength of the specimens has been reported as a quantitative comparison of the welding parameters. Figure 63 displays the ultimate tensile strength of the specimens. The 2024-T3 bottom sheet parent material has a tensile yield strength of 48 ksi (331 MPa) and an ultimate tensile strength of 65 ksi (448 MPa), while the 7075-T6 top sheet parent material has a tensile yield strength of 72 ksi (496 MPa) and an ultimate tensile strength of 80 ksi (552 MPa) [166]. Some interesting trends can be seen in Figure 63. Tensile strength increased with increasing rotation rate for all welding speeds. Tensile strength increased with increasing welding speed at the 1200 rpm and 1500 rpm rotation rates, but decreased

at the 900 rpm rotation rate. Only the lowest welding speed was tested at 600 rpm. The strength of the welds made at 1500 rpm approach the ultimate strength of 2024, the weaker of the two materials.

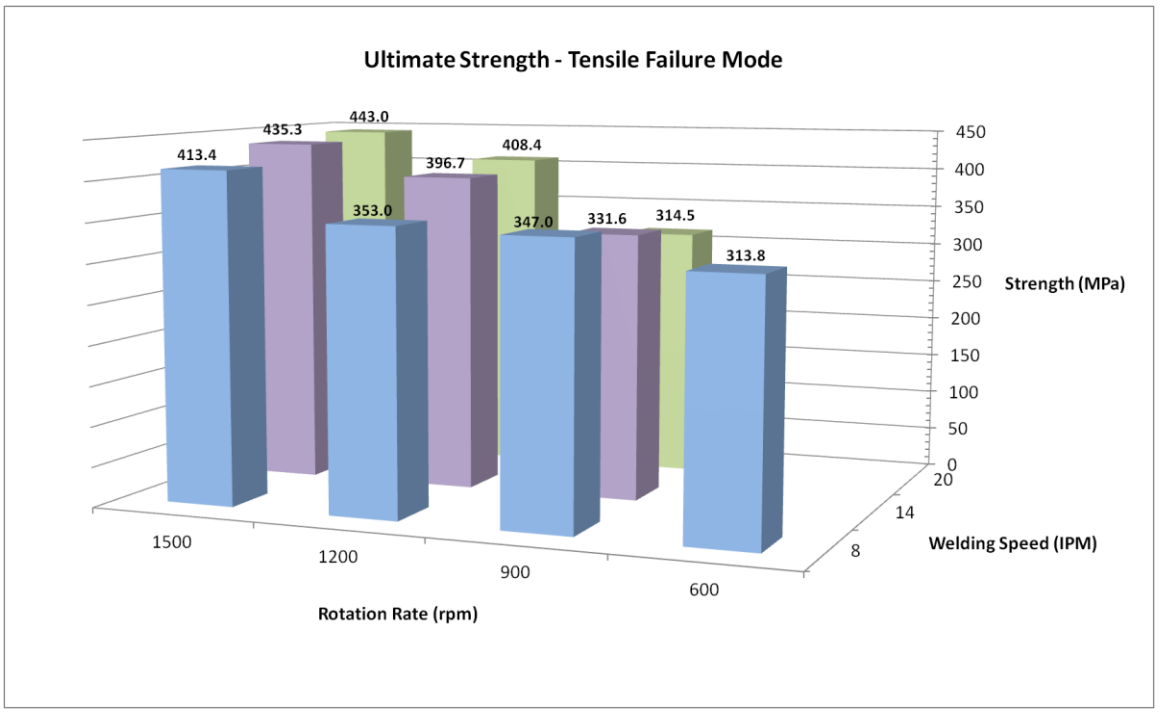

Figure 63: Ultimate Tensile Strength of Welded Samples

In general, the strongest welds occurred at higher rotation rates, at which there is less probability of a cold lap defect. These weld specimens tended to fail in the 2024 parent material, at what is likely the edge of the HAZ, as seen in Figure 62(a). At lower rotation rates, weld specimens tended to fail at the retreating side of the 7075 top sheet, as seen in Figure 62(c). Further analysis of common lap joint defects and failure modes was beyond the scope of this study, as the main focus was on developing a system for in-process detection of sealant application flaws.

Based on these results, the parameters selected for the sealant flaw detection study were 1500 rpm and 14 IPM. This combination had the second highest strength (a 97% joint efficiency based on 2024 ultimate strength), and its specimens had more consistent failure modes than the 20 IPM welding speed at 1500 rpm. It was also believed that traversing at a lower speed could lead to a higher probability of detecting a flaw because there is a longer time window from which to extract data for a particular sealant gap or thin spot, and for this reason, 14 IPM was a more desirable parameter than 20 IPM.

Experimental Methods

The sealant selected for use in this study was PR-1432-GP, manufactured by PRC-DeSoto. PR-1432-GP is a two-part, dichromate polysulfide compound that can be applied by spray or brush in the uncured state [167]. The sealant thickness must be controlled precisely between 0.002 inch and 0.004 inch during application [68]. A weld matrix was designed that included control welds with proper sealant application and welds with 1 inch long gaps in sealant or 1 inch long thin sections of sealant. Welds were performed with sealant in both the cured and uncured states, and in a full application and an edge application, where sealant is not applied directly in the tool path. Welds with machined gaps of 0.003 inch depth were also performed for comparison purposes. Figure 64 depicts these various configurations with transparent top sheets so that the sealant layer is visible. Prior to sealant application, both top and bottom sheets were cleaned with a 50% MEK and 50% toluene solvent using lint-free wipes and then cleaned again using pre-wetted isopropyl alcohol wipes.

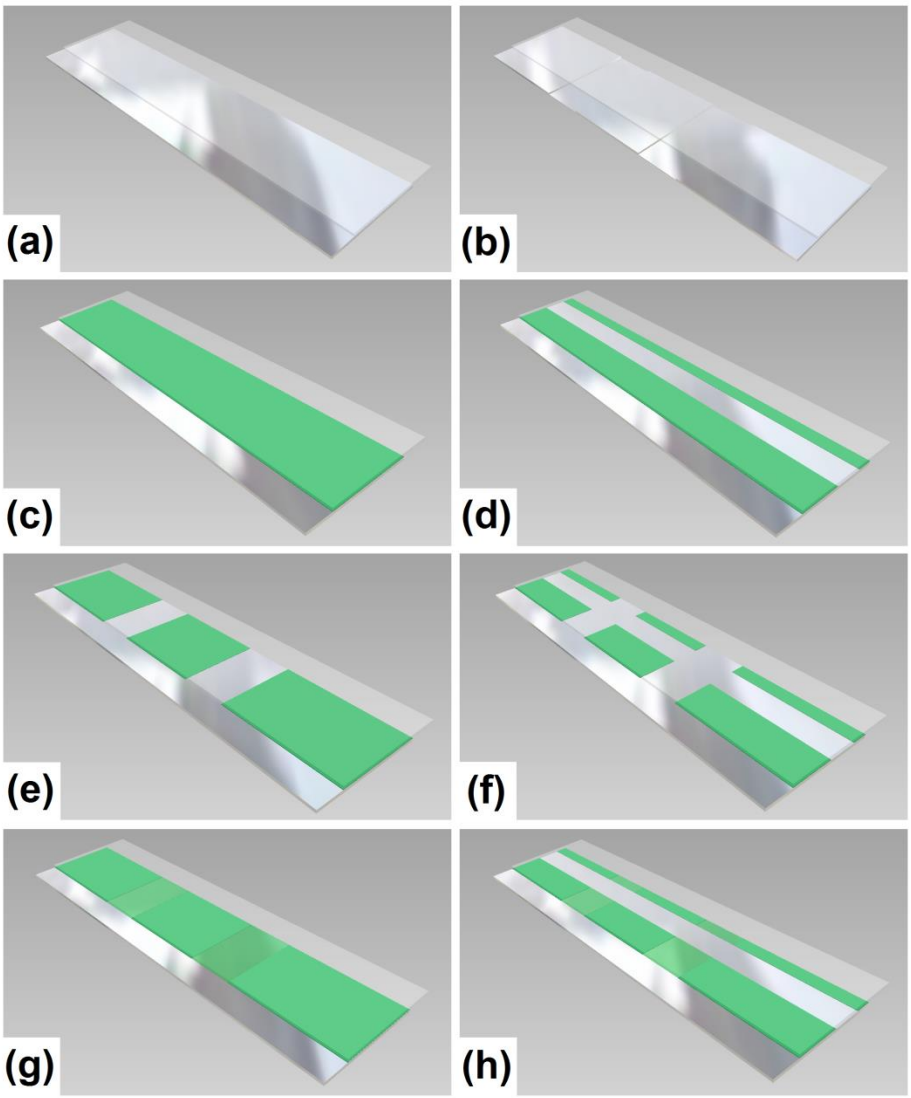

Figure 64: Sealant Configurations: (a) No Sealant; (b) Machined Gaps; (c) Full Sealant; (d) Edge Sealant; (e) Full Gap; (f) Edge Gap; (g) Full Thin Sealant; (h) Edge Thin Sealant

The two part sealant was mixed and then diluted with the same solvent so that it could be controlled to between a 0.002 and 0.004 inch thickness using a roller with a 0.25 inch nap. The sealant thickness was measured with a Gardco WF-2110 precision wet film thickness gauge. Copper tape was used to mask the non-sealant areas of the samples. Figure 65 shows the application process for the full gap and edge gap samples.

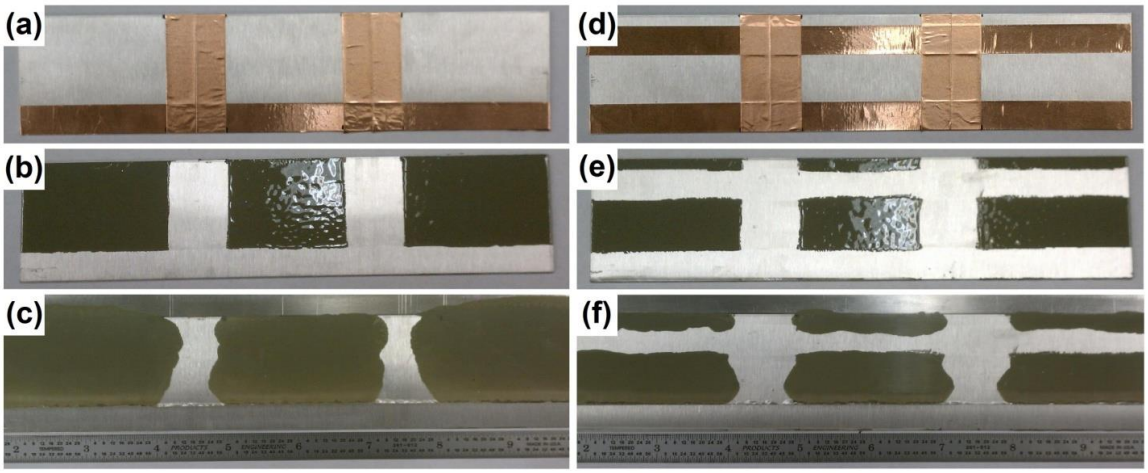

Figure 65: Sealant Application: (a) Full Gap Masked; (b) Full Gap Applied; (c) Full Gap Clamped; (d) Edge Gap Masked; (e) Edge Gap Applied; (f) Edge Gap Clamped

Figure 65 (c) and (f) show how the sealant wets out additionally after the top sheet is applied and the sample is clamped. This was shown by replacing the top sheet with a piece of clear acrylic and then clamping the sample normally. Clamping the full gap sample reduced the sealant gap width to a minimum of 0.375 inch. Clamping the edge gap sample reduced the sealant gap width to a minimum of 0.625 inch; however, the gap remained 1 inch at the tool path. Welds with uncured sealant were performed within 1 hour of sealant application. For welds with cured sealant, the top sheet was positioned after the sealant had been applied, and the sample was then clamped and allowed to cure for approximately 95 hours, which is a more than sufficient cure time for this sealant [167]. Weld samples with thin sealant sections were created in the cured state only. First, a layer of sealant approximately 0.001 inch thick was applied and allowed to cure without the top sheet in place. Next, the samples were masked, and an additional layer of sealant was applied at a thickness of approximately 0.001 to 0.003 inch. Figure 66 shows the samples after this step.

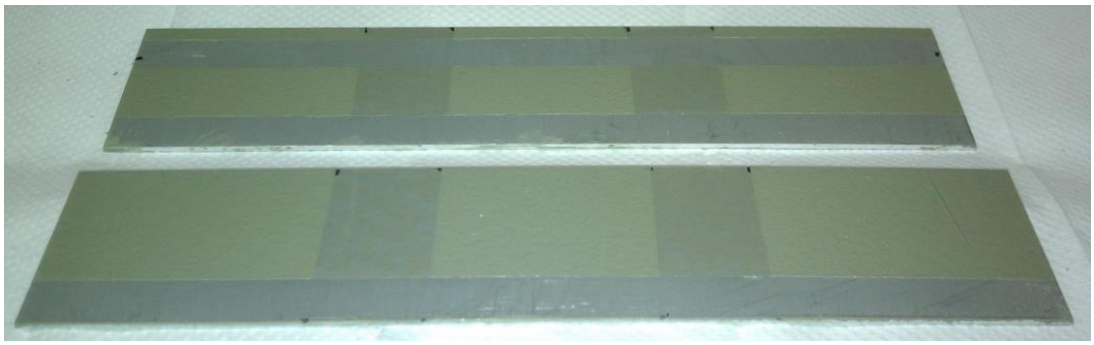

Figure 66: Thin Sealant Samples

Finally, the top sheet was positioned and the samples were clamped and allowed to cure. Welds were performed under a fume hood to minimize vapor exposure. Axial force (F_z) and torque (T) signals were collected using a custom force measurement system [107, 108, 109].

Data Analysis

First-Order Comparisons

Figure 67 displays the first-order force data for a machined gap weld and both cured and uncured sealant welds in the full gap configuration. The axial force decreased by approximately 1000 N while welding over a machined gap of 0.003 inch. This confirms a finding of Fleming, et al. [133]. This same trend can be observed in Figure 67 (b) for cured sealant in a full application. A decrease in axial force is not noticeable for the uncured sealant weld in Figure 67 (c), and a significant variation in the torque signal was not noticeable for any of the cases. While variations in the first-order data are evident for only certain configurations, these preliminary results were encouraging.

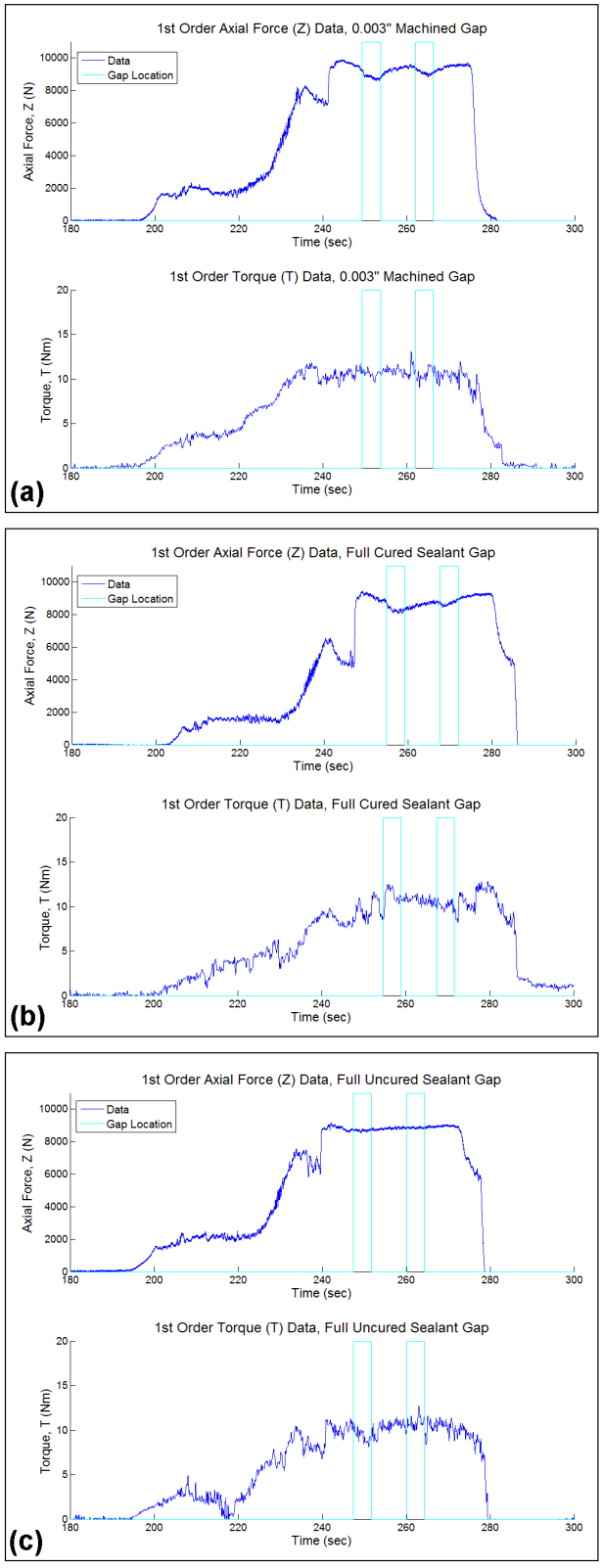

Figure 67: First-Order Force Data: (a) Machined Gap; (b) Full Cured Sealant Gap; (c) Full Uncured Sealant Gap

The decrease in axial force for the full cured sealant gap weld served as an indicator that techniques used to detect machine gaps may indeed work to detect sealant application flaws. Additionally, Fleming, et al. found that machined gaps smaller than 0.0012 inch that did not create noticeable changes in the first-order axial force data could be detected by computing the frequency spectra of the forces and then reducing the data to lower dimensional subspaces using techniques such as Principle Component Analysis or Linear Discriminant Analysis [133].

Frequency Analysis and Dimensional Reduction

The frequency domain of data from force or acoustic sensors has been demonstrated to be an excellent source of information for quality control in manufacturing, including in both FSW [129] and inertia welding, or solid-state friction welding [128]. In order to extract meaningful information from the sealant welds, the data was windowed by selecting 1 second long portions of axial force and torque data from the welds at certain locations. For gap or thin sealant welds, windows of data were selected from the flawed regions only, and for control welds, substantially more windows of data were selected from throughout the welds. These windows of force data were then normalized and transformed from the time domain to the frequency domain using the Fourier transform, which was computed in Matlab using the Fast Fourier Transform (FFT) method.

After the FFT was computed, each data set extracted from the welds was represented by a frequency spectrum, from which 25 frequency bins were selected. This means that the frequency information from each point of interest in any class (gap, thin

sealant, or control) was represented in a 25 dimensional space. In order to discriminate sealant flaws from control welds, dimensional reduction techniques were utilized that would remove redundancies in the data and allow for direct qualitative comparisons of the data classes in a lower dimensional space.

Principle Component Analysis (PCA) is an unsupervised technique, given no knowledge of the class labels, that searches data for directions of maximum variance and then projects the data onto them, creating a lower dimensional representation of the data [168]. This was performed by grouping each sealant flaw data set with its respective control data set, normalizing the data, computing the covariance matrix, computing and ranking the variances (eigenvalues) by magnitude, and computing the respective principle components (eigenvectors) which were then projected onto the original data [169].

Linear Discriminant Analysis (LDA) is a supervised technique in which class label information is provided to the algorithm. LDA seeks to minimize within-class scatter and maximize between-class scatter [168]. This is accomplished by maximizing equation (12), in which S_B is the between-class scatter and S_W is the within-class scatter, defined in equations (13) and (14), respectively, where x_i is a frequency data set, μ_c is the class mean, and $\bar{x}$ is the mean across all data classes.

$$J(w) = \frac{\boldsymbol{w}^T S_B \boldsymbol{w}}{\boldsymbol{w}^T S_W \boldsymbol{w}} \tag{12}$$

$$S_B = \sum_c (\mu_c - \bar{x})(\mu_c - \bar{x})^T \tag{13}$$

$$S_W = \sum_c \sum_{i \in c} (x_i - \mu_c)(x_i - \mu_c)^T \tag{14}$$

The objective of maximizing equation (12) can be achieved by solving:

$$S_B \boldsymbol{w} = \lambda S_W \boldsymbol{w} \tag{15}$$

which is a generalized eigen-problem. In a technique similar to what was done with PCA, the eigenvectors were computed and ordered by magnitude of the eigenvalues. The ordered vectors were then projected onto the original data.

For a visual comparison of C number of data classes, it is necessary to have C – 1 vectors to project onto. This means that discriminating between uncured sealant gap and control welds could be performed on a line plot, but for the cured sealant welds, which include gaps, thin spots, and control data, the visual discrimination must be performed on a 2D plot. For purposes of uniformity, all data was plotted on 2D plots, which display the data projections from the two principle components corresponding to the greatest two eigenvalues. Additionally, continuous windowing and PCA analysis was explored with the sealant flaw welds in order to examine the potential for developing a real-time flaw detection system using a completely unguided technique. The entire traverse sections of the welds were divided into 0.5 second data windows and the data was processed as before. Plots of the 1st component of PCA vs. traverse position were then generated to see if the results indicated the location of the sealant flaws.

Results

In order to examine the effect of input signal selection on sealant flaw detection ability, PCA results using axial force and torque were compared for different sealant

configurations. Figure 68 displays a sample of these comparisons for the full cured sealant configuration. PCA was selected for this examination because it is an unguided technique, and any subtle differences in class separation would be easily discernible. A more robust technique, such as LDA, might mask such differences.

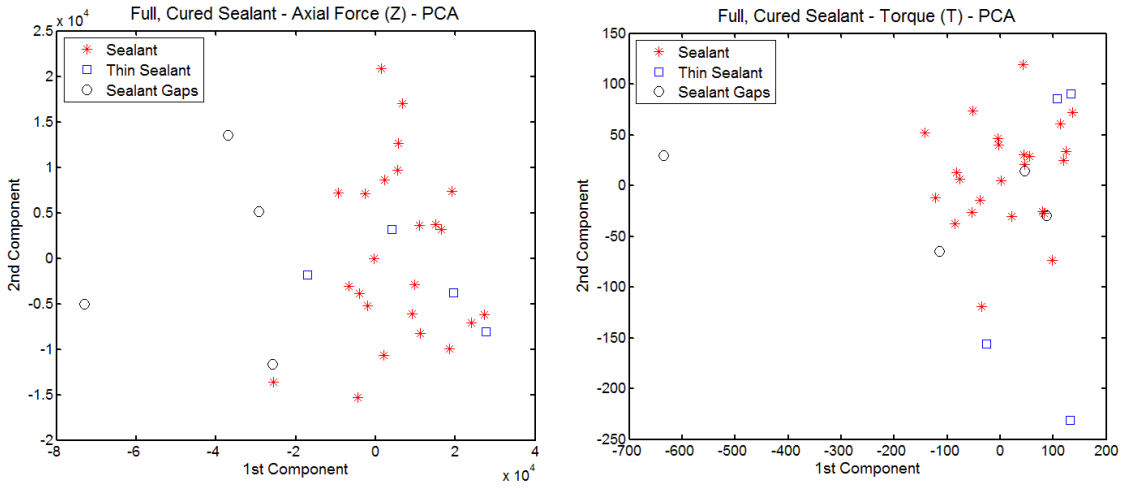

Figure 68: Input Signal Comparison

It is evident from Figure 68 that axial force is the more effective input signal based on the separation of the sealant gaps from the sealant data points in the case of full cured sealant. This was the most dramatic case, and although additional sealant configurations are not shown here, torque did not prove to be a more effective input signal for any of the sealant configurations. It is for this reason that axial force was selected as the input signal for the remainder of the analysis.

Figures 69 and 70 display the results of PCA and LDA, respectively. Examining the results of PCA, it can be seen that for the full cured sealant configuration, sealant data and sealant gaps are linearly separable in the 1st component.

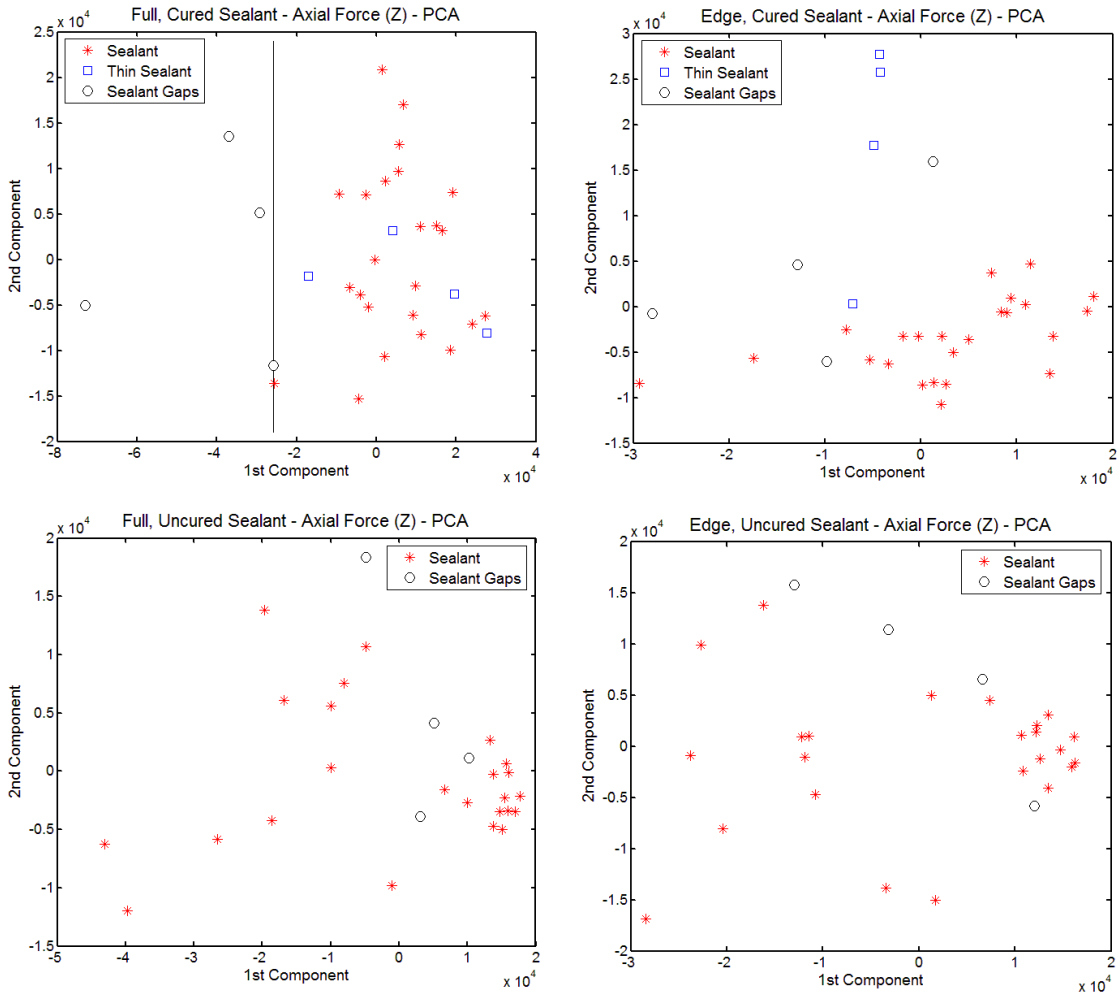

Figure 69: Results of PCA

This is the configuration that most closely mimics a machined gap due to the rigid nature of the cured sealant. Thin sealant data are not linearly separable using PCA for either the full or edge configurations. A very interesting observation is that the flaws in the edge cured configuration appear to be closer to being separable than the flaws in the full uncured configuration. This shows that the state of the sealant (cured or uncured) is a more important factor than initial sealant location in the weld path when it comes to flaw detection ability. For the cured sealant welds, the full configuration is more separable

than the edge configuration, but there is no such distinction for the uncured sealant welds, most likely because when welding with uncured sealant in a full application, the sealant is supposed to be squeezed away from the joint line to the faying surface by the pressure of the tool. This type of sealant migration is evident in Figure 71, which displays macrographs of the welded samples.

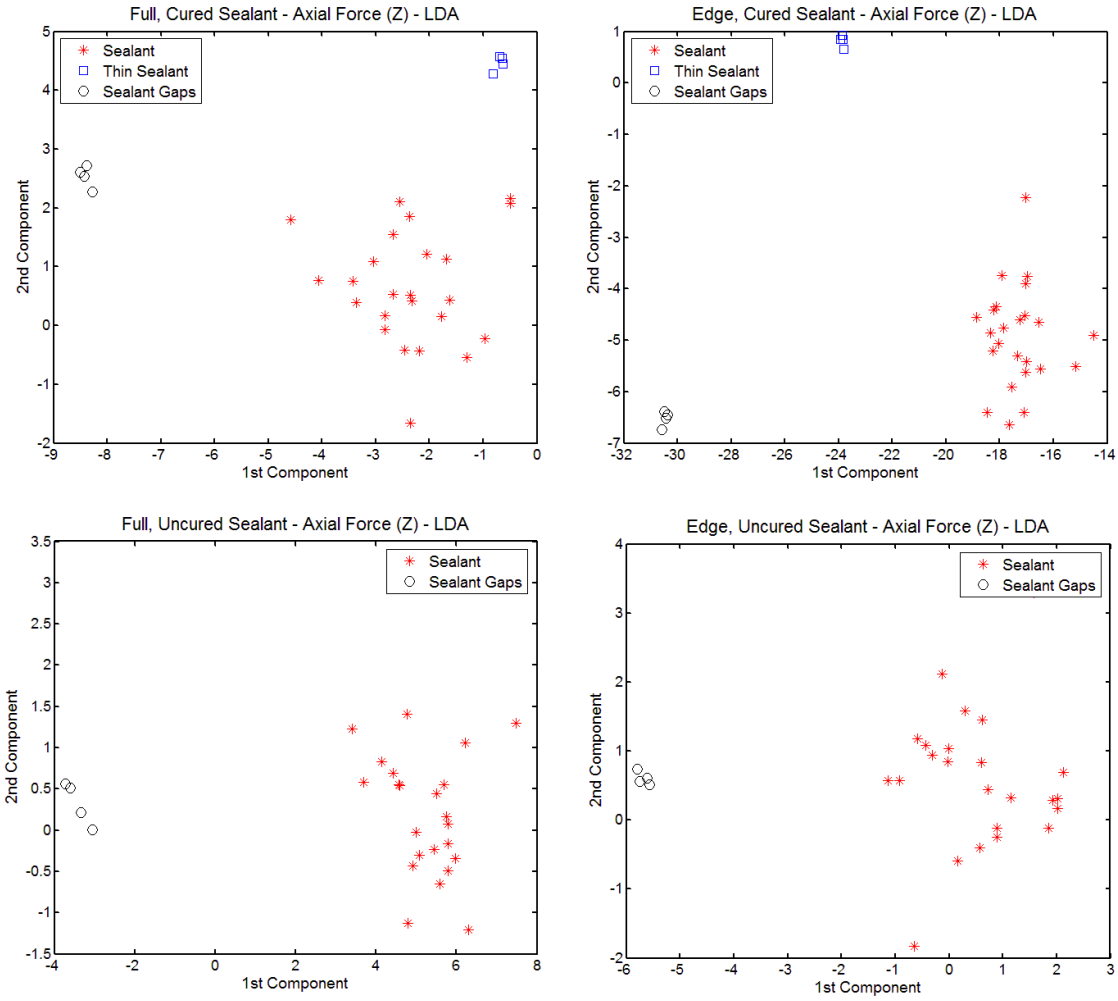

Figure 70: Results of LDA

Examining Figure 70, it can be seen that when LDA is used, sealant gaps and thin sealant become linearly separable from control data for all sealant configurations regardless of sealant state or initial location in the weld path. This is an excellent result, in that these findings could be used as the foundation for a robust real-time detection system that could detect flaws in even uncured sealant, which is most commonly used in FSW.

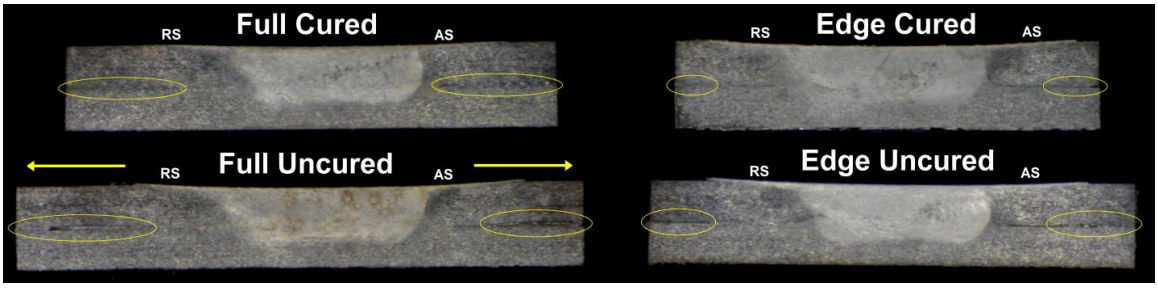

Figure 71: Macrographs of Welded Samples (Sealant Circled)

Figure 72 displays the results of continuous PCA analysis for a full cured sealant weld. The results of this technique were inconsistent from weld to weld. Figure 72 displays a successful case however in which gaps could be detected when data points in the 1st component of PCA fell below a detection threshold while the tool was passing over a sealant gap. Due to the inconsistency of this technique, it would likely not be a good technique to use for a successful real-time detection system.

A successful real-time flaw detection system will most likely be based on a robust, guided technique, like LDA, with a set of training data, rather than an unguided technique like PCA. Such a system may include the steps outlined in Figure 73. A processor would continually collect and analyze force data from a welding process and then cyclically compare it to training data to classify weld sections as good or bad.

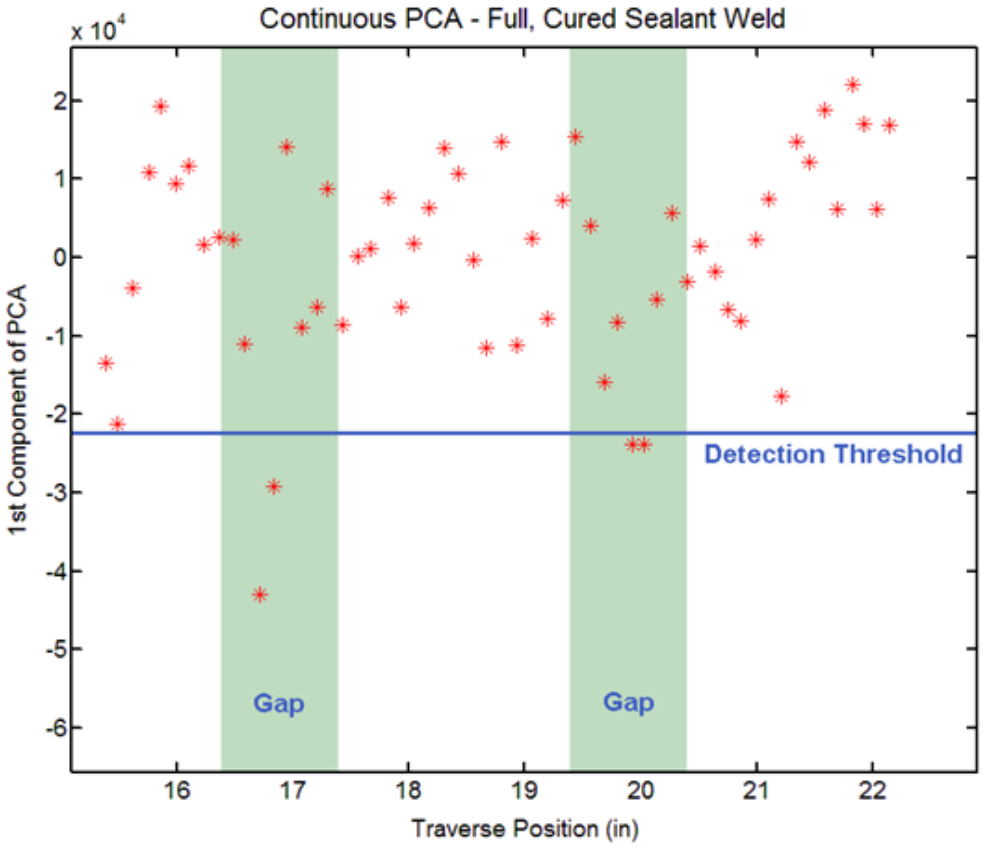

Figure 72: Continuous PCA with Full Cured Sealant

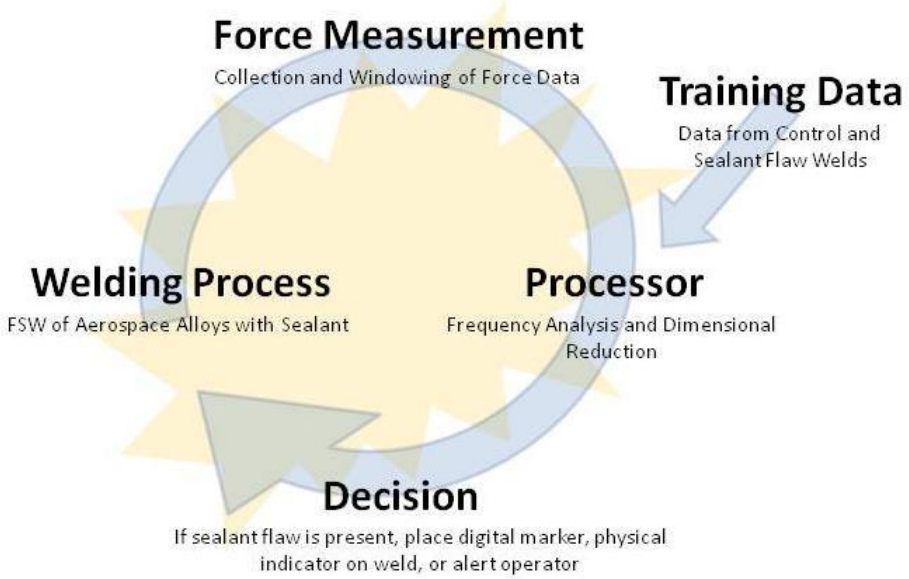

Figure 73: Flow Chart for Real-Time Sealant Flaw Detection

This would enable manufacturers to make informed decisions about accepting or rejecting parts, based on the quality of sealant application. On larger structures, such as aircraft assemblies, the potential may also exist for sealant flaw locations to be repaired using alternate sealant application methods. This type of system was preliminarily investigated by running offline simulations with an LDA classifier using previously collected training and test data from control welds and machined gap welds. The built-in MATLAB function, *classify*, was used to classify F_z frequency data windows, with some overlap, in a cyclical manner as either coming from good weld sections or weld sections with a gap.

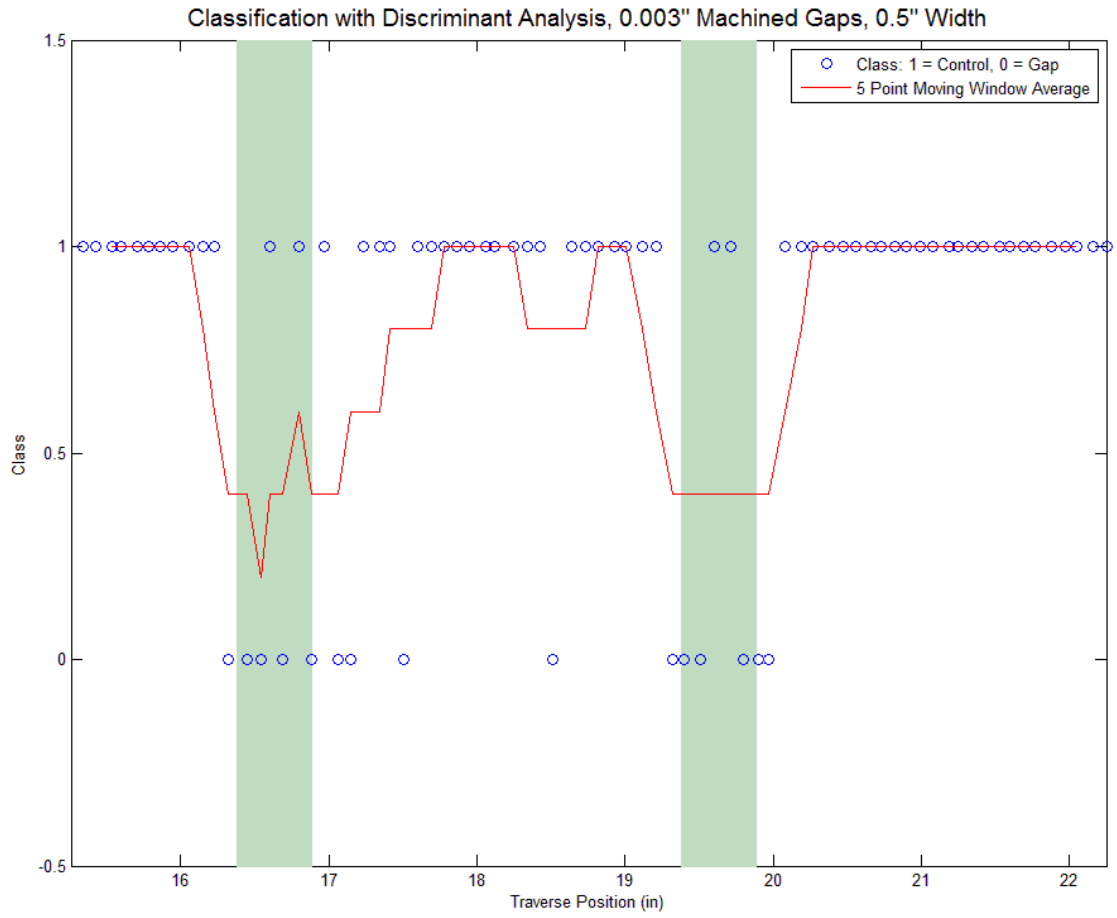

Figure 74: Output of Simulation of Real-Time Gap Detection Using LDA Classifier

When plotted, each output point was either a 1 (indicating good or control) or a 0 (indicating the presence of a gap), and then a moving window average was used to smooth the detection function and eliminate any artifacts. A threshold could then be selected, and if the average dips below that threshold, a gap would be detected. Figure 74 displays the output of this simulation for the 0.5 inch wide machined gap case. Appendix A contains more details about the simulations, including the inputs, variables, and the complete code. It can be seen however in Figure 74 that if the proper threshold were selected, perhaps 0.5, the output of the moving window average would dip below the threshold at the gap locations, enabling a real-time error signal.

Discussion and Conclusions

A technique that has been successfully used to detect machined gaps in FSW lap joints was tested on dissimilar lap joints of 2024-T3 and 7075-T6 alloys with a variety of PR-1432-GP sealant configurations, including in both cured and uncured states and in full and edge applications, to determine if flaws in the sealant application could be detected. A number of techniques for dimensional reduction and class discrimination were examined. The general conclusions which can be drawn from the results are:

1) Sealant flaws, such as gaps or thin spots, can indeed be discriminated from control welds with proper sealant application.

2) The success of this technique depends on the input force signal used, the sealant configuration, and the dimensional reduction method used.

3) A successful real-time flaw detection system will mostly likely be based on a robust, guided technique, such as LDA, with a set of training data, rather than an unguided technique like PCA.

This technology may be critical as FSW continues to be adopted as a rivet replacement technology in aerospace and related industries. Future work will continue to focus on determining the readiness of this technology for production implementation. Additional simulations may be done with an LDA classifier or there are other candidate technologies, such as neural networks, that should perhaps be investigated as methods for real-time classification. Implementation of a small-scale real-time system in the laboratory would then be appropriate.

CHAPTER IV

THROUGH-THE-TOOL TRACKING OF BLIND SEALANT PATHS

This chapter is published in:

Gibson, B.T., Cox, C.D., Ballun, M.C., Cook, G.E., Strauss, A.M., "Automatic Tracking of Blind Sealant Paths in Friction Stir Lap Joining," *AIAA Journal of Aircraft*, Vol 51, No 3, 2014, pp. 824 – 832. DOI: 10.2514/1.C032470

Abstract

An automatic joint tracking technique that employs an extremum seeking controller is evaluated as a method for automatically tracking sealant paths that have been applied in dissimilar friction stir lap joints of 2024 and 7075 aluminum alloys. Sealants are commonly used to prevent the ingress of corrosion at the faying surfaces of lap joints, and in this study, an attempt is made to exploit sealant presence to reduce necessary robotic path planning procedures. Controller parameters are tuned and baseline tracking performance is established with milled channels, which are used to replicate the force signature of sealant, and the tracking technique is then evaluated with Pelseal® 2077 sealant applied in a prescribed fashion in both cured and uncured states. Mechanical testing is conducted to determine the implications for weld strength when welding parameters are selected primarily for successful tracking. Results are promising and demonstrate a new level of interaction between sealants and robotic control techniques.

Introduction

In recent years, Friction Stir Welding (FSW) has deservedly garnered much attention from aerospace manufacturers [141]. As a rivet replacement technology on aviation structures, FSW has proven to offer numerous advantages [140]. These include weight savings, a reduction in parts, significantly faster joining speeds, increased joint strength, and lower manufacturing costs. This was demonstrated dramatically in the manufacture of the Eclipse 500 very light jet, which has a total of 263 friction stir welds that replaced 7,378 would-be conventional fasteners. FSW was used to create integrally stiffened skin panels for the cabin, aft fuselage, and wings and proved to be an indispensable technology in the quest to establish an entirely new class of aircraft [124, 149, 150]. Other manufacturers have incorporated the use of FSW into their aircraft or are evaluating the technology for use on future generations of aircraft: Embraer has tested fuselage sections fabricated with FSW for inclusion on the Legacy 450 and Legacy 500 models [152, 153], Bombardier has evaluated FSW tooling for use in a regional aircraft application [154], and Airbus has worked to incorporate longitudinal fuselage skin panels joined with FSW into multiple aircraft, including the A340 and A350 models [155, 156]. The incumbent materials for aviation structures are 2xxx and 7xxx series aluminum alloys. It is common for a 7xxx series structural member, such as a stringer, frame, rib, or wing spar, to be welded to a 2xxx series aircraft skin panel in a lap joint configuration. This particular combination of materials has been the focus of several studies in both butt and lap weld configurations [67, 69, 142, 143, 144, 145, 146]. One challenging aspect of the welding process that has not been as widely studied until recently, however, is the incorporation of corrosion preventative measures. In some applications, sealant is

applied between sheets before joining, and the heat of subsequent welding then accelerates the sealant curing process [159]. The cured sealant then prevents ingress of crevice corrosion and, in some cases, the potential for galvanic corrosion, at the faying surfaces of the joint throughout the service life of the welded component. The purpose of this study however, is to demonstrate that sealant presence within a weld seam can potentially be beneficial during the manufacturing phase as well. It will be shown that the force signature of sealant, if applied in a prescribed way, can be exploited in order to simplify robotic welding procedures and enable automatic tracking of a desired path.

Sealants

Sealants are typically viewed as an added complexity or necessary evil when they are incorporated into a joining operation as they can potentially impact both joint strength and fatigue life of welds made with previously established weld schedules and procedures. It can also be very difficult to control sealant application, even when using manual methods [68]. It is for these reasons that joining with sealants has recently become a research area of much interest. Li et al. evaluated the effectiveness of PRC 1750 sealant at preventing crevice corrosion in FSW lap welds of 7075-T6 in 2 mm (0.080 inch) thickness. Sealant was applied as a 1.6 mm (1/16 inch) bead in two configurations, either directly in the tool path or adjacent to the tool path, and welding was performed with sealant in both the cured and uncured states. In all cases, sealant prevented the ingress of corrosion after a 500 hour salt fog exposure, and furthermore, the presence of sealant in the weld negatively impacted shear strength at a significant level for only one parameter combination [160]. Doering investigated the effectiveness of

sealants at restoring the fatigue life of friction stir welded joints subjected to a corrosive immersion. Silicone rubber, applied in the uncured state, and nylon-11, applied as a pre-fabricated sheet, were evaluated as faying surface sealants in lap joints of 3.18 mm (0.125 inch) thick anodized 2024-T8 on top of anodized 357-T6 cast T-rails. Results indicate that the two sealants are suited for differing operational environments. Silicone rubber sealant showed promise in restoring the performance of samples in corrosion fatigue, while the nylon-11 performed best in the ambient environment, significantly contributing to fatigue life [162]. Aside from continuous linear welding, Brown evaluated swept friction stir spot welds (FSSW) of 2024-T3 in 1 mm (0.040 inch) thickness with multiple surface treatments and with PR-1432-GP sealant applied in the joint before welding. It was shown that the sealant prevented crevice corrosion and only slightly decreased joint strength while minimally impacting fatigue life [161]. And, as was discussed in the preceding chapter, quality evaluation of the sealant application can be performed in-process and that there exists potential for further exploitation of the sealant force signature. Dissimilar lap welds of 2024-T3 and 7075-T6 alloys were made with sealant that included intentionally introduced application flaws, such as gaps or thin spots. Using collected force signals along with signal processing and dimensional reduction techniques, it was shown that sealant application flaws were qualitatively separable from control sections with no flaws. This result could form the basis of a robust in-process quality control system for assuring that sealant is applied properly. Systems of this nature are becoming critical pieces of technology as more and more processes apart from welding itself, such as sealing and dispensing, are being performed by industrial robots in

aerospace manufacturing [163]. In other words, robots must work in concert with sealants from application, to welding, to quality control.

Robotic Welding

In order to create quality robotic friction stir welds, it is critically important to maintain the proper tool-workpiece contact condition. This condition includes the proper plunge depth, or alignment in the vertical direction, and proper lateral tool positioning relative to the joint line. Different techniques are employed to achieve these objectives. Force control is commonly used to maintain the proper plunge depth, as position control can fall short due to dimensionally inconsistent workpieces, complex curved surfaces, or deflection of the welding robot caused by large process forces [43]. Axial force can be controlled by manipulating the plunge depth, welding speed, or the rotation rate, but choosing plunge depth as the controlling variable enables a continuous adjustment of vertical tool position to maintain a desired condition [110]. It has been shown that controlling torque by manipulating plunge depth is also highly effective, and it provides a deeper understanding of the welding process while being simple and low cost to implement [115]. In order to achieve a desired lateral tool alignment relative to the joint line throughout the weld, it is usually necessary to use a planned path technique with compensation or employ some type of joint tracking methodology. There are two issues that can arise when using a planned path technique on an industrial robot. There are often slight differences between the actual work cell and the offline virtual programming environment, and the relatively large forces associated with FSW can cause robot deflection and deviation from the planned path [121, 170]. It has been demonstrated

however, that process forces can be monitored and correlated to path deviations, enabling real-time corrections [122]. The other option is to use a joint tracking technique, of which, vision-based tracking systems are both effective and quite popular, but they require additional external equipment, including one or more cameras as well as image processing software that interfaces with the robot controller. There are also joints, such as the blind T-joint, which lack top-side visual characteristics that can be easily exploited for tracking purposes. To address these issues, Fleming et al. developed a through-the-tool tracking technique for FSW that, in concept, parallels through-the-arc sensing methods used in arc welding. Cook had shown previously that these methods, when utilized in arc welding, can lend simplicity to manufacturing operations while also being low cost and effective [171]. Fleming et al. showed that when blind T-joints are joined with FSW, a maximum axial force exists when the tool is aligned properly with the vertical workpiece member [123]. An extremum-seeking technique was developed that weaves the tool laterally while taking periodic axial force measurements in order to make lateral position adjustments that maintain maximum axial force and thus, proper alignment [126]. This technique was also evaluated and shown to be effective when used on lap joints with an overlap width equal to the tool shoulder diameter. In that configuration, both axial force and torque were effective feedback signals, with torque having slightly better characteristics [127]. In the present study, the technique will be used to track not the force signature of the lap joint configuration itself, but features within the joint such as sealant.

Automatic Joint Tracking

The tracking technique developed by Fleming et al. is a lateral position detection and control system known as WeaveTrack [100]. WeaveTrack employs an extremum-seeking control technique, in which the objective is to track a varying maximum or minimum value rather than achieve stabilization about a known reference point, as in traditional control [172]. When WeaveTrack is activated, the FSW tool weaves back and forth laterally while traversing, creating a trapezoidal pattern which can be seen in Figure 75.

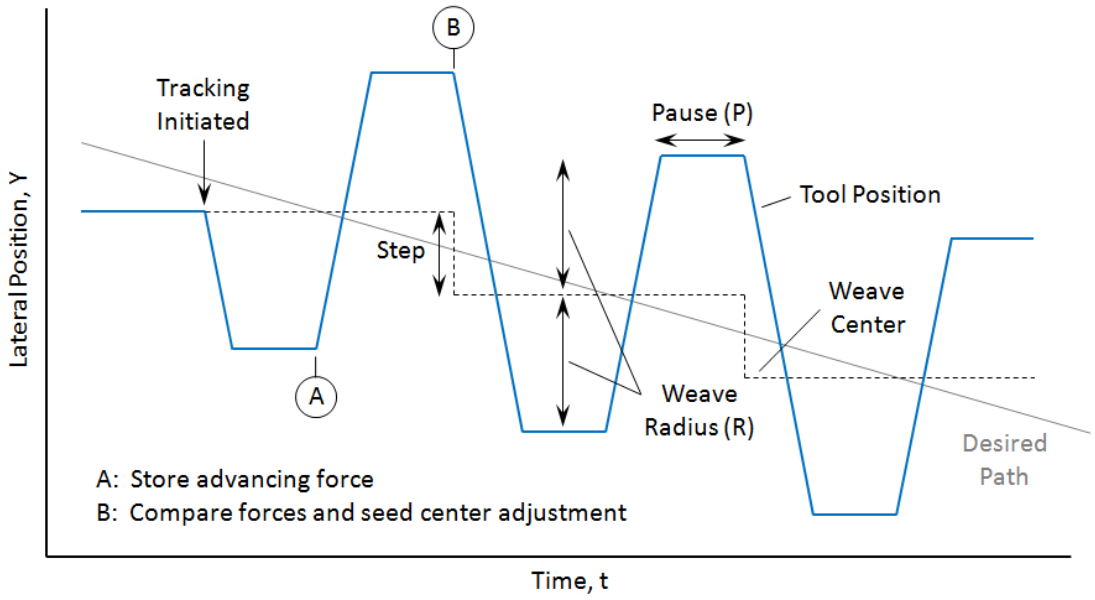

Figure 75: Three WeaveTrack Cycles

This pattern creates a perturbation in the force feedback signal that can be exploited by the extremum-seeking control technique, given that a force variation with lateral position is present in the particular joint configuration being welded. In one cycle of WeaveTrack, the tool first moves to the advancing side, then pauses for a prescribed

amount of time before moving to the retreating side and pausing again. During the pauses at the extremes of the weave, running averages of the force feedback signal are collected, and at the end of each cycle, the forces readings are compared. After the comparison, three outcomes can result: the weave center can step to the advancing side, step to the retreating side, or stay the same, if the force difference is below a certain threshold. In this study, the weave center is adjusted towards the direction of lower axial force, in contrast to the prior work done by Fleming et al. [126, 127]. The step threshold is also a new aspect of the technology, implemented for the present study. There are multiple parameters that affect the performance of the controller. These include the weave radius (R), the pause length (P), the step size, the lateral velocity (V_{Lat}), and the step threshold. The welding speed (V_{Tra}) also affects the profile of the tool path, and thus the performance of the controller. These parameters must be tuned to achieve proper tracking. The shape and degree of lateral change in the desired path must also be considered when choosing parameters, as the potential rate of change associated with the chosen controller parameters must be greater than or equal to the greatest rate of change in the desired path. The difference in these quantities has been denoted the weave margin (WM) and is defined in Equation 16, which assumes a step is executed in each cycle.

$$\frac{step}{V_{Tra}\left(2P+\frac{4R+step}{V_{Lat}}\right)} = WM \times m \tag{16}$$

where m = maximum slope of desired path (amount of lateral change / traverse distance)

This weave margin serves as a safety factor for tracking. It gives the controller the capacity to make incorrect decisions periodically due to errant force readings and still be

able to recover and track properly. The weave margin will be reported along with the other parameters selected in this study. In order to choose parameter values and then test the controller's ability to track a desired path, however, the force signature of the desired path must first be determined.

Technical Approach

The objective of this study is to demonstrate the automatic tracking of a desired path defined by sealant boundaries at the faying surfaces of a lap joint. The sealant is to be applied on the bottom sheet on each side of the desired path in such a manner that when the top sheet is put in place and clamped, the sealant will wet out while still leaving a clean path in the middle for the tool to travel through. This concept is depicted in Figure 76 with a transparent top sheet so that a generic sealant path is visible.

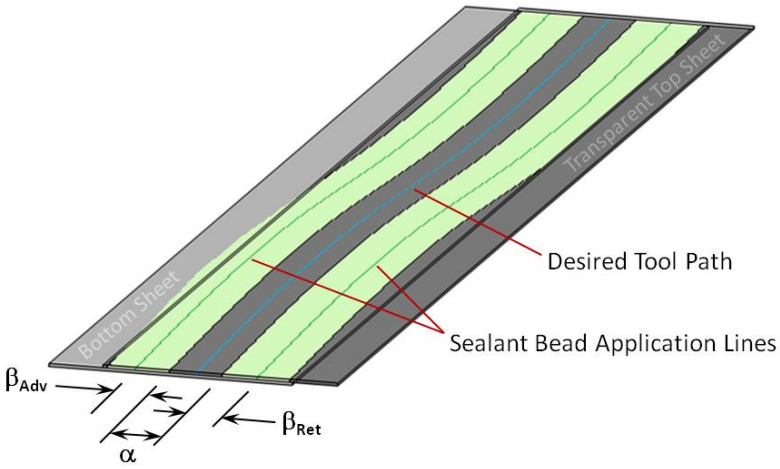

Figure 76: Sealant Path Tracking Concept

This scenario was simulated in the first stage of this study by milling channels in the bottom sheet material. As demonstrated in the preceding chapter, milled features can

replicate the axial force (F_Z) signature of sealant and are more consistent and repeatable in nature. The material selected for the study was 2024-T3 and 7075-T6 bare sheets in 1.6 mm (0.063 inch) thickness. Dissimilar lap welds were created with 7075-T6 as the top sheet and 2024-T3 as the bottom sheet. A two piece tool was used throughout the study that has a flat, scrolled shoulder, 15.9 mm (0.625 inch) in diameter. The probe is threaded and fluted with a cup feature on the terminal end and is 6.35 mm (0.25 inch) in diameter with the length adjusted so that it penetrated the bottom sheet by 30% of the top sheet thickness. This is the same tool pictured in Figure 60 of the preceding chapter. A fixed heel plunge depth of 0.05 mm (0.002 inch) and a tilt angle of 2 degrees were used for all welds.

Offset Study

To determine the force signature of sealant boundaries adjacent to the region of tool travel, a series of conventional welds were created with varying lateral tool offsets to each side of milled channels in the bottom sheet. The channels represent the desired paths, while the untouched parent material on each side of the milled channels mimic the additional thickness of a sealant layer in a lap joint. The milled channels were 17.46 mm (0.6875 inch) wide (representing α in Figure 76) and 0.13 mm (0.005 inch) deep. The depth was selected to be the same order of magnitude thickness as a typical sealant layer [68]. The width was selected to be slightly greater than the tool shoulder diameter. This was done intentionally to reduce the possibility of having a bi-modal response in axial force, which could result if the tool shoulder could bridge the channel and would be a bad input condition for the extremum-seeking controller. Figure 77 shows a layout of the

samples for this portion of the study. Two different configurations were experimented with: plunging the tool into the parent material (as pictured) or into the channel at the start of the weld.

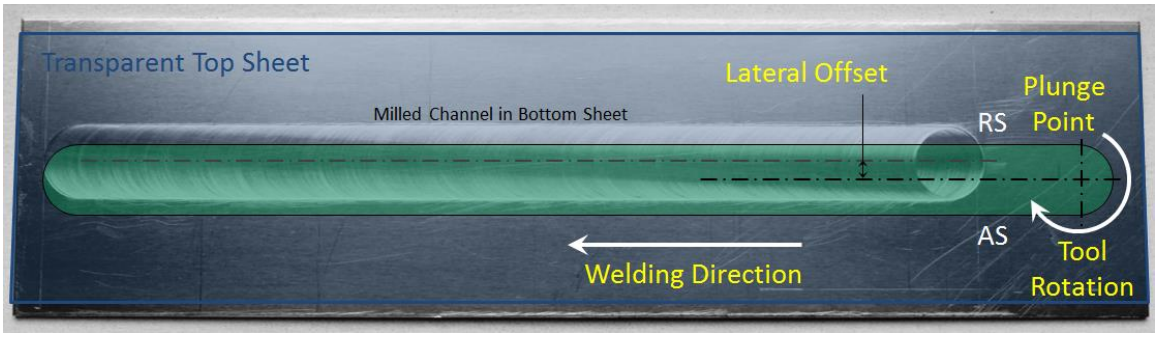

Figure 77: Milled Channel Sample Configuration

It was believed that plunging into the channel at the start could cause problems with weld initiation and loss of material consolidation under the shoulder, so for the offset study, the tool was plunged into the parent material and then traversed into the channel. Samples were approximately 23 cm (9 inch) in length, and force response data was then selected from the channel region only. The first round of welds was performed with relatively coarse lateral offset steps of 1.59 mm (0.0625 inch). Welding speed and rotation rate were 20.3 cm/min (8 IPM) and 1500 rpm, respectively. These parameters were chosen because it was shown in the preceding chapter they produce high strength, quality welds with this material and tool combination. Figure 78 displays the resulting axial force response data along with depictions of tool position relative to the channel location. A box-and-whisker style plot was chosen to display axial force from 25.4 mm (1 inch) of weld from the channel region of each sample. The maximum whisker length was set at three times the interquartile range (3*IQR) in order to encompass all data and show no

outliers. The notches in each box at the median indicate if there is a significant difference between the data sets at a 95% confidence level.

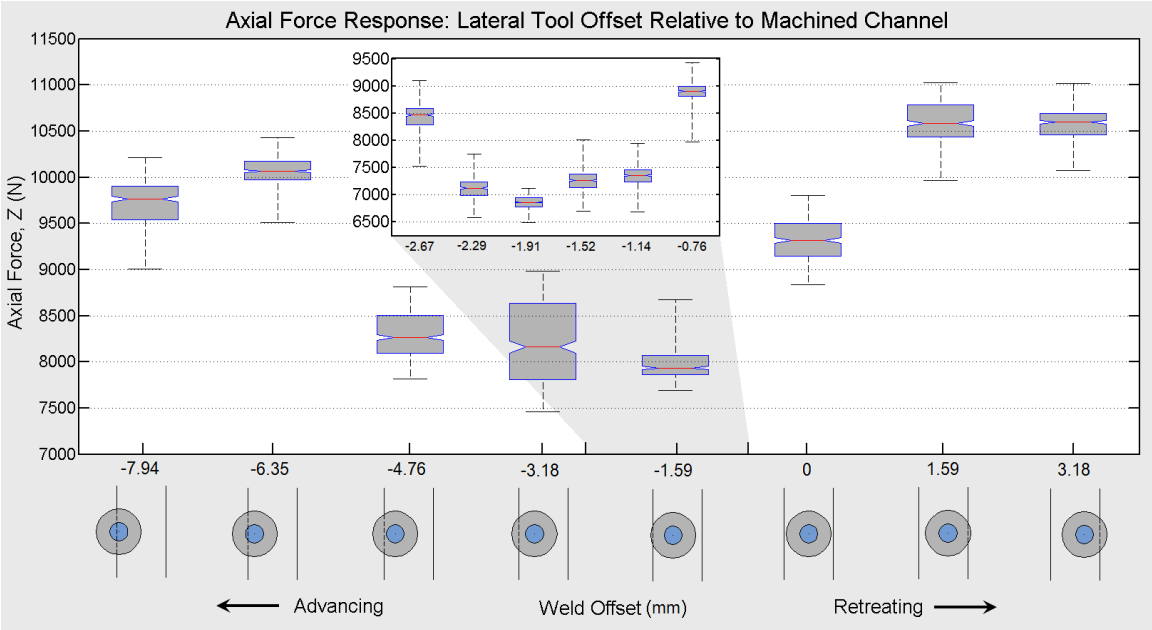

Figure 78: Offset Study Response Data

The data shows that there is a significant variation in axial force with lateral position. The greatest reduction in force does not occur when the tool is directly centered on the channel as one might expect however. The overall trend is centered about a region somewhere to the advancing side of center, when the retreating side of the tool is well within the channel. This parallels an observation by Fleming et al. that the greatest force response with lateral position variation in T-joints occurs slightly off-center, with the retreating side of the tool closer to the vertical member, the feature responsible for force variation [123]. This result is due to the inherent nature of material flow in FSW, which was characterized by early experimental and modeling efforts [5, 6, 7] and which contemporary models, capable of explaining weld structural features, have shown to be

dependent on tool geometry, including features such as threads [24, 25]. Flow fields and resulting dominant currents within the FSW process can lead to variations in weld structure from advancing to retreating sides. Figure 79, which shows an image of the back side of an offset study weld, provides evidence of this type of asymmetry.

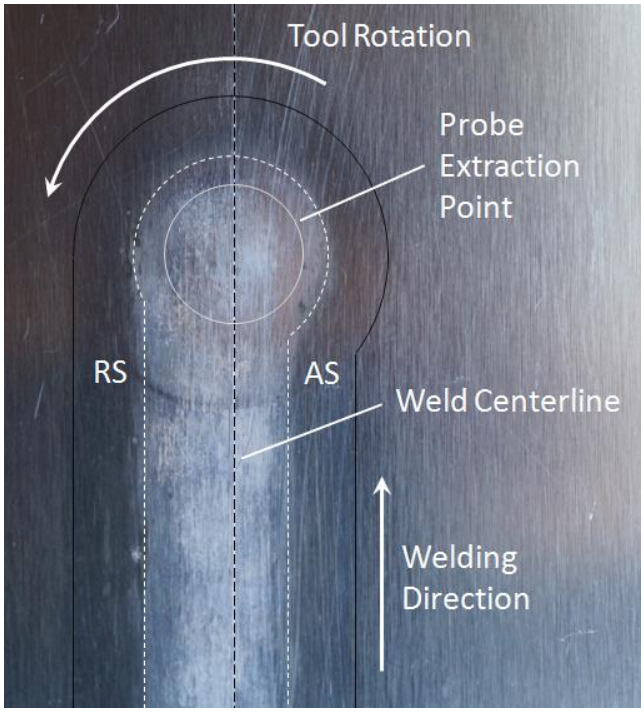

Figure 79: Weld Root Revealing Asymmetric Material Flow

It can be seen that material which has been thermo-mechanically affected by the tool probe and forged against the backing anvil is offset to the retreating side. This phenomenon transcends joint configuration, as in addition to T-joints and lap joints, its presence in butt joints sometimes dictates the tool probe be intentionally offset from the joint interface to account for asymmetry or to reduce tool wear and have better joining characteristics in dissimilar metal welds [61]. In order to determine the position of minimum axial force, or the position that will ultimately become the desired position for

tracking, with greater confidence, another offset study was conducted with a finer resolution of 0.38 mm (0.015 inch) centered about the region of lowest axial force in the coarse study. Welds were again conducted at 1500 rpm, but the welding speed was reduced to 10.2 cm/min (4 IPM) to more closely resemble the lower welding speeds shown previously to be necessitated by tracking [126, 127]. The results of this study are shown in the smaller window in Figure 78. Again, a strong variation in axial force with lateral position is evident, with the magnitude of the force values slightly lower due to the reduced welding speed. The minimum axial force occurred at a tool offset of 1.91 mm (0.075 inch) to the advancing side of the channel center. This relative tool-channel position therefore, is the one that the extremum-seeking controller will attempt to maintain throughout the weld when tracking is activated.

Tracking Milled Channels

Before attempting to track sealant paths, tracking machined channels was performed in order to expedite the controller tuning process and establish baseline performance data with a rigid feature, as opposed to sealant, which wets out and can be squeezed further away from the joint line by pressure from the tool when in the uncured state. Two tracking scenarios were examined: Tracking a path with a straight, unchanging desired lateral position with an initial offset and tracking a path with a continuously changing desired lateral position. Tracking a straight path with an initial offset tests the ability of WeaveTrack to get on track if not started properly or to get back on track if there is ever an overshoot condition. The initial offset chosen for these experiments was 2.5 mm (0.1 inch). Tracking a path with a continuously changing

desired lateral position is a critical performance aspect of WeaveTrack. It must execute this task well in order to have satisfactory performance in any future application. The slope (*m*) of the desired path selected for these experiments was 0.028 mm lateral/mm traverse (inch lateral/inch traverse). Coupons 26.7 cm (10.5 inch) in length were created with the necessary milled channels. Controller parameters were tuned through an iterative experimental process. Table 2 displays two resulting parameters sets that were chosen for these experiments.

Table 2: WeaveTrack Parameter Sets

Parameter	Set 1	Set 2	Units
Rotational Speed	1500	1200	rpm
Welding Speed	10.2 (4)	7.6 (3)	cm/min (IPM)
Weave Radius	0.89 (0.035)	1.02 (0.040)	mm (inch)
Step Size	0.36 (0.014)	0.64 (0.025)	mm (inch)
Pause	1.3	1.3	seconds
Lateral Velocity	15.2 (6)	15.2 (6)	cm/min (IPM)
Threshold	75	20	N
Weave Margin (if m = 0.028 mm/mm)	1.81	4.01	

Parameter Set 1 was selected for the initial offset welds. It has a tool rotational speed and a welding speed equal to that of the finer resolution offset study. Figure 80 displays the tracking results from this portion of the study. Welds are started conventionally (non-weaving) with offsets to the advancing and retreating sides, and then WeaveTrack is turned on at approximately 250 seconds. It is observed that the controller is able to find the desired path and follow it, although some overshoot is evident in the advancing side offset case. WeaveTrack is then turned off at approximately 355 seconds. Figure 81

shows an example of the surface finish which results from weaving and the contrast between it and the conventional surface finish after weaving is turned off.

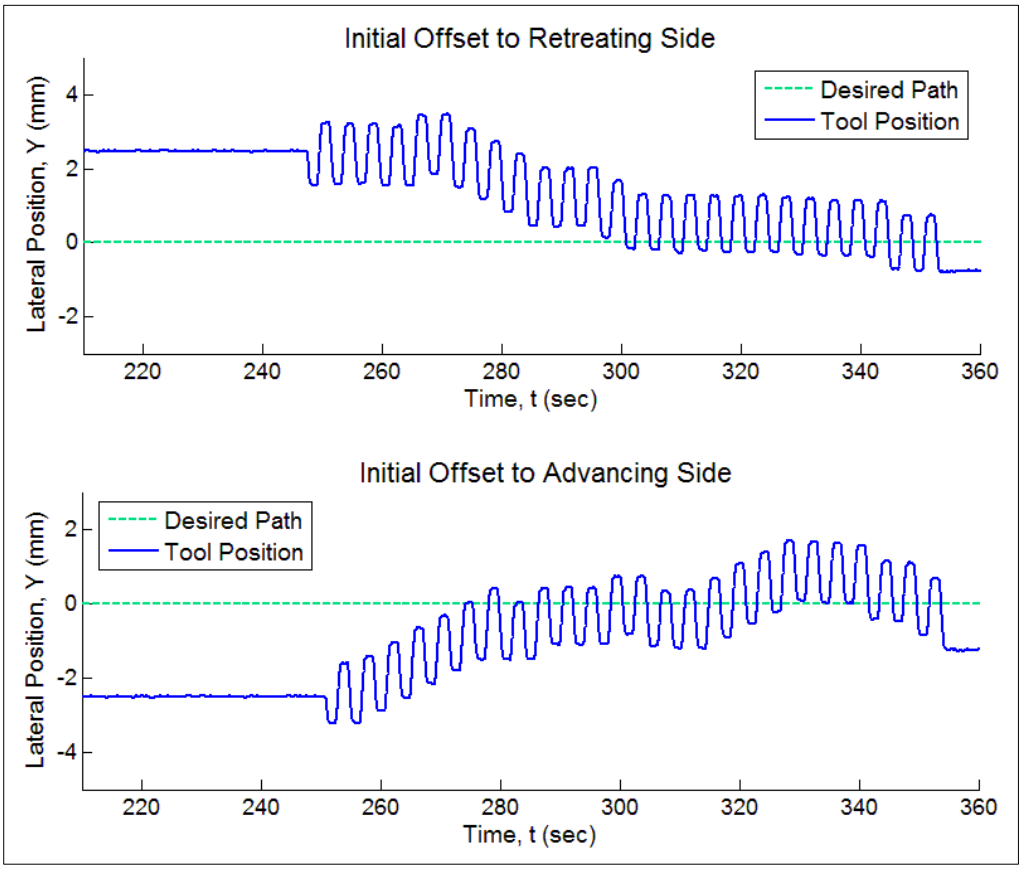

Figure 80: Tracking Results for Straight Paths with Initial Offsets

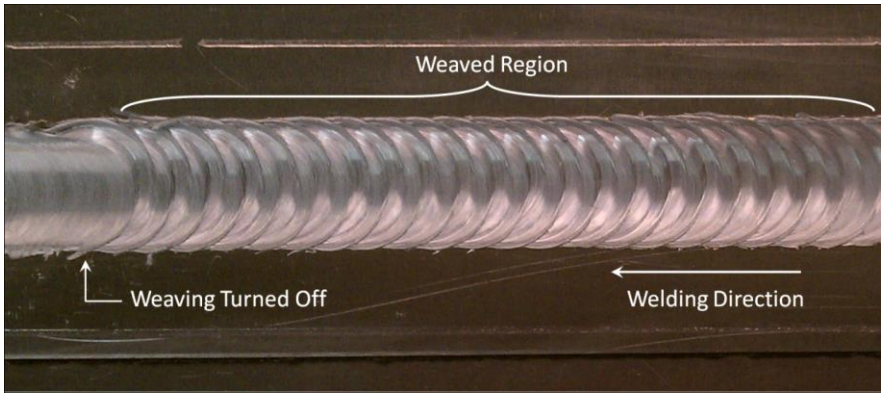

Figure 81: Surface Finish Example

For tracking a path with a continuously changing desired lateral position, Parameter Set 2 was selected. This parameter set has a reduced rotational rate and welding speed along with an increased weave radius and step size. It was believed these changes would create improved conditions for tracking. Three trials of this experiment with milled channels are documented here and are then repeated with sealant in both the cured and uncured state. Figure 82 displays the tracking results from Trial 1 of tracking a continuously changing path.

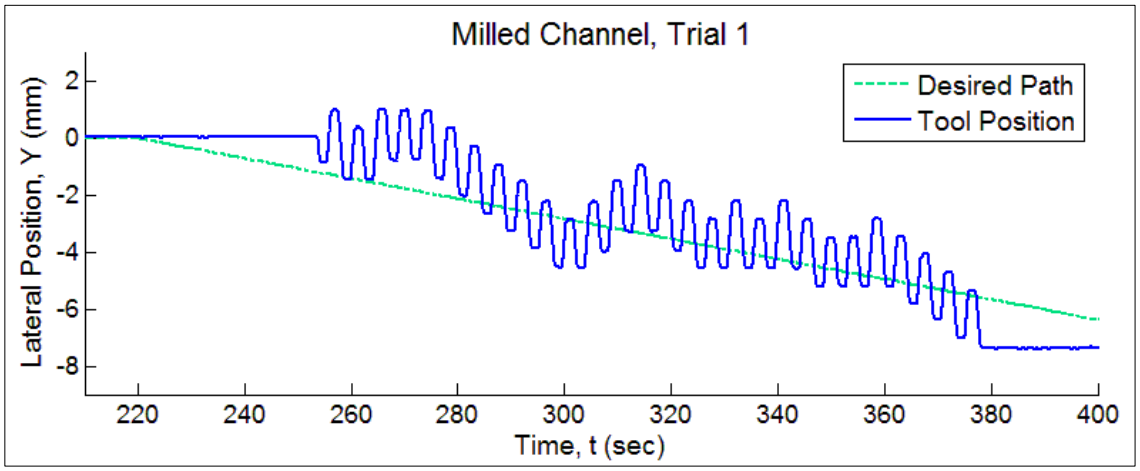

Figure 82: Tracking Results for a Continuously Changing Path

The weld is started conventionally with the tool initially on the desired path. At the onset, before tracking is turned on, the tool deviates from the channel, and then WeaveTrack is turned on at approximately 250 seconds. It is observed that the controller is able to find the path and track it throughout the weld after a very slight overshoot and oscillation. Tracking is then turned off at approximately 380 seconds. This positive performance was encouraging and served as a proof of concept in theory for tracking sealant paths. In order to quantify the performance of WeaveTrack at tracking these

continuously changing desired paths, an error determination method was developed. This is illustrated in Figure 83 with a magnified section of milled channel Trial 1.

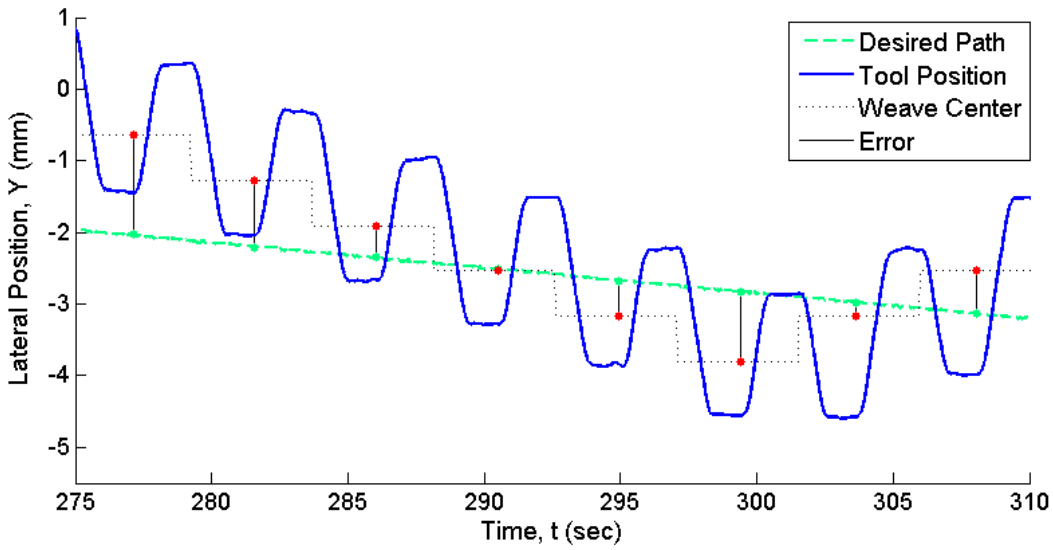

Figure 83: Error Determination Methodology

The error is calculated once per weaving cycle as the absolute value of the difference between the center of the weave and corresponding point on the desired path, as measured in the lateral direction. In Figure 83, this error is represented with vertical lines. The error measurement occurs at the center of the weaving cycle in time as well. This quantifiable determination of tracking performance enabled the comparison of tracking milled channels to tracking cured and uncured sealant paths. Error data from three trials of tracking milled channels, all conducted with the same parameters, is displayed in Table 3 along with data from sealant trails, which were conducted after methods for applying sealant properly were developed.

Sealant Application Methods

The sealant chosen for use in these experiments was Pelseal® 2077, which is a one-part fluoroelastomer sealant, formulated with Viton®, from DuPont Performance Elastomers. It requires no separate curative agent for activation and can be applied simply with a caulking gun in a bead configuration [173]. The challenge in applying this sealant to create a desired path of previously established width (α) and slope (m) was to figure out the offset, or β in Figure 76, between the edge of the desired path and the sealant application lines. This distance is a function of the sealant properties and the clamping characteristics of the robotic welding setup. Application and clamping trials were performed with a piece of clear acrylic in place of the top sheet so that the sealant would be visible as it dispersed under the pressure of clamping. Trials were also initially performed with a sealant analog.

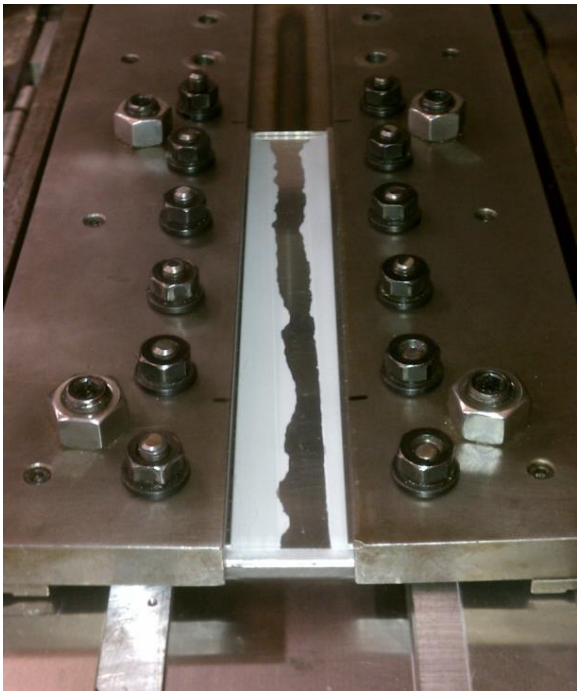

Figure 84: Sealant Application Trial with Clear Acrylic Top Sheet

Titebond® 7301 is a latex caulk that is both economical and easy to clean up. It also has the same viscosity as Pelseal® 2077 [174]. Dual beads 1.5 mm (0.06 inch) in diameter were applied to a 26.7 cm (10.5 inch) long bottom sheet of 2024 with varying offsets and clamped in repeated trials until satisfactory results were achieved. The edges of the desired path were also scored on the bottom sheet to aid in slowing the ingress of sealant. Figure 84 displays a satisfactory 7301 sealant application trial with the clear acrylic top sheet.

The offsets selected for use in the tracking experiments with the actual 2077 sealant were β_{Adv} = 14.3 mm (0.563 inch) and β_{Ret} = 12.7 mm (0.5 inch). The reason for the difference in offsets is attributable to the uniqueness of the clamping setup and the coupon size. It is likely that in any future application of this technology, the offsets would have to be determined for the specific robotic welding setup. Prior to applying sealant for tracking trials, both the top and bottom sheets were cleaned with a 50% methyl ethyl ketone and 50% toluene solvent using lint free wipes. They were then cleaned a second time using pre-wetted isopropyl alcohol wipes. For welds with sealant in the uncured state, samples were welded within 20 minutes of sealant application. For welds with sealant in the cured state, sealant was applied, the top sheet was placed on and clamped, and then the samples were allowed to cure for approximately 72 hours before welding, which is the minimum recommended cure time for 2077 sealant [173].

Sealant Path Tracking

Three tracking trials for both cured and uncured sealant are documented here. All welds were performed with Set 2 parameters, just as the three milled channel tracking welds were. Figure 85 displays results from one of the trials with uncured sealant, and Figure 86 displays results from a cured sealant trial.

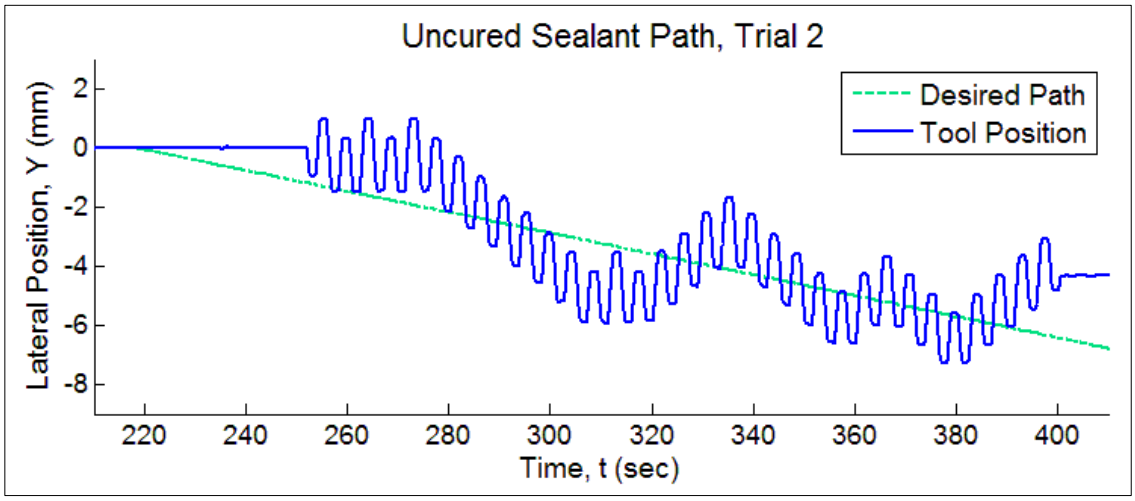

Figure 85: Tracking Results for a Continuously Changing Uncured Sealant Path

In both examples, the conventional weld at the start initially deviates from the desired path, and then WeaveTrack is turned on at approximately 250 seconds. The tracking results are characterized by overshoot, oscillation, and some deviation from the path, but in general the weld path followed the desired direction. This was common across the sealant welding trials. Table 3 displays all error data for the sealant trials as well as the trials with milled channels.

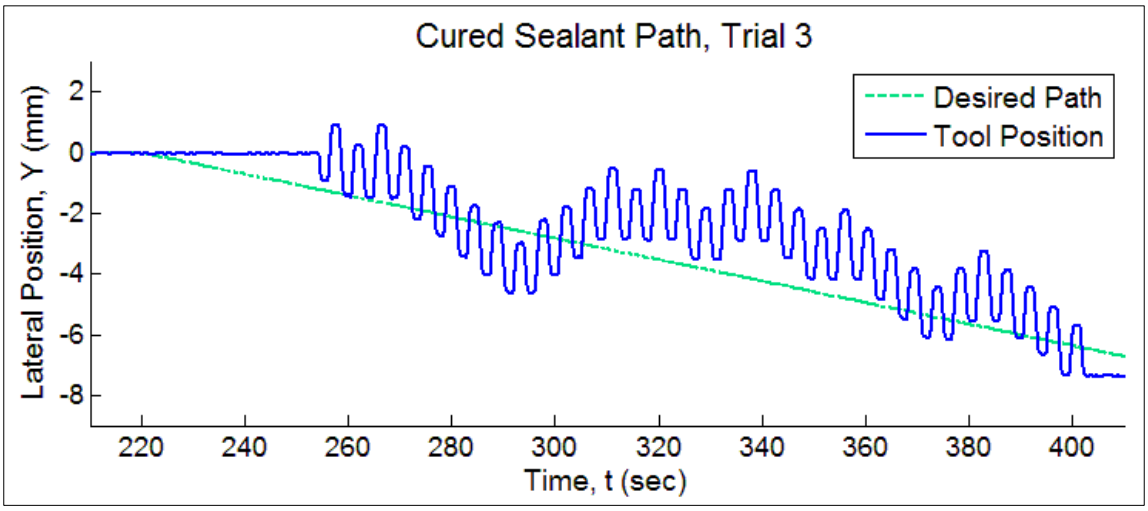

Figure 86: Tracking Results for a Continuously Changing Cured Sealant Path

The maximum, minimum, mean, and standard deviation were computed for the error set of each individual trial.

Table 3: Tracking Error Data

Path Configuration		Lateral Position Error, mm (inch)			
		Max	Min	Mean	Standard Deviation
Milled Channel	Trial 1	1.88 (0.074)	0.02 (0.001)	0.76 (0.030)	0.53 (0.021)
	Trial 2	2.98 (0.117)	0.04 (0.002)	1.33 (0.052)	0.79 (0.031)
	Trial 3	3.43 (0.135)	0.01 (0.000)	1.63 (0.064)	0.88 (0.035)
	Composite	**3.43 (0.135)**	**0.01 (0.000)**	**1.26 (0.050)**	**0.83 (0.033)**
Cured Sealant	Trial 1	3.22 (0.127)	0.18 (0.007)	1.74 (0.069)	0.83 (0.033)
	Trial 2	3.76 (0.148)	0.04 (0.002)	1.12 (0.044)	0.97 (0.038)
	Trial 3	2.84 (0.112)	0.01 (0.000)	1.24 (0.049)	0.71 (0.028)
	Composite	**3.76 (0.148)**	**0.01 (0.000)**	**1.37 (0.054)**	**0.88 (0.035)**
Uncured Sealant	Trial 1	5.47 (0.215)	1.05 (0.041)	3.31 (0.130)	1.06 (0.042)
	Trial 2	3.25 (0.128)	0.04 (0.002)	0.99 (0.039)	0.73 (0.029)
	Trial 3	2.23 (0.088)	0.01 (0.000)	1.21 (0.048)	0.60 (0.024)
	Composite	**5.47 (0.215)**	**0.01 (0.000)**	**1.87 (0.074)**	**1.35 (0.053)**

Then the three error sets within each path configuration were lumped together, and the four metrics were again computed to create a composite look at each configuration as a whole. It can be observed that by all four metrics, WeaveTrack exhibited the best performance with the milled channel configuration. The cured sealant configuration had the next best performance, again by all four metrics, and then uncured sealant was last. The performance of WeaveTrack with cured sealant was close to that of the milled channel configuration. This is perhaps not surprising, given that cured sealant should be rigid in nature and resistant to migration within the joint resulting from tool pressure. With uncured sealant, it is likely that the sealant path dimensions were altered slightly by pressure from the tool as it caused dispersion beyond that of clamping. Nevertheless, results as a whole were encouraging. The classification of each tracking result as a success or failure cannot be done without a tolerance defining an acceptable level of path deviation, which is not established here. That type of metric will likely always be application driven, particularly with lap welds, in which there are no natural limitations to tool position deviation in the lateral direction, provided adequate sheet overlap. The error data in Table 3, however, serves as a quantitative comparison of the path configuration types and may perhaps be used in the future to gauge gains in performance as controller parameters are further tuned or sealant application methods are refined.

Weld Properties

It has been demonstrated that WeaveTrack can employed in order to track blind sealant paths in lap joints; however, there were additional aspects of weaving that required further investigation. It has been shown previously that weaving has the

potential to increase joint strength, particularly in lap welds [101, 126, 127]. The lateral movement of the tool has the effect of increasing the thermo-mechanically affected zone (TMAZ) width, which is critical to strength in lap joints. Weaving causes the probe to sweep a volume of material larger than itself, in a fashion similar to that of other FSW technologies, such as Skew-Stir™ or Com-Stir™, which were designed with similar objectives in mind [35, 175]. Unfortunately, as discussed previously, tracking necessitates lower welding speeds, which is not ideal, as a downward trend in strength with decreasing welding speed was documented in the preceding chapter for this particular tool-material combination at the tool rotation rates used in the present study. The consequences of this trade-off and the question of whether weaving could help recover any strength loss needed to be investigated. The interaction of the weaving process with sealants was also of great interest. Ideally, in a full sealant application, the pressure from the FSW tool causes sealant at the joint line to be squeezed away from the weld zone. This promotes sealing of the faying surfaces while removing the sealant as a contaminant from the nugget. It was believed that weaving may further aid in this process, although it was unclear to what degree, as in the present study sealant was applied only adjacent to the tool path to begin with. A weld matrix was designed that included conventional welds, non-tracked (or stationary) weaved welds, sealant free welds, and welds with sealant in both the cured and uncured states. All welds were made at 1200 rpm and 7.6 cm/min (3 IPM), and weaved welds were made with Set 2 parameters, excluding the step size and threshold, as the weave center did not step but remained fixed throughout the weld. Coupons were configured such that the advancing side was adjacent to the top sheet lapped edge. This places any top sheet thinning or cold

lap defect that may be present in the load path during tension-shear testing. This configuration has been shown to have more desirable characteristics [68, 160]. Sealant was applied with the same methods as before, with the exception that $\beta_{Adv} = \beta_{Ret} = 12.7$ mm (0.5 inch) due to the change in sample configuration. Samples with cured sealant were prepared and clamped for 72 hours prior to welding, and then all samples were welded at the same time and allowed to naturally age for approximately 120 hours before testing. Four 12.7 mm (0.5 inch) wide tension-shear samples were pulled from each weld, and the results were averaged for each condition. Figure 87 shows the resulting ultimate loads in tension-shear.

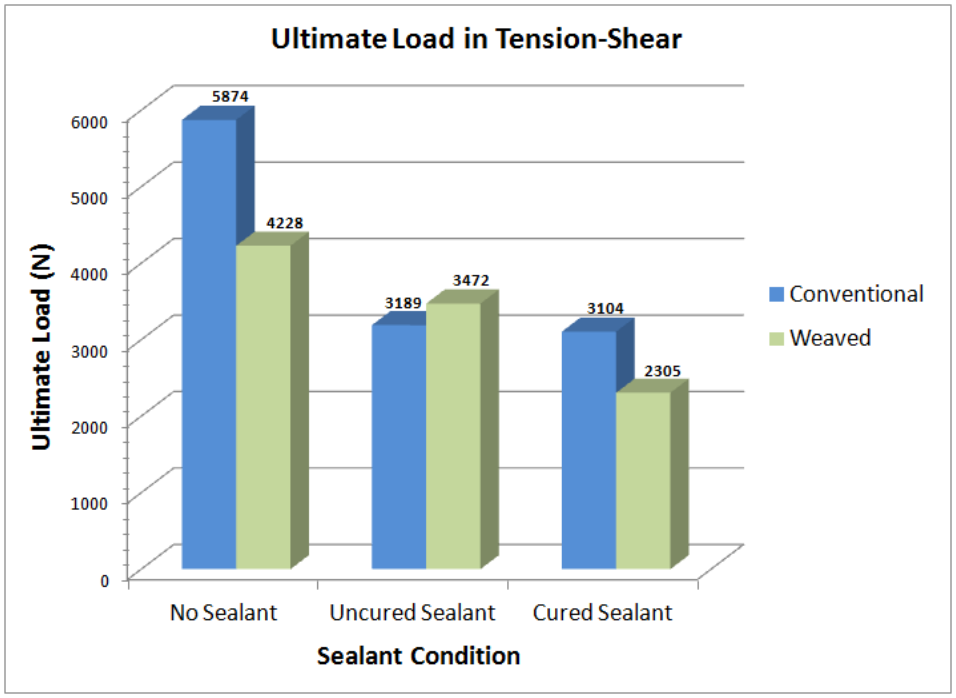

Figure 87: Strength Results

All samples exhibited pull-out fracture mode, failing in the top sheet at either the nugget or slightly to the retreating side of the nugget. Hammer S-Bend tests were conducted as

well, and all samples failed in the top sheet at the same location. When comparing the strength of coupons without sealant to those made with sealant, the potential detrimental effects of sealant on weld strength are obvious. A 46% decrease in strength was observed when comparing conventional weld samples without sealant to those with uncured sealant. Conventional weld samples with cured sealant exhibited a similar decrease in strength. This is a potential effect of sealant that must be contended with when designing joining operations. The weld parameters in the present study have been optimized for tracking, not strength of welded coupons with sealant. Weaving also had a detrimental impact on strength for the samples without sealant and with cured sealant. While in several cases it has been demonstrated that weaving can increase joint strength, Hendricks found that weaving with large weave radii can cause decreases in lap weld joint strength and, in extreme cases, surface defects consisting of voids repeated at the interval of the weave cycle [101]. Although no surface voids were observed, the weave radius of 1.02 mm (0.040 inch) used in this study is at the higher end of the weave radii that have been tested in the literature, and weaved welds tended to fracture along the peaks and valleys of the weaved surface texture. On the other hand, weaving did slightly increase joint strength in the case of uncured sealant, although what is observed is not statistically significant. In order to see if weaving led to increased migration of sealant from the weld zone, and thus a potentially stronger weld, macrographs of each weld configuration were made for comparison. These are pictured in Figure 88. Polished cross sections were etched with Keller's reagent, and the distances between layers of faying surface sealant were measured and are indicated on the macrographs. General observations about the macrographs include the presence of a classic hooking defect on

the advancing side of all the samples. Defects on the retreating side vary from sample to sample. Some samples exhibit a classic top sheet thinning, or cold lap, defect, while others a more severe up-tick of the bottom sheet into the top, reminiscent of a hooking defect. Drastic differences between the appearances of weaved samples can be attributed to the sectioning of samples without regard to location in the weaving cycle.

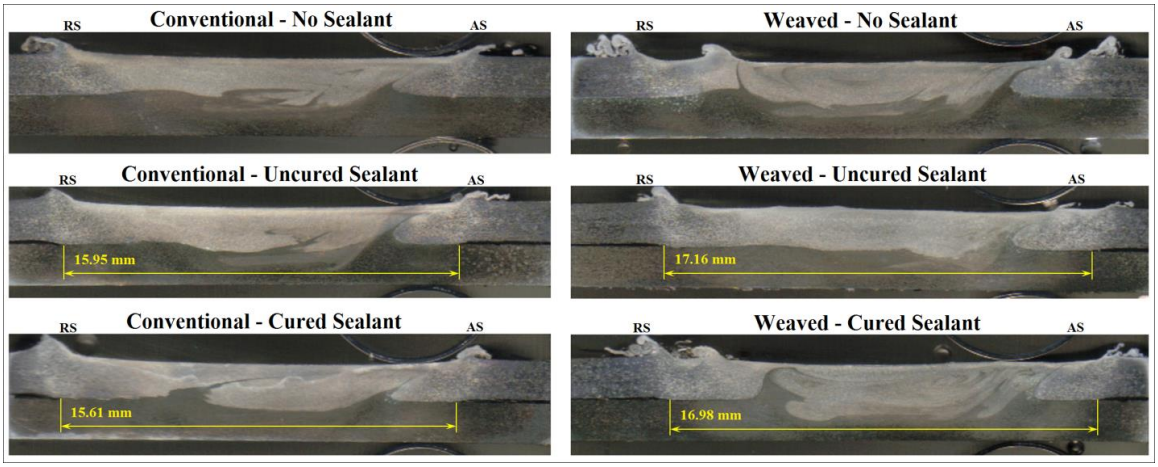

Figure 88: Weld Macrographs; Faying Surface Sealant is Visible at Edges

With regard to sealants, it can be observed that uncured sealant is squeezed farther away from the weld zone than cured sealant in both the conventional and weaved cases. Furthermore, weaving causes additional migration of sealant in both the cured and uncured states. The largest spread between faying surface sealant layers occurs in the case of weaving with uncured sealant, which may explain why this weaving configuration saw a slight increase in strength over its conventionally welded counterpart. In general, results indicate that one must consider the interactions between sealants and process variants like weaving when selecting parameters for a joining operation.

Discussion and Conclusions

An extremum seeking control technique known as WeaveTrack, which has been shown previously to enable joint tracking in certain joint configurations, has been evaluated as a method for tracking blind sealant paths in lap joints of aerospace alloys. The force signature of such a sealant feature was first determined by using machined channels to replicate the presence of sealant in a controlled and repeatable fashion, and milled channels were also used to in the first round of tracking experiments to tune controller parameters and establish baseline performance. Tracking sealant paths in both the cured and uncured states was then attempted and characterized.

While tracking results were characterized by some overshoot, oscillation, and path deviation, they also indicated that the fundamental concept was sound and that performance could perhaps be improved by further tuning controller parameters and refining sealant application methods. This is an exciting prospect for manufacturers and a new level of interaction between sealant and robotic control techniques. The potential exists for desired paths to be laid out in sealant and then automatically tracked without having to pre-program planned path operations. Tracking with cured sealant exhibited lower error than tracking with uncured sealant, while tracking milled channels outperformed both sealant configurations. As previously discussed, classifying each tracking result as a success or failure cannot be done without having a tolerance for acceptable deviation in the lateral direction. This metric is not established here, as it will likely always be application driven, particularly with lap welds. As the tool axis is practically normal to the planar joint interface (minus the small tilt angle), there are not natural boundaries for tool position, as are found with butt joint or T-joint configurations.

A quality lap weld can still result even after significant tool displacement in the lateral direction, and limitations arise perhaps only when sheet overlap widths, and thus tool positional boundaries, are established in particular applications.

The dynamics of sealant within the joint interface, however, have been shown to be critical for both tracking capability and for joint strength. Typically, with uncured sealant in a full application, it is desired that pressure from the tool squeeze the sealant away from the weld zone to the faying surfaces of the joint. This migration removes sealant as a contaminant from the weld zone, which enables the creation of quality, defect free welds. In the present study, sealant was applied only adjacent to the tool path to begin with, and it was shown that further migration of the sealant from the weld zone can be either beneficial or harmful, depending on the perspective. From a tracking perspective, sealant migration is not desired, as evidenced by the cured sealant samples having lower error than the uncured sealant samples. For better tracking performance, it is desired for the feature within the joint to be more rigid. From a strength perspective however, sealant migration is desired. Samples with uncured sealant exhibited higher strengths than their cured counterparts for both conventional and weaved welds, and the one case where weaving resulted in increased strength was with sealant in the uncured state. This case had the highest spread of sealant from the weld zone, as measured in the macrograph. Therefore, a potential trade off situation exists between tracking performance and strength that must be considered when designing a joining operation.

Potential future work should be focused on this trade off, improving tracking performance while maintaining joint strength as a priority. One aspect that affects both of these items is the desired path width (α). In this study, the width was initially chosen

to be slightly wider than the tool shoulder to avoid a bi-modal force response as the tool offset from the path varied. The response was indeed not bi-modal, but oscillation was observed in the tracking results, and a weave radius that is on the higher end of those that have been tested in the literature was necessary for detecting the force signature of the path. If the desired path width could be decreased while maintaining a uni-modal force response, the weave radius could likely be decreased, which is desired from a strength perspective, and oscillation in tracking could perhaps be reduced as well. Another aspect that could be studied is reduction of the surface texture that results from weaving. This could perhaps be accomplished by altering tool shoulder geometry or welding parameters such as the tool tilt angle. A smoother surface texture would perhaps result in decreased stress concentrations and paths along which welds tended to fail during tension-shear testing. There are additional aspects of tracking with sealant that deserve attention as well, including the incorporation of regulation style force control for maintaining desired plunge depth, allowing one or more tracking parameters to vary proportionally to magnitude differences in axial force at the comparisons, or optimizing the extremum seeking controller parameters for performance in general. These items have been discussed previously by Fleming et al. in the tracking of other joint configurations [126, 127], and it is likely that the incorporation of sealant would add complications that must be taken into account in each of these areas. It is known, for example, that the presence of sealant within a lap joint can complicate force control. The sealant acts as an insulating layer causing uneven heating, and a result, the top sheet more readily softens, which leads to a drop in axial force for which a controller will try to compensate by plunging the tool deeper [176]. These types of interactions between sealants and control

techniques must be studied and improvements made to existing technology to enable the creation of quality welds with the desired characteristics on a consistent basis.

CHAPTER V

JOINING 2198 ALUMINUM-LITHIUM ALLOY WITH WEAVING AND PULSING VARIANTS AND SEALANT

This chapter is published in:

Gibson, B.T., Ballun, M.C., Cook, G.E., Strauss, A.M., "Friction Stir Lap Joining of 2198 Aluminum-Lithium Alloy with Weaving and Pulsing Variants," *SME Journal of Manufacturing Processes*, Vol 18, No 4, 2015, pp. 12 - 22.
DOI: 10.1016/j.jmapro.2014.12.002

Abstract

Lap joints of 2198-T8 Al-Li alloy in 0.063 inch sheet thickness were friction stir welded to investigate the combination of this material and assembly method for the manufacturing of aerospace structures. Along with conventional friction stir welding (FSW), weaved FSW and pulsed FSW (PFSW) were evaluated to determine the potential impact of these variant technologies on weld strength. Additionally, a more traditional flat shoulder tool geometry operated with a tilt angle was compared to a tapered shoulder tool geometry operated at a zero degree tilt angle, which offers the possibility of simplifying robotic welding operations. Faying surface sealant, the use of which is critical in aerospace applications, was investigated as well, to determine its impact on weld strength and to characterize its interactions with welding parameters and process variants.

Introduction

As composite and metallic airframe construction methods compete for dominance in the aerospace marketplace, much attention has been paid to the support technologies that are key enablers of these methodologies. In the production of metallic fuselages, wings, and other aerostructures, friction stir welding (FSW) has rapidly gained acceptance as a rivet replacement technology [140] which, when paired with new alloys, has enabled metallic construction methodologies to remain relevant and maintain a semblance of 'leading-edge' technology. Specifically, FSW enables the joining of metallic structures at significantly higher rates than riveting, along with having the advantages of reduced weight, reduced part count, increased joint strength, and lower overall manufacturing costs. Major aircraft manufacturers including Airbus, Embraer, and Bombardier, along with Eclipse Aerospace, in particular, have all committed resources to evaluating existing and developing new FSW technologies and incorporating them into the production of metallic airframe structures [124, 149, 150, 152, 154, 155].

The dominant materials utilized in these metallic structures have been 2xxx and 7xxx series aluminum alloys, forming the aircraft skin and high strength structural members, respectively. A significant amount of research has been focused on friction stir welding this particular dissimilar combination of materials in both butt and lap joint configurations [67, 69, 142, 143, 144, 145, 146]. Recently however, more modern alloys, including the third generation of aluminum-lithium (Al-Li) alloys, have emerged enabling metallic structures to keep pace with composites on the critical fronts of weight efficiency, cost, and safety. More specifically, the latest iteration of Al-Li alloys exhibits improved performance with respect to density, stiffness, isotropy, fatigue crack growth

resistance, fracture toughness, and corrosion resistance [177, 178]. These alloys have also paired well with FSW as a joining method to offer an intriguing combination for manufacturers to consider [179, 180]. The research community has taken notice as well, with a perhaps telling amount of work being conducted on FSW of Al-Li alloys [181, 182, 183, 184, 185, 186, 187, 188, 189, 190, 191, 192, 193], with particular emphasis on 2198. Other Al-Li alloys receiving attention including 2199, viewed as a viable candidate for aircraft skin, and 2099 extrusions, which would be used to form internal structural members [194].

An additional aspect of FSW utilization in the construction of metallic structures for aerospace applications that has been studied recently is the incorporation of corrosion prevention measures. Faying surfaces of joints are subject to in-service crevice or galvanic corrosion attack, and as such, technology has been developed that allows for sealants to be applied within the joints prior to welding [159]. Sealants migrate away from the joint line during welding, cure, and then protect against corrosion for the life of the joint. Specific research in this area has focused on sealant performance and impact on weld quality [160, 162], extension to friction stir spot welding [161], in-process quality evaluation of sealant application, the focus of Chapter III of this dissertation, and the exploitation of sealant presence to enable automatic path tracking, which is the focus of Chapter IV of this dissertation; the latter topics, referenced throughout the present chapter, are indicative of the trend towards increased use of industrial robots in aerospace manufacturing for tasks other than part handling or conveyance, such as sealing and dispensing [163].

Given the aforementioned trends in aerospace manufacturing, involving advanced materials, joining methods, and corrosion prevention, the objectives of the present study are to build upon previous work in these areas and focus on some remaining unanswered questions. More specifically, these objectives focus on joining Al-Li with FSW, the exploration of FSW process variants, the impact of tool geometry, the incorporation of sealant within the joints, and the interactions of these items. The objectives are:

1) Determine optimal parameters for joining thin section 2198-T8 Al-Li sheet in a lap joint configuration. Incorporate FSW variants *pulsing* (cyclical variation in tool rotation rate) and *weaving* (cyclical variation in lateral tool position), both of which were introduced in Chapter II of this dissertation, and determine the resulting effects on weld shear strength.

2) Compare the traditional lap joining themes of flat shoulder geometry, high tilt angle, and high welding speed with a non-traditional combination of a tapered tool shoulder and welding at 0 degrees tilt, which effectively eliminates a degree-of-freedom required of a welding robot.

3. Examine the interaction of welding parameters and tool geometry with the dynamics of sealant within the weld joint. Conclude how this interaction would affect in-process sealant quality evaluation and automatic sealant path tracking capabilities.

Weaving, or weaved FSW, is a process variant that arose from the development of a lateral position detection and control system for FSW [100]. This is a through-the-tool joint tracking technique that was inspired in part by successful through-the-arc sensing techniques in arc welding [171]. Fleming et al. first determined that blind FSW T-joints have a characteristic axial (Z) force signature as the position of the tool varies laterally

relative to the location of the vertical member [123]. An extremum-seeking control technique known as WeaveTrack was then developed that weaves the tool side to side laterally while monitoring force values and makes periodic lateral position adjustments to seek a varying maximum force and thus track the workpiece [126]. A diagram of this cyclical process is displayed in Figure 75 of Chapter IV. Parameters affecting the performance of WeaveTrack include the weave radius (R), the lateral velocity, the pause length (P), the step size, the step threshold, and the welding speed. It has also been demonstrated that WeaveTrack is effective at tracking lap joints with an overlap width equal to the tool shoulder diameter with either axial force or torque (T) as the feedback signal [127] and at tracking blind paths outlined by between-sheet sealant in lap joints with the controller modified to track a varying minimum axial force, which was demonstrated in Chapter IV. The effect of weaving the tool side to side laterally on the mechanical properties of the joints has been examined as well, as it was suspected that weaving action would promote increases in the thermo-mechanically affected zone (TMAZ) width, which is critical for lap joint strength and has been the driver of other FSW tool designs and technologies [35, 175]. Hendricks conducted the most comprehensive study, focused on lap joining Al 6061 in 0.125 inch thickness. It was found that weaving can indeed increase the strength of lap joints as compared to conventionally welded counterparts, with weave radius standing out as a critical parameter. Diminishing returns with increasing weave radii or even detrimental effects and a repeating surface defect were possible at the highest weave radii tested [101]. A characteristic, scalloped surface finish along which lap welds tended to fail in tension-shear testing was documented in Chapter IV for weaving as well. An examination of

these issues, both the advantages and disadvantages of weaving, has inspired aspects of the present study, especially with regard to flat versus tapered shoulder geometry and the resulting weld surface finish.

Pulsing, or Pulsed FSW (PFSW), is another technology that has grown from the exploration of potential extensions of arc welding techniques into FSW processes. The pulsation of welding current can be beneficial in the arc welding of aluminum alloys with regard to heat dissipation and the prevention of hot cracking [96]. It was believed that the pulsation of parameters, such as tool rotation rate or welding speed, in FSW could have benefits as well, ranging from improved process symmetry to increased heat dissipation and material mixing. The first FSW process variant that involved the pulsation of parameters was Re-stir^{TM}, or reversal stir welding, which was developed by TWI. In this process, the tool rotation is pulsed in full reversal mode either before or after one full tool rotation. The motivation behind this process development was to achieve symmetry and disrupt the advancing-retreating paradigm dictated by conventional FSW, which can lead to characteristic defects, such as hooking defects or top sheet thinning defects in lap welds, on either side of the joint. Preliminary investigations into effectiveness of Re-stir^{TM} at achieving this goal were promising [35]. Another investigation into pulsing began with the issue of tool oscillation. Eberl et al. pulsed the welding speed to reduce tool oscillation in the joining of dissimilar alloys, but found there were unanticipated secondary benefits, including enhanced mixing of the alloys, reduced volumetric flaws, and higher tensile strength [97]. Perhaps the most comprehensive study of pulsed FSW parameters to date however was conducted by Ballun and focused on joining 0.25 thick Al 6061 in a butt joint configuration.

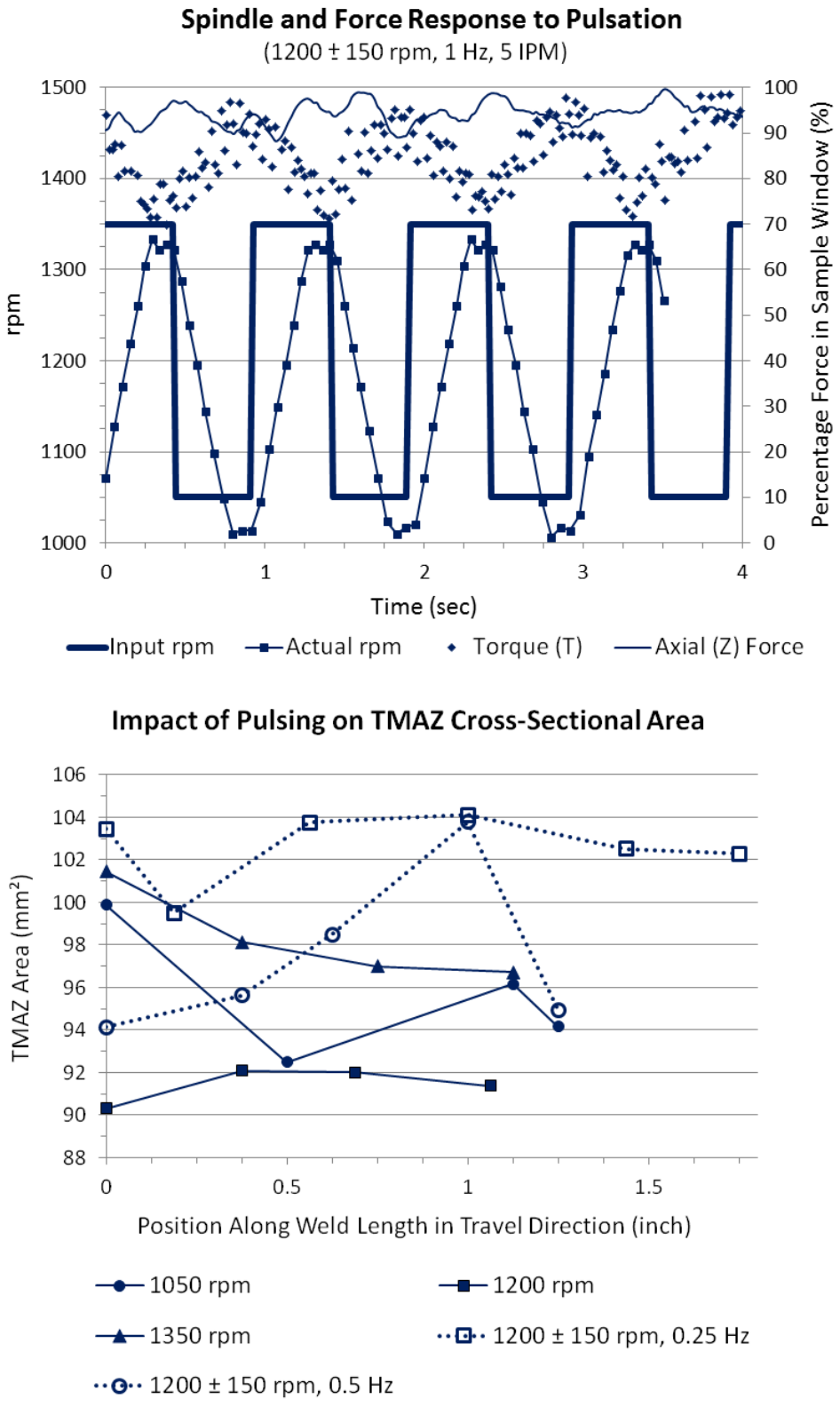

Figure 89: PFSW Process Response and TMAZ Area Data Documented by Ballun [98, 99]

Plasticine was joined as well, as a workpiece analog, to enable better understanding of the effects of pulsation on material flow via striking visual characteristics. Tool rotation rate was pulsed at ±150 rpm as a square wave input at varying means and frequencies, and the response of the welding robot spindle was characterized and the effect on welding forces examined. Figure 89 displays process response data from this examination. Then, through rigorous materials testing, the effect of pulsation on weld strength and weld structure, specifically the cross-sectional area of the TMAZ, was examined. It was determined that pulsing did not have a statistically significant impact on weld strength when compared to conventional welds (within the limited parameter windows of the study), but pulsing did however facilitate a statistically significant increase in TMAZ area, the data for which is also displayed in Figure 89. The greatest increase occurred at the 1200 ± 150 rpm, 0.25 Hz freq, and 5 inch per minute (IPM) parameter set [98, 99]. This increase in TMAZ area held great promise for potential PFSW of lap joints, for which a large TMAZ, or wide joint interface, is critical for preventing interfacial fracture. This potential process improvement of friction stir lap joining via parameter pulsation did indeed inspire aspects of the present study.

Technical Approach

Material and Tool Selection

The material selected for this study was 2198-T8 Al-Li alloy. Sheets of this material in 0.125 inch thickness were provided by Spirit AeroSystems of Wichita, KS. In order to create lap joints that were representative of stiffener-to-skin joints that might be

found in a typical aerospace application, the 0.125 inch thick sheets were milled down to 0.0625 inch thickness. This gauge reduction was performed by Tennessee Metal Works of Nashville, TN. For simplicity, the sheets were milled from one surface, which is not ideal in terms of achieving consistent through-thickness properties, but this compromise made part holding manageable in the absence of a vacuum table. The as-received and milled surface roughness of the sheets was characterized after the reduction. This was measured with a TR200 Handheld Roughness Tester, and the collected data is displayed in Table 4.

Table 4: As-Received and Milled Surface Roughness

	Mean, Ra (um)	RMS, Rq (um)	Max Peak-to-Valley, Rt (um)
As Received - Transverse	0.892	1.081	4.678
As Received - Longitudinal	0.410	0.500	2.279
Milled Surface	0.360	0.427	1.758

By all three roughness parameters documented, the milled surfaces of the sheets exhibited lower roughness than the as-received material, which was a desirable outcome. In order to further characterize the parent material, especially considering the method and degree of gauge reduction, tensile specimens of unwelded, milled sheets were tested to establish baseline strength in both longitudinal and transverse directions. Table 5 displays the collected tensile data. The level of ultimate tensile strength (UTS) observed was more than satisfactory when compared to published values for 2198, and the level of anisotropy, at only 4.2% (calculated as a percent difference of UTS values), was relatively impressive considering Al-Li alloys have been historically notorious for this

undesirable property. In this study, milled surfaces of the 2198 coupons were placed against each other, leaving factory surfaces outward, to form lap joint configurations which were then welded perpendicular to the rolling direction so that specimens would be pulled longitudinally during tension-shear testing.

Table 5: Parent Material Strength

	σ_y (0.2% Offset, MPa)	UTS (MPa)
2198-L	391.5	522.7
2198-T	345.0	501.4

As specified in the objectives, two tools were selected for comparison in this study. These tools featured the same probe design with differing shoulder geometries: a flat, scrolled shoulder which was operated at a tilt angle of 2 degrees; the other a tapered, scrolled shoulder which was operated at a tilt angle of 0 degrees. Photographs of the tools are displayed in Figure 90.

Figure 90: FSW Tools: Flat Shoulder (Left) and Tapered Shoulder (Right)

The diameter of the flat shoulder was 0.625 inch, while the tapered shoulder extended from the probe to the boundary of the 1 inch diameter tool shank with a change in height of 0.058 inch, or at an angle of approximately 8.8 degrees. The flat shoulder tool was operated with a heel plunge depth of 0.002 inch, and the shoulder plunge of the tapered shoulder tool was set such that the width of shoulder-workpiece engagement was approximately 0.625 inch as well. The probes in the two-piece tools were set to length so that they penetrated the bottom sheet by 30% of the top sheet thickness. Both tools featured a 0.25 inch diameter, threaded, fluted probe with a cup feature on the terminal end.

Parameter Selection

An experimental weld matrix was designed to accommodate both tool designs and the three welding processes: conventional, weaved, and pulsed FSW. Welding speed and rpm were varied along with special parameters for the process variants, including the weaving parameters introduced previously and the pulsing rpm magnitude and frequency. The weld matrix was designed with two dominant regimes in mind as well: a strength regime and a tracking regime, which refers to the typically lower than ideal welding speeds necessitated by weaving for the primary purpose of tracking a desired path [126, 127]. Initial welding trials with the tapered shoulder tool and previous experience with the flat shoulder tool, documented in Chapter IV, also indicated that the two geometries were suited for different operating windows, specifically with respect to rpm. All of these issues were taken into account to allow for direct comparisons across factors and levels of the weld matrix, which is shown in Table 6. Three welding speeds and three

rotation rates were tested. For the weaved welds, parameter sets were selected to satisfy both the strength and tracking regimes. All weaved welds were stationary, with the step size and step threshold (force) set to zero, meaning the tool was weaved laterally side to side while following a straight, planned path.

Table 6: Experimental Weld Matrix

No	Shoulder	Welding Type	Speed (IPM)	rpm	Special Information
1	Flat	Conventional	14	1500	n/a
2	Flat	Conventional	8	1200	n/a
3	Flat	Conventional	3	900	n/a
4	Flat	Weaved	14	1500	R = 0.015 in, P = 0.85 sec
5	Flat	Weaved	8	1200	R = 0.015 in, P = 1.3 sec
6	Flat	Weaved	3	900	R = 0.040 in, P = 1.3 sec
7	Flat	Weaved	3	900	R = 0.015 in, P = 1.3 sec
8	Flat	Pulsed	14	1500	+/- 150 rpm, Freq = 0.70 Hz
9	Flat	Pulsed	8	1200	+/- 150 rpm, Freq = 0.40 Hz
10	Flat	Pulsed	3	900	+/- 150 rpm, Freq = 0.15 Hz
11	Tapered	Conventional	14	900	n/a
12	Tapered	Conventional	8	1200	n/a
13	Tapered	Conventional	3	900	n/a
14	Tapered	Weaved	14	900	R = 0.015 in, P = 0.85 sec
15	Tapered	Weaved	8	1200	R = 0.015 in, P = 1.3 sec
16	Tapered	Weaved	3	900	R = 0.040 in, P = 1.3 sec
17	Tapered	Weaved	3	900	R = 0.015 in, P = 1.3 sec
18	Tapered	Pulsed	14	900	+/- 150 rpm, Freq = 0.70 Hz
19	Tapered	Pulsed	8	1200	+/- 150 rpm, Freq = 0.40 Hz
20	Tapered	Pulsed	3	900	+/- 150 rpm, Freq = 0.15 Hz

The lateral rate for all weaved welds was 6 IPM. With strength as the objective, the pause length (P) and the weave radius (R) were selected as 1.3 seconds and 0.015 inch, respectively; values which were supported by the findings of Hendricks [101]. The pause length was reduced at the highest welding speed however. To test parameters dictated by

a tracking objective, the weave radius was selected as 0.040 inch, a level which is supported by the findings of Chapter IV. For pulsed rpm welds, a square wave input of magnitude 150 rpm was selected to build upon the work conducted by Ballun on the same welding robot. As the welding speed was varied, the pulsing frequency was modified to maintain a pulse length equal to that of the best case for TMAZ area increase documented by Ballun, which was a 0.333 inch pulse length at 0.25 Hz and 5 IPM [98]. Lap joint coupons were welded with the advancing side of the tool adjacent to the lapped edge, which is important to note given the sheet interface-load path interaction during mechanical testing. This particular configuration has shown repeatedly to exhibit better mechanical properties, provided the hooking-defect turns upward and any top-sheet thinning that is present is relatively easy to mitigate given proper parameter selection. All samples in the matrix were welded and then allowed to naturally age for a minimum of 3.5 weeks prior to mechanical testing.

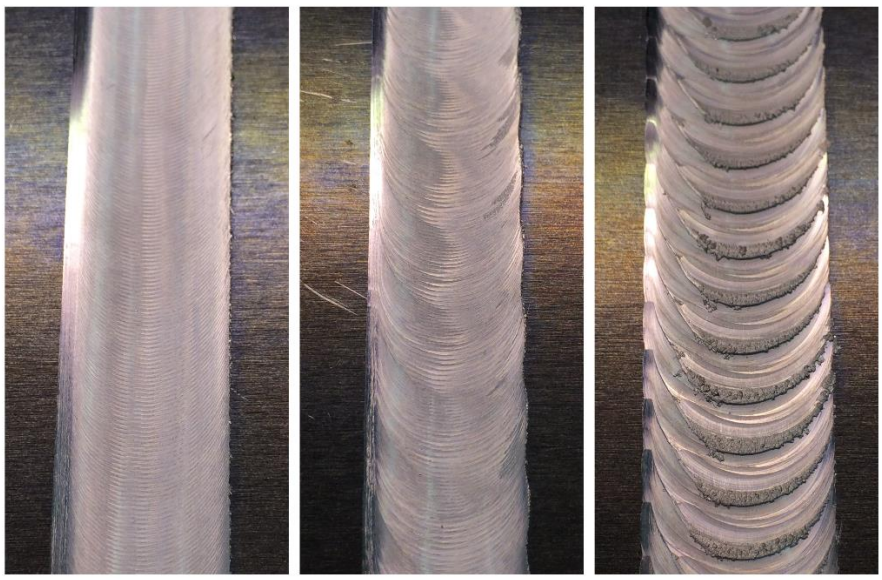

Figure 91: Representative Weld Surface Finishes Created with the Tapered Shoulder Tool: Conventional FSW, Pulsed FSW, and Weaved FSW (Left to Right)

Figure 91 displays a sample of representative weld surface finishes that result from the different process variants. Welds shown were created with the tapered shoulder tool, and the effect of process variants on material flow is certainly visually evident on the surface.

Evaluation Methods

Mechanical evaluation of the welds included tension-shear testing and hammer S-bend testing, which has been shown to be indicative of weld performance in fatigue loading. Three 0.5 inch wide specimens were taken from each weld for tension-shear testing to capture variation and allow for statistical analysis of the strength data. Single-factor (with replication) Analysis of Variance (ANOVA) was performed in order to determine if differences in strength, in particular comparisons of interest across factors/levels of the weld matrix, were statistically significant at a confidence level of 95% (alpha = 0.05). Weld surface finish and modes of fracture in tension-shear were also visually inspected to evaluate differences originating from tool geometry. In certain cases, welds were selected to be repeated with faying surface sealant applied in the joint prior to welding to determine its effect on mechanical properties as well. Macrographic cross-sections of these welds were created in order to quantify the level of sealant migration within the joint and the interaction of tool geometry with this phenomenon. Polished macrographs were etched with Keller's reagent and subsequently imaged.

Sealant Application Methods

The faying surface sealant used for select welds was Pelseal® 2077, which is formulated with Viton®, from DuPont Performance Elastomers. It is a one-part

fluoroelastomer sealant requiring no separate curative compound that can be applied with a caulking gun in a bead configuration [173]. Sealant was applied in select welds with the objective of sealing the faying surfaces while leaving a clean path for the tool to travel through during welding, a scenario that was developed and characterized for the purpose of automatic sealant path tracking in Chapter IV. Dual beads of sealant, 0.06 inch (1.5 mm) in diameter, were applied 1.6875 inch apart, centered about the weld path, which was outlined by scored lines on the bottom sheet 0.6875 inch apart to slow the ingress of sealant during clamping and welding. Welds were made with the sealant in the uncured state, meaning sealant application, placement of the top sheet, clamping, and welding occurred within a 20 minute timeframe. Both the top and bottom sheets were cleaned prior to sealant application using first, a 50% methyl ethyl ketone and 50% toluene solvent with lint free wipes, followed by a second cleaning with pre-wetted isopropyl alcohol wipes.

Results

The weld strength data was divided into three groups for presentation: the 1200 rpm, 8 IPM parameter set, which was common across all welding type and shoulder profile combinations, a high welding speed, or 14 IPM, parameter set, which includes 1500 rpm and 900 rpm tool rotation rates, depending on the shoulder profile, and a tracking regime, or 900 rpm, 3 IPM data set, which was also common across all welding type and shoulder profile combinations and included two different weave radii as well. Figure 92 displays the weld strength data for the 1200 rpm, 8 IPM parameter set and Figure 93 displays the weld strength data for the high welding speed parameter set.

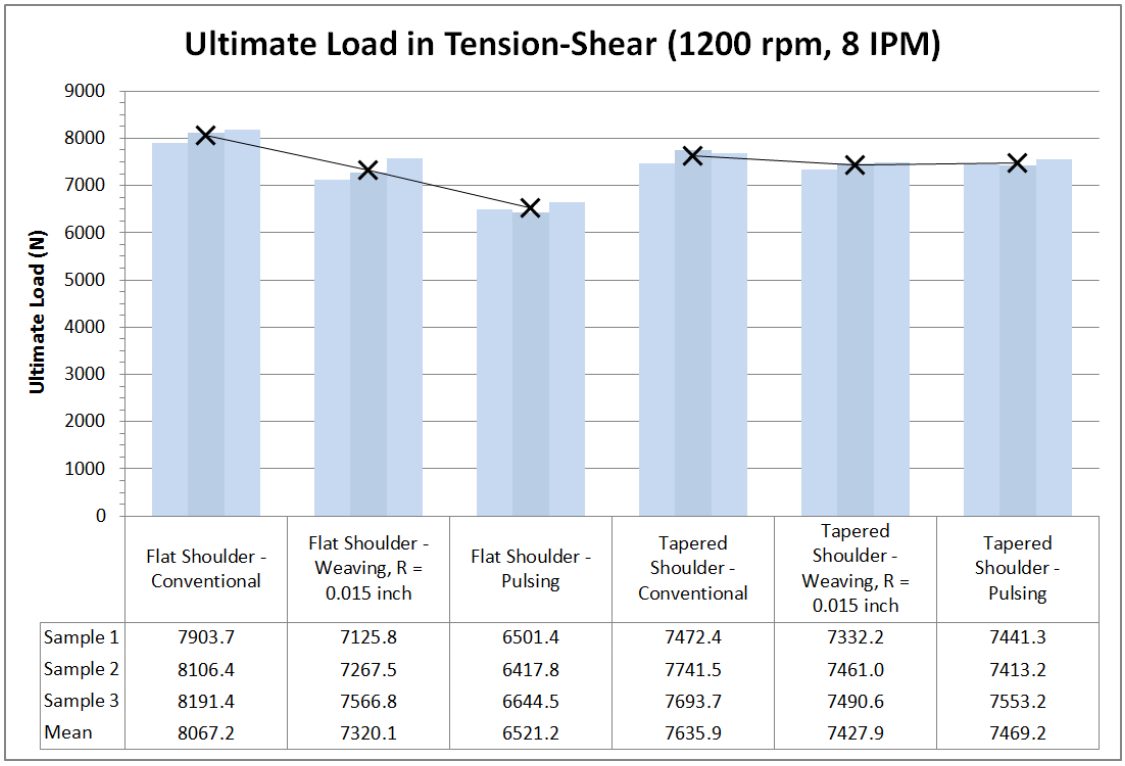

	Flat Shoulder - Conventional	Flat Shoulder - Weaving, R = 0.015 inch	Flat Shoulder - Pulsing	Tapered Shoulder - Conventional	Tapered Shoulder - Weaving, R = 0.015 inch	Tapered Shoulder - Pulsing
Sample 1	7903.7	7125.8	6501.4	7472.4	7332.2	7441.3
Sample 2	8106.4	7267.5	6417.8	7741.5	7461.0	7413.2
Sample 3	8191.4	7566.8	6644.5	7693.7	7490.6	7553.2
Mean	8067.2	7320.1	6521.2	7635.9	7427.9	7469.2

Figure 92: Weld Strength for the 1200 rpm, 8 IPM Parameter Set

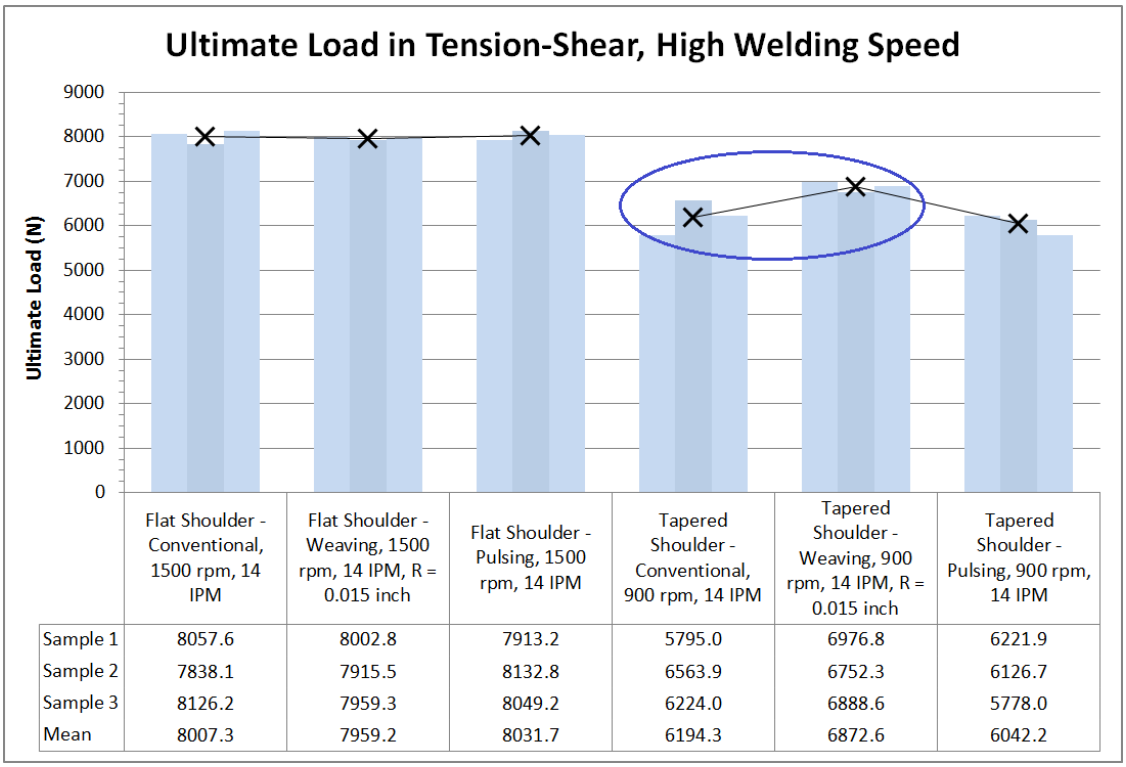

	Flat Shoulder - Conventional, 1500 rpm, 14 IPM	Flat Shoulder - Weaving, 1500 rpm, 14 IPM, R = 0.015 inch	Flat Shoulder - Pulsing, 1500 rpm, 14 IPM	Tapered Shoulder - Conventional, 900 rpm, 14 IPM	Tapered Shoulder - Weaving, 900 rpm, 14 IPM, R = 0.015 inch	Tapered Shoulder - Pulsing, 900 rpm, 14 IPM
Sample 1	8057.6	8002.8	7913.2	5795.0	6976.8	6221.9
Sample 2	7838.1	7915.5	8132.8	6563.9	6752.3	6126.7
Sample 3	8126.2	7959.3	8049.2	6224.0	6888.6	5778.0
Mean	8007.3	7959.2	8031.7	6194.3	6872.6	6042.2

Figure 93: Weld Strength at the High (14 IPM) Welding Speed

Differences in strength due to shoulder profile and process variants are evident without statistical analysis in many cases. These interactions are discussed further in the following section. The highest weld strength documented was conventional welding with the flat shoulder tool at 1200 rpm and 8 IPM. If the failure mode for this case was approximated as a tensile failure in one sheet of the lap joint, which is a simplification of most failure modes observed, the 8067.2 N would translate to a 400.1 MPa tensile stress, or 76.6% of the UTS documented in Table 5. One documented case of a process variant increasing weld strength over that of its conventionally welded counterpart is highlighted in Figure 93. This was the case of weaving with the tapered shoulder tool, and statistical analysis was used to determine if the increase in strength was significant. The slight increase in mean strength for the pulsing variant over its conventionally welded counterpart with the flat shoulder tool, also in Figure 93, was not selected for further investigation. Figure 94 displays the weld strength data for the tracking regime, or the 900 rpm and 3 IPM, welds. Overall strengths were indeed lower for this regime, as expected, but differences in weld strength relating to tool shoulder geometry are strikingly evident in Figure 94. Tracking of blind sealant paths was documented with flat shoulder geometry at a weave radius (R) of 0.040 inch and relatively low welding speed and tool rotation rate in Chapter IV, but the impact of these parameters, selected primarily for successful tracking, on weld strength was a concern. The data documented in Figure 94, and highlighted by arrows for the particular variant and weave radius of interest, suggests that a change in shoulder geometry while leaving all other factors the same might in itself facilitate a dramatic increase in weld strength.

As discussed previously, the two shoulder geometries do seem suited for differing

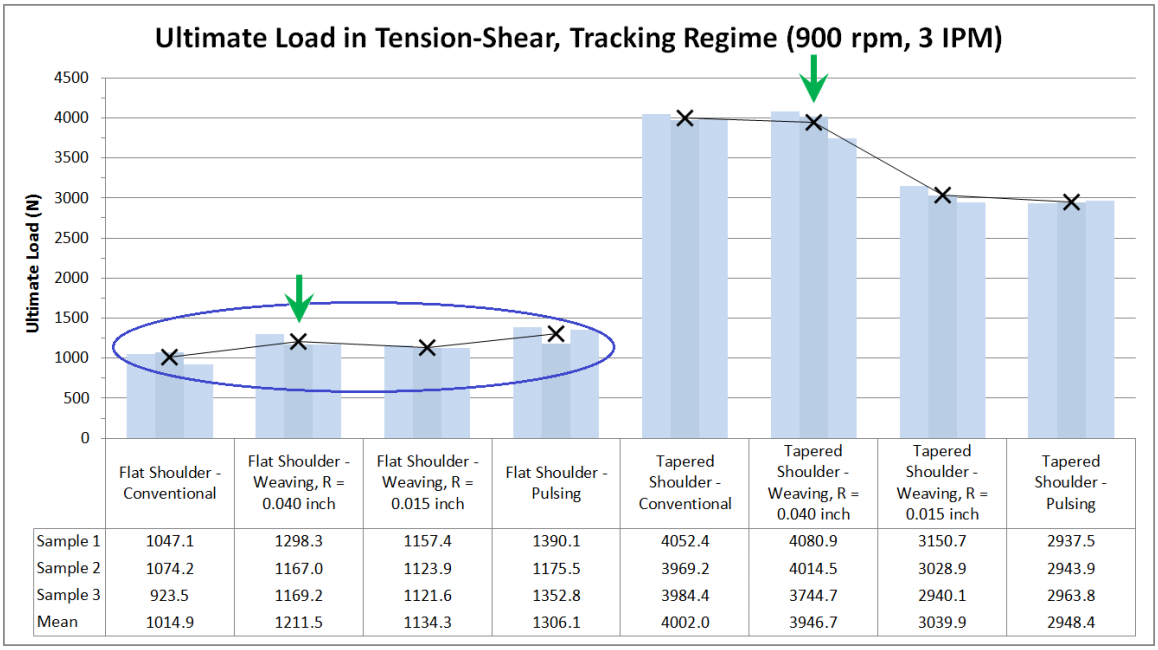

	Flat Shoulder - Conventional	Flat Shoulder - Weaving, R = 0.040 inch	Flat Shoulder - Weaving, R = 0.015 inch	Flat Shoulder - Pulsing	Tapered Shoulder - Conventional	Tapered Shoulder - Weaving, R = 0.040 inch	Tapered Shoulder - Weaving, R = 0.015 inch	Tapered Shoulder - Pulsing
Sample 1	1047.1	1298.3	1157.4	1390.1	4052.4	4080.9	3150.7	2937.5
Sample 2	1074.2	1167.0	1123.9	1175.5	3969.2	4014.5	3028.9	2943.9
Sample 3	923.5	1169.2	1121.6	1352.8	3984.4	3744.7	2940.1	2963.8
Mean	1014.9	1211.5	1134.3	1306.1	4002.0	3946.7	3039.9	2948.4

Figure 94: Weld Strength for the Tracking Regime

operating windows, especially with respect to tool rotation rate, but another factor may indeed be weld surface finish, in that the combination of a flat shoulder and weaving can result in a scalloped surface finish along which welds fail in testing, whereas a tapered shoulder might leave a more desirable surface finish in theory. Figure 95 displays the as-welded surface finish of the weaved tracking regime welds at R = 0.040 inch for both shoulder geometries. While both tools leave behind a surface finish characteristic of weaving, that of the tapered shoulder tool is more desirable with less weld flash; and, this difference in shoulder-workpiece interaction did indeed translate into differences in weld failures during mechanical testing. Figure 96 displays fractured tension-shear specimens for both the flat and tapered shoulder tools in the tracking regime for conventional welding, weaving at R = 0.040 inch, and weaving at R = 0.040 inch with sealant. Sealant weld coupons were designed to have larger faying surfaces, which explains the difference in general specimen appearance from non-sealant to sealant in the figure.

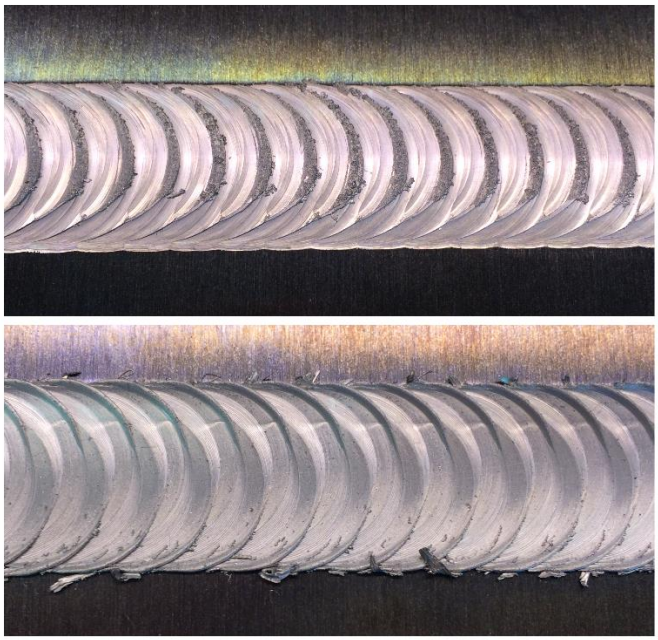

Figure 95: Surface Finish of Weaved Tracking Regime Welds (at R = 0.040 inch); Tapered Shoulder Tool (Top), Flat Shoulder Tool (Bottom)

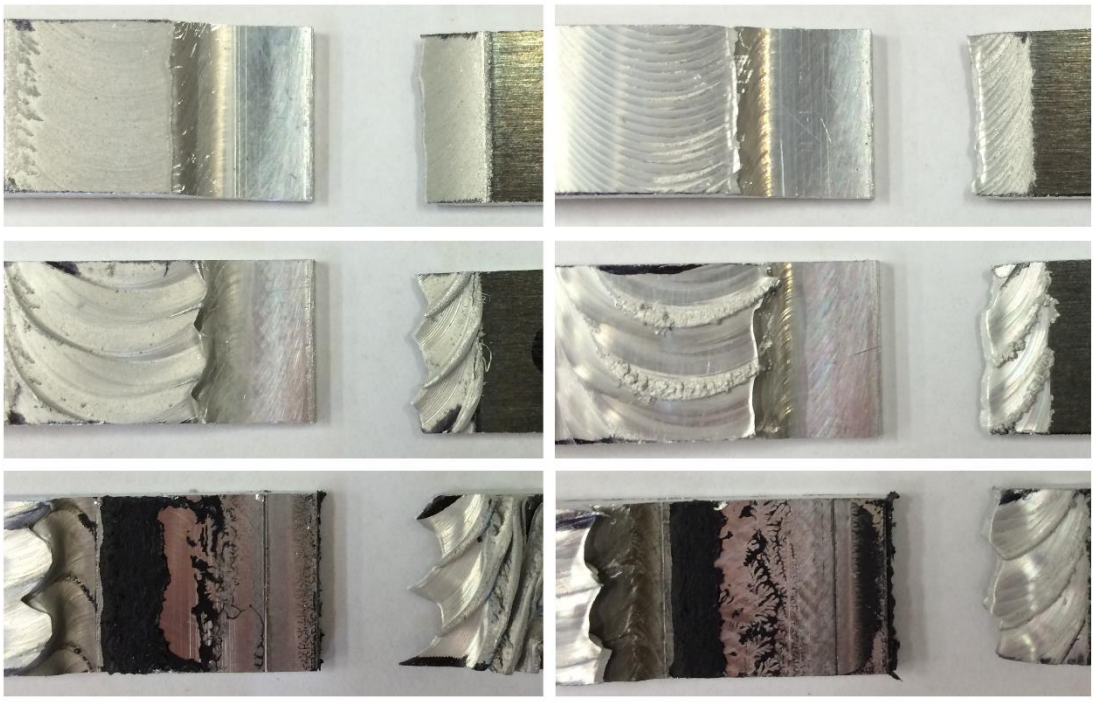

Figure 96: Tension-Shear Fracture Surfaces in the Tracking Regime; Conventional, Weaving at R = 0.040 inch, and Weaving at R = 0.040 inch with Sealant (From Top to Bottom); Flat Shoulder Tool (Left) and Tapered Shoulder Tool (Right)

No specimens in the study failed in interfacial fracture, which is a desirable outcome and an indicator of adequate TMAZ width; all specimens failed in pull-out fracture in either the top or bottom sheet. Conventionally welded specimens exhibited fractures that were similar in nature for both tools. Differences in appearance begin to arise however when weaved welds and weaved welds with sealant are examined. It is evident from the jagged fracture surfaces that weaved welds failed along the peaks and valleys of the scalloped surface finish. The presence of sealant within the joint exacerbated this effect, which may in part be due to the insulative nature of the sealant, leading to greater softening of the top sheet during welding. This trend of less desirable fracture surface from conventional to weaving to weaving with sealant was more pronounced however with the flat shoulder tool. The tapered shoulder tool reduced the severity of this effect, which helps to explain the dramatic difference in weld strength for the two tool geometries in the tracking regime. The effect of sealant on the shape of the sheet interface and resulting weld strength will be discussed further in this section.

Also of great interest in Figure 94 are increases in weld strength for each of the process variants over their conventionally welded counterpart with the flat shoulder tool. This is highlighted in the figure and is an excellent outcome that is discussed more in the following section as well. Again, the question of whether these increases in strength, along with the strength increase highlighted in Figure 93, were statistically significant was addressed with ANOVA. These outcomes are summarized in Table 7. An F value greater than F-critical or a P-Value lower than alpha (0.05) indicates a significant difference, or a greater than 95% probability that the two sample sets in question originated from different underlying populations.

Table 7: ANOVA Results

	Groups	F-Critical	F	P-Value	Significant
	- Flat Shoulder, 3 IPM, 900 rpm -				
Conventional (Weld 3)	Weaving, R = 0.040 inch (Weld 6)	7.708647	9.57377	0.036427	✓
Conventional (Weld 3)	Weaving, R = 0.015 inch (Weld 7)	7.708647	6.235521	0.066974	
Conventional (Weld 3)	Pulsing (Weld 10)	7.708647	12.97517	0.022716	✓
	- Tapered Shoulder, 14 IPM, 900 rpm -				
Conventional (Weld 11)	Weaving, R = 0.015 inch (Weld 14)	7.708647	8.559016	0.043003	✓
	- Flat Shoulder, Weaving, R = 0.040 inch, 3 IPM, 900 rpm -				
No Sealant (Weld 6)	Sealant (Weld 6S)	7.708647	46.26744	0.00244	✓
	- Tapered Shoulder, Weaving, R = 0.040 inch, 3 IPM, 900 rpm -				
No Sealant (Weld 16)	Sealant (Weld 16S)	7.708647	0.064795	0.811623	

At the high welding speed with the tapered shoulder tool, weaving at R = 0.015 inch facilitated a statistically significant increase in weld strength. In the tracking regime with the flat shoulder tool, both weaving at R = 0.040 inch and pulsing facilitated statistically significant increases in weld strength. The case of weaving at R = 0.015 inch was very nearly significant. Because testing a tracking regime was closely tied to and inspired by the idea of tracking blind sealant paths in lap joints, select welds in the this regime were repeated with faying surface sealant applied in the joint prior to welding. Again, these were the weaved welds with R = 0.040 inch for both shoulder geometries. Figure 97 displays the measured weld strengths for these welds alongside their non-sealant counterparts. Welding at these parameters with the flat shoulder tool and with sealant saw a statistically significant decrease in weld strength to the lowest level documented in the study. However, with the tapered shoulder tool, again weld strength was much higher, but too the presence of sealant did not have a significant impact on weld strength when compared to the non-sealant counterpart. The outcomes of these statistical analyses can be found in Table 7 as well.

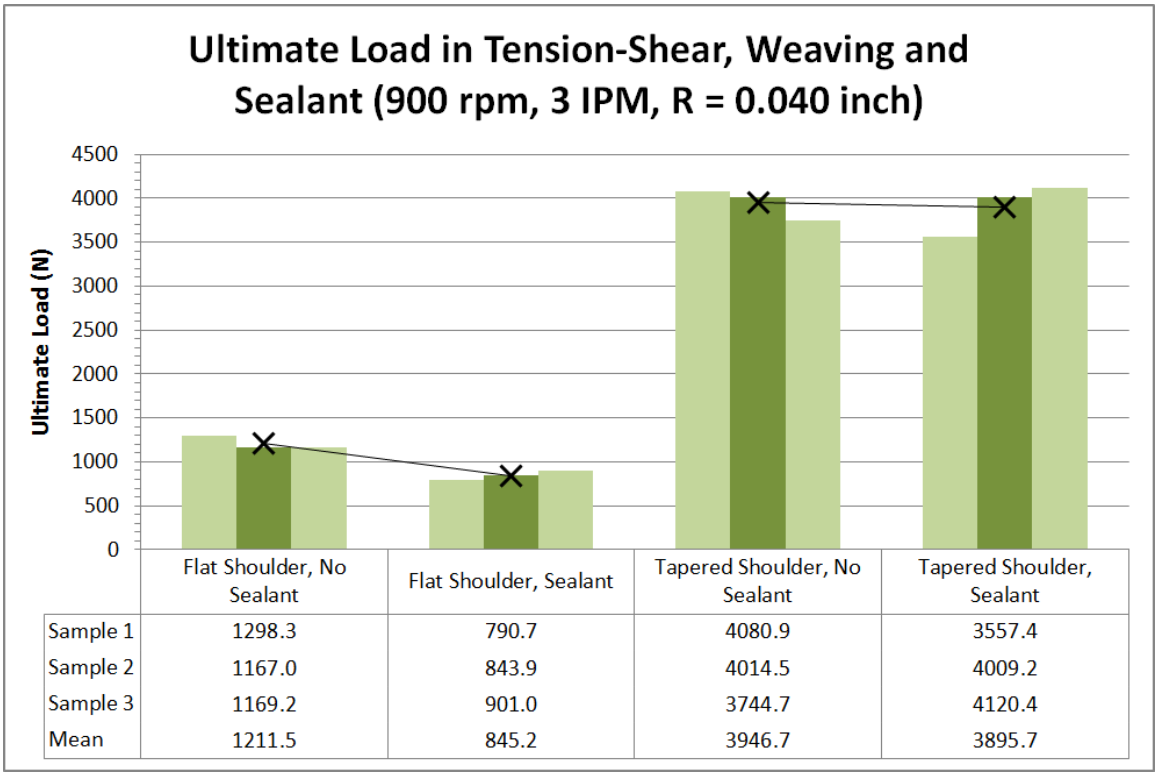

	Flat Shoulder, No Sealant	Flat Shoulder, Sealant	Tapered Shoulder, No Sealant	Tapered Shoulder, Sealant
Sample 1	1298.3	790.7	4080.9	3557.4
Sample 2	1167.0	843.9	4014.5	4009.2
Sample 3	1169.2	901.0	3744.7	4120.4
Mean	1211.5	845.2	3946.7	3895.7

Figure 97: Weld Strength for Sealant Welds at Tracking Parameters

It was suspected that the interaction between tool shoulder geometry and sealant migration within the joint was related to the difference in sealant impact on weld strength for the different shoulder geometries. Ideally, when high strength is the objective, as opposed to tracking performance for instance, pressure from the tool during welding forces sealant to migrate away from the joint line to the faying surfaces. To compare the degree of sealant migration for the tool geometries, macrographs of the sealant welds were examined. These are displayed in Figure 98. With the tapered shoulder tool there was indeed a wider spread of sealant from the joint line, which helps to explain the different trends in strength between the two tools with regard to sealant. Also visible in Figure 98 are the joint interfaces and characteristic lap weld defects created by each tool. While a hooking defect on the advancing side and top sheet thinning on the retreating

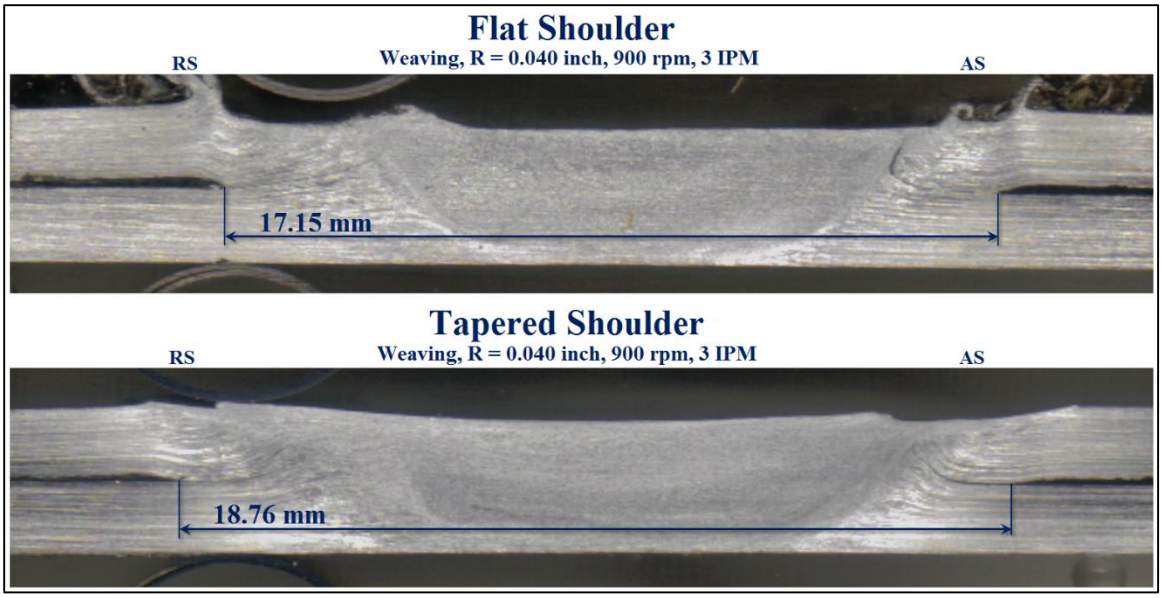

Figure 98: Macrographs of Sealant Welds

side are evident for both tool geometries, these are more severe with the flat shoulder tool, and in general, it is evident that the tapered shoulder tool, especially at the parameters of the tracking regime, creates in a more desirable sheet interface shape and is capable of mitigating the potential negative effects of sealant on mechanical properties.

Discussion and Conclusions

The overall objective of this research was to study the friction stir welding of 2198 Al-Li alloy in a lap joint configuration for aerospace applications. Within this broad objective, a number of issues were explored. These included the incorporation of process variants, the comparison of tool geometries and corresponding tilt angles, and the application of faying surface sealant within the joints prior to welding. More specifically, variants included pulsing and weaving, and parameters for these variants were selected in order to build upon the findings of more preliminary studies. The use of a tapered

shoulder tool operating at a zero degree tilt angle, which could reduce the degree of freedom requirement for welding robots, was compared to the more traditional combination of a flat shoulder tool operating at a relatively high tilt angle and welding speed. The purpose of including sealant in the study was to examine the interactions of tool geometry and process parameters with sealant migration in the joint and determine how this would impact advancements made previously with regard to sealant quality evaluation and control.

With respect to tool geometry, lap welding with a tapered shoulder tool at zero degrees tilt angle was demonstrated to be completely feasible. While the highest strength welds in the study were created with the flat shoulder tool, the two tools seemed suited for different operating windows of tool rotation rate and welding speed, and more experience has been accrued with the flat shoulder tool. Operation of the tapered shoulder tool could indeed be optimized with a larger parameter study. It is interesting to note, however, that much higher weld strengths were possible with the tapered shoulder tool at 3 IPM in the tracking regime, suggesting that this tool geometry may extend operating windows for welding speeds lower than that typically encountered in the literature for the more traditional combination of a flat shoulder tool operated at a tilt angle.

With respect to process variants, there were multiple cases where either weaving or pulsing increased weld strength over the conventionally welded counterparts at statistically significant levels. Differences in weld strength across factor/levels of the matrix were characterized as either marginal or significant using single-factor ANOVA. Further analysis, such as two-factor ANOVA, could have been performed to explore

interactions between variants, tool geometry, and parameter levels, but these interactions are readily evident upon examination of the strength plots in Figures 92 - 94. Tool geometry and variants do indeed interact, such that sometimes variants have an effect on weld strength, and sometimes they do not. Likewise, parameter sets, or levels of tool rotation rate and welding speed, can affect whether variants contribute to strength or not. Strength increases facilitated by variants were more common when the conventional or initial base strength was relatively low, suggesting that the tool was being operated outside of its ideal parametric window. Normally, a tool would not intentionally be operated outside of its ideal window for strength, if that window has been characterized, but there are cases when other process objectives may dictate this be done. One such case is joint tracking, which the literature has shown can dictate that lower than normal welding speeds be used. Another case is when high strength tool materials are used in the welding of high melting point or highly abrasive alloys. Tool materials that are wear resistant are often more brittle and prone to facture, which can dictate that more conservative parameters be used to protect the tool [55]. In cases such as this, process variants might be used to recapture some of the weld strength lost. Another advantage to using process variants, pulsing in particular, is that there exists the potential for tool geometry to be simplified. Some of the most significant work aimed at improving tool design and functionality was performed by TWI in an effort to create more desirable weld structure in lap joints. This involved increasing TMAZ width to prevent interfacial fracture and reducing the severity of joint-line remnant defects [35]. The resulting tools, including SkewStir™ and the Flared Triflute™, were great improvements to prior technology, but unfortunately involve more complex designs that are difficult and costly

to manufacture. Because it has been shown that pulsing, as well as weaving, can similarly promote increases in the size of the TMAZ, which in some cases translates into increased weld strength, these variants might allow for the use of simplified tool geometry that is less expensive to manufacture and comes with shorter lead times.

Also in this study, certain welds were selected to be repeated with faying surface sealant applied in the joint prior to welding. This is a critical aspect of welding in the manufacture of structures for aerospace applications. It was shown that the presence of sealant within the joint exacerbated undesirable characteristics, such as unusual fracture surfaces in the case of weaving. Macrographs of welds with sealant also revealed joint-line remnant defects for both tool geometries. The tapered shoulder geometry did show promise however in mitigating some of the negative aspects of welding with sealant. In addition to creating a more desirable sheet interface shape at the parameters with which sealant was used, the tapered shoulder design facilitated sealant migration further away from the joint line than did the flat shoulder. This is desirable in cases where weld strength is the primary objective. As mentioned throughout this study, however, there are cases when sealant rigidity can actually be a beneficial property. When sealant is resistant to migration within the joint, it has a stronger force signature, meaning processes like sealant quality evaluation and automatic tracking of blind sealant paths perform much more reliably, as demonstrated in Chapters III and IV, respectively. Because the degree of sealant migration and the sealant force signature are strongly related, it is likely that these processes would be impacted by a change in tool geometry, especially with regard to sensitivity in a detection and control context. It is anticipated that a sealant quality evaluation process could potentially be implemented without a prior evaluation of

force magnitude or frequency characteristics related to a change in tool geometry, provided a technique is utilized that does not require training data. The force signature of a tapered shoulder tool interacting with a path feature in the joint would likely have to first be characterized in order to implement a robust sealant tracking process. And, while sensitivity may be affected and controller parameters require tuning, it is anticipated that the benefits of welding with tapered shoulder geometry would not preclude the implementation of a successful tracking process.

CHAPTER VI

CROSS-STUDY STRENGTH EVALUATION

Introduction

The purpose of this chapter is to examine and compare both the base material properties and the mechanical properties of welds made with aluminum alloys 2024-T3 and 7075-T6 in Chapter III and Chapter IV with those made with the aluminum-lithium alloy 2198-T8 in Chapter V. The examination takes place in the context of the search for new materials that can improve upon the performance of incumbent alloys for aerospace applications and the weld strengths that can be achieved by joining these materials with FSW. One of the primary motivators for upgrading to more advanced materials is the promise of weight reduction, while maintaining the strength, toughness, or fatigue crack growth performance dictated by the application. As previously discussed in the aerospace section of the literature review, one the most high profile material transitions that involved FSW was the switch from 2219 to 2195 in NASA's construction of the space shuttle external tank. This material upgrade resulted in a 7,500 lb reduction in the dry structural weight of the tank and involved the inclusion of 700 feet of FSW welds [81, 139]. This weight reduction allowed for payload increases that were critical for the transport of large deliveries to the International Space Station [195].

Similarly, manufacturers in commercial aviation are seeking to reduce the weight of assemblies by replacing incumbent 2xxx and 7xxx aluminum alloys with more advanced alloys, of which, aluminum-lithium alloys, in sheet, plate, and extrusions, are

receiving much attention. As mentioned in Chapter V, two candidate alloys are 2099 extrusions for stringers and 2199 sheet for aircraft skins [194, 195]. Giummarra et al. conducted a trade study aimed at achieving weight reduction while maintaining or improving material performance under conditions specific to Bombardier advanced aircraft designs. Three areas were chose for examination: lower wing skin, lower wing stringers, and the fuselage skin. It was found that by adjusting the alloy and tempering practices, significant weight reduction was possible while maintaining performance metrics in these areas. Figure 99 displays the estimated weight savings for the lower wing skin compared to skin manufactured with the baseline 2024-T351 plate material.

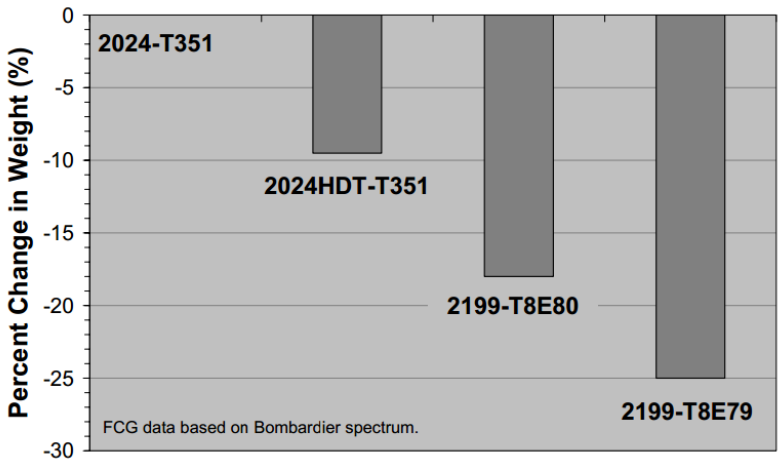

Figure 99: Bombardier Lower Wing Weight Comparisons for Various Alloys Documented by Giummarra et al. [195]

It is shown that a weight reduction of up to 25% was possible with the proper selection of alloy and tempering practice. The authors therefore highlighted the importance of material supplier-customer relationship in aerospace. The weight saving improvement was attributed to lower density and better fatigue crack growth resistance of 2199 [195].

Material Properties

Like 2199, the 2198 alloy welded in Chapter V is a third-generation aluminum-lithium alloy. A hallmark of the third-generation alloys is that they contain less than 2% lithium, unlike their second-generation predecessors. Table 8 displays the chemical composition of 2198 alongside other third-generation aluminum-lithium alloys that have been discussed here.

Table 8: Chemical Composition (Nominal wt% values) for Some Third-Generation Al-Li Alloys [194]

Alloy	Li	Cu	Mg	Ag	Zr	Mn	Zn
2195	1.0	4.0	0.4	0.4	0.11		
2198	1.0	3.2	0.5	0.4	0.11	0.5 max	0.35 max
2099	1.8	2.7	0.3		0.09	0.3	0.7
2199	1.6	2.6	0.2		0.09	0.3	0.6

The addition of lithium to a 2xxx series material, alloyed largely with copper but containing other elements as well, leads to alloy weight reduction, due to the lower density of lithium, and increased strength due to the participation of lithium in the formation of strengthening precipitates. While 2198 in various tempers generally does not exhibit the tensile strength of 7075-T6 for example, its lower density results in a material with a high specific strength, or strength-to-weight ratio, which can rival or surpass that of 7075-T6. Examining the aircraft skin candidate materials, 2198-T8 exhibits both higher ultimate strength and lower density than 2024-T3. This is shown in Table 9, which displays the ultimate tensile strength, density, and resulting specific strength properties of the alloys welded in Chapters III, IV, and V of this dissertation.

Table 9: Specific Strength of Select Alloys

	2198-T8	7075-T6	2024-T3
UTS* (MPa)	522.7	545.2	449.3
Density° (g/cm^3)	2.64	2.81	2.78
Specific Strength	**198.0**	**194.0**	**161.6**
	*Measured experimentally °Reference values		

Ultimate tensile strength values were determined experimentally in the preceding chapters by conducting tensile tests of unwelded parent material specimens, and density values were supplied by reference. And, while base material properties and performance largely influence structural design decisions, another critical aspect is joining methodology and the resulting overall structural performance than can be achieved. Accordingly, the objective of the following section is to compare weld strengths across common welding parameter sets and best-case parameter sets for the different materials welded in Chapters III, IV, and V.

Weld Strength

The initial lap weld parameter study with 2024-T3 and 7075-T6 alloys in Chapter III included rotations rates of 600, 900, 1200, and 1500 rpm and welding speeds of 8, 14, and 20 IPM. This was a fairly broad spectrum of parameters that was intended to allow for optimization with respect to weld strength in tension-shear. Welding parameters of Chapter IV were initially selected from this parameter set as well. The experimental weld matrix for the 2198-T8 alloy used in Chapter V was designed with several criteria in mind. This included the accommodation of process variants and varying tool geometry,

while maintaining common parameter sets across factors and levels of the matrix. It also was designed, however, with knowledge gained from the first parameter study with 2xxx and 7xxx series alloys. Rotation rates and welding speeds were selected to, in some cases, exactly match previous parameter combinations. And, while differences in optimized welding parameters from alloy to alloy can certainly be expected, this makes for nonetheless interesting comparisons. Figure 100 displays weld strengths for all common, conventionally welded parameter combinations of rotation rate and welding speed for Chapters III and V.

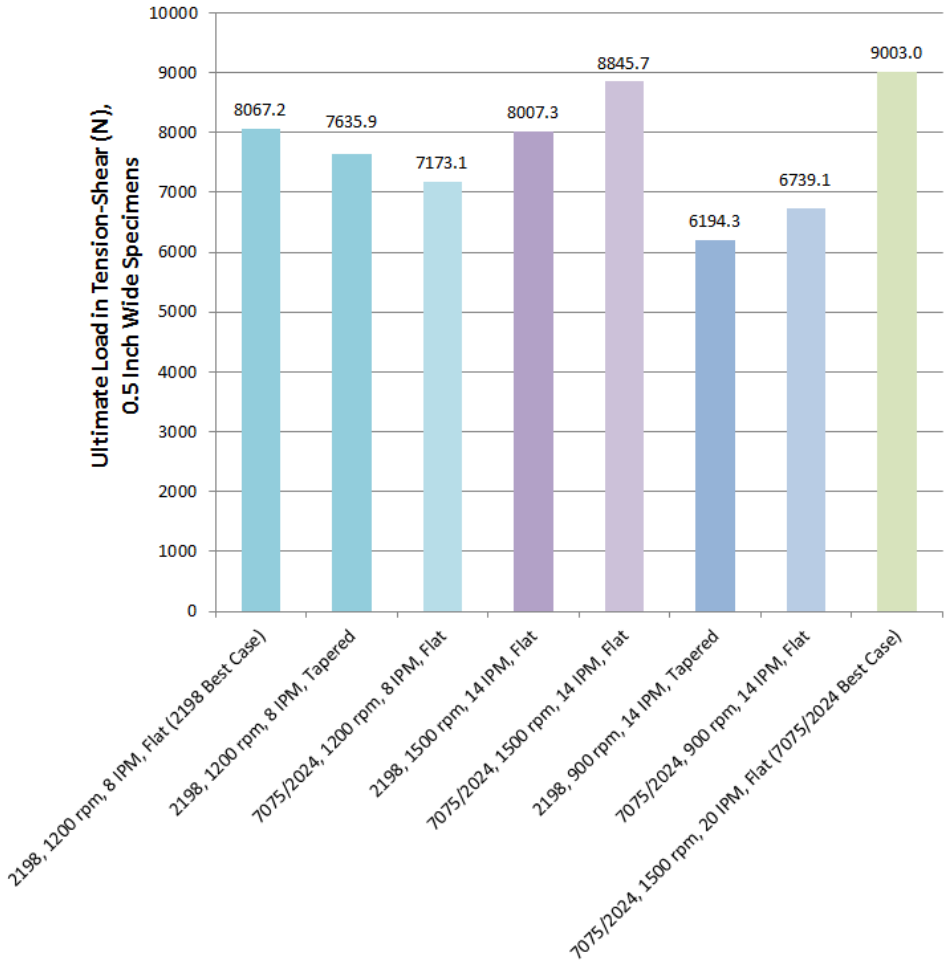

Figure 100: Weld Strength for Common Parameter Sets across Chapters III and V

Weld strength is reported as ultimate load in tension-shear for 0.5 inch wide test specimens. Select tensile strength values first reported in Figure 63 of Chapter III for 2024-T3 and 7075-T6 welds were converted to this convention for comparison purposes. Data is grouped and color coded by parameter combination, with darker colors representing welds made with 2198-T8 and lighter corresponding colors representing dissimilar welds of 2024-T3 and 7075-T6. Tool shoulder geometry is denoted, given the differences of Chapter V, and best cases for each alloy are designated as well. Overall, results indicate that the strengths achievable with the different alloys tested are comparable. The effects that varying parameter combinations and tool shoulder geometries have on strength are evident as well. The best-case parameter set used with the incumbent alloys exhibits higher strength than the best-case with 2198-T8, but it should be noted that a larger optimization study was performed with the incumbent alloys, and the strength achievable with 2198-T8 could likely be improved with a similar, large study. This was an encouraging outcome, in that it underscored the potential improvements to aerostructure design that are made possible with the use of advanced alloys, due to both their superior base material properties and the joint strengths that are attainable with FSW. It is for this reason that manufacturers currently have such high interests in incorporating these materials into their products.

CHAPTER VII

ADAPTIVE CONTROL OF PROCESS TORQUE FOR THE PURPOSE OF ESTIMATING TOOL WEAR

This chapter is published in:

Gibson, B.T., Cook, G.E., Prater, T., Longhurst, W.R., Strauss, A.M., Cox, C.D., "Adaptive Torque Control of Friction Stir Welding for the Purpose of Estimating Tool Wear," *Proceedings of the Institution of Mechanical Engineers, Part B: Journal of Engineering Manufacture*, Vol 225, No 8, 2011, pp. 1293 - 1303.
DOI: 10.1177/2041297510393629

Abstract

An adaptive torque controller for FSW is presented that can estimate parameters such as probe radius that may be changing throughout the welding process. Implementing an adaptive controller with this capability would be of interest to industry sectors in which FSW is performed on high melting point alloys or metal matrix composites. Welding these materials has shown a greatly accelerated rate of tool wear. Simulations were conducted to examine how extreme tool wear would affect controller performance and how accurately the controller could estimate the probe radius. A simplified wear model consisting of a linear decrease in probe radius was used to verify controller performance. Next, a wear model consistent with wear patterns seen in the welding of highly abrasive materials was developed. Results indicate that torque is controlled effectively while a change in system dynamics is experienced, as would be expected with adaptive control, but also that the tool profile is accurately estimated after an initial identification period.

Introduction

FSW is currently employed in a wide range of industries, including aerospace, land transportation, railway, and marine, and the advantages of FSW are numerous. The joining technique allows for the welding of dissimilar materials or materials that are difficult or impossible to fusion weld. In addition, FSW is an energy efficient process that requires no shielding gas or filler material. There are no fumes, arc flash, or spatter associated with the process, and the relatively low temperatures result in low distortion and low residual stresses. The welding process involves a non-consumable (ideally) rotating tool, consisting of a probe and shoulder, which traverses the joint line of materials to be joined. Heat is generated through both friction and plastic deformation of the welded material. A number of tool designs have been tested and optimized to maximize material flow and interrupt oxide layers at the interface of the materials [35]. Tools commonly have threaded cylindrical probes; however, probes may take other forms with asymmetrical geometry. Shoulders are often scrolled to enhance the material containment ability of the tool. A significant area of concern in the area of tool design, especially when probe and shoulder features are incorporated, however, is tool wear.

Steel tools are commonly used for the welding of low melting-point alloys such as aluminum. Steel becomes inadequate though when more abrasive materials, such as Metal Matrix Composites (MMCs), are welded. The abrasive nature of the imbedded particles leads to greatly accelerated tool wear [8, 196]. Figure 101 displays the progressive nature of tool wear on MMC. Tool wear can potentially alter the material flows within the weld seam [197]. It would not be unusual for tools that have experienced significant wear to produce less than adequate vertical flows, which can lead

to voids that run the length of the weld [196]. Figure 102 displays cross sections of welds performed with highly worn or "self-optimized" tool geometry.

Figure 101: Progressive Tool Wear on MMC at 2000 rpm, 7 IPM; (1) New Probe, (2) 8 Inches of Weld, (3) 16 Inches of Weld, (4) 24 Inches of Weld

Statistical models have been developed to predict the volume percentage of tool wear that will occur based on weld parameters.

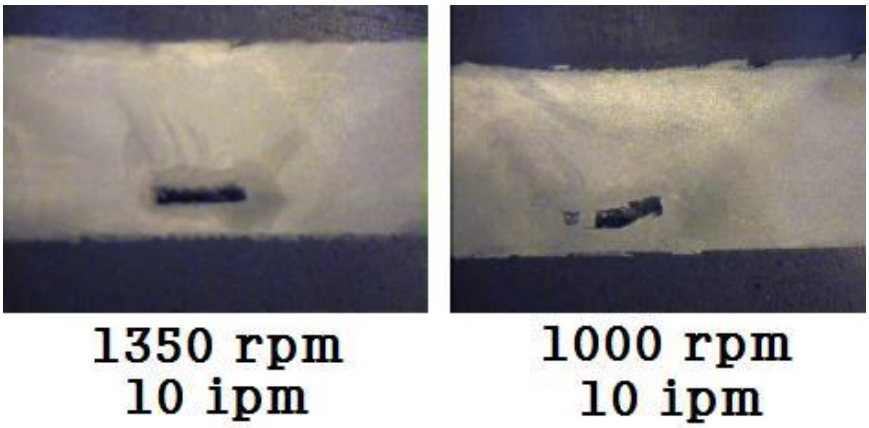

Figure 102: Weld Defects Resulting From Worn Trivex™ Tool

In a study by Prater et al., a formula was developed through statistical analysis that predicts the amount of wear on a steel trivex tool while welding MMC (Al 359/SiC/20P) [53]. The percent tool wear is given by Equation 17:

$$W = 0.584(l) - 1.038(v) + 0.009(\omega) - 6.028 \quad (17)$$

where W is the percent tool wear, l is the weld length in inches, v is the traverse rate in inches per minute, and ω is the tool rotation speed in rpm. The model was tested against experimental results over a range of welding parameters and produced a maximum error of only 13.4% [53]. While these types of models are valuable for predicting the amount of wear that may take place over a given weld, it is more desirable to have an in-process prediction of tool wear based on force and/or torque feedback signals. An estimate of this type is more likely to produce an accurate picture of the amount of wear that is taking place at a given time.

As discussed in previous chapters, the forces and torque experienced by a FSW tool during welding can vary greatly depending on the welded material, tool geometry, joint configuration, and weld parameters. The axial force (Fz) is most significant and can range in values from 1 to 15 kN for aluminum welds [30]. Torque values, which strongly depend on tool design and weld parameters, can be as high as 60 Nm [32]. Planar forces are often measured for research purposes as well. These forces are the traversing force (Fx) and the side force (Fy), and they are usually much lower in magnitude when compared to the axial force. Because FSW is often performed at the end of compliant industrial robots and on materials that may exhibit significant thickness variations, it is usually necessary to employ some type of force control, torque control, or a hybrid control to limit loads on the robot joints and links and to keep the tool properly engaged with the material surface [110]. To account for the compliant nature of industrial robots and material variation, force control with plunge depth as the controlling variable or torque control with plunge depth as the controlling variable are most commonly used. Force and torque control have proved to be advantageous in other ways, as well. When

force control is used with rotation speed as the controlling variable, increased weld strength can be achieved. When force control is used with traverse speed as the controlling variable, heat distribution or weld input energy along the weld seam can be controlled [43]. Longhurst et al. used a PID control architecture tuned with the Ziegler-Nichols method to successfully implement torque control in FSW [115]. Implementing adaptive torque control in FSW will allow the welding process to be referenced to a model, which will allow for the estimation of in-process weld parameters, including tool profile.

Controller Design

Concept

A conceptual flowchart for controlling torque and estimating tool wear is shown in Figure 103. Weld parameters that are used in the simulation of FSW are also fed into the adaptive torque controller and process model. This is where tool wear estimates are produced, based on a comparison of the model and the actual process. The model-based partitioned controller was developed using Craig's method [198]. Craig's method has been used successfully in other industrial applications, such as adaptive voltage control in arc welding [199].

Adaptive Control

In FSW, the torque experienced by the tool depends on, among other factors, plunge depth. Therefore, traditionally, plunge depth is changed to maintain a constant

desired torque value during steady-state welding (not during tool plunge or tool retraction). When extreme tool wear is experienced, the relationship between plunge depth and torque is not fixed. To implement adaptive control, a process constant, Kpt, is introduced to the control loop. Kpt is a variable gain that changes with tool wear. The torque control loop may be seen in Figure 104.

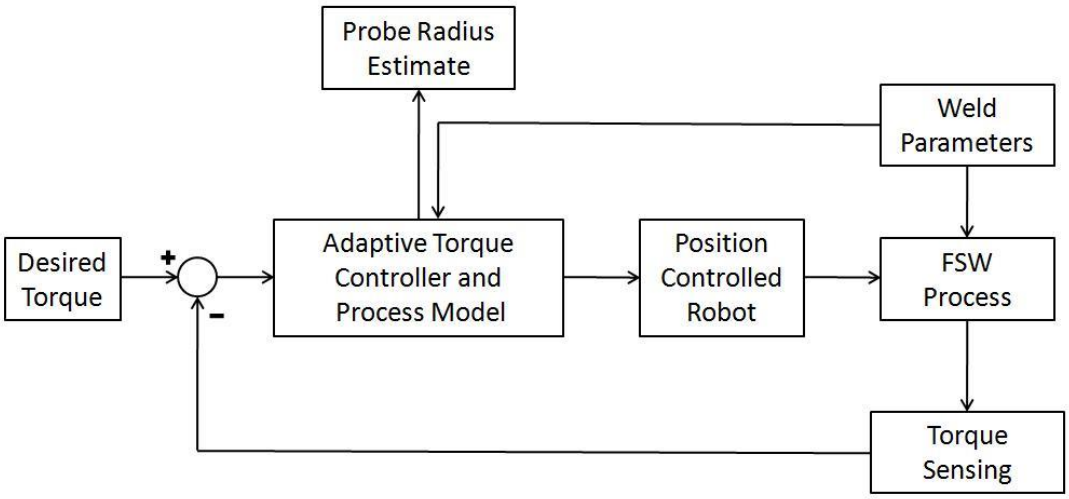

Figure 103: Adaptive Control Flowchart

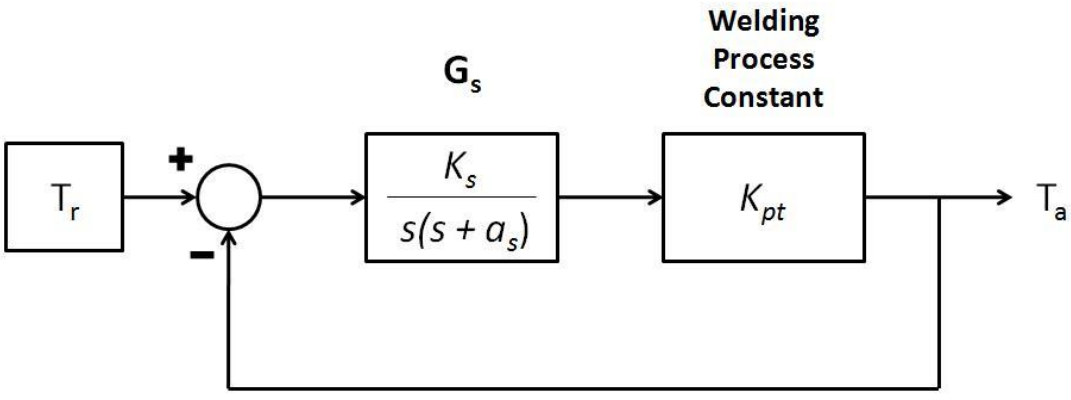

Figure 104: Closed Loop Torque Control

Design of Adaptive Controller

The transfer function of the servo motor controlling tool plunge has been adapted from a study by Longhurst [43] and simplified so it can be applied to an adaptive controller using Craig's method [198]. The transfer function is given by:

$$G_s(s) = \frac{P}{T_m} = \frac{K_s}{s(s+0.25)} \tag{18}$$

where P represents position and T_m represents motor torque. If $P*K_{pt} = T_a$ is used in (18), the differential equation may be written as:

$$\ddot{T_a} + 0.25\dot{T_a} = K_s K_{pt} T_m \tag{19}$$

Equation (19) may be rewritten in the form

$$\frac{1}{K_s K_{pt}}\ddot{T_a} + \frac{0.25}{K_s K_{pt}}\dot{T_a} = T_m \tag{20}$$

Equation (20) reveals that $C_1 = 0.25/K_s K_{pt}$ and $C_2 = 1/K_s K_{pt}$. Equation (20) may be rewritten

$$C_2\ddot{T_a} + C_1\dot{T_a} = T_m \tag{21}$$

Equation (21) is a nonlinear second-order differential equation because C_1 and C_2 vary inversely with K_{pt}, which changes nonlinearly with probe radius.

The adaptive controller is partitioned into a model-based portion and a servo portion. The control law for the model-based portion is

$$T_m = \alpha T_m{}' + \beta \tag{22}$$

Equating (21) and (22) yields

$$C_2\ddot{T}_a + C_1\dot{T}_a = \alpha T_m{}' + \beta \tag{23}$$

Parameters α and β must be chosen such that the system will appear as the linear second-order system

$$T_m{}' = \ddot{T}_a \tag{24}$$

To satisfy equations (23) and (24), α and β must be selected as

$$\alpha = C_2$$
$$\beta = C_1\dot{T}_a$$

The controller employs estimates of constants C_1 and C_2 that will be denoted $\widehat{C_1}$ and $\widehat{C_2}$. Parameter errors $\widetilde{C_1}$ and $\widetilde{C_2}$will also be established that are $\widetilde{C_1} = C_1 - \widehat{C_1}$ and $\widetilde{C_2} = C_2 - \widehat{C_2}$. A proportional-plus-derivative control law is selected such that

$$T_m = \widehat{C_2}\ddot{T}_a + \widehat{C_1}\dot{T}_a \tag{25}$$

or $$T_m = \widehat{C_2}T_m{}' + \widehat{C_1}\dot{T}_a \tag{26}$$

where $T_m{}' = \ddot{T}_r + K_v\dot{e} + K_p e$ and $e = T_r - T_a$. T_r represents the reference torque.

Equating (21) and (26) and substituting for T_m' yields

$$C_2\ddot{T}_a + C_1\dot{T}_a = \widehat{C_2}\left[\ddot{T}_r + K_v\dot{e} + K_p e\right] + \widehat{C_1}\dot{T}_a \tag{27}$$

The error equation can be realized by rearranging equation (27) as

$$C_2\ddot{T}_a + [C_1 - \widehat{C_1}]\dot{T}_a = \widehat{C_2}\ddot{T}_r + \widehat{C_2}[K_v\dot{e} + K_p e]$$

then $\left[C_2 - \widehat{C_2}\right]\ddot{T}_a + \left[C_1 - \widehat{C_1}\right]\dot{T}_a = \widehat{C_2}\left[\ddot{T}_r - \ddot{T}_a\right] + \widehat{C_2}[K_v\dot{e} + K_p e]$

and finally $\widetilde{C_2}\ddot{T}_a + \widetilde{C_1}\dot{T}_a = \widehat{C_2}[\ddot{e} + K_v\dot{e} + K_p e]$

The error equation may be written as $\ddot{e} + K_v\dot{e} + K_p e = \frac{1}{\widehat{C_2}}[\widetilde{C_2}\ddot{T}_a + \widetilde{C_1}\dot{T}_a]$ (28)

Equation (28) may be written in matrix form as

$$\ddot{e} + K_v\dot{e} + K_p e = \frac{1}{\widehat{C_2}} W(\ddot{T}_a, \dot{T}_a)\Phi \tag{29}$$

where $W\left(\ddot{T}_a, \dot{T}_a\right) = [\ddot{T}_a \quad \dot{T}_a]$ and $\Phi = \begin{bmatrix}\widetilde{C_2} \\ \widetilde{C_1}\end{bmatrix}$

The estimation of parameters C_1 and C_2 is driven by system error, or more specifically, the filtered servo error signal. The filtered servo error is given by

$$E_s(s) = (s + \psi)E(s) \tag{30}$$

When the Laplace transform of the error equation is substituted into (30), the result is

$$E_s(s) = \frac{s+\psi}{s^2 + K_v s + K_p}\left(\frac{1}{\widehat{C_2}} W\left(\ddot{T}_a, \dot{T}_a\right)\Phi\right) \tag{31}$$

Assuming the strictly positive real lemma is satisfied, the state-space representation is

$$\dot{x} = Ax + B\left(\frac{1}{\widehat{C_2}} W\left(\ddot{T}_a, \dot{T}_a\right)\Phi\right) \tag{32}$$

$$e_1 = Cx$$

and $x = [e \quad \dot{e}]^T$

Also, matrices $\wp$ and $\mathbb{Q}$ are positive definite such that $\wp > 0$, $\mathbb{Q} > 0$, and

$$A^T\wp + \wp A = -\mathbb{Q} \tag{33}$$

$$\wp B = C^T$$

A Lyapunov function to ensure stability was selected as

$$v(x, \Phi) = x^T \wp x + \Phi^T \Gamma^{-1} \Phi \tag{34}$$

the derivative of which is

$$\dot{v}(x, \Phi) = \dot{x^T} \wp x + x^T \wp \dot{x} + \dot{\Phi^T} \Gamma^{-1} \Phi + \Phi^T \Gamma^{-1} \dot{\Phi}$$

or $$\dot{v}(x, \Phi) = -x^T \mathbb{Q} x + 2\Phi^T (W^T \frac{1}{\widehat{C_2}} e_1 + \Gamma^{-1} \dot{\Phi}) \tag{35}$$

where Γ is a diagonal matrix of estimator gains $\gamma_1$and γ_2.

By choosing $\dot{\Phi} = -\Gamma W^T \frac{1}{\widehat{C_2}} e_1$, the estimator equations become

$$\dot{\widehat{C_2}} = \frac{\gamma_2 \ddot{T_a}}{\widehat{C_2}} e_1 \quad \text{and} \quad \dot{\widehat{C_1}} = \frac{\gamma_1 \dot{T_a}}{\widehat{C_2}} e_1 \tag{36}$$

The adaptive torque controller was constructed in MATLAB's Simulink. The Simulink model is shown in Figure 105. Estimator equations (36) are implemented in the Adaptive Estimator block in the model. Estimates are fed into Alpha (α) and Beta (β) blocks which then form the control law (22). The Reference Torque block is a second-order filter whose input is a constant desired torque value with an added perturbation for adaptation purposes. The adaptation scheme is driven by error; therefore, a constant torque value alone would not allow the controller to adapt to changing system dynamics. The perturbation is a 1 Hz sine wave with an amplitude of 0.04. The FSW process is modeled in the Parameters block using the Nunes Rotating Plug model [26].

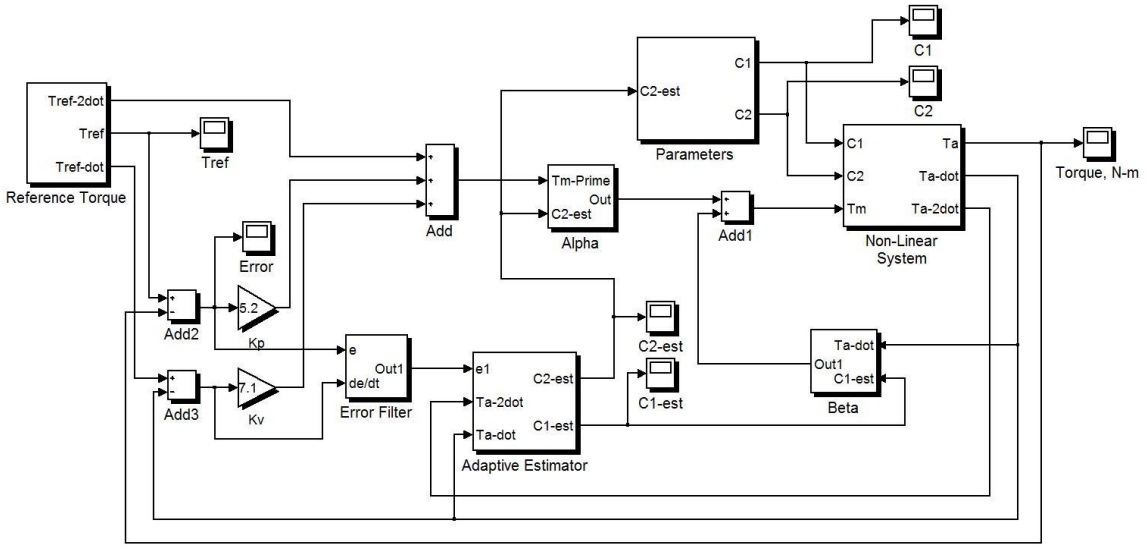

Figure 105: Adaptive Torque Controller, Simulink Model

Process Model

As previously discussed, in an experimental and theoretical study, Nunes et al. developed a model for material flow in the FSW process [26]. This model is known as the Rotating Plug model, and it is illustrated in Figure 17. Nunes et al. theorized that a thin layer of welded material sticks to and rotates with the probe. Immediately outside of this thin layer of material is a narrow shear zone in which plastic deformation occurs. This constitutes the primary flow. Secondary material flows are created by threads on the probe, assuming a threaded probe is used. The torque on the tool may be determined by assuming it arises from the interactions between the rotating plug and the surrounding material. Also, it is assumed that the rotating plug is sufficiently thin such that it has the same dimensions as the probe. Torque arising from secondary flows is ignored to allow for a simplified model. With these assumptions, the torque on the tool is given by Equation 3. Also in their study, Nunes et al approximated the shear flow stress with:

$$\sigma = \beta(T_m - T)^2 \quad (37)$$

in which T_m is the melting temperature of the welded material, T is the temperature at the shear zone, and β is a material constant. Also, the temperature at the shear zone is given by:

$$T = 530°C - \sqrt{\frac{9765(T-30°C)}{RPM}} \quad (28)$$

Nunes et al. adjusted the constant, 9765, so that equation (28) would match experimental results. In the present study, the Rotating Plug model has been used to simulate the FSW process in the Parameters block of the Simulink model in Figure 105. The FSW process determines the variable gain K_{pt}, on which constants C_1 and C_2 depend. Initial welding parameters and materials were selected to align with the research of Nunes et al. [26] so that values of temperature and shear stress obtained from simulations could be confirmed with the experimental data collected in the Nunes study.

Simulation Results

Welding Simulation

Simulations in this research were designed to replicate extreme tool wear. A 2195 Al-Li material was selected to align with research performed by Nunes et al. [26]. For this material, T_m = 530º C and β = 0.26 psi/K^2 [200]. A MMC material was not selected because the FSW model does not capture the effects of imbedded particles on torque. Tool rotation speed and traverse speed were selected as 700 rpm and 2 IPM (50.8

mm/min), respectively. These welding parameters not only align with the research conducted by Nunes et al. [26] but also fall within the more restrictive operating envelope for particle reinforced materials defined by studies by Feng et al. [201] and Marzoli et al. [202]. Significant tool wear was simulated over the course of a single 8 inch (203.2 mm) sample weld, meaning the simulation time in Simulink was 240 seconds. The FSW tool used in the simulation featured a shoulder diameter of ¾ inch (19.05 mm) and a cylindrical probe of ¼ inch (6.35 mm) diameter and ¼ inch (6.35 mm) length. The reference torque was selected as 21 Nm, which is slightly lower than the process torque indicated by the Nunes model for the selected parameters. This means that the controller will slightly retract the FSW tool to lower the torque to the desired level. It was necessary to select a lower desired torque because the Nunes model does not capture additional torque generated by the shoulder plunging below the surface of the material.

Controller Tuning

The controller was tuned by simulating a step in probe radius at 120 seconds. The step change in radius is shown in Figure 106. Using a step change is not representative of any type of phenomenon that would be seen in FSW, but rather an effective simulation to run for optimizing controller performance. Estimator gains, $\gamma_1$and γ_2, and the error filter gain ψ were tuned so that estimates of C_1 and C_2 would adapt quickly with a relatively low amount of overshoot or undershoot. Figure 107 displays the estimates of parameters C_1 and C_2. After the tuning process was completed, the selected gains were γ_1= 1.7, γ_2= 1.4, and ψ = 2. Because it adapted faster than the estimate of C_1, the estimate of C_2 was

selected to be used to derive the estimate of tool profile. C2-est was fed back to the FSW model in the Parameters block in Figure 105 to be used to estimate tool profile.

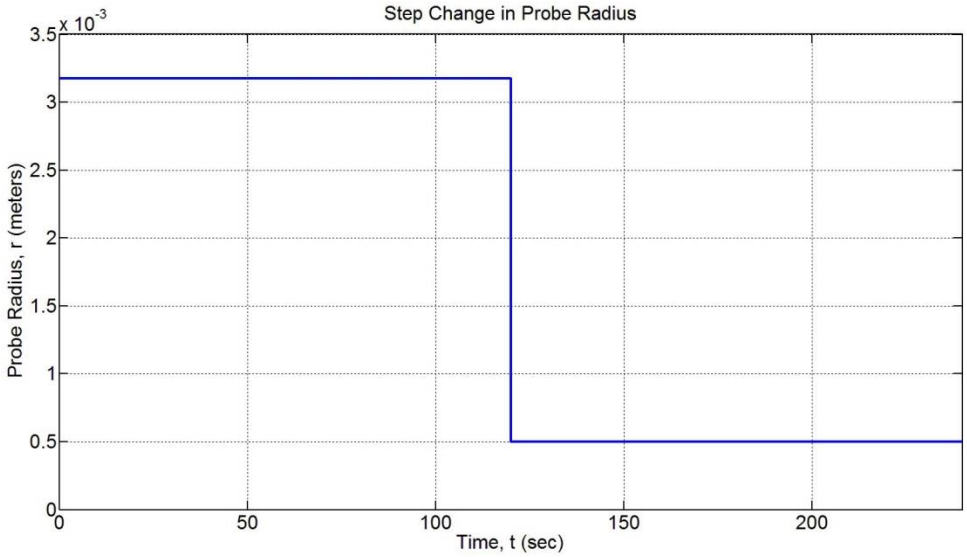

Figure 106: Step Change in Probe Radius for Controller Tuning Purposes

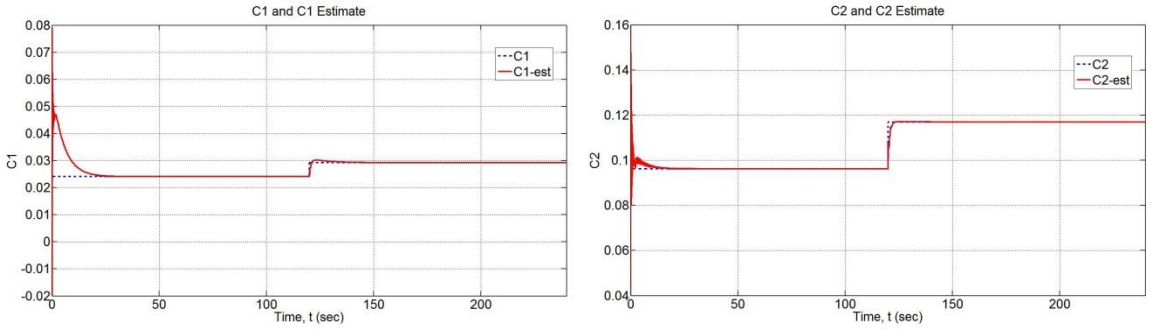

Figure 107: Controller Estimates with Step Change in Probe Radius

Simulation of Uniform Probe Wear

A simple tool wear model was simulated by assuming a linear change in probe radius over the length of the weld. Experiments have shown that assuming a linear relationship between tool wear and distance traversed is valid, given particular rotation

speeds and traverse rates [53]. The linear decrease in probe radius began at 20 seconds and continued throughout the simulation. The linear change in probe radius created non-linear changes in parameters C_1 and C_2. Figure 108 shows how the controller identified and adapted to these non-linear changes.

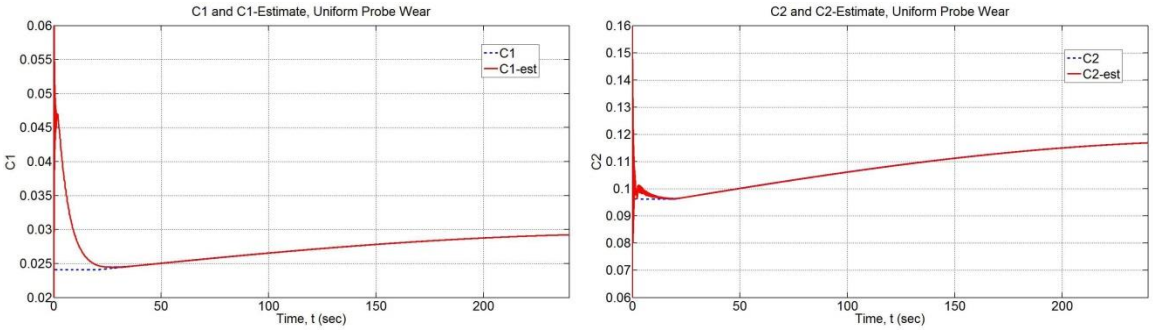

Figure 108: Nonlinear Changes in Controller Parameters While Simulating Uniform Probe Wear

The adaptation scheme of the controller was used to estimate the probe radius. Figure 109 displays the actual change in probe radius and the controller estimate.

Figure 109: Estimation of Uniform Probe Wear

After an initial identification period, the controller estimated the probe radius accurately while controlling torque with very low error. Figure 110 shows the error in torque while uniform tool wear is simulated.

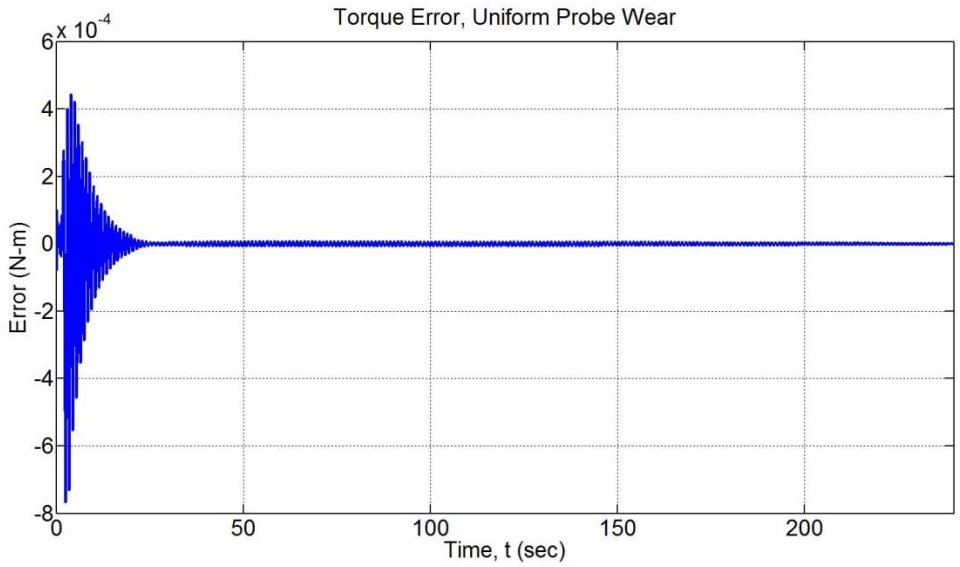

Figure 110: Torque Error While Simulating Uniform Probe Wear

Simulation of Non-Uniform Probe Wear

The uniform probe wear simulation proved that the adaptive controller not only controlled torque properly during FSW, but that it can also accurately identify welding parameters that are changing throughout the weld. The uniform probe wear model is not representative of wear modes that are seen in FSW however. In order to create a more realistic tool wear simulation, a wear model was developed that follows patterns seen in previous studies. A change in probe radius was again simulated, but that change was correlated to a change in cross sectional area of the probe. In studies of tool wear, cross-sectional area, which is proportional to volume, is most often used to characterize the

wear patterns. The probe length was segmented into five regions, each of which constitutes 20% of the initial cross sectional area. Tool wear was simulated by governing, beginning at the start of the weld, the percentage that each region constitutes of the whole. These percentage values were matched to experimental data obtained by Prater et al. [53]. Figure 111 displays the tool wear simulation model, which is based on a 24 inch (609.6 mm) MMC weld at 1500 rpm and 7 IPM (177.8 mm/min).

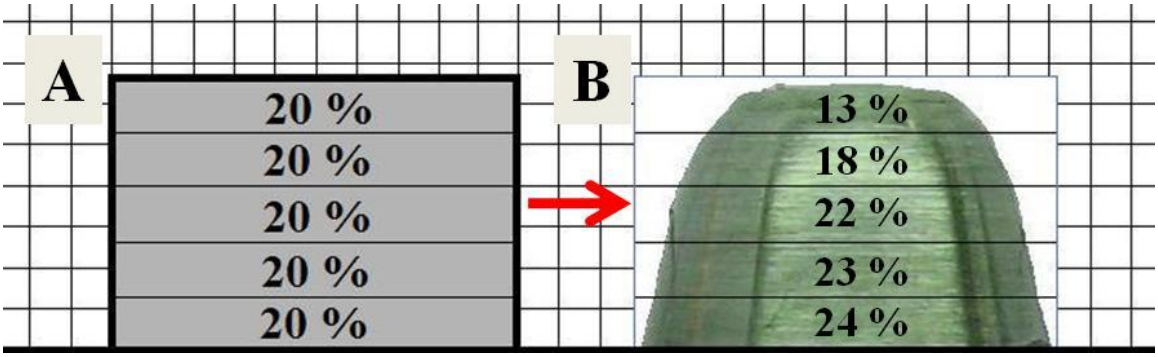

Figure 111: Non-Uniform Tool Wear Model; A) Original Probe Depiction, B) Probe after 24 inches of weld

The cross-sectional percentages were determined using a digital image of the probe and the pixel count tool in a digital image software package. Other common methods for quantifying tool wear include microscopy, weighing, mechanical gauging, profilometry, and the use of radiotracers. Because it is known how each region changes in size proportionately to one another, at any given time during the simulation the controller can estimate the average radius of the regions. Figure 112 shows a diagram of the average radii. A wear rate could also be predicted for t_5, which would represent wear in the axial direction. To simulate tool wear using the newly developed non-uniform wear model, weld parameters in the simulation were changed to 1500 rpm and 7 IPM (177.8 mm/min).

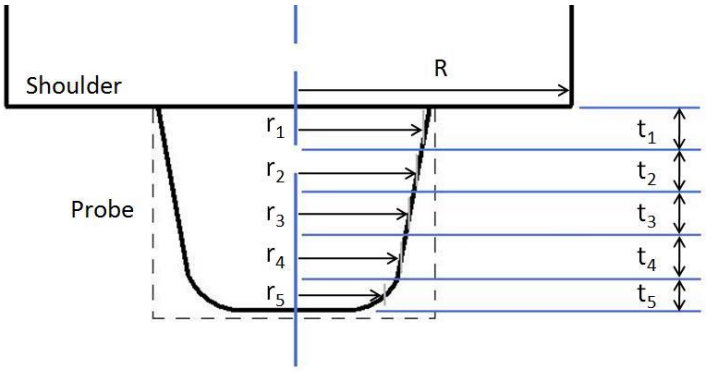

Figure 112: Non-Uniform Probe Wear Model for Radial Estimation

To replicate a 24 inch (609.6 mm) weld, the simulation was run for 206 seconds. Total probe cross-sectional area was varied linearly from 4.032E-5 m^2 to 3.34E-5 m^2 to account for the 17.16% decrease seen by Prater et al. [53], and the five regional cross-sectional area percentages were varied linearly from their initial values of 20% to the new percentages shown in Figure 111. Figure 113 shows how the controller estimated the radius of each region.

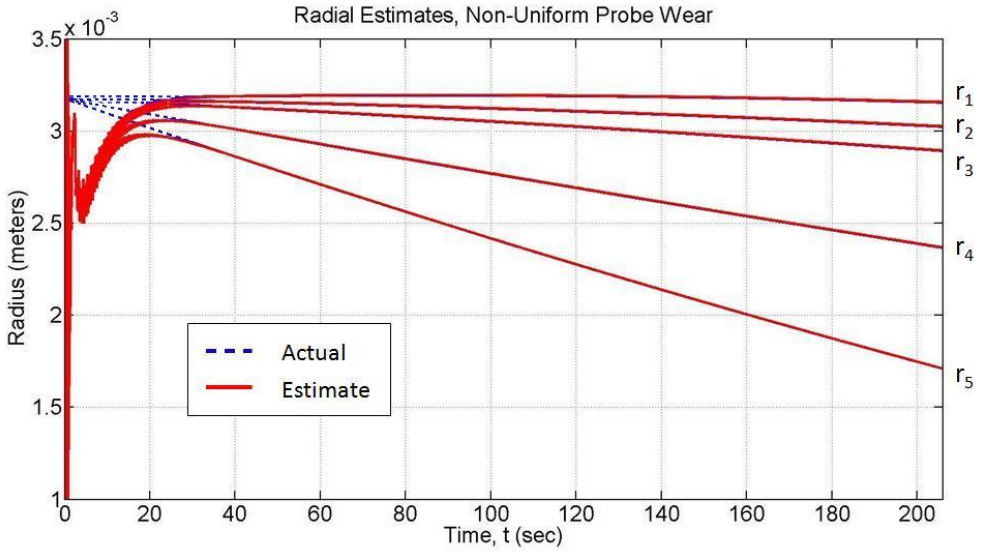

Figure 113: Radial Estimates While Non-Uniform Tool Wear is Experienced

Finally, the wear estimation output of the controller was configured to estimate the percent tool wear based on cross-sectional area, which is the most common characterization of tool wear. Figure 114 shows the actual percent tool wear and the controller estimate of the same. Figure 115 shows the error in the percent tool wear estimation.

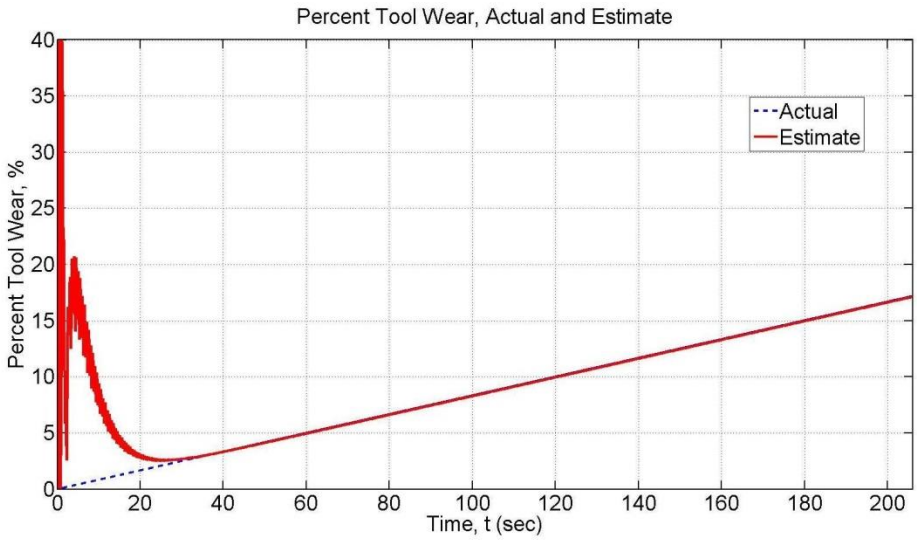

Figure 114: Percent Tool Wear Estimation

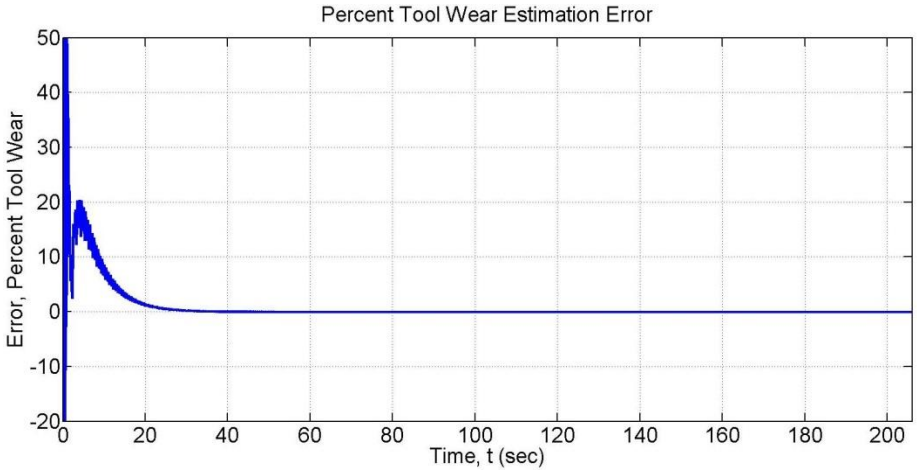

Figure 115: Percent Tool Wear Estimation Error

Discussion and Conclusions

The adaptive torque controller developed for estimating parameters during the FSW process was simulated using two different wear models. First, controller performance was tested by assuming a simple wear model, which involved uniform wear of the probe radius. Next, a non-uniform wear model was developed using the results of FSW experiments in which welding was performed on highly abrasive MMC. This model involved sectioning the probe into five regions and specifying how each region changed in relation to one another based on cross-sectional area. In both cases, the results were:

1) The controller adapted to the changing system dynamics caused by extreme tool wear and controlled torque with very low error.

2) The controller identified parameters that were changing throughout the weld, such as probe radius or probe cross-sectional area, after an initial identification period.

In the case of uniform probe wear, the controller accurately estimated the probe radius after 20 seconds. In the case of non-uniform probe wear, the controller accurately estimated the radii of all five regions after approximately 30 seconds. The percent tool wear by area was accurately estimated after approximately 30 seconds as well. This means that for a traverse rate of 7 ipm, as in the simulations, the controller can estimate tool profile after approximately 3 to 4 inches of weld. For most industrial applications, this identification period would be sufficiently small.

Empirical models have been developed by Prater et al. [53] and others that are valuable in predicting the amount of tool wear that may take place over the course of a weld, given a particular rotation speed and traverse rate. While these models are extremely valuable in process planning, there are variables such as material variation of both the tool and the welded material that can reduce the accuracy of these models. Of greater value is knowing the actual amount of tool wear that has taken place at any point throughout the weld. The implementation of adaptive torque control allows for this capability. Figure 115 indicates that after approximately 30 seconds, there is zero error in the estimation of percent tool wear.

Having an in-process estimate of tool wear may be especially useful when a tool is used that exhibits features such as threads on the probe. In most industrial applications of FSW, tool design and tool material are selected only after extensive testing to ensure any tool wear will not be detrimental to weld quality; however, tool features such as threads are often the weak link of tool design. The wear estimation capabilities of the adaptive torque controller would allow operators to know when tool features such as threads have experienced significant wear, which may lead to weld defects resulting from insufficient flows. Tool changes could therefore be performed when process feedback signals indicate they are needed, rather than on a set schedule. This could result in savings of both time and money for manufacturers who use FSW. Furthermore, because of the radial estimation capabilities displayed in Figure 113, is possible to know when during the process certain locations on the probe experience more wear than others. This may lead designers to create more robust tools that can handle the demands of custom industrial FSW applications.

Using adaptive torque control in FSW may prove to be advantageous in other ways as well. Although adaptive control may not be necessary for controlling torque during the steady-state welding process, it may prove to be useful for controlling torque during tool plunge or retraction, during which there are non-linear phenomena that would necessitate adaptive control. Appropriate future work would focus on developing a model for thread wear prediction and implementing adaptive control of FSW for experimental validation of simulation results. Implementation would allow for the direct comparison of controller estimates to offline pre and post-weld FSW tool measurements.

CHAPTER VIII

DISCUSSION AND CONCLUSIONS

Discussion

The over-arching theme of research presented in this dissertation was addressing challenges in the utilization of FSW as a primary joining technology for the manufacture of lightweight structures in the aerospace industry. Advances were targeted in corrosion prevention, robotic path planning procedures, tool wear, the incorporation of process variants, and the joining of a novel, candidate alloy for aerospace. The goal was for contributions to enhance the knowledge base, create areas of strength for manufacturers using FSW, and enable new users of FSW to emerge.

In Chapter III, the development of a method for enabling in-process quality evaluation of friction stir welded lap joints of aerospace alloys with sealant was documented. The goal of the project was to address the detection of gaps or thin sections of sealant that exist at the time of welding and to determine their presence using in-process signals rather than post-weld evaluation techniques. In this sense, the welding process itself would become a diagnostic tool. The use of sealants are required for aerospace applications of FSW in order to prevent the ingress of corrosion at the faying surfaces, or joining interfaces, of the weld. Sealants can be applied between the sheets of a lap weld prior to welding. Both the inspiration for this project and the technical guidance was provided by Spirit AeroSystems. Aluminum alloys 2024-T3 and 7075-T6 in 0.063 inch (1.6 mm) thick sheets were welded in a dissimilar combination in order to

simulate a stiffer-to-skin lap joint of an aerospace application. Varying configurations of PR-1432-GP sealant, which included control sections, gap sections, and thin sections, were applied in the joints, with two initial locations relative to the weld path as well. It was shown that through digital signal processing of the collected process forces, including computation of the frequency spectra and dimensional reduction using Principle Component Analysis and Linear Discriminant Analysis, weld sections with sealant flaws could indeed be separated from control sections with proper sealant application. Using PCA, gaps in cured sealant in a full application were linearly separable from high quality control sections, and when LDA was utilized, all data classes became linearly separable. Generally, it was concluded that the success of the technique depended on the selected feedback signal, axial force or torque, the curing state of the sealant, the initial sealant location within the joint, and the dimensional reduction technique used. It was noted based on PCA results that the state of the sealant, cured or uncured, played a more significant role in detection success than the initial sealant location, given the likely connection between sealant rigidity and force signature. This connection would be further examined in the work of Chapter IV. Finally, methods of performing sealant evaluation in real-time, such as using an LDA classifier, were examined and preliminarily simulated.

The findings of Chapter III were quite promising in that they could enable manufacturers to make informed decisions about accepting or rejecting parts, based on the quality of sealant application, and without performing post-weld analysis. On larger structures, such as aircraft assemblies, the potential may also exist for sealant defect locations to be repaired using alternate sealant application methods. This may be critical

technology as FSW continues to be adopted as a rivet replacement technology in aerospace and related industries. And, in addition to creating a new level of interaction between welding robots and sealants, this work demonstrated a new method of quality control in joining: welding itself as a diagnostic tool. A significant amount of information can indeed be extracted from the interactions between the welding tool and the workpiece, potentially reducing or even eliminating the need for post-weld evaluation.

In Chapter IV, a method of automatically tracking desired weld paths without using a pre-programmed planned path technique or any additional sensors was presented. This type of technique is alternatively known as through-the-tool tracking, and it is based on the concept of exploiting process force signals that are generally readily available. The work of Chapter IV built upon an observation in Chapter III that sealant can have a significant force signature, particularly when it is in the cured state. A lateral position control system, which utilizes an extremum-seeking controller, was evaluated at tracking desired weld paths outlined by faying surface sealant that was applied in a bead configuration prior to the placement of the lap joint top sheet. Again, 2024-T3 and 7075-T6 aluminum alloys were utilized in a dissimilar combination for this project. Controller parameters were first tuned using milled channels as a consistent sealant analog, which was appropriate based on the findings of Chapter III. Then, sealant tracking trials were performed with sealant in the cured and uncured states. It was shown that, while results were characterized by some overshoot and oscillation, the concept of tracking blind sealant paths was indeed plausible. Tracking cured sealant paths outperformed tracking uncured sealant paths, and the milled channel analogs exhibited the lowest error. An

error limit or more advanced performance metric was not established due to the nature of the lap joining itself, which can tolerate large deviations in lateral tool position and still yield sound welds, unlike butt joining. In that sense, tool positional limitations in lap joining are usually highly application specific. In general, however, these results were promising and offer new possibilities for manufacturers in that the potential exists for desired paths to be laid out in sealant and then automatically tracked without requiring the development of pre-programmed planned path operations. This is potentially important given the current transition, being driven by increasing product demand, from manual to robotic operations for a number of processes in aerospace manufacturing. Additionally, the attractiveness of this technique might well be magnified in small-lot manufacturing of custom hardware, for which significant planning, work-cell development, and setup is often cost prohibitive.

Mechanical testing was also performed to determine the effects of weaving, or the perturbation of lateral position necessitated by the control technique, on weld strength, particularly when parameters are selected primarily to achieve successful tracking. This was of significant interest for a number of reasons. It was shown in Chapter III that weld strength of dissimilar 7075/2024 joints tends to decrease with decreasing welding speed, and tracking does indeed tend to necessitate lower welding speeds. It was thought, however, that weaving might enable the recovery of weld strength due to its nature of facilitating increased TMAZ width, which is critical for lap weld strength and has been the focus of other developments in tool design and process variants. Also of interest was the interaction between weaving and the dynamics of sealant within the joint. Normally, for achieving high strength alone, it is desired that sealant be squeezed away from the

weld zone by pressure from the tool. It was thought that weaving might facilitate this migration, which could be viewed as a positive or negative, depending on whether the objective is strength, or tracking performance, for which a more rigid feature is ideal. Results indicated that sealant could indeed have a detrimental impact on weld strength, which was anticipated, but that weaving could also have a detrimental impact on weld strength. While this was somewhat surprising, the literature does indicate that there are diminishing returns for weld strength with increasing weave radii, and beyond a point, large weave radii can be detrimental to weld strength, even resulting in repeating surface void defects. The weave radius used was indeed on the high end of radii tested in the literature, and while no voids were detected, the surface of weaved welds were highly textured, or scalloped, and weaved welds tended to fail along the peaks and valleys of this surface texture during tension-shear testing. Macrographs indicated, however, that weaving did indeed facilitate sealant migration, and the widest spread of sealant, which occurred with weaving and sealant in the uncured state, corresponded with a slight increase in weld strength for a weaved weld over its conventionally welded counterpart. In general, these results highlighted the potential advantages and disadvantages of weaving and revealed areas in which much more investigation was required. For instance, the reduction of weave radii and the modification of tool geometry or welding parameters to achieve a more desirable surface finish. Accordingly, these items became the focus of much of the work documented in Chapter V.

The objective of the research documented in Chapter V was to further explore the use of process variants, including weaved FSW, which was preliminarily explored in Chapter IV, and pulsed FSW (PFSW) which is a variant technology that had displayed

promise for improving the characteristics of lap joints. An additional item of interest was tool shoulder geometry and its relation to process parameters, surface finish, and welding robot degree-of-freedom requirements. A traditional flat shoulder tool operated at a tilt angle and relatively high welding speed, which is a combination that is pervasive throughout the literature, was compared to a tapered shoulder tool operated at zero degrees tilt. The hope was that a tapered shoulder geometry would reduce the prominent, scalloped surface texture that was documented for weaving in Chapter IV; additionally, there is the benefit that lap welding with a tool at zero degrees tilt would effectively eliminate a degree-of-freedom required of welding robots and would simplify robot programming procedures. Faying surface sealant was included in the study as well for select welds in order to characterize its interactions with welding parameters and variant technologies. All these items were investigated by lap welding 0.063 inch (1.6 mm) thick 2198-T8, which is a third-generation Aluminum-Lithium alloy that is receiving significant attention from aerospace manufacturers as a candidate material for the replacement of incumbent 2xxx and 7xxx series alloys. The weld matrix was designed to take into account knowledge gained from previous experience with 7075 and 2024 alloys however, and variant parameters, such as weave radius and pulsing frequency, were selected to build upon prior work from others in the literature. Select parametric levels of interest were evaluated with ANOVA to determine if observed differences in weld strength were significant.

Results indicated a number of interesting relationships. It was demonstrated that the two shoulder geometries create different sheet interface shapes and are perhaps suited for differing operating conditions. Lap welding with a tapered shoulder tool was shown

to be completely feasible, however, and this geometry may actually extend the parametric window of welding speed lower than that achievable with a flat shoulder tool. There were also multiple cases of process variants, pulsing and weaving, increasing weld strength over conventionally welded counterparts at significant levels. The occurrence of this was more common when the base, or conventional, weld strength was relatively low, indicating that the tool was being operated outside of its desired parametric window for achieving high weld strength. Discussion of this finding in Chapter V highlights applications that might dictate a tool be operated at less than ideal conditions, such as for joint tracking or to prevent breakage of a wear-resistant, brittle tool material, and where process variants might prove beneficial in recapturing some of the sacrificed weld strength. The potential for process variants to allow for simplified, inexpensive tool geometries is discussed as well, in that they similarly promote increases in TMAZ area like complex tool designs that are more expensive to manufacture. Regarding sealants, it was shown that shoulder geometries and sealant migration within the joint can potentially interact, with the tapered shoulder geometry facilitating an increased spread of sealant from the joint line. This can be viewed as either a benefit, from the perspective of weld strength, or a detriment, as operations which depend on a strong sealant force signature, such as in-process evaluation of sealant quality or tracking, are potentially affected. It was concluded, however, that the use of non-traditional or innovative shoulder geometries would not preclude the implementation of such operations, given that care is taken to characterize differences that result from a change in tool geometry.

The purpose of Chapter VI was to examine and compare the weld strength data from Chapter III, which was focused on joining 7075-T6 and 2024-T3 alloys in a

dissimilar combination, and Chapter V, which was focused on joining 2198-T8 with both conventional welding and process variants. The weld matrix of Chapter V was intentionally designed to include some common parameter sets with the study on 7075 and 2024 alloys documented in Chapter III; and, while optimized weld parameters are nearly certain to differ with respect to varying alloy combinations, this made for nonetheless interesting comparisons. Further, material base properties were compared, and the best case scenarios for weld strength were examined as well. Overall, it can be said that the strengths documented for the 7075/2024 welds and the 2198 welds were comparable. Differences in strength levels arising from alloy, tool geometry, and process parameters were evident. It was noted that a larger parameter optimization study had been performed in Chapter III for 7075/2024 alloys, and perhaps the strength of 2198 alloy welds could be increased with a similar, large study. However, results provide justification for the interest of manufacturers in utilizing Al-Li alloys, in that material performance is relatively high, and slightly lower strengths are even acceptable given the exceptional specific strength, or strength-to-weight ratio, provided that other metrics, such as toughness or fatigue crack growth resistance, are satisfied as well.

Finally, the work of Chapter VII addressed an area of need for potentially all manufacturers using FSW. An adaptive FSW torque controller that has the capability to estimate parameters, such as probe radius, that may be changing throughout the welding process was designed and simulated. A controller of this type could potentially be valuable to all manufacturers who use FSW, but it may be of particular interest to those who weld high melting point alloys or highly abrasive alloys and therefore have a significant need to implement tool wear prediction and mitigation practices. Controller

performance was characterized by simulating extreme tool wear, which represented a change in system dynamics, both with a simplified wear model and with a wear model that recreated patterns of wear documented in the welding of highly abrasive Metal Matrix Composite (MMC) material, and then determining how well process torque was controlled and tool profile estimated. A process model was used to simulate welding outputs to provide the required torque signal. Results showed that the controller could effectively control process torque as system dynamics are changing, which was an anticipated advantage of adaptive control, but it was also shown that the controller could identify and provide a continuous estimate of tool profile throughout the welding process. This is impactful in that wear estimation capability of this nature could potentially allow manufacturers to know when tool geometry, which may include features such as threads, has experienced significant wear, often leading to weld defects caused by insufficient material flow. Tool changes could then be performed only when process feedback signals indicate they are needed, rather than on a pre-determined schedule. Tool designs could also be modified to better resist wear using knowledge from in-process signals revealing how and when tools experience the most significant wear. These results could yield savings of both time and money for manufacturers who use FSW.

The research findings that have been presented here highlight the improvements and innovations that are possible for a thermo-mechanical process like FSW when it is characterized and refined, through the multiple and varied avenues of experimentation, mechanical evaluation, sensing, signal processing, and modeling and simulation. It has been shown that meaningful signals can be extracted from the process and correlated with phenomena of interest, to enable improvements to the process that make it more efficient,

regarding aspects such as quality evaluation, robotic programming, or tool wear. It has been shown that variant technologies, or modifications to the conventional FSW process, can lead to potential improvements as well. Throughout the research that has been presented, however, the interconnected nature of FSW is ever-present. Joint configuration, workpiece thickness, alloy, tool geometry, tool features, tilt angle, welding speed, rotation rate, and variant technologies can all have significant impacts on the welding process. These items interact, and when even one is modified, there can be both predicted and unforeseen outcomes. Understanding this interconnected nature, for instance the interaction between tool geometry and welding parameters in forming a lap joint sheet interface shape, how the load path through the selected joint orientation interacts with the sheet interface shape thereby dictating weld strength, and how optimizing parameters for strength can affect how signals are monitored and thus the performance of in-process quality evaluation or tracking, can greatly aid in reaching desired outcomes or meeting application requirements. It is anticipated that the pursuit of understanding of complex problems of this nature will continue to drive joining research forward.

Direction of Future Work

Any future work that may build upon, or be related to, the research that has been presented here would most effectively be focused in a few, specific areas. It is anticipated that in-process quality evaluation or quality assurance (QA) will receive significant attention in the field moving forward, and rightfully so, given its potential for reducing or eliminating expensive and time consuming post-weld evaluation. Additional

areas deserving of attention, however, include joining advanced, application specific alloys, further examination of process variants, pulsing in particular, and the development of a through-the-tool joint tracking technique that does not require lateral position perturbation, or weaving. Regarding alloys, the materials welded and documented in this dissertation were selected to represent the incumbent aerospace alloys as well as an advanced, candidate material for their replacement. It is clear that there is significant interest in the aerospace community in utilizing aluminum-lithium alloys, in particular 2198, 2199, and 2099. Any effort aimed at advancing the knowledge of how to most efficiently join these materials would be of great value. In the automotive industry as well, there is significant interest in transitioning away from steels and utilizing lightweight alloys for bodies. Any work addressing the joining of these materials, either with linear FSW or FSSW, would be enhanced by industry guidance on selecting the most appropriate alloys. Regarding process variants, it is clear that there is the potential for tool rotation rate pulsation to create improved process characteristics. Future work in this area should focus on the potential for tool geometry to be simplified, while maintaining adequate TMAZ area in lap joining using pulsation. Any work revealing that pulsation would enable the use of simple, inexpensive tool geometry, would truly be groundbreaking. Additionally, pulsing has so far been evaluated only on aluminum alloys. There may be yet unforeseen potential advantages to using the FSW variant on steels or titanium, for which tool geometry is typically significantly different. Finally, regarding joint tracking, it has been shown that weaving enables the extraction of information from process signals that indicates the relative lateral position of the tool with respect to workpiece features. Weaving can facilitate increases in joint strength as

well, but it has been shown that this is not universal. There is evidence that suggests, however, that workpiece features might produce signatures that are discernable in multiple signals, such as axial force and side force, for example, that together would enable not just the determination of relative position, but ultimate position resolution, which would eliminate the need for lateral perturbations of the tool. Characterizing multiple signatures for a variety of joint configurations and enabling non-weaving through-the-tool joint tracking would be of significant value.

APPENDIX A

REAL-TIME WELD CLASSIFICATION SIMULATION CODE

Classify Function:

Class = classify(sample, training, group, method)

Sample = set of frequency data to be classified
Training = multiple sets of training frequency data
Group = labels corresponding to training sets, i.e. (1 = Good, 0 = Gap)
Method = string denoting algorithm

Variables Affecting Detection:

Control training data (amount and type)
Gap training data (amount and type)
Method (‘diaglinear’, etc…)
Window Length
Overlap
Number of frequency bins
Size of running average
Threshold

Example Using Machined Gaps:

Control Training Files:
LapNormal1, 174500 start index, 1 sec window length, 0.5 sec spaces
LapNormal2, 220000 start index, 1 sec window length, 0.5 sec spaces

Gap Training File:
LapMGap1, 1 sec window length, 0.25 space, offset1 = 0, offset2 = 2.0357

Frequency Data:
100 frequency bins

For best results, a selection of LapNormal2 data sets were used (after some trial and error optimization)

This is the Classifier.m file in which weld data from a single weld is analyzed in a cyclical manner to classify data windows as either good or bad (gap). The file analyzed in this example is the LapMGap5 weld, which has 0.003" deep gaps that are 0.5" wide. The setup of the training and group matrices is not shown here.

```
%% Analysis of Sealant Welds

%% Definition of variables
filename = 'LapMGap5.txt';

%% Load and parse data
%data = csvread(filename);


%*****  User Inputs  *****%
TotalTime = 480; %Enter total recorded time (seconds)
TraverseStart = 14.485;  %Enter starting position (inches)
FirstGapIn = 1.9;  %Enter distance to first gap edge (inches)
GapLength = 0.5;  %Enter gap length (inches)
WindowLength = 1; %Window length (seconds)
Overlap = 3; %1 = NoOverlap   2 = Half Overlap    3 = 2/3 Overlap   4 = 3/4 overlap
NumFreqBins = 100;  %Number of frequency bins


%*****  Loading and Processing Data  *****%
t = data(:,3)/1000;  %time is converted from milliseconds to seconds
Z = data(:,7); %Z-force
tra = data(:,13); %traverse location

SizeZ = size(Z);
fs = floor(SizeZ(1,1)/TotalTime);  %Sampling Frequency

for i = 1:SizeZ;
   if tra(i) > TraverseStart + 0.75;
      BeginIndex = i; %Data index of first edge
      break
   end
end

for i = 1:SizeZ;
   if tra(i) > TraverseStart + 7.75;
      EndIndex = i; %Data index of last edge
      break
   end
end
```

```
 %*****  Windowing  *****%
WindowDataSize = floor(fs*WindowLength); %Number of data points per window
NumOfWindows = floor((EndIndex - BeginIndex) / (WindowDataSize/Overlap)); %Number of windows

WindowedData = zeros(WindowDataSize,1);
class = zeros(NumOfWindows,1);
average = zeros(NumOfWindows-4,1);
TraPos = zeros(1,NumOfWindows);
AveTraPos = zeros(NumOfWindows-4,1);
%Bin = zeros(NumFreqBins,1);


%*****  Plotting  *****%
boundaries = [50 t(BeginIndex) t(EndIndex) 300]';
Zvalues = [0 10000 0 0]';
[xZ yZ] = stairs(boundaries, Zvalues);

figure(1)
%subplot(131)
axis([180, 290, 0, 10200])
hold('all');
plot(t(:,1),Z(:,1))  %Blue
plot(xZ, yZ,'LineWidth',1,'Color',[1 0 0])  %Red
title({'1st Order Axial (Z) Force Data, 0.003" Gaps'},'FontSize',14)
ylabel('Axial Force, Z (N)')
xlabel('Time (sec)')

figure(2)
%subplot(121)
axis([tra(BeginIndex), tra(EndIndex), -0.5, 1.5])
box('on');
grid('off');
hold('all');

area([(TraverseStart + FirstGapIn) (TraverseStart + FirstGapIn + GapLength)], [5 5],'FaceColor',[0.8314 0.8157 0.7843],...
   'EdgeColor',[0.8314 0.8157 0.7843]);
area([(TraverseStart + FirstGapIn) (TraverseStart + FirstGapIn + GapLength)], [-5 -5],'FaceColor',[0.8314 0.8157 0.7843],...
   'EdgeColor',[0.8314 0.8157 0.7843]);
area([(TraverseStart + FirstGapIn + 3) (TraverseStart + FirstGapIn + 3 + GapLength)], [5 5],'FaceColor',[0.8314 0.8157 0.7843],...
   'EdgeColor',[0.8314 0.8157 0.7843]);
area([(TraverseStart + FirstGapIn + 3) (TraverseStart + FirstGapIn + 3 + GapLength)], [-5 -5],'FaceColor',[0.8314 0.8157 0.7843],...
```

```
   'EdgeColor',[0.8314 0.8157 0.7843]);

plot2 = scatter(TraPos,class);
plot2b = line(AveTraPos,average,'color',[1 0 0]);

xlabel('Traverse Position (in)');
ylabel('Class');
title({'Classification with Discriminant Analysis, 0.003" Machined Gaps, 0.5" Width'},'FontSize',14);
legend1 = legend([plot2, plot2b], 'Class: 1 = Control, 0 = Gap', '5 Point Moving Window Average');

%figure(3)
% subplot(122)
% plot3 = bar(Bin);
% axis([0, 110, 0, 25000])
% xlabel('Frequency (Hz)');
% ylabel('Magnitude');
% title({'Frequency Data'},'FontSize',14);


%*****Looping Through Data for Classification*****%
Index = BeginIndex;

for i = 1:NumOfWindows;
    WindowedData = Z(Index : Index + WindowDataSize - 1);
    WindowedMean = mean(WindowedData); %Finding mean value (scalar) of data in window
    WindowedData = WindowedData - WindowedMean; %Subtracting mean from all data points in window
    TraPos(1,i) = tra(Index + floor((WindowDataSize/2))); %Traverse position in middle of window for plot
    %FFT
    FrequencyData = abs(fft(WindowedData,fs));
    %Bin
    Bin = FrequencyData(1:NumFreqBins);
    %Classify
    class(i,1) = classify(Bin', training, group,'diaglinear');
    %Running Average
    if i > 4
       average(i-4) = (class(i-4) + class(i-3) + class(i-2) + class(i-1) + class(i))/5;
       AveTraPos(i-4) = TraPos(i-2);
    end
    %Update Plot
    set(plot2,'YData',class,'XData',TraPos);
    set(plot2b,'YData',average,'XData',AveTraPos);
```

```
    %set(plot3,'YData',Bin);
    drawnow

    Index = Index + floor(WindowDataSize/Overlap); %Stepping to next window
end


%Optional Plots of Frequency Data
% for i = 1:13;
% k = 0:(NumFreqBins - 1);
% fk = k;
% figure(i+1),bar(fk,FrequencyData(1:NumFreqBins,i))
% title('FFT')
% end

%Create legend
%legend1 = legend('show');
%set(legend1,'Position',[0.705 0.8426 0.1835 0.0639]);
```

REFERENCES

[1] Thomas, W.M., Nicholas, E.D., Needham, J.C., Murch, M.G., Templesmith, P., Dawes, C.J., "Improvements Relating to Friction Welding," EPO Patent EP0615480, 8 Nov 1995.

[2] Midling, O.T., Morley, E.J., Sandvik, A., "Friction Stir Welding," EPO Patent EP0752926, 27 May 1998.

[3] Threadgill, P.L., "Terminology in Friction Stir Welding," *Science and Technology of Welding and Joining*, Vol 12, No 4, 2007, pp. 357 - 360.

[4] Nandan, R., DebRoy, T., Bhadeshia, H.K.D.H., "Recent Advances in Friction-Stir-Welding – Process, Weldment Structure and Properties," *Progress in Materials Science*, Vol 53, No 6, 2008, pp. 980 - 1023.

[5] Colligan, K., "Material Flow Behavior During Friction Stir Welding of Aluminum," *Welding Journal*, Vol 78, No 7, 1999, pp. 229s - 237s.

[6] Reynolds, A.P., "Visualization of Material Flow in Autogenous Friction Stir Welds," *Science and Technology of Welding and Joining*, Vol 5, No 2, 2000, pp. 120 - 124.

[7] Arbegast, W.J., "Modeling Friction Stir Joining as a Metalworking Process," *Hot Deformation of Aluminum Alloys III*, The Minerals, Metals & Materials Society, Warrendale, PA, January 2003.

[8] Mishra, R.S., Mahoney, M.W., Eds., "Friction Stir Welding and Processing," ASM International, Materials Park, OH, 2007.

[9] Arbegast, W.J., "A Flow-Partitioned Deformation Zone Model for Defect Formation During Friction Stir Welding," *Scripta Materialia*, Vol 58, No 5, 2008, pp. 372 - 376.

[10] Krishnan, K.N., "On The Formation of Onion Rings in Friction Stir Welds," *Materials Science and Engineering*, Vol A327, 2002, pp. 246 - 251.

[11] Yang, B., Yan, J., Sutton, M.A., Reynolds, A.P, "Banded Microstructure in AA2024-T351 and AA2524-T351 Aluminum Friction Stir Welds, Part I. Metallurgical Studies," *Materials Science and Engineering*, Vol A364, 2004, pp. 55 - 65.

[12] Schneider, J., Beshears, R., Nunes, A.C., "Interfacial Sticking and Slipping in the Friction Stir Welding Process," *Materials Science and Engineering*, Vol A435-436, 2006, pp. 297 - 304.

[13] Longhurst, W.R., "FSW Void Sensing Research," Unpublished Report, Vanderbilt University, 2012.

[14] Qian, J.W., Li, J.L., Xiong, J.T., Zhang, F.S., Li, W.Y., Lin, X., "Periodic Variation of Torque and its Relations to Interfacial Sticking and Slipping During Friction Stir Welding," *Science and Technology of Welding and Joining*, Vol 17, No 4, 2012, pp. 338 - 341.

[15] London, B., Mahoney, M., Bingel, W., Calabrese, M., Bossi, R.H., Waldron, D., "Material Flow in Friction Stir Welding Monitored with Al-SiC and Al-W Composite Markers," *Friction Stir Welding and Processing II*, The Minerals, Metals & Materials Society, Warrendale, PA, March 2003.

[16] Zhao, Y.H., Lin, S.B., Qu, F.X., Wu, L., "Influence of Pin Geometry on Material Flow in Friction Stir Welding Process," *Materials Science and Technology*, Vol 22, No 5, 2006, pp. 45 - 50.

[17] Lammlein, D.H., DeLapp, D.R., Fleming, P.A., Strauss, A.M., Cook, G.E., "The Application of Shoulderless Conical Tools in Friction Stir Welding: An Experimental and Theoretical Study," *Materials & Design*, Vol 30, 2009, 4012 – 4022.

[18] Lammlein, D.H., Gibson, B.T., DeLapp, D.R., Cox, C.D., Strauss, A.M., Cook, G.E., "Friction Stir Welding of Small Diameter Pipe: An Experimental and Numerical Proof of Concept for Automation and Manufacturing," *Proceedings of the Institution of Mechanical Engineers, Part B: Journal of Engineering Manufacture*, Vol 226, No 3, 2012, pp. 383 – 398.

[19] Lammlein, D.H., "Friction Stir Welding of Spheres, Cylinders, and T-Joints: Design, Experiment, Modeling, and Analysis," Ph. D. Dissertation, Vanderbilt University, 2010.

[20] Schmidt, H., Hattel, J., "A Local Model for the Thermomechanical Conditions in Friction Stir Welding," *Modeling and Simulation in Materials Science and Engineering*, Vol 13, No 1, 2005, pp. 77 - 93.

[21] Colegrove, P.A., Shercliff, H.R., Zettler, R., "Model for Predicting Heat Generation and Temperature in Friction Stir Welding from the Material Properties," *Science and Technology of Welding and Joining*, Vol 12, No 4, 2007, pp. 284 – 297.

[22] Roy, G.G., Nandan, R., DebRoy, T., "Dimensionless Correlation to Estimate Peak Temperature During Friction Stir Welding," *Science and Technology of Welding and Joining,* Vol 11, No 5, 2006, pp. 606 – 608.

[23] Querin, J.A., Schneider, J.A., "Developing an Alternative Heat Indexing Equation for FSW," *Welding Journal*, Vol 91, 2012, pp. 76s – 82s.

[24] Schneider, J.A., Nunes, A.C., "Characterization of Plastic Flow and Resulting Microtextures in a Friction Stir Weld," *Metallurgical and Materials Transactions B,* Vol 35B, 2004, pp. 777 – 783.

[25] Schwartz, M., Ed., "Innovations in Materials Manufacturing, Fabrication, and Environmental Safety," Taylor and Francis Group, Boca Raton, FL, 2011.

[26] Nunes, A.C., Bernstein, E.L., McClure, J.C., "A Rotating Plug Model for Friction Stir Welding," *Proceedings of the 81st American Welding Society Annual Convention*, 2000.

[27] Nunes, A.C., "Wiping Metal Transfer in Friction Stir Welding," *Proceedings of the TMS Annual Meeting*, 2001.

[28] Querin, J.A., "Deconvoluting the Link Between Weld Tool Geometry and Process Parameters," Ph.D. Dissertation, Mississippi State University, 2010.

[29] Melendez, M., Tang, W., Schmidt, C., McClure, J.C., Nunes, A.C., Murr, L.E., "Tool Forces Developed During Friction Stir Welding," Unpublished NASA Technical Document, Marshall Space Flight Center, 2003.

[30] Cook, G.E., Crawford, R., Clark, D.E., Strauss, A.M., "Robotic Friction Stir Welding," *Industrial Robot: An International Journal*, Vol 31, No 1, 2004, pp. 55 – 63.

[31] Crawford, R., Cook, G.E., Strauss, A.M., Hartman, D.A., Stremler, M.A., "Experimental Defect Analysis and Force Prediction Simulation of High Welding Pitch Friction Stir Welding," *Science and Technology of Welding and Joining,* Vol 11, No 6, 2006, pp. 657 – 665.

[32] Crawford, R., Cook, G.E., Strauss, A.M., Hartman, D.A., "Modelling of Friction Stir Welding for Robotic Implementation," *International Journal of Modelling, Identification, and Control,* Vol 1, No 2, 2006, pp. 101 – 106.

[33] Atharifar, H., Lin, D., Kovacevic, R., "Numerical and Experimental Investigations on the Loads Carried by the Tool During Friction Stir Welding," *Journal of Materials Engineering and Performance,* Vol 18, No 4, 2009, pp. 339 – 350.

[34] Ulysse, P., "Three-Dimensional Modelng of the Friction Stir-Welding Process," *International Journal of Machine Tools & Manufacture,* Vol 42, 2002, pp. 1549 – 1557.

[35] Thomas, W.M., Johnson, K.I., Wiesner, C.S., "Friction Stir Welding – Recent Developments in Tool and Process Technologies, *Advanced Engineering Materials*, Vol 5, No 7, 2003, pp. 485 – 490.

[36] Thomas, W.M., Norris, I.M., Staines, D.G., Watts, E.R., "Friction Stir Welding – Process Developments and Variant Techniques," *Proceedings of the SME Summit*, Oconomowoc, Milwaukee, August 3 - 4, 2005.

[37] Trivex™ Tool for Friction Stir Welding, Connect, No 124, May – June 2003, TWI <http://www.twi.co.uk/news-events/publications/connect/archive/2003/may-june/trivex-tool-for-friction-stir-welding/> 26 Oct 2012.

[38] Elangovan, K., Balasubramanian, V., "Influences of Tool Pin Profile and Welding Speed on the Formation of Friction Stir Processing Zone in AA2219 Aluminum Alloy," *Journal of Materials Processing Technology*, Vol 200, 2008, pp. 163 – 175.

[39] Liu, F.C., Ma, Z.Y., "Influence of Tool Dimension and Welding Parameters on Microstructure and Mechanical Properties of Friction Stir Welded 6061-T651 Aluminum Alloy*," Metallurgical and Materials Transactions A*, Vol 39A, 2008, pp. 2378 – 2388.

[40] Colligan, K.J., Xu, J., Pickens, J.R., "Welding Tool and Process Parameter Effects in Friction Stir Welding of Aluminum Alloys," *Friction Stir Welding and Processing II*, The Minerals, Metals & Materials Society, Warrendale, PA, March 2003.

[41] Scialpi, A., De Filippis, L.A.C., Cavaliere, P., "Influence of Shoulder Geometry on Microstructure and Mechanical Properties of Friction Stir Welded 6082 Aluminum Alloy," *Materials and Design,* Vol 28, 2007, pp. 1124 – 1129.

[42] Sorensen, C., Nielsen, B., "Exploring Geometry Effects for Convex Scrolled Shoulder, Step Spiral Probe FSW Tools," *Friction Stir Welding and Processing V,* The Minerals, Metals & Materials Society, Warrendale, PA, 2009.

[43] Longhurst, W.R., "Force Control of Friction Stir Welding," Ph.D. Dissertation, Vanderbilt University, 2009.

[44] Longhurst, W.R., Strauss, A.M., Cook, G.E. "The Identification of Key Enablers for Force Control of Robotic Friction Stir Welding," *American Society of*

Mechanical Engineers Journal of Manufacturing Science and Engineering, Vol 133, No 3, 2011, pp. 1- 11.

[45] Longhurst, W.R., "Torque Control of Friction Stir Welding," Status Review and Update for NASA SBIR/STTR 2010 Phase I Contract NNX11CI39P, Longhurst Engineering, 2011.

[46] Longhurst, W.R., Cox, C.D., Gibson, B.T., Cook, G.E., Strauss, A.M., DeLapp, D.R., "Applied Torque Control of Friction Stir Welding Using Motor Current as Feedback," *Proceedings of the Institution of Mechanical Engineers, Part B: Journal of Engineering Manufacture,* Submitted June 2013, Under Review.

[47] Burford, D.A., "Friction Stir Welding Tool Having a Counterflow Pin Configuration," U.S. Patent 7,942,306. 17 May 2011.

[48] Trapp, T.J., Fisher, J.J., Bernath, J.J., Method of Friction Stir Welding and Retractable Shoulderless Variable Penetration Friction Stir Welding Tool for Same," U.S. Patent 7,234,626. 26 June 2007.

[49] Ding, R.J., Oelgoetz, P.A., "Auto-Adjustable Pin Tool for Friction Stir Welding, U.S. Patent 5,893,507. 13 April 1999.

[50] Thompson, B., Root, J., George, R., Eff, M., Sedha, S., "Development of an All-in-One Exit Hole Elimination Technique for Thin Section Aluminum," *Proceedings of the 9th International Symposium on Friction Stir Welding*, TWI, Cambridge, UK, May 2012.

[51] Thomas, W.M., Threadgill, P.L., Nichols, E.D., "Feasibility of Friction Stir Welding Steel, *Science and Technology of Welding and Joining*, Vol 4, 1999, pp. 365 - 372.

[52] Lienert, J., Stellwag, W.L., Grimmett, B.B., Warke, R.W., "Friction Stir Welding Studies on Mild Steel," *Supplement to the Welding Journal,* 2003, pp. 2S – 9S.

[53] Prater, T.J., Strauss, A.M., Cook, G.E., Machemehl, C., Sutton, P., Cox, C.D., "Statistical Modeling and Prediction of Wear in Friction Stir Welding of a Metal Matrix Composite (Al 359/SiC/20p), *Journal of Manufacturing and Technology Research*, Vol 2, 2010, pp 1 - 13.

[54] Prado, R.A., Murr, L.E., Shindo, D.J., Soto, K.F., "Tool Wear in the Friction Stir Welding of Aluminum Alloy 6061+Al2O3: A Preliminary Study, *Scripta materialia,* Vol 45, 2001, pp. 75 - 80.

[55] Prater, T.J., "Predictive Process Modeling of Tool Wear in Friction Stir Welding of Metal Matrix Composites," Ph.D. Dissertation, Vanderbilt University, 2012.

[56] Leonhardt, T., Thompson, B., "Past, Present, and Future Developments of Tungsten Tool Materials for Friction Stir Welding of Steel and Hard Metals," *Proceedings of the 9th International Symposium on Friction Stir Welding*, TWI, Cambridge, UK, May 2012.

[57] Kolluri, M., Luzginova, N.V., Schuring, E.W., Kyffin, W., Martin, J., "Friction Stir Welding of P91 Steel with an Improved W-Re Tool Material for Nuclear Applications," *Proceedings of the 9th International Symposium on Friction Stir Welding*, TWI, Cambridge, UK, May 2012.

[58] Arbegast, W.J., "Friction Stir Welding After a Decade of Development, *Friction Stir Welding and Processing IV*, The Minerals, Metals & Materials Society, Warrendale, PA, 2007.

[59] Miyake, M., Sato, Y.S., Kokawa, H., Takaku, Y., Omori, T., Ishida, K., Imano, S., Park, S.H.C., Hirano, S., "Material Properties Governing Wear of Co-Based Alloy Tool During Friction Stir Welding of Steels," *Proceedings of the 9th International Symposium on Friction Stir Welding*, TWI, Cambridge, UK, May 2012.

[60] Mochizuki, N., Takasugi, T., Kaneno, Y., Oki, S., Hirata, T., "Application of Ni-Base Dual Two-Phase Intermetallic Alloy to FSW Tools for Joining SUS430 Plates," *Proceedings of the 9th International Symposium on Friction Stir Welding*, TWI, Cambridge, UK, May 2012.

[61] Rai, R., De, A., Bhadeshia, H.K.D.H., DebRoy, T., "Review: Friction Stir Welding Tools," *Science and Technology of Welding and Joining*, Vol 16, No 4, 2011, pp. 325 – 342.

[62] DebRoy, T., De, A., Bhadeshia, H.K.D.H., Manvatkar, V.D., Arora, A., "Tool Durability Maps for Friction Stir Welding of an Aluminum Alloy," *Proceedings of the Royal Society A*, Published online in advance of print, 25 July 2012.

[63] Dodds, S., Jones, H., Cater, S., "The Use of Novel Methods in Determining the Wear of Friction Stir Tooling," *Proceedings of the 9th International Symposium on Friction Stir Welding*, TWI, Cambridge, UK, May 2012.

[64] Zhang, Y.N., Cao, X., Larose, S., Wanjara, P., "Review of Tools for Friction Stir Welding and Processing," *Canadian Metallurgical Quarterly*, Vol 51, No 3, 2012, pp. 250 – 260.

[65] Colegrove, P.A., Shercliff, H.R., Hyoe, T., "Development of the Trivex Friction Stir Welding Tool for Making Lap Welds," *Proceedings of the 5th International Symposium on Friction Stir Welding*, TWI, Cambridge, UK, 2004.

[66] Thomas, W.M., Staines, D.G., Norris, I.M., de Frias, R., "Friction Stir Welding – Tools and Developments," *FSW Seminar,* Porto, Portugal, 2002.

[67] Cederqvist, L., Reynolds, A.P., "Factors Affecting the Properties of Friction Stir Welded Aluminum Lap Joints", *Welding Journal*, Vol 80, No 12, 2001, pp. 281S – 287S.

[68] Sylva, G., Sr. FSW Engineer, Spirit AeroSystems, Personal Communication, 2011 [retrieved 28 June 2011 – 5 July 2011].

[69] Dubourg, L., Merati, A., and Jahazi, M., "Process Optimisation and Mechanical Properties of Friction Stir Lap Welds of 7075-T6 Stringers on 2024-T3 Skin," *Materials and Design*, Vol 31, No. 7, 2010, pp. 3324 – 3330.

[70] Jana, S., Hovanski, Y., Grant, G.J., Mttlin, K., "Effect of Tool Feature on the Joint Strength of Dissimilar Friction Stir Lap Welds," *Friction Stir Welding and Processing VI*, The Minerals, Metals & Materials Society, Warrendale, PA, 2011.

[71] Cox, C.D., "Friction Stir Welded Magnesium Alloy AZ31B in a Lap Joint Configuration, M.S. Thesis, Vanderbilt University, 2010.

[72] Cox, C.D., Lammlein, D.H., Cook, G.E., Strauss, A.M., "Effects of Rotation and Traverse Speeds on Lap Joints of Friction Stir Welded Mg AZ31B H24," *Proceedings of the AWS Professional Program at FABTECH*, Atlanta, GA, Nov 2 - 4, 2010.

[73] Yang, Q., Li, X., Chen, K., Shi, Y.J., "Effect of Tool Geometry and Process Condition on the Strength of a Magnesium Friction Stir Lap Linear Weld," *Friction Stir Welding and Processing VI*, The Minerals, Metals & Materials Society, Warrendale, PA, 2011.

[74] Yazdanian, S., Chen, Z.W., Littlefair, G., "Mechanical Properties of Al and Mg Alloy Welds Made Using Friction Stir Lap Welding," *Friction Stir Welding and Processing VI*, The Minerals, Metals & Materials Society, Warrendale, PA, 2011.

[75] Aldanondo, E., Arruti, E., Alvarez, P., Acheverria, A., "Mechanical and Microstructural Properties of FSW Lap Joints," *Friction Stir Welding and Processing VII*, The Minerals, Metals & Materials Society, Warrendale, PA, 2013.

[76] Skinner, M., Edwards, R.L., "Improvements to the FSW Process Using the Self-Reacting Technology, *Materials Science Forum*, Vols 426 – 432, 2003, pp. 2849 – 2854.

[77] Sylva, G., Edwards, R., Sassa, T., "A Feasibility Study for Self Reacting Pin Tool Welding of Thin Section Aluminum," *Proceedings of the 5th International Symposium on Friction Stir Welding*, TWI, Cambridge, UK, May 2004.

[78] Colligan, K., "Tapered Friction Stir Welding Tool," U.S. Patent 6,669,075. 30 Dec 2003.

[79] Colligan, K.J., Pickens, J.R., "Friction Stir Welding of Aluminum Using a Tapered Shoulder Tool," *Friction Stir Welding and Processing III*, The Minerals, Metals & Materials Society, Warrendale, PA, 2005.

[80] Colligan, K.J., O'Donnell, A.K., Shevock, J.W., Smitherman, M.T., Hostetter, G.J., "Friction Stir Welding of Thin Aluminum Using Fixed Gap Bobbin Tools," *Proceedings of the 9th International Symposium on Friction Stir Welding*, TWI, Cambridge, UK, May 2012.

[81] Ding, J., Carter, B., Lawless, K., Nunes, A.C., Russell, C., Suites, M., et al., "A Decade of Friction Stir Welding R&D At NASA'S Marshall Space Flight Center and a Glance into the Future," NASA Report, 2008, <http://ntrs.nasa.gov/archive/nasa/casi.ntrs.nasa.gov/20080009619_2008009118.pdf>.

[82] Carter, R.W., "Auto-Adjustable Tool for Self-Reacting and Conventional Friction Stir Welding," U.S. Patent 6,758,382. 6 July 2004.

[83] Schneider, J.A., Nunes, A.C., Brendel, M.S., "The Influence of Friction Stir Weld Tool Form and Welding Parameters on Weld Structure and Properties: Nugget Bulge in Self-Reacting Friction Stir Welds," *Proceedings of the 8th International Symposium on Friction Stir Welding*, TWI, Cambridge, UK, May 2010.

[84] Hilgert, J., dos Santos, J.F., Huber, N., "Numerical Simulation in Bobbin Tool FSW Process Development," *Proceedings of the 9th International Symposium on Friction Stir Welding*, TWI, Cambridge, UK, May 2012.

[85] Chen, J., Fujii, H., Sun, Y., Morisada, Y., Kondoh, K., "Effect of Material Flow by Double-Sided Friction Stir Welding on Weld Structure and Mechanical Properties of Magnesium Alloy," *Proceedings of the 9th International Symposium on Friction Stir Welding*, TWI, Cambridge, UK, May 2012.

[86] Sinclair, P., "Heated Friction Stir Welding: An Investigation into How Preheating Aluminum 6061 Affects Process Forces, M.S. Thesis, Vanderbilt University, 2009.

[87] Sinclair, P., Longhurst, W.R., Cox, C.D., Lammlein, D.H., Strauss, A.M., Cook, G.E., "Heated Friction Stir Welding: An Experimental and Theoretical

Investigation into How Preheating Influences Process Forces," *Materials and Manufacturing Processes*, Vol 25, 2010, pp. 1283 – 1291.

[88] Riichi, S., Takehiko, T., Susumu, H., Naoki, Y., Yuuta, K., "On Pre-Heating Effect for Friction Stir Welding of Aluminum Alloy – A Feasibility Study of Friction Stir Welding with Heating of Aluminum Alloy, *Quarterly Journal of the Japan Welding Society*, Vol 24, No 3, 2006, pp. 281 – 286.

[89] Kou, S., Cao, G., "Arc-Enhanced Friction Stir Welding, U.S. Patent 7,078,647. 18 July 2006.

[90] Scutelnicu, E., Birsan, D., Cojocaru, R., "Research on Friction Stir Welding and Tungsten Inert Gas Assisted Friction Stir Welding of Copper," *Recent Advances in Manufacturing Engineering*, pp. 97 – 102. < http://www.wseas.us/e-library/conferences/2011/Barcelona/MEQAPS/MEQAPS-16.pdf> 1 Nov 2012.

[91] Palm, F., "Laser Supported Friction Stir Welding Method," U.S. Patent 6,793, 118. 21 Sept 2004.

[92] Cabage, B., "New Way to Weld: ORNL Team Adds Laser Tech to Expand the Reach of a New Welding Technique," *Oak Ridge National Laboratory Reporter*, No 84, 2006, 1 – 4.

[93] Tweedy, B.M., Arbegast, W., Allen, C., "Friction Stir Welding of Ferrous Alloys Using Induction Preheating," *Friction Stir Welding and Processing III*, The Minerals, Metals & Materials Society, Warrendale, PA, 2005.

[94] Grant, G.J., Khaleel, M., Eberhardt, J.J., Arbegast, B., Stone, G., Howard, S., Allen, C., "Friction Stir Joining and Processing of Advanced Materials Including MMCs, High Strength Weight Reduction Materials," FY 2005 Progress Report, 112 – 121. <http://www1.eere.energy.gov/vehiclesandfuels/ pdfs/hswr_2005/fy05_hswr_4h.pdf> 1 Nov 2012.

[95] Ferrando, W.A., Lammlein, D., Posada, M., Floyd, A., "The Concept of Electrically-Assisted Friction Stir Welding and Application to Processing of Various Metals," *Proceedings of the 9th International Symposium on Friction Stir Welding*, TWI, Cambridge, UK, May 2012.

[96] Balasubramanian, V., Ravisankar, V., Reddy, G.M., "Effect of Pulsed Current Welding on Mechanical Properties of High Strength Aluminum Alloy," *International Journal of Advanced Manufacturing Technology*, Vol 36, 2008, pp. 254 - 262.

[97] Eberl, I., Hantrais, C., Ehrtsrom, J.C., Nardin, C., "Friction Stir Welding Dissimilar Alloys for Tailoring Properties of Aerospace Parts." *Science and Technology of Welding and Joining*, Vol 15, No 8, 2010, pp. 699 - 705.

[98] Ballun, M.C., "Development and Investigation of Pulsed Friction Stir Welding," M.S. Thesis, Vanderbilt University, 2013.

[99] Ballun, M.C., Cox, C.D., Gibson, B.T., Cook, G.E., Strauss, A.M., "Pulsed Friction Stir Welding: A Preliminary Process Variation Study," Pending Submission.

[100] Fleming, P.A., Lammlein, D.H., Cook, G.E., Wilkes, D.M., Strauss, A.M., DeLapp, D.R., Hartman, D.A., "Lateral Position Detection and Control for Friction Stir Systems," U.S. Patent 7,850,057 B2. Filed 30 May 2008.

[101] Hendricks, C.E., "The Mechanical Effects of WeaveTrack on Friction Stir Welds in a Lap Configuration," M.S. Thesis, Vanderbilt University, 2009.

[102] Johnson, D., "Creating an Affordable Option for Friction Stir Welding," National Instruments Website, <http://sine.ni.com/cs/app/doc/p/id/cs-11860> 2010.

[103] Burton, K.A., Matlack, M.P., Bommer, H.L., "Friction Stir Welding Load Confirmation System", U.S. Patent No. US 7,571,654 B2. 18 Nov 2008.

[104] "Low Cost Friction Stir Welder: History," LowStir, <http://www.lowstir.com/Webpages/History.html> 2013.

[105] Mitchell, J.E., "The experimental Thermo-Mechanics of Friction Stir Welding," M.S. Thesis, Vanderbilt University, 2002.

[106] Blignault, C., Hattingh, D.G., Kruger, G.H., Van Niekerk, T.I., James, M.N., "Friction Stir Weld Process Evaluation by Multi-Axial Transducer," *Measurement*, Vol 41, 2008, pp. 32 - 43.

[107] Gibson, B.T., "Custom Low-Cost Force Measurement Methods in Friction Stir Welding," M.S. Thesis, Vanderbilt University, 2011.

[108] Gibson, B.T., Cox, C.D., Longhurst, W.R., Strauss, A.M., Cook, G.E., "Exploiting Robotic Link Deflection for Low-Cost Force Measurement in Manufacturing," *Measurement*, Vol 45, 2012, pp. 140 - 143.

[109] Gibson, B.T., Cox, C.D., Aguilar, J.R., Ballun, M.C., Strauss, A.M., Cook, G.E., "Low-Cost Wireless Force Sensor Design with Applications in Friction Stir Welding," *9th International Trends in Welding Research Conference*, Chicago, IL, June 4 - 8, 2012.

[110] Longhurst, W.R., Strauss, A.M., Cook, G.E., Cox, C.D., Hendricks, C.E., Gibson, B.T., Duwant, Y.S., "Investigation of Force Controlled Friction Stir Welding for Manufacturing and Automation," *Proceedings of the Institution of Mechanical Engineers, Part B: Journal of Engineering Manufacture*, Vol 224, No 6, 2010, pp. 937 – 949.

[111] Smith, C., "Robotic Friction Stir Welding Using a Standard Industrial Robot," *Proceedings of the 2nd International Symposium on Friction Stir Welding*, TWI, Cambridge, UK, 2000.

[112] Rosio Friction Stir Welding Robot: Friction Stir Robot for Welding Challenging Joints, ESAB Welding & Cutting, 2013 <http://www.esabna.com/us/en/products_catalog.cfm?Product_ID=965> 6 Sept 2013.

[113] De Backer, J., Verheyden, B., "Robotic Friction Stir Welding for Automotive and Aviation Applications," M.S. Thesis, University West, Sweden, 2009.

[114] Cook, G.E., Smartt, H.B., Mitchell, J.E., Strauss, A.M., Crawford, R., "Controlling Robotic Friction Stir Welding," *Welding Journal*, Vol 82, No 6, 2003, pp. 28 – 34.

[115] Longhurst, W.R., Strauss, A.M., Cook, G.E., Fleming, P.A., "Torque Control of Friction Stir Welding for Manufacturing and Automation*," International Journal of Advanced Manufacturing Technology*, Vol 51, No 9, 2010, pp. 905 – 913.

[116] Mutambara, A.G.O., "Design and Analysis of Control Systems," CRC Press, Boca Raton, FL, 1999.

[117] Bres, A., Monsarrat, B., Dubourg, L., Birglen, L., Perron, C., Fahazi, Baron, L., "Simulation of Friction Stir Welding Using Industrial Robots*," Industrial Robot: An International Journal*, Vol 37, No 1, 2010, pp. 36 – 50.

[118] Campbell, C.L., Fullen, M.S., M.J., Skinner, "Welding Head," U.S. Patent 6,199,745 B1. 13 March 2001.

[119] Fehrenbacher, A., Duffie, N.A., Ferrier, N.J., Pfefferkorn, F.E., Zinn, M.R., "Toward Automation of Friction Stir Welding Through Temperature Measurement and Closed-Loop Control," *ASME Journal of Manufacturing Science and Engineering*, Vol 133, No 5, 2011, pp. 1 - 12.

[120] Soron, M., Kalaykov, I., "Generation of Continuous Tool Paths Based on CAD Models for Friction Stir Welding in 3D," *Proceedings of the 15th Mediterranean Conference on Control and Automation*, Athens, Greece, 27 – 29 July 2007.

[121] De Backer, J., Christiansson, A.K., Oqueka, J., Bolmsjö, G., "Investigation of Path Compensation Methods for Robotic Friction Stir Welding," *Industrial Robot: An International Journal*, Vol 39, No 6, 2012, pp. 601 – 608.

[122] Soron, M., De Backer, J., Christiansson, A.K., Ilar, T., "A Local Model for Online Path Corrections in Friction Stir Welding," *Friction Stir Welding and Processing Conference*, Lille, France, 28 – 29 Jan 2010.

[123] Fleming, P.A., Lammlein, D.H., Wilkes, D.M., Cook, G.E., Strauss, A.M., DeLapp, D.R., Hartman, D.A., "Misalignment Detection and Enabling of Seam Tracking for Friction Stir Welding," *Science and Technology of Welding and Joining*, Vol 14, No 1, 2009, pp. 93 - 96.

[124] Christner, B., Hansen, M., Skinner, M., Sylva, G., "Friction Stir Welding System Development for Thin Gauge Aerospace Structures," *Proceedings of the 4th International Symposium on Friction Stir Welding*, TWI, Cambridge, UK, May 2003.

[125] Martin, J.P., Stanhope, C., Gascoyne, S., "Novel Techniques for Corner Joints using Friction Stir Welding," *Friction Stir Welding and Processing VI*, The Minerals, Metals & Materials Society, Warrendale, PA, 2011.

[126] Fleming, P.A., Hendricks, C.E., Wilkes, D.M., Cook, G.E., Strauss, A.M., "Automatic Seam-Tracking of Friction Stir Welded T-Joints," *International Journal of Advanced Manufacturing Technology*, Vol 45, 2009, pp. 490 - 495.

[127] Fleming, P.A., Hendricks, C.E., Cook, G.E., Wilkes, D.M., Strauss, A.M., Lammlein, D.H., "Seam-Tracking for Friction Stir Welded Lap Joints," *Journal of Materials Engineering and Performance*, Vol 19, No 8, 2010, pp. 1128 - 1132.

[128] Dave, V.R., Hartman, D.A., King, W.H., Cola, M.J., Vaidya, R.U., "Strategy for Small-Lot Manufacturing: In-Process Monitoring and Control," *Los Alamos Science*, No 28, 2003.

[129] Boldsaikhan, E., Corwin, E.M., Logar, A.M., Arbegast, W.J., "The Use of Neural Network and Discrete Fourier Transform for Real-Time Evaluation of Friction Stir Welding," *Applied Soft Computing*, Vol 11, 2011, pp. 4839 – 4846.

[130] Boldsaikhan, E., Burford, D., "Generalized e-NDE Algorithm for Friction Stir Welding," *Proceedings of the 9th International Symposium on Friction Stir Welding*, TWI, Cambridge, UK, May 2012.

[131] Burford, D., Boldsaikhan, E., "Early Detection of Volumetric Defects Using e-NDE During Friction Stir Welding," *Proceedings of the 9th International Symposium on Friction Stir Welding*, TWI, Cambridge, UK, May 2012.

[132] Boldsaikhan, E., McCoy, M., "Analysis of Tool Feedback Forces and Material Flow During Friction Stir Welding," *Friction Stir Welding and Processing VII*, The Minerals, Metals & Materials Society, Warrendale, PA, 2013.

[133] Fleming, P.A., Lammlein, D.H., Wilkes, D.M., Fleming, K., Bloodworth, T., Cook, G.E., Strauss, A.M., DeLapp, D.R., Lienert, T., Bement, M., Prater, T., "In-Process Gap Detection in Friction Stir Welding," *Sensor Review*, Vol 28, No 1, 2008, pp. 62 – 67.

[134] Thomas, W.M., Kallee, S.W., Staines, D.G., Oakley, P.J., "Friction Stir Welding – Process Variants And Developments In The Automotive Industry, *SAE World Congress*, 3 – 7 April 2006, TWI < http://www.twi.co.uk/technical-knowledge/published-papers/friction-stir-welding-process-variants-and-developments-in-the-automotive-industry-april-2006/> 6 Nov 2012.

[135] Kallee, S.W., "NZ Fabricators Begin to use Friction Stir Welding to Produce Aluminum Components and Panels," *New Zealand Engineering News*, Aug 2006, TWI < http://www.twi.co.uk/technical-knowledge/published-papers/nz-fabricators-begin-to-use-friction-stir-welding-to-produce-aluminium-components-and-panels-august-2006/> 6 Nov 2012.

[136] "High-Tech Production of Aluminum Bodies," Audi of America News Channel, 17 Feb 2011 <http://www.audiusanews.com/newsrelease.do;jsessionid=ACFEB6C0C51AFA18EAFC7D0CA293D38C?&id=2238&allImage=1&teaser=high-tech-production-aluminum-bodies&mid=111> 6 Nov 2012.

[137] Meyer, A., "FSW in Automotive Mass Production – The New Mercedes SL," *Proceedings of the 9th International Symposium on Friction Stir Welding*, TWI, Cambridge, UK, May 2012.

[138] "Honda Develops New Technology to Weld Together Steel and Aluminum and Achieves World's First Application to the Frame of a Mass-Production Vehicle," Honda Motor Co., Ltd., 6 Sept 2012 <http://world.honda.com/news/2012/4120906Weld-Together-Steel-Aluminum/index.html> 7 Nov 2012.

[139] "Space Shuttle Technology Summary: Friction Stir Welding," NASA, 2001 <http://www.nasa.gov/centers/marshall/pdf/104835main_friction.pdf> 9 Sept 2013.

[140] Dracup, B.J, Arbegast, W.J. "Friction Stir Welding as a Rivet Replacement Technology," U.S. Patent 6,779,707. 24 Aug 2004.

[141] Arbegast, W.J., "Friction Stir Welding: After a Decade of Development," *Friction Stir Welding and Processing IV*, The Minerals, Metals & Materials Society, Warrendale, PA, 2007.

[142] Aldanondo, E., da Silva, A., Alvarez, P., Lizarralde, A., Echeverria, A., "Dissimilar Friction Stir Welding of AA2024-T3 and AA7075-T6 Aluminum Alloys," *Friction Stir Welding and Processing V*, The Minerals, Metals & Materials Society, Warrendale, PA, Feb 2009.

[143] Baumann, J. A., Lederich, R.J., Bolser, D.R., Talwar, R., "Property Characterization of 2024Al/7075Al Bi-Alloy Friction Stir Welded Joints," *Friction Stir Welding and Processing II*, The Minerals, Metals & Materials Society, Warrendale, PA, March 2003.

[144] Cavaliere, P., Cerri, E., and Squillace, A., "Mechanical Response of 2024-7075 Aluminum Alloys Joined by Friction Stir Welding," *Journal of Materials Science*, Vol 40, No 14, 2005, pp. 3669 – 3676.

[145] Cavaliere, P., Nobile, R., Panella, F.W., Squillace, A., "Mechanical and Microstructural Behavior of 2024-7075 Aluminum Alloy Sheets Joined by Friction Stir Welding," *International Journal of Machine Tools and Manufacture*, Vol 46, No 6, 2006, pp. 558 – 594.

[146] Widener, C.A., Talia, J. E., Tweedy, B.M., Burford, D.A., "Corrosion in Friction Stir Welded Dissimilar Aluminum Alloy Joints of 2024 and 7075," *Friction Stir Welding and Processing IV*, The Minerals, Metals & Materials Society, Warrendale, PA, 2007.

[147] Mittelstedt, C., Schroder, K.U., "Local Postbuckling of Hat-Stringer-Stiffened Composite Laminated Plates Under Transverse Compression," *Composite Structures*, Vol 92, No 12, 2012, pp. 2830 – 2844.

[148] "Reproducing Stressed Skin Effect in Aircraft Models," Rogerio "Rato" Marczak, 2013 < http://www.ratomodeling.com/articles/stressed_skin/> 17 Sept 2013.

[149] Christner, B., McCoury, J., and Higgins, S., "Development and Testing of Friction Stir Welding as a Joining Method for Primary Aircraft Structure," *Proceedings of the 4th International Symposium on Friction Stir Welding*, TWI, Cambridge, UK, May 2003.

[150] Maxwell, D., "The Great Eclipse: A Dream Design Bankrupted by Marketing and Mismanagement and Saved by a Sensible Business Strategy," Dog Ear Publishing, Indianapolis, IN, 2011.

[151] Eclipse Jet in Flight, Total Eclipse Twin-Engine Jets, Eclipse Aerospace, <http://www.eclipse.aero/total_eclipse.php> 16 Oct 2012.

[152] Fernandez, F., "Friction Stir Welding Applied on Mid-Size Aircraft," *Proceedings of the 8th International Symposium on Friction Stir Welding*, TWI, Cambridge, UK, May 2010.

[153] Fortes, L., "FSW Applied on Mid Size Aircraft," *Presented at the 20th Aeromat Conference*, Dayton, Ohio, 2009.

[154] Freeman, J., Moore, G., Thomas, B., Kok, L., "Advances in FSW for Commercial Aircraft Applications," *Proceedings of the 6th International Symposium on Friction Stir Welding*, TWI, Cambridge, UK, Oct. 2006.

[155] "Airbus to Use Friction Stir Welding," The Aluminum Association <http://www.aluminum.org/AM/Template.cfm?Section=Home&CONTENTID=22762&TEMPLATE=/CM/ContentDisplay.cfm> 20 May 2013.

[156] Shepherd, G., "The Evaluation of Friction Stir Welded Joints on Airbus Aircraft Wing Structure," *Proceedings of the 4th International Symposium on Friction Stir Welding*, TWI, Cambridge, UK, May 2003.

[157] Specs, Eclipse 550 Twin-Engine Jets, http://www.eclipse.aero/550.php?n=1> 17 Sept 2013.

[158] Brown, J., Burford, D., "Friction Stir Fabrication of Spar T-Joints Made From 7075 Aluminum," *Friction Stir Welding and Processing VI*, The Minerals, Metals & Materials Society, Warrendale, PA, 2011.

[159] Christner, B., "Welded Joints with Polymer Sealant," U.S. Patent 7,225,966. 5 June 2007.

[160] Li, T., Ritter, G., Kapustka, N., Lederich, R., "Friction Stir Lap Joining of Al 7075 With Sealant," *Friction Stir Welding and Processing IV*, The Minerals, Metals & Materials Society, Warrendale, PA, 2007.

[161] Brown, J.M., "The Effects of Sealants and Surface Treatments on the Faying Surface of Swept Friction Stir Spot Welds", MS Thesis, Wichita State University, 2008.

[162] Doering, K.T.N. "Fatigue of Friction Stir Welded Lap Joints with Sealants," MS Thesis, Missouri University of Science and Technology, 2009.

[163] Presher, P. "Robotic Advances in Aerospace Manufacturing", 4 April 2013, Design News <http://www.designnews.com/author.asp?section_id=1386&doc_id=261140&dfpPParams=ind_182,aid_261140&dfpLayout=blog> 20 May 2013.

[164] Alloy 2024 Sheet and Plate: Material Specifications, Alcoa Mill Products, <http://www.alcoa.com/mill_products/catalog/pdf/alloy2024techsheet.pdf> 19 Sept 2013.

[165] Alloy 7075 Sheet and Plate: Material Specifications, Alcoa Mill Products, <http://www.alcoa.com/mill_products/catalog/pdf/alloy7075techsheet.pdf> 19 Sept 2013.

[166] MMPDS-01, Metallic Materials Properties Development and Standardization Handbook, U.S. Department of Transportation, 2003.

[167] PR-1432-GP Corrosion Inhibitive Coating: Technical Data Sheet, PPG Aerospace, PRC-DeSoto <http://www.ppg.com/coatings/aerospace/ sealants1/pr_1432gp.pdf> 19 Sept 2013.

[168] Welling, M., "Fisher Linear Discriminant Analysis," Department of Computer Science, University of Toronto, 2007, <http://www.ics.uci.edu/~welling/ classnotes/papers_class/ Fisher-LDA.pdf> 19 Sept 2013.

[169] Shlens, J., "A Tutorial on Principle Component Analysis," Center for Neural Science, New York University, 2009, http://www.snl.salk.edu/~shlens/pca.pdf> 19 Sept 2013.

[170] Smith, C.B., Schroeder, K., Fehrenbacher, A., "An Automated Path Planning and Programming System with Real-Time Adaptive Control for Friction Stir Processing of Cast Surfaces," *Proceedings of the 9th International Symposium on Friction Stir Welding*, TWI, Cambridge, UK, May 2012.

[171] Cook, G.E., "Robotic Arc Welding: Research in Sensory Feedback Control," *IEEE Transactions on Industrial Electronics*, Vol IE-30, No 3, 1983, pp. 252 - 268.

[172] Zhang, C., Ordonez, R., "Extremum-Seeking Control and Applications: A Numerical Optimization-Based Approach," Springer-Verlag, London, UK, 2012.

[173] Pelseal 2077 and Pealseal 2531, Technical Data, Pelseal Technologies, LLC <http://www.bhdistributors.com/Images/Interior/pelseal%202077%20&%202531 %20tds.pdf> 29 May 2013.

[174] Titebond Painter's Caulk, Physical Properties, Franklin International <http://www.titebond.com/product.aspx?id=033a84f9-90a0-4ba3-9ff4-975990cef7ea> 29 May 2013.

[175] "Com-stir™ - Compound Motion for Friction Stir Welding and Machining," *Connect*, No 124, May/June 2003, p. 8, TWI <http://www.twi.co.uk/news-

events/connect/archive/2003/may-june-2003/com-stir-tm-compound-motion-for-friction-stir-welding-and-machining/> 29 May 2013.

[176] Sylva, G., M&P Engineering, Eclipse Aerospace, Personal Communication, 2012 [retrieved 8 Nov 2012 – 12 Nov 2012].

[177] Liu, J., "Advanced Aluminum and Hybrid Aerostructures for Future Aircraft," *Materials Science Forum*, Vols 519-521, 2006, pp. 1233-1238.

[178] Rioja, R.J., Liu, J., "The Evolution of Al-Li Base Products for Aerospace and Space Applications," *Metallurgical and Materials Transactions A*, Vol 43A, 2012 pp. 3325 - 3337.

[179] Dursun, T., Soutis, C., "Recent Developments in Advanced Aircraft Aluminum Alloys," *Materials and Design*, Vol 56, 2014, pp. 862 - 871.

[180] Pacchione, M., Telgkamp, J., "Challenges of the Metallic Fuselage," *Proceedings of the 25th International Congress of the Aeronautical Sciences*, 2006.

[181] Astarita, A., Squillace, A., Scala, A., Prisco, A., "On the Critical Technological Issues of Friction Stir Welding T-Joints of Dissimilar Aluminum Alloys," *Journal of Materials Engineering and Performance*, Vol 21, No 8, 2012, pp. 1763 - 1771.

[182] Bitondo, C., Prisco, U., Squillace, A., Buonadonna, P., Dionoro, G., "Friction-Stir Welding of AA 2198 Butt Joints: Mechanical Characterization of the Process and of the Welds Through DOE Analysis," *International Journal of Advanced Manufacturing Technology*, Vol 53, 2011, pp. 505 - 516.

[183] Bitondo, C., Prisco, U., Squillace, A., Giorleo, G., Buonadonna, P., Dionoro, G., Campanile, G., "Friction Stir Welding of AA2198-T3 Butt Joints for Aeronautical Applications," *International Journal of Material Forming*, Vol 3, No 1, 2010, pp. 1079 - 1082.

[184] Buffa, G., Campanile, G., Fratini, L., Prisco, A., "Friction Stir Welding of Lap Joints: Influence of Process Parameters on the Metallurgical and Mechanical Properties," *Materials Science and Engineering A*, Vol 519, 2009, pp. 19 - 26.

[185] Cavaliere, P., Cabibbo, M., Panella, F., Squillace, A., "2198 Al-Li Plates Joined by Friction Stir Welding: Mechanical and Microstructural Behavior," *Materials and Design*, Vol 30, 2009, 3622 - 3631.

[186] Cavaliere, P., De Santis, A., Panella, F., Squillace, A., "Effect of Anisotropy on Fatigue Properties of 2198 Al-Li Plates Joined by Friction Stir Welding", *Engineering Failure Analysis*, Vol 16, 2009, pp. 1856 - 1865.

[187] Le Jolu, T., Morgenever, T.F., Denquin, A., Gourgues-Lorenzon, A.F., "Effect of Welding Defects on Plastic Behavior and Fatigue Lifetime of Friction Stir Welded Al-Cu-Li Alloy," *Proceedings of the 13th International Conference on Fracture*, Beijing, China, June 2013.

[188] Li, W., Jiang, R., Zhang, Z., Ma, Y.E., "Effect of Rotation Speed to Welding Speed Ratio on Microstructure and Mechanical Behavior of Friction Stir Welded Aluminum-Lithium Alloy Joints," *Advanced Engineering Materials*, Vol 15, No 11, 2013, pp. 1051 - 1058.

[189] Ma, Y.E., Irving, P., "Residual Stress Effects and Fatigue Behavior of Friction-Stir-Welded 2198-T8 Al-Li Alloy Joints," *AIAA Journal of Aircraft*, Vol 48, No 4, 2011, pp. 1238 - 1244.

[190] Ma, Y.E., Liu, B.Q., Zhao, Z.Q., "Damage Tolerance Properties of 2198-T8 Integral Fuselage Panel Between Double Friction Stir Weld Joints," *Applied Mechanics and Materials*, Vols 138-139, 2012, pp. 651 - 656.

[191] Ma, Y.E., Xia, Z.C., Jiang, R.R., Li, W.Y., "Effect of Welding Parameters on Mechanical and Fatigue Properties of Friction Stir Welded 2198 T8 Aluminum-Lithium Alloy Joints," *Engineering Fracture Mechanics*, Vol 114, 2013, pp. 1 - 11.

[192] Ma, Y.E., Zhao, Z.Q., Liu, B.Q., Li, W.Y., "Mechanical Properties and Fatigue Crack Growth Rates in Friction Stir Welded Nugget of 2198-T8 Al-Li Alloy Joints," *Materials Science and Engineering A*, Vol 569, 2013, pp. 41 - 47.

[193] Rao, J., Payton, E.J., Somsen, C., Neuking, K., Eggeler, G., Kostka, A., dos Santos, J.F., "Where Does the Lithium Go? A Study of the Precipitates in the Stir Zone of a Friction Stir Weld in a Li-Containing 2xxx Series Al Alloy," *Advanced Engineering Materials*, Vol 12, No 4, 2010, pp. 298 - 303.

[194] Prasad, N.E., Gokhale, A., Wanhill, R.J.H. (Eds.), *Aluminum-Lithium Alloys: Processing, Properties, and Applications*, Butterworth-Heinemann, Oxford, UK, 2013.

[195] Giummarra, C., Thomas, B., Rioja, R.J., "New Aluminum Lithium Alloys for Aerospace Applications," *Proceedings of the Light Metals Technology Conference*, 2007.

[196] Prater, T., "An Investigation into the Friction Stir Welding of Al 6061 and Al 6061/SiC/17.5p Using Diamond Coatings," M.S. Thesis, Vanderbilt University, 2008.

[197] Fernandez, G.J., Murr, L.E., "Characterization of Tool Wear and Weld Optimization in the Friction-Stir Welding of Cast Aluminum 359+20% SiC Metal Matrix Composite", *Materials Characterization*, Vol. 52, 2004, pp. 65 – 75.

[198] Craig, J.J.,"Introduction to Robotics: Mechanics and Control," 3rd ed. Pearson Prentice Hall, Upper Saddle River, New Jersey, USA, 2005, pp. 290 - 312.

[199] Koseeyaporn, P., Cook, G.E., Strauss, A.M. , "Adaptive Voltage Control in Fusion Arc Welding", *IEEE Transactions on Industry Applications*, Vol 36, No 5, 2000, pp. 1300 - 1307.

[200] Talia, J.E., Nunes, A.C., "Cracking During Welding of 2195 Aluminum-Lithium Alloy: Experimental Approaches Towards Mechanism," *Aluminum-Lithium Alloys for Aerospace Workshop*, NASA Conference Publication 3287, 1994.

[201] Feng, A.H., Xiao, B.I., Ma, Z.Y., "Effect of Microstructural Evolution on Mechanical Properties of Friction Stir Welded AA2009/SiCp Composite," *Composites Science and Technology*, Vol 68, 2008, pp. 2141 - 2148.

[202] Marzoli, L.M., Strombeck, A.V., Dos Santos, J.F., Gambaro, C., Volpone, L.M., "Friction Stir Welding of an AA6061/Al2O3p Reinforced Alloy*," Composites Science and Technology*, Vol 66, 2006, pp. 363 - 371.